ON TIME-FREQUENCY ANALYSIS OF HEART RATE VARIABILITY

Huibert Goosen van Steenis

ON TIME-FREQUENCY ANALYSIS OF HEART RATE VARIABILITY

OVER TIJD-FREQUENTIE ANALYSE VAN HARTRITME VARIABILITEIT

Proefschrift

ter verkrijging van de graad van doctor
aan de Erasmus Universiteit Rotterdam
op gezag van de Rector Magnificus

Prof.dr.ir. J.H. van Bemmel

en volgens het besluit van het College voor Promoties.

De openbare verdediging zal plaatsvinden op
woensdag 30 oktober 2002 om 15.45 uur
door

Huibert Goosen van Steenis
geboren te Herwijnen

Promotiecommissie

Promotoren	Prof.dr. M.W. Hengeveld Prof.ir. K.H. Wesseling
Overige leden	Prof.dr.ir. N. Bom Dr.ir. L.J.M. Mulder Dr. J.A. Kors
Copromotor	Dr. J.H.M. Tulen

De werkzaamheden beschreven in dit proefschrift werden uitgevoerd op de afdeling Psychiatrie van het Erasmus MC. De afdeling Psychiatrie wil ik bedanken voor de financiële bijdrage in de kosten van dit proefschrift.

Het gedicht van Ida Gerhardt werd geplaatst met de welwillende toestemming van Em. Querido's Uitgeverij b.v., Amsterdam.

Drukwerk: Ridderprint offsetdrukkerij b.v., Ridderkerk.

ISBN 90-9016246-1

Spreuk bij het werk

Als ik nu in dit land
maar wat alléén mag blijven,
dan zal de waterkant
het boek wel voor mij schrijven.

Dit is wat ik behoef
en hiertoe moest ik komen,
het simpele vertoef
bij dit gestadig stromen.

Het water gaat voorbij,
wiss'lend gelijk gebleven, -
het heeft stilaan in mij
een nieuw begin geschreven.

Ik weet met zekerheid,
hier vind ik vroeg of later
het woord dat mij bevrijdt
en levend is als water.

Ida Gerhardt

In herinnering:
Vader † 28-03-2002
Moeder † 12-10-2000
Rien † 22-11-1988

Contents **page**

Chapter 1 Introduction 11

Chapter 2 Heart rate variability and its analysis 23

Chapter 3 Heart rate variability spectra based on non-equidistant sampling: the spectrum of counts and the instantaneous heart rate spectrum 39
Medical Engineering and Physics 16:355-362, 1994

Chapter 4 Quantification of autonomic cardiac regulation in psycho-pharmacological research 61
In: Measurement of heart rate and blood pressure variability in man. Methods, mechanisms and clinical applications of continuous finger blood pressure measurement. A.J. Man in 't Veld, G.A. van Montfrans, G.J. Langewouters, K.I. Lie, G. Mancia (eds.). Alphen aan den Rijn: Van Zuiden Communications BV, The Netherlands, 1995, chapter 8, pp:61-72

Chapter 5 Examining nonequidistantly-sampled cardiovascular time series by means of the Wigner-Ville distribution 79
In: Computers in psychology: applications, methods, and instrumentation. Maarse FJ, Akkerman AE, Brand AN, Mulder LJM, and Van der Stelt MJ (eds). Lisse: Swets & Zeitlinger chapter 13, pp:151-166, 1994. ISSN 0925-9244

Chapter 6 The exponential distribution applied to nonequidistantly sampled cardiovascular time series 99
Computers and Biomedical Research 29:174-193, 1996

Chapter 7 Quantification of the dynamic behavior over time of narrow-band components present in heart rate variability by means of the instantaneous amplitude and frequency 127
Submitted

Chapter 8 The instantaneous frequency of cardiovascular time series: a comparison of methods 161
Computer Methods and Programs in Biomedicine, accepted

Chapter 9 Time-frequency parameters of heart rate variability – using instantaneous amplitude and frequency to unravel the dynamics of cardiovascular control processes 187
IEEE Engineering in Medicine and Biology Magazine, in press

Chapter 10 Summary and concluding remarks 221
Samenvatting 227

Appendix Time-frequency analysis 241
Glossary 265
Abbreviations 274

Dankwoord 277

Curriculum Vitae 279

List of publications 280

CHAPTER 1
INTRODUCTION

1 Background

The human heart does not beat in a constant rhythm, but there are fluctuations in time between two consecutive heartbeats (see figure 1). These fluctuations are spontaneous, or they can be evoked by physical or mental stimulation or by pharmacological interventions. Heart rate is the number of heartbeats per minute. Thus the heart rate shows both random and apparent periodical fluctuations with variable amplitude and frequency (see figures 2A,3A). These beat-to-beat fluctuations in heart rate are called heart rate variability (HRV) (Task Force p:354, 1996).

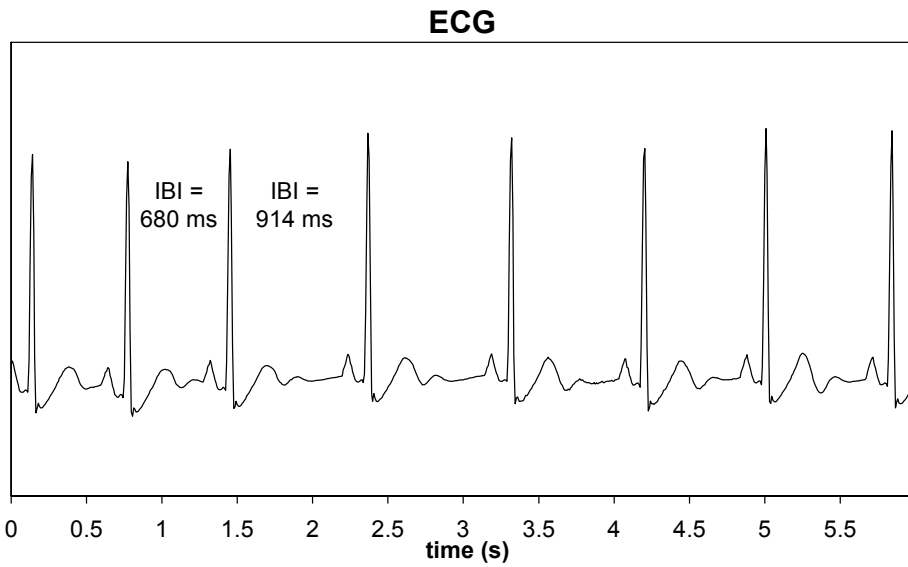

Figure 1. Example of an ECG recording: 6 s recording of a healthy woman of 36 years. IBI = interbeat interval.

Although the causes of HRV are still debated, the periodical fluctuations in heart rate are frequently studied to obtain quantitative estimates of sympathetic and parasympathetic processes of neurocardiac function. It has been demonstrated that HRV follows a 1/f spectral course down to frequencies of 10^{-5} Hz (Kobayashi et al., 1982; Di Rienzo et al., 1995). The beat-to-beat fluctuations in heart rate present in periods up to several minutes (2-5 min) are called short-term variability.

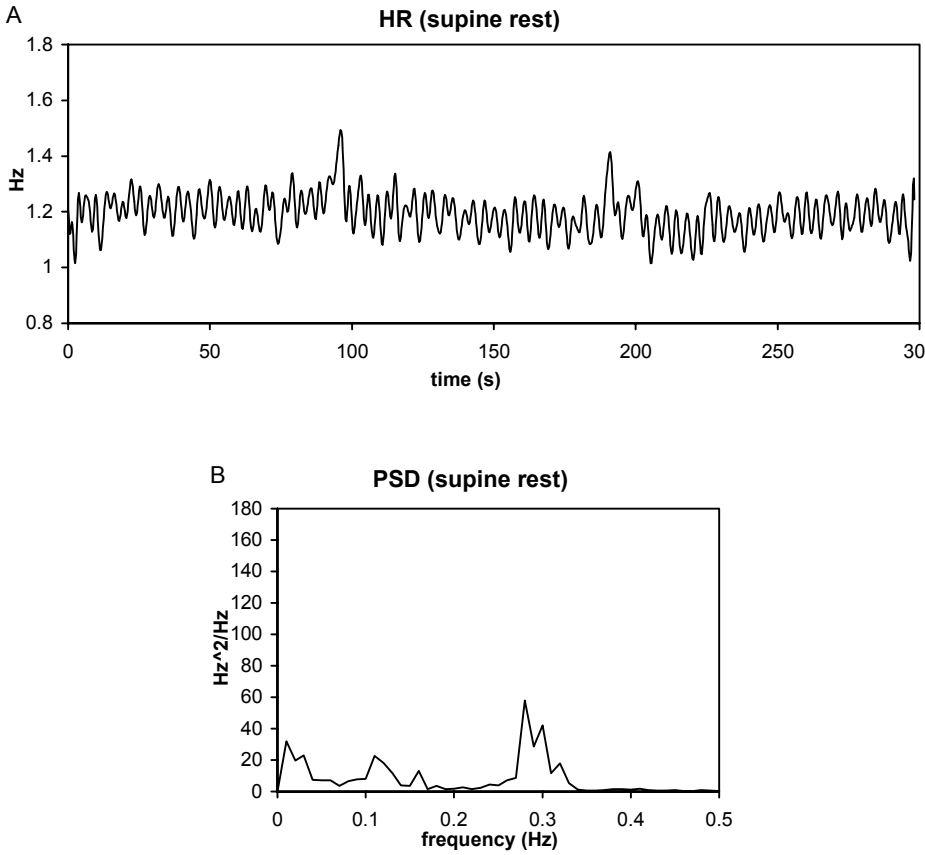

Figure 2. Heart rate (HR). A: an example of an equidistantly sampled low-pass filtered cardiac event series (see chapter 2) of about 5 min during supine rest, recorded from a healthy male volunteer; mean heart rate is 72 beats per minute. B: the corresponding power spectral density (PSD) function.

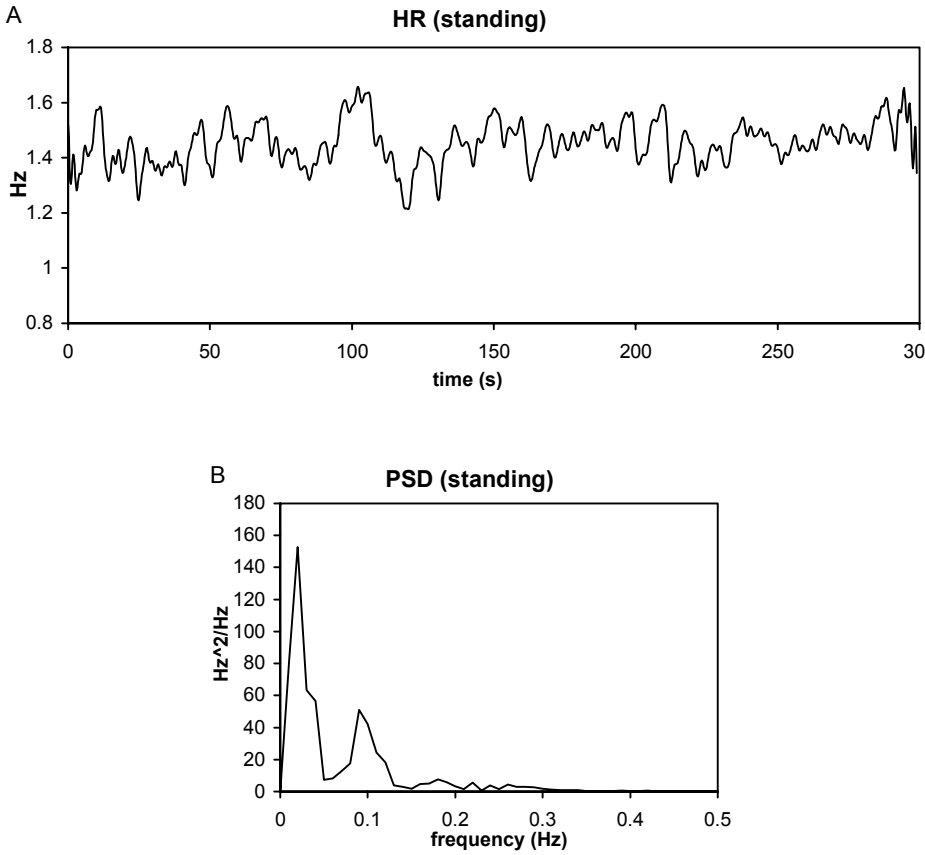

Figure 3. Heart rate (HR). A: a low-pass filtered cardiac event series of about 5 min during orthostatic challenge, recorded from the same person as shown in figure 2; mean heart rate is 87 beats per minute. B: the corresponding power spectral density (PSD) function.

In the range of short-term variability, three peaks can often be distinguished at frequencies near 0.04, 0.1, and 0.3 Hz (see figures 2B,3B) (e.g., Hyndman et al., 1971; Sayers, 1973; Kitney, 1975; Akselrod et al., 1981; Kamath et al., 1993; Task Force, 1996). The first peak, at 0.04 Hz, is of uncertain origin. The 0.1 Hz peak is probably mediated by the baroreflex and reflects the variable sympathetic tone of the autonomic nervous system. The peak near 0.3 Hz may reflect parasympathetic (vagal) tone linked with respiration. In the study of HRV, these peaks are called the characteristic frequency components, bands, or rhythms. It has been shown that the ratio of the powers of the heart rate fluctuations in the last two mentioned frequency areas might be indicative of a sympathovagal balance (e.g., Malliani et al., 1991; Parati et al., 1995). Several closed-loop blood pressure control models have been put forward to explain the short-term variations in heart rate in terms of baroreflex and/or cardiopulmonary reflexes (e.g., Wesseling et al., 1985; Ten Voorde, 1992; Van Roon, 1998).

In clinical research, most attention has been paid to the study of HRV. HRV can be derived non-invasively from a surface ECG. As a non-invasive tool, the study of HRV has provided valuable information regarding neurocardiac functioning in autonomic nervous system diseases such as neonatal autonomic developmental dysfunction, autonomic neuropathy (e.g., diabetes mellitus, autonomic failure), hypertension, heart failure, and coronary heart disease. For instance, population-based studies have indicated that reduced HRV, primarily due to reduced vagal effectiveness, predicts cardiac events, cardiovascular mortality, and the onset of hypertension (Bigger et al., 1993; Tsuji et al., 1996; Singh et al., 1998; Kikuya et al., 2000).

In affective and anxiety disorders, abnormalities of the autonomic nervous system and a higher-than-expected rate of sudden death from cardiac disease have been reported (e.g., Malzberg, 1937; Black et al., 1985; Hayward, 1995). Within psychiatric research, HRV-analysis has been applied to assess if dysfunctions in sympathetic and parasympathetic neurocardiac regulation may explain these phenomena. Several clinical studies have demonstrated that depressed patients show decreased HRV, possibly due to vagal withdrawal (Dalack et al., 1990; Miyaki et al., 1991). However, other studies only found limited evidence for alterations in HRV in depressed patients (Yeragani et al., 1991; Tulen et al., 1996). The issue of comorbidity between cardiac diseases and psychiatric symptoms is complicated to resolve. This may be due to the cardiovascular (side-)effects of many psychoactive drugs, such as tricyclics and MAO-Is. Furthermore, the presence of cardiovascular

risk factors, e.g., smoking, reduced physical activity, and altered lipid levels, in many psychiatric populations also complicates this issue.

2 Why time-frequency analysis?

It is customary to study HRV in the time-domain or in the frequency domain. For instance, the variance of an HRV-signal within a time-interval is a time-domain parameter expressing the power of the HRV in that interval. The variance is computed by integrating the squared amplitude of the HRV-signal over that interval. The squared amplitude of a signal is called the instantaneous power (e.g., Boashash p:438, 1991; Cohen p:4, 1995). The power spectral density of a signal computed over a time-interval is defined by the squared amplitude of the finite Fourier transform of the signal averaged over that time-interval (e.g., Bendat p:130, 1986; Boashash p:437, 1991; Cohen p:7, 1995). This reflects the power of each frequency component averaged over that time-interval. The power of an HRV-signal within a frequency band is a frequency-domain parameter and is obtained by integrating the power spectral density of the signal over that frequency band.

However, the instantaneous power and the power spectral density, alone and in combination, are not sufficient to fully describe the properties of an HRV-signal. From a power spectral density function we learn which frequency components are present, but it does not tell us when they are present, since the phase information is lost when computing the power spectral density. Similarly, the instantaneous power describes which time components are present, but not the frequency range of a time component. (e.g., Boashash p:422, 1991). In other words, the power spectral density does not reveal the frequency components in time and the instantaneous power does not show the time components in frequency.

Statistics measured in a 5 min interval of HRV probably differ from those measured in the next 5 min and from those measured in the entire 10 min interval. When the differences are statistically significant, the signal is called non-stationary. If this is the case, there may be significant changes of the frequency components of the signal in time (cf., Boashash p:418, 1991). Their presence in time cannot be derived from the power spectral density computed over the 10 min interval. And their powers cannot be interpreted unambiguously, because frequency components of different duration and amplitude may produce similar peaks in the power spectral density function. For instance, if a frequency component is present during 20 s within the 10 min interval with an amplitude of, say, 10 units, the power spectral density is similar to a situation where the frequency component is present during 5 s with an amplitude

of 20 units. Thus the need arises for a description that represents the power of the signal simultaneously in the time- and frequency-domains. Such time-frequency representations are often called ‘distributions’ for historical reasons. The phase spectrum of the raw signal contains the information that is necessary to localize the frequency components in time. Especially, the instantaneous frequency is a means to localize the frequency components in time. Therefore, the phase information of the raw signal is included in the computation of a time-frequency representation. Time-frequency signal analysis does not assume stationarity, whereas power spectral analysis does (e.g., Boashash p:418, 1991).

If there are transients in HRV, which is often the case, a time-frequency representation can be employed to describe them. This means a greatly improved interpretation of HRV-signals of experimental and clinical populations. Especially if a time-frequency method can be used that provides a qualitative and quantitative description of the dynamic changes in frequency and amplitude with a high resolution in time. We expect that these methods facilitate the study of very fast ‘instantaneous’ changes in sympathetic and parasympathetic processes. Furthermore, the time-frequency method should allow the quantification of transient and sustained changes in the characteristic frequency components to study responsiveness of the cardiovascular control system to various physical, mental or pharmacological stimuli.

This thesis describes time-frequency techniques that we have developed to study cardiovascular control mechanisms applicable to psychiatric and psycho-physiological research.

3 Aim of the research

The aim of this research is to develop a time-frequency method suitable to study HRV in greater detail. The following approach was used:

- two known time-frequency representations were applied to HRV to understand its advantages and disadvantages in describing HRV in frequency and in amplitude, over time;
- a new method was developed that describes the time-varying fluctuations in the characteristic frequency bands of HRV by means of the instantaneous frequency and the instantaneous amplitude with an optimal time-resolution;
- an index was developed to separate the oscillatory from the irregular periods in the instantaneous frequency;

- from the instantaneous amplitude and frequency, we derived summarizing parameters which we applied to describe the changes in the instantaneous amplitude and frequency over time for the oscillatory and irregular periods separately.

4 Outline of the thesis

Chapter 2 presents an overview of existing techniques to analyze HRV in the time-domain, the frequency-domain, and the time-frequency domain.

Chapter 3 describes methods for frequency analysis on non-equidistantly sampled HRV-signals. It paves the way for the application of time-frequency techniques to such signals.

Chapter 4 summarizes the results of experiments using the frequency-domain techniques of chapter 3. The spectral estimates of heart rate and blood pressure variability were computed. They described changes in sympathetic and para-sympathetic cardiovascular processes as a result of pharmacological challenge tests (clonidine, lorazepam, epinephrine, norepinephrine) in healthy volunteers. They also described the effects of antidepressant treatment (imipramine, mirtazapine) on the autonomic cardiovascular control processes of depressed patients.

Chapters 5 and 6 demonstrate the applicability of two known time-frequency representations. This was done by visualizing and analyzing the instantaneous spectral changes in HRV, blood pressure, and respiratory signals. These signals were obtained from healthy subjects, patients with pure autonomic failure, and depressed patients. The signals were measured during supine rest, mental stress, and orthostatic challenge.

Chapter 7 presents a new method to describe the time-varying properties of HRV by the instantaneous amplitude and frequency. A measure of the instantaneous bandwidth, the instantaneous bandwidth coefficient, was developed to separate irregular and oscillatory periods in the instantaneous frequency.

In chapter 8, the instantaneous frequency was compared to three other methods: the discrete time-frequency transform, the circular mean direction of the time-slices of the Wigner-Ville distribution, and the central finite difference of the instantaneous phase.

In chapter 9, our new method was applied to HRV-data obtained from healthy subjects during supine rest and orthostatic challenge. A number of summarizing parameters were defined to quantitatively describe changes in the instantaneous amplitude and frequency over time.

Chapter 10 summarizes the advantages of our time-frequency method in conjunction with its relevance for clinical research.

References

Akselrod S, Gordon D, Ubel FA, Shannon DC, and Cohen RJ. Power spectrum analysis of heart rate fluctuation: a quantitative probe of beat-to-beat cardiovascular control. Science 213:220-222, 1981.

Bendat JS and Piersol AG. Random Data, Analysis and Measurements Procedures, 2nd edition. New York: John Wiley and Sons, Inc., 1986.

Bigger JT, Fleiss JL, Rolnitzky LM, Steinman RC. The ability of several short-term measures of RR variability to predict mortality after myocardial infarction. Circulation 88: 927-934, 1993.

Black DW, Warrack G, and Winokur G. Excess mortality among psychiatric patients. The Iowa record-linkage study. JAMA 253:58-61, 1985.

Boashash B. Time-frequency signal analysis. In: Advances in Spectrum Analysis and Array Processing, Vol. 1. S. Haykin, Ed. Englewood Cliffs, NJ: Prentice Hall, pp:418-517, 1991.

Cohen L. Time-Frequency Analysis. Englewood Cliffs, NJ: Prentice Hall Inc, 1995.

Dalack GW and Roose SP. Perspectives on the relationship between cardiovascular disease and affective disorder. J Clin Psychiatry 51(suppl): 4-9, discussion 10-1, 1990.

Hayward C. Psychiatric illness and cardiovascular disease risk. Epidemiol Rev 17:129-138, 1995.

Hyndman BW, Kitney RI, and Sayers BMcA. Spontaneous rhythms in psysiological control systems. Nature 233:339-341, 1971.

Kamath MV and Fallen EL. Power spectral analysis of heart rate variability: a noninvasive signature of cardiac autonomic function. Crit Rev in Biomed Eng 21(3):245-311, 1993.

Kikuya M, Hozawa A, Ohokubo T, Tsuji I, Michimata M, Matsubara M, Ota M, Nagai K, Araki T, Satoh H, Ito S, Hisamichi S, and Imai Y. Prognostic significance of blood pressure and heart rate variabilities: the Ohasama study. Hypertension 36:901-906, 2000.

Kitney RI. Entrainment of the human RR interval by thermal stimuli. J Physiol 252:37P-38P, 1975.

Kobayashi M and Musha T. 1/f Fluctuations of heartbeat period. IEEE Trans Biomed Eng BME-29:456-457, 1982.

Malliani A, Pagani M, Lombardi F, and Cerutti S. Cardiovascular neural regulation explored in the frequency domain. Circulation 84:482-492, 1991.

Malzberg B. Mortality among patient with involution melancholia. Am J Psychiatry 93:1231-1238, 1937.

Miyawaki E, Salzman C. Autonomic nervous system tests in psychiatry: implications and potential uses of heart rate variability. Integr Psychiatry 7:21-28, 1991.

Parati G, Saul JP, di Rienzo M, and Mancia G. Spectral analysis of blood pressure and heart rate variability in evaluating cardiovascular regulation. A critical appraisal. Hypertension 25:1276-1286, 1995.

Di Rienzi M, Parati G, Castiglioni P, Mancia G, and Pedotti A. The wide band spectral analysis: a new insight into modulation of blood pressure, heart rate and baroreflex sensitivity. In: Computer Analysis of Cardiovascular Signals. Di Rienzi M, Mancia G, Parati G, Pedotti A, and Zanchetti A (eds). Amsterdam: IOS Press pp:67-74, 1995.

Sayers BMcA. Analysis of heart rate variability. Ergonomics 16:17-32, 1973.

Singh JP, Larson LG, Tsuji H, Evans JC, O'Donnell CJ, and Levy D. Reduced heart rate variability and new-onset hypertension: insights into pathogenesis of hypertension: the Framingham Heart Study. Hypertension 32:293-297, 1998.

Steeghs P. Local power spectra and seismic interpretation (Ph.D. Thesis). Delft: Delft University of Technology, 1997.

Task force of the European society of cardiology and the North American society of pacing and electrophysiology. Heart rate variability – standards of measurement, physiological interpretation, and clinical use. Eur Heart J 17:354-381, 1996.

Ten Voorde BJ. Modeling the baroreflex: a systems analysis approach (Ph.D. Thesis). Amsterdam: Free University Amsterdam, 1992.

Tsuji H, Larson MG, Venditti FJ Jr, Manders ES, Evans JC, Feldman CL, and Levy D. Impact of reduced heart rate variability on risk for cardiac events. The Framingham Heart Study. Circulation 94:2850-2855, 1996.

Tulen JHM, Bruijn JA, De Man KJ, Pepplinkhuizen L, Van den Meiracker AH, and Man in 't Veld AJ. Cardiovascular variability in major depressive disorder and effects of imipramine or mirtazapine (org 3770). Journal of Clinical Psychopharmacology 16:135-145, 1996.

Van Roon AM. Short-term cardiovascular effects of mental tasks – physiology, experiments and computer simulations (Ph.D. Thesis). Groningen: University of Groningen, 1998.

Wesseling KH and Settels JJ. Baromodulation explains short-term blood pressure variability. In: Psychophysiology of Cardiovascular Control. Orlebeke JF, Mulder G, Van Doornen LJP (eds). New York & London: Plenum Press pp:69-97, 1985.

Yeragani VK, Pohl R, Balon R, Ramesh C, Glitz D, Jung I, Sherwood P. Heart rate variability in patients with major depression. Psychiatry Research 37:35-46, 1991.

CHAPTER 2
HEART RATE VARIABILITY AND ITS ANALYSIS

This chapter introduces the concept of heart rate variability and defines various representations of heart rate variability that can be used for various analysis techniques, such as spectral analysis. Spectral analysis and time-frequency analysis are explained. The chapter ends with a section on the instantaneous amplitude and frequency of narrow frequency bands.

1 Heart rate and heart rate variability

The human heart contracts and relaxes rhythmically, with each contraction pumping blood from the veins to the arteries. The complete cycle of contraction and relaxation is called a heartbeat or cardiac cycle. Each heartbeat is initiated by an electric impulse, called an action potential. The action potentials are generated in the sinoatrial node of the heart, which is a specialized group of cells in the right atrial wall of the heart (e.g., Guyton et al., 1996). Contraction and relaxation of the heart are preceded by electrical phenomena that can be measured on the skin by means of an electrocardiogram (ECG). This complex of electric phenomena or waves in one cardiac cycle is depicted in figure 1 (e.g, Guyton et al., 1996).

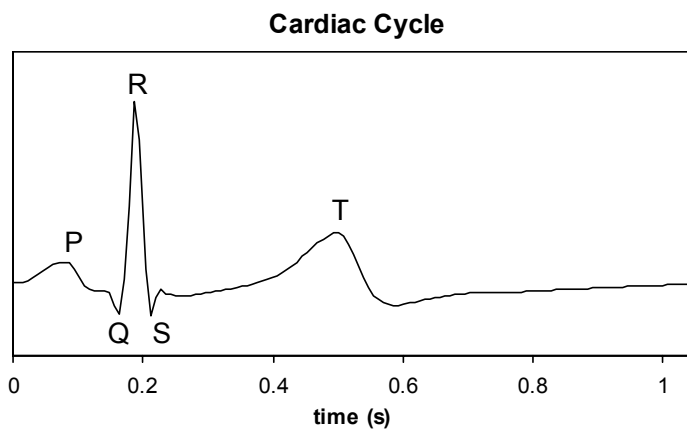

Figure 1. An example of one cardiac cycle or heart beat.

Heart rate (HR) is the occurrence rate of the cardiac cycle per unit time, conventionally, per minute (e.g., Rompelman, 1980; Guyton et al., 1996). Heart rate is also called heart rhythm. To determine this rate, it should be sufficient to measure the time-intervals between adjacent sinoatrial action potentials. However, these are not detectable in the ECG. The nearest to this action potential is the P-wave. Thus the period of time between two adjacent P-waves could be measured, but the onset of a P-wave is not sharply defined. In general, the sharp R-waves of the QRS-

complex are easier to detect and the period between two consecutive R-waves is called the R-R interval or **interbeat interval** (IBI). The interbeat intervals determine in practice the heart rate. It should be noted that the P-R interval shows slight fluctuations. This causes small differences between the heart rate measured from the onset of P- or from the R-waves. Since this thesis deals with small fluctuations in heart rate, the effect must be mentioned, but it is almost always ignored in practice (Rompelman, 1980).

The generation of action potentials is a rhythmic process. Repetitive self-induced discharges cause potential depolarizations in the cell membranes of the sinoatrial node and thereby firing action potentials. This results in a fairly constant heart rhythm (e.g., Guyton et al., 1996). However, the heart rhythm is modulated by the autonomic nervous system. Varying sympathetic and parasympathetic nervous activity modulates the firing rate of the sinoatrial node. Therefore, the duration of the cardiac cycle varies. These variations in duration are called beat-to-beat fluctuations (of the cardiac cycles). The beat-to-beat fluctuations in heart rate are called heart rate variability (HRV) (Task Force p:354, 1996). HRV may be studied in the time-domain, the frequency-domain, or in the time-frequency domain. An HRV-representation is the beat-to-beat information derived from the ECG that is of interest for HRV-analysis and ordered in such a way that it is accessible to the analysis techniques (De Boer pp:20,28, 1985; De Boer et al., 1985) and can be related to other physiological processes (Rompelman p:124, 1987; Mulder p:5, 1988). This information may consist of a listing of interbeat intervals derived from the ECG or a listing of inverses of interbeat intervals, called **instantaneous heart rates**. The interbeat intervals are expressed in s, the instantaneous heart rates are expressed in s^{-1}, or more conventionally in beats per minute.

2 Various HRV-representations

When we state that the oscillations in the heart rate are called heart rate variability there are still several ways in which this can be described and displayed. A first and obvious way is to make a list of the successive interbeat interval values or instantaneous heart rate values that are measured by detecting the R-waves from the ECG. Since these values occur with increasing time, the various interbeat interval or instantaneous heart rate values in the list may be ordered by means of an increasing index. An indexed list of interbeat intervals is called an **interbeat interval time series**. An indexed list of instantaneous heart rates is called a **heart rate time series**. The index may be a number starting from 1 and increasing with 1: (1,2,3,4...).

When the list is plotted on a horizontal axis the heart rate values are plotted at regular horizontal distances. Often the regular horizontal increment is taken as the average interbeat interval in seconds. This transforms the horizontal axis to a time axis. In this case the indices are equidistantly spaced and the list is called an **equidistant time series**.

The index may also be the R-wave occurrence time. In that case the values are placed at the instant of detection of the second R-wave of the R-wave pair between which the interbeat interval or the instantaneous heart rate value was measured. When we plot a time series indexed by R-wave occurrence time, the values of the list are now plotted at irregular horizontal intervals. This is because the heart rate in general is not constant. The horizontal axis is now naturally a time axis and the list is called a **non-equidistant time series**.

This leads to the definition of four different HRV-representations (see figures 2 and 3):

- The **interbeat interval series** is an equidistant interbeat interval time series.
- The **heart rate series** is an equidistant heart rate time series.
- The **interbeat interval function** is a non-equidistant interbeat interval time series.
- The **instantaneous heart rate function** is a non-equidistant heart rate time series.

These representations were studied by various authors, for instance, Rompelman et al. (1977), De Boer (pp:29-32,49, 1985), and Janssen et al. (1993).

There are still more HRV-representations. Another representation of heart rate variability is obtained by replacing the R-wave by a narrow positive spike of constant unit impulse generated at the instant that the R-wave is detected (see figure 4). If each R-wave is called an event, the series of events is called an R-wave event series or **cardiac event series** (CES) (e.g., Hyndman et al., 1975a; 1975b; Rompelman et al., 1977; 1985). It is further possible to multiply each constant spike by the value of the interbeat interval obtained at that instant, multiplied with the duration of the preceding R-R interval. The result is called the **interbeat interval event series**. The equivalent for the instantaneous heart rate is called the **heart rate event series** (e.g., Mulder, 1988; Van Steenis, 1994).

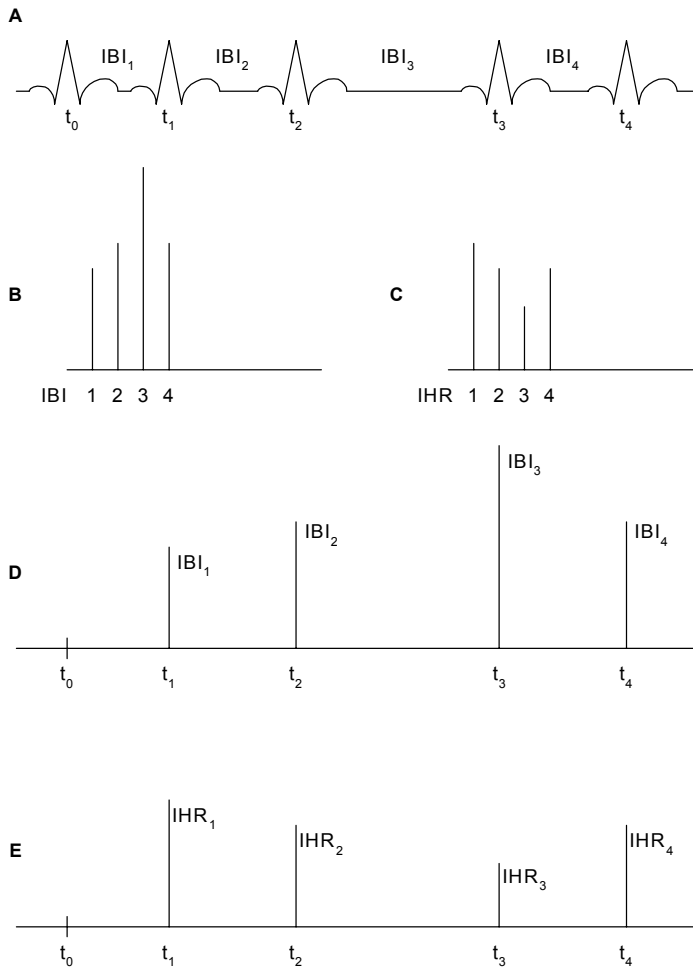

Figure 2. HRV-representations (e.g., Rompelman et al., 1977; De Boer p:49, 1985; Janssen et al., 1993). Abbreviations: IBI = interbeat interval; IHR = instantaneous heart rate.

A: ECG with R-waves at t_i, and interbeat intervals $\mathrm{IBI}_i = t_i - t_{i-1}$, the instantaneous heart rates IHR_i are the inverses of IBI_i;

B: interbeat interval series: the IBI_i are indexed by number i;

C: heart rate series: the IHR_i are indexed by number i;

D: interbeat interval function: the IBI_i are placed as a function of time t_i;

E: instantaneous heart rate function: the IHR_i are placed as a function of time t_i.

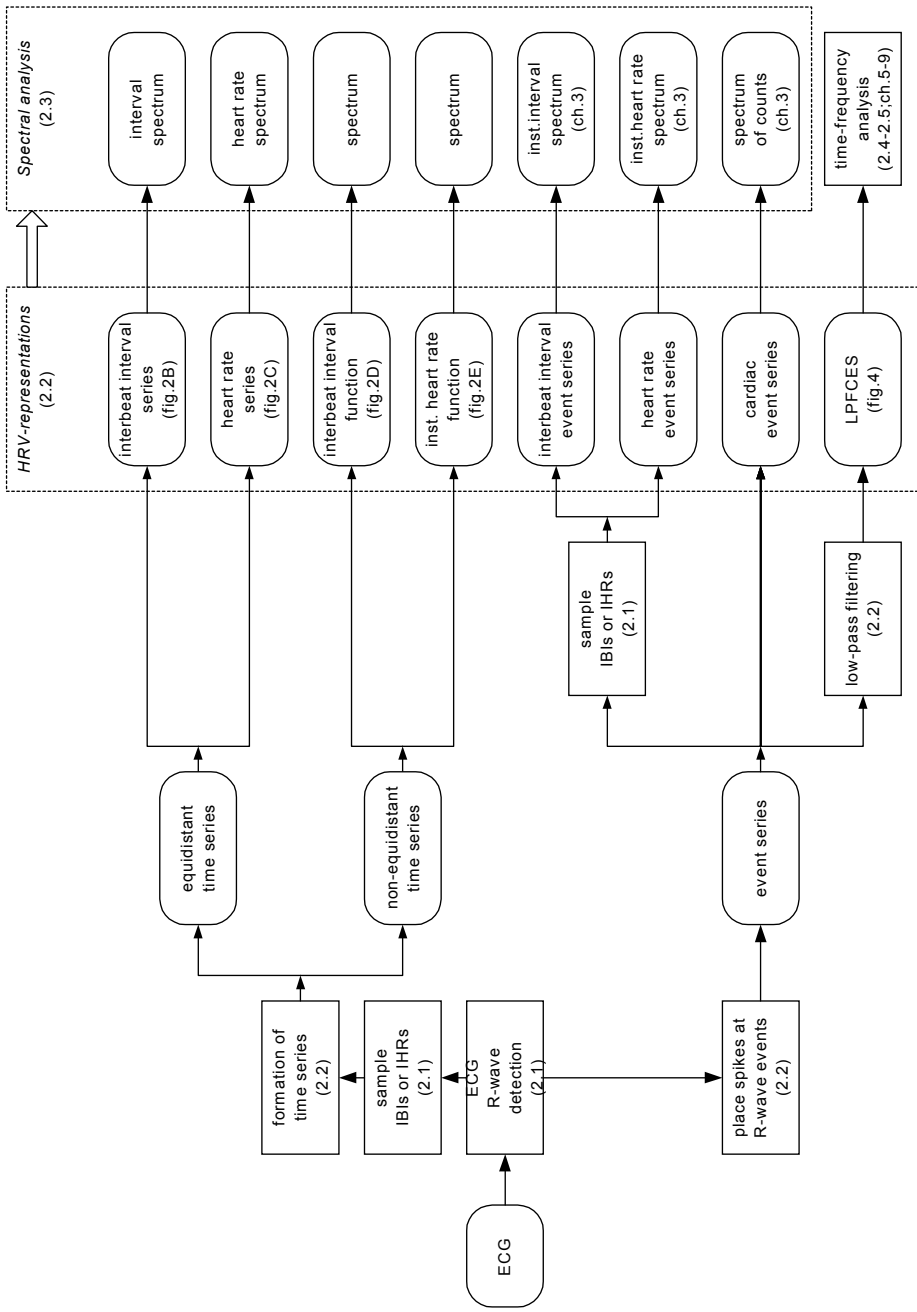

Figure 3. Summary of the sections 2 and 3. Abbreviations: ECG = electrocardiogram; IBI = interbeat interval; IHR = instantaneous heart rate; LPFCES = low-pass filtered cardiac event series; inst. = instantaneous. The numbers refer to sections and figures of chapter 2.

The unit spikes of the CES are placed at irregular distances. An equidistant time-series may be obtained by filtering the CES with some low-pass filter and sampling this signal. Often a cutoff frequency of 0.5 Hz is used. This result is called the **low-pass filtered cardiac event series** (see figure 3) (e.g., Hyndman et al., 1975a; 1975b; Rompelman et al., 1977; French et al., 1971; Peterka et al., 1978). We used a zero-phase low-pass finite impulse response (FIR)-filter (Oppenheim et al., 1999). This filter is non-causal. The pass-band is the frequency interval [0, 0.5]. The -6 dB point is at 0.5 Hz. The transition band between 0.4863 Hz and 0.5137 Hz is '$\cos^2$-shaped' (see figure 5). The low-pass filtered cardiac event series is comparable with heart rate, because whenever the heart rate is higher, there are more spikes with smaller intervals between them, and consequently, the filter output will be higher (see figure 4). To use this signal digitally it must be sampled, in our case with a sample frequency of 4 Hz.

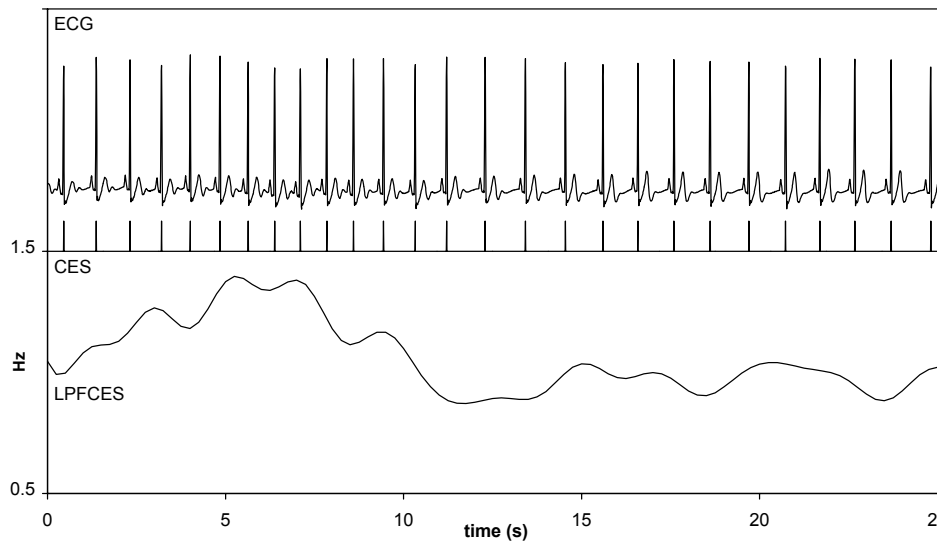

Figure 4. From ECG to LPFCES: the R-waves in the ECG (upper graph) are detected and represented by spikes placed at the R-wave occurrence times. This constitutes a function of time, called the cardiac event series (CES, middle graph). The CES is filtered with a zero-phase low-pass FIR-filter with cutoff frequency of 0.5 Hz. This results in a low-pass filtered cardiac event series (LPFCES) (e.g., De Boer p:32, 1985).

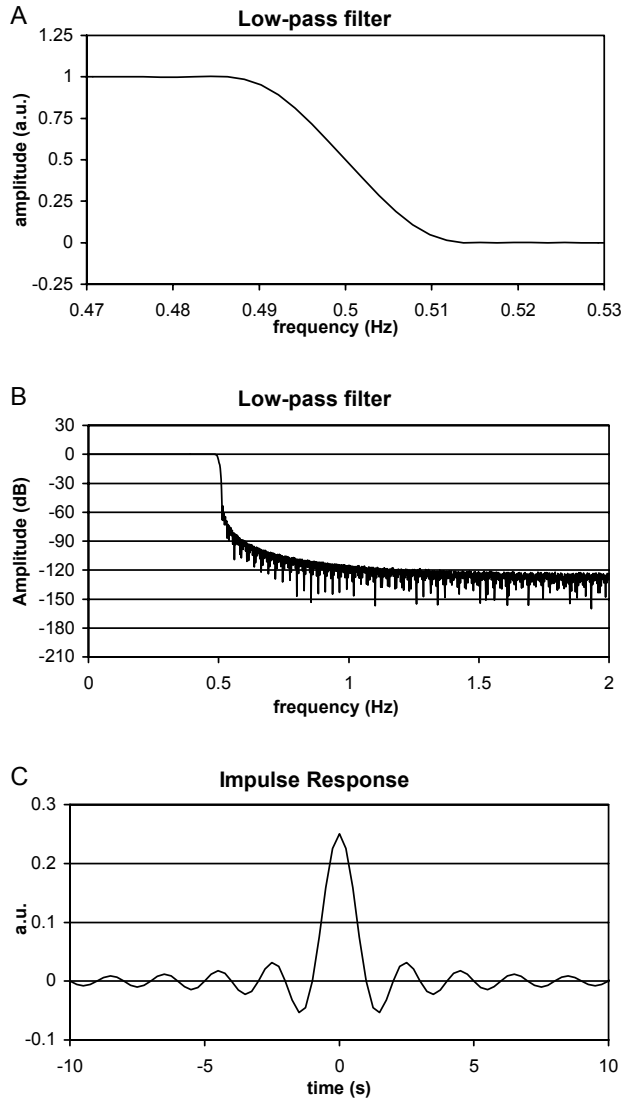

Figure 5. To obtain a low-pass filtered cardiac event series, the cardiac event series is filtered with a zero-phase low-pass FIR-filter. The –6 dB point is at 0.5 Hz. The pass-band ranges from 0 to 0.5 Hz. The transition band ranges from 0.4863 to 0.5137 Hz and has a $\cos^2$-shaped slope. Figure A shows the transition band. Figure B shows the amplitude of the frequency response in dB. Figure C shows the truncated impulse response of this filter. The total duration is 183 s. Note that this FIR-filter is non-causal.

Although we now already have eight representations, all with slightly different properties, several more can be defined and have been in use. This makes HRV-studies confusing for the uninitiated. In the study of time-frequency analysis of HRV (chapters 7,8, and 9), we limited ourselves to the use of the low-pass filtered cardiac event series, based on its slightly superior properties for our purpose (e.g., Rompelman, 1980; Rompelman et al., 1977; Mulder pp:8,51-52, 1988). However, the use of any other representation may serve just as well when the fluctuations are small with respect to the average heart rate.

3 Spectral analysis of heart rate variability

In the previous sections we have described how heart rate (and interbeat interval) can be derived from the ECG and how a number of slightly different representations of heart rate variability came into use. When looking at abritrary HRV-signals it appears that often both noise-like and sinusoidal-like variability components are present (see figures 2A and 3A of chapter 1). The overall picture may be quite confusing and at times when the sinusoidal oscillations are small in amplitude they may even become invisible in the noise. However, these ‘invisible’ oscillations may become ‘visible’ by means of spectral analysis. What is spectral analysis?

Let us take an interval of heart rate variability of, say, 100 s. To this interval we apply a discrete Fourier transform and we obtain the same signal as before but in yet another form or representation. The result of this Fourier transform is a list of all the frequencies, from the fundamental harmonic (here 0.01 Hz) up, that occur in the heart rate variability with their amplitude and their phase in the form of a complex number. This means that to each frequency in the list, a complex number is assigned by the transform. This is called a spectrum. In the spectrum we can usually observe the noisy component separated from the sinusoidal component since they usually differ in frequency. The noise is usually concentrated towards the fundamental harmonics (those from 0.01 Hz up), whereas the sinusoidal components are predominant near 0.1 Hz and near 0.3 Hz (see figures 2B and 3B of chapter 1). Thus we have now obtained a much clearer picture of the sinusoids in the heart rate variability signal.

There is nothing special about the spectrum. Given the spectrum, the original data can be reconstructed by means of another discrete Fourier transform and so forth and so on. The absolute values of the complex numbers of the spectrum are often squared. The result is called the power spectrum (or power spectral density function). Because of the squaring action the phase is lost and the high amplitudes

are emphasized with respect to the smaller amplitudes. A further effect is that we clearly see the amplitude of the sinusoid of a particular frequency but from the spectrum alone we do not know at which point in time this frequency occurred. In fact, the spectrum gives an average of the amplitude of an oscillation at a certain frequency over the entire 100 s duration of the signal. We gain some, we loose some.

Spectral analysis of HRV-representations signals was used at an early stage by Penaz et al. (1968), and by Sayers (1973), to name just two pioneers. Spectral analysis can be applied to each of the HRV-representations of section 2. Some spectra have names. We just mention these names. The power spectral density function

- of an interbeat interval series is called the **interval spectrum**;
- of a heart rate series is called the **heart rate spectrum**;
- of a CES is called the **spectrum of counts**;
- of an interbeat interval event series is called **the instantaneous interval spectrum**;
- of an heart rate event series is called the **instantaneous heart rate spectrum**.

This is shown in figure 3. The different techniques of spectral analysis were studied by Luczak et al. (1973), Hyndman et al. (1975a; 1975b), Mohn (1976), Rompelman et al. (1982), Rompelman (1985; 1987), Pomeranz et al. (1985), De Boer (ch.3, 1985), Mulder (pp:51-57, 1988), Van Steenis et al. (1994), Parati et al. (1995), and many more.

Two examples of spectra of counts are shown in figures 2B and 3B of chapter 1. Mulder (1988) developed a computer program, called CARSPAN, to compute the power spectral density function of a CES and of an interbeat interval event series.

4 Time-frequency analysis of heart rate variability

Let us return to the 100 s interval of HRV (section 3). Suppose we sampled the interval with a sample frequency of 1 Hz. Then the interval of 100 s delivers 100 data-points. The time-resolution is 1 s, and the frequency range of the power spectrum of this interval ranges from 0 until 0.5 Hz in steps of 0.01 Hz. Suppose now there appears a sinusoid with a frequency of 0.2 Hz at the 20^{th} second and disappears at the 40^{th} second. Then we observe a peak in the power spectrum at 0.2 Hz. However, from the spectrum alone we do not know at which points in time this sinusoid occurred. Suppose, for the sake of clarification, that at each second of the time-interval, we are able to compute a list of frequencies that occur at that instant, together with their amplitude and their phase. Of each list we can compute the power

spectrum. This results in a list of 100 power spectra: one for each instant in the time-interval, i.e., they are computed instantaneously. We call these spectra: instantaneous power spectra. When we plot this list of instantaneous power spectra, ordered according to increasing time, we see that there appears a frequency component of 0.2 Hz in the 20th second. It stays in the successive spectra until the 39th second, after which the sinusoid disappears. Furthermore, if the amplitude of the sinusoid varies in time, the heights of the peaks in the instantaneous spectra varies correspondingly. Such a list of instantaneous power spectra is called a time-frequency representation: it represents the power of a signal simultaneously in time and frequency. The strength of a time-frequency representation is that it visualizes time-varying frequency components in a signal when they come and go. In the next section we discuss some forms of time-frequency representations that are used in the study of HRV. In the chapters 5 and 6 we applied two time-frequency representations to HRV.

5 The instantaneous amplitude and frequency of narrow frequency bands

In the example of section 3 we observed 2 frequency peaks, one near 0.1 Hz and one near 0.3 Hz. However, in general these peaks are not narrow, but they have a width or spread (see figures 2B and 3B of chapter 1). As peaks they do not stand alone, but protrude above a general background. Take, for example, the peak near 0.1 Hz. How was this peak brought about? Is it the result of a sinusoid of which the frequency is fluctuating in time? Or is it the result of a sinusoid of which the amplitude is fluctuating in time? Maybe it is a combination of both? With a time-frequency representation this complex component can be visualized. However, we want to go a little further and analyze, for example, this component near 0.1 Hz quantitatively. In the instantaneous spectra (see section 4) of the time-frequency representation we see this component changing in amplitude, in frequency location, and in spread, with increasing time. The next step is that we want to compute these parameters at each independent instant of the time-interval. If we manage to do this, the amplitude is called the instantaneous amplitude, the frequency is called the instantaneous frequency, and the spread is called the instantaneous bandwidth of this component in the signal.

What are independent instants in practice? Suppose we filter the signal of section 3 with a low-pass filter. After the low-pass filter, the original samples of the signal become dependent because the signal does no longer change as quickly and

adjacent samples become linked or correlated. We say that the signal is over-sampled. Suppose each four adjacent points are dependent and every fifth instant is independent. The 1st point, the 5th point, the 9th point, and so on, are independent instances. Adjacent disjoint time-intervals of 4 s are likewise independent. Suppose we can compute a value of a signal property in these intervals: one value for each interval. Then we can say that the resulting adjacent values in time are placed at independent instances. This means that these properties are instantaneous properties. Otherwise, computations over a shorter time interval yield adjacently dependent points in time; if computed over a longer time interval, the values of the properties will be averaged. We now define that a signal property, which can be computed within the time-resolution of the signal, is an instantaneous property (see chapter 7).

The next step in the time-frequency analysis of HRV is the analysis of the characteristic frequency bands of HRV by means of the instantaneous amplitude, frequency, and a measure of the instantaneous bandwidth. After filtering the HRV-signal with a filter corresponding with one of the characteristic frequency bands, we can determine the time-resolution of the filtered signal and compute these parameters instantaneously. This is described in chapter 7, 8, and 9.

References

De Boer RW. Beat-to-beat blood-pressure fluctuations and heart-rate variability in man: physiological relationships, analysis techniques and a simple model (Ph.D. Thesis). Amsterdam: University of Amsterdam, 1985.

De Boer RW, Karemaker JM, and Strackee J. Description of heart-rate variability data in accordance with a physiological model for the genesis of heart beats. Psychophysiology 22:147-155, 1985.

French AS and Holden AV. Alias-free sampling of neuronal spike trains. Kybernetic 5:165-171, 1971.

Guyton AC and Hall JE. Textbook of Medical Physiology. Ninth Edition. Philadelphia, PA: Saunders, 1996.

Hyndman BW and Mohn RK. A model of the cardiac pacemaker and its use in decoding the information content of cardiac intervals. Automedica 1:239-252, 1975a.

Hyndman BW and Gregory JR. Spectral analysis of sinus arrhythmia during mental loading. Ergonomics 18:255-270, 1975b.

Janssen MJA, Swenne CA, De Bie J, Rompelman O, and Van Bemmel JH. Methods in heart rate variability analysis: which tachogram should we choose? Computer Methods and Programs in Biomedicine 41:1-8, 1993.

Luczak H and Laurig W. An analysis of heart rate variability. Ergonomics 16:85-97, 1973.

Mohn RK. Suggestions for the harmonic analysis of point process data. Comput Biomed Res 9:521-530, 1976.

Mulder LJM. Assessment of cardiovascular reactivity by means of spectral analysis (Ph.D. Thesis). Groningen: University of Groningen, 1988.

Oppenheim AV, Schafer RW, and Buck JR: Discrete-Time Signal Processing, 2nd edition. Englewood Cliffs, NJ: Prentice Hall, 1999.

Parati G, Saul JP, di Rienzo M, and Mancia G. Spectral analysis of blood pressure and heart rate variability in evaluating cardiovascular regulation. A critical appraisal. Hypertension 25:1276-1286, 1995.

Penaz J, Roukens J, and Vanderwaal HJ. Spectral analysis of some spontaneous rhythms in the circulation. In: Biokybernetik, Drische H and Tiedt N (eds). Leipzig: K.Marx Universitat pp:233-236, 1968.

Peterka RJ, Sanderson AC, and O'Leary DP. Practical considerations in the implementation of the French-Holden algorithm for sampling neuronal spike trains. IEEE Trans Biomed Eng BME-25:192-195, 1978.

Pomeranz B, MacAulay RJB, Caudill MA, Kutz I, Adam D, Gordon D, Kilborn KM, Barger AC, Shannon DC, Cohen RJ, and Benson H. Assessment of autonomic function in humans by heart rate spectral analysis. Am J Physiol 248:H151-H153, 1985.

Rompelman O. The assessment of fluctuations in heart-rate. In: The study of heart-rate variability. Kitney RI, Rompelman O (eds). Oxford: Clarendon Press pp:59-77, 1980.

Rompelman O. Spectral analysis of heart-rate variability. In: Psychophysiology of Cardiovascular Control. Orlebeke JF, Mulder G, Van Doornen LJP (eds). New York & London: Plenum Press pp:315-331, 1985.

Rompelman O. Hartritmevariabiliteit – meting, verwerking, interpretatie (Ph.D. Thesis). Delft: Delft University of Technology, 1987.

Rompelman O, Coenen AJRM, and Kitney RI. Measurement of heart-rate variability: part 1 – comperative study of heart-rate variability analysis methods. Med & Biol Eng & Comput 15:233-239, 1977.

Rompelman O, Snijder JBIM, and van Spronsen CJ. The measurement of heart rate variability spectra with the help of a personal computer. IEEE Trans Biomed Eng BME-29:503-510, 1982.

Sayers BMcA. Analysis of heart rate variability. Ergonomics 16:17-32, 1973.

Task Force of the European society of cardiology and the North American society of pacing and electrophysiology. Heart rate variability – standards of measurement, physiological interpretation, and clinical use. Eur Heart J 17:354-381, 1996.

Van Steenis HG, Tulen JHM, and Mulder LJM. Heart rate variability spectra based on non-equidistant sampling: the spectrum of counts and the instantaneous heart rate spectrum. Medical Engineering and Physics 16:355-362, 1994.

CHAPTER 3
HEART RATE VARIABILITY SPECTRA BASED ON NON-EQUIDISTANT SAMPLING: THE SPECTRUM OF COUNTS AND THE INSTANTANEOUS HEART RATE SPECTRUM

Medical Engineering and Physics 16:355-362, 1994

H.G. van Steenis[1,3], J.H.M. Tulen[2,3], L.J.M. Mulder[4]

[1]Department of Clinical Neurophysiology, University Hospital Rotterdam Dijkzigt
[2]Department of Psychiatry, Erasmus University Rotterdam
[3]Section Pathophysiology of Behaviour, Erasmus University Rotterdam
[4]Experimental and Occupational Psychology, University of Groningen

This paper compares two methods to estimate heart rate variability spectra, i.e., the spectrum of counts and the instantaneous heart rate spectrum. Contrary to Fourier techniques based on equidistant sampling of the interbeat intervals, the spectrum of counts and the instantaneous heart rate spectrum are based on non-equidistant sampling: the values are determined at R-wave occurrence times. A consequence of the non-equidistant occurrence of the R-peaks in a heart rate signal is the appearance of the sidebands of the harmonic components of the mean heart rate in the spectra. These sidebands contaminate the signal components in the spectrum. The sideband distortion in the instantaneous heart rate spectrum was found to be smaller than in the spectrum of counts. Simulations using the IPFM-model were made to quantify this difference. On basis of these simulations, sideband distortion appeared to be dependent on the mean heart rate, the modulation depth and the modulation frequency.

1 Introduction

Spectral analysis of beat-to-beat fluctuations in heart rate can be used as a quantitative and non-invasive technique for the study of the functioning of short-term cardiovascular control. Fluctuations in heart rate are believed to contain information related to sympathetic and parasympathetic activity within the cardiovascular control system (Hyndman et al., 1971; Sayers, 1973; Akselrod et al., 1981; 1985).
From the electrocardiogram (ECG), the R-wave occurrence times are determined and the interval lengths (interbeat interval: IBI) between consecutive R-waves, as well as the heart rate, are measured. It has been shown that the variations in the interbeat interval time series do not produce a random pattern (Sayers, 1980), but show certain frequency-specific properties (Sayers, 1973; Akselrod et al., 1981). Therefore, spectral analysis is an important method to describe frequency-dependent aspects of heart rate variability. The following frequency bands are recognized in the heart rate variability spectrum (Sayers, 1973; Mulder, 1988):
a) variations related to temperature regulation of the body (0.02–0.06 Hz, low frequency band);
b) variations related to intrinsic characteristics of the blood pressure control system (0.06–0.14 Hz, mid frequency band) and
c) variations mainly related to respiratory activity (0.14–0.50 Hz, high frequency band).

Several techniques have been developed to estimate heart rate variability spectra. Baselli et al. (1985; 1986) used a parametric method for autoregressive

spectral analysis of heart rate time series. This method calculates a number of parameters which are used to describe the spectrum.

Non-parametric methods in general make use of a discrete Fourier transform (Bendat and Piersol, 1986). Some of these methods are based on equidistant sampling of the interbeat interval lengths (Sayers, 1973; 1980; Mohn, 1976; De Boer et al., 1984), or inverse interval lengths (Mohn, 1976; De Boer et al., 1984). The intervals (figure 1a), or inverse interval lengths (figure 1b), are placed equidistantly as a function of interval number. Spectra can then be calculated using a fast Fourier transform (FFT) (Cooley and Tukey, 1965). This is a fast way to calculate the spectra, but the disadvantages are that the number of data points has to be a power of two and the spectra are functions of 'cycles per beat' instead of 'cycles per second' (De Boer et al., 1984). Such an approach may become a problem when time relations between signals have to be studied (such as between heart rate and respiration), because this method may introduce relative time shifts between time series which are not constant as a function of time.

Other methods are based on interpolation of non-equidistantly sampled interbeat intervals. Firstly, the intervals are placed non-equidistantly at R-wave occurrence times (figure 1c) (Luczak and Laurig, 1973), or the inverse interval lengths are placed non-equidistantly at the R-wave occurrence times (figure 1d) (Womack, 1971). Then the time series is interpolated and the resulting signal is sampled equidistantly. From these sampled data points, the spectrum can be estimated using a fast Fourier transform. The disadvantage is that a zero order interpolation often results in a discontinuous signal and a first order interpolation also results in unwanted effects in the spectrum (Luczak and Laurig, 1973; De Boer et al., 1984). Berger et al. (1986) used a series of interpolated inverse intervals.

In this paper we evaluate two other methods, based on non-equidistant sampling, to estimate the heart rate variability spectrum. These methods are:

1) the spectrum of counts (SOC) (Rompelman, 1985): at each R-wave occurrence time, a delta function of unit area is placed (figure 1e); this sequence of delta functions is transformed with a discrete Fourier transform in order to estimate the power spectrum;

2) the instantaneous heart rate spectrum (IHRS): at each R-wave occurrence time, the interbeat interval length is measured. A delta function of unit area, but with weight (or amplitude) equal to the inverse interval length, is placed at the R-wave occurrence time (figure 1d); a discrete Fourier transform is applied to estimate the power spectrum of this time series. This IHRS is based on a method of Mulder (1988).

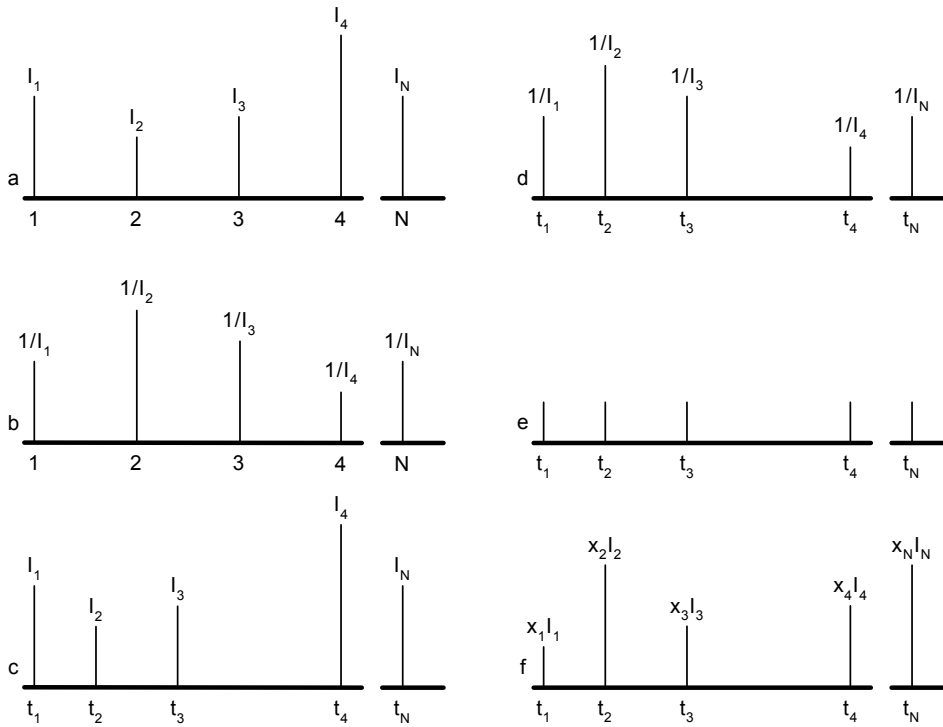

Figure 1: Methods to sample a heart rate variability signal.

a) A series of interbeat interval lengths as function of interval number, the intervals are sampled equidistantly.

b) A series of inverse interval lengths as function of interval number, the intervals are sampled equidistantly.

c) A series of interbeat interval lengths as function of time, the intervals are sampled non-equidistantly at R-wave occurrence times.

d) A series of inverse interval lengths as function of time, the intervals are sampled non-equidistantly at R-wave occurrence times.

e) A series of delta pulses as a function of time, the pulses are placed non-equidistantly at R-wave occurrence times.

f) A series of delta pulses as a function of time, the pulses are placed non-equidistantly at R-wave occurrence times and have weights equal to the sample of the signal multiplied by the time-interval passed since the former sample, i.e. $I_i = t_i - t_{i-1}$.

Although the discrete Fourier transform takes a longer calculation time, the SOC and IHRS have the great advantage that any number of data points can be used, while the spectra are now functions of 'cycles per second' and no unwanted interpolation effects will occur.

A consequence of the non-equidistant character of the sequence of delta-functions or the (inverse) interval series is the appearance of the sidebands of the harmonic components of the mean heart rate in the spectra. These sidebands contaminate the signal components in the spectrum. Although the two methods to estimate the heart rate variability spectra (i.e., SOC and IHRS) are essentially equivalent, the appearance of the sideband components is different. After a description of the methods to calculate the SOC and the IHRS, the effects of the distortion in the spectra due to the sidebands of the harmonic frequencies are evaluated in this paper.

2 Theory

A standard fast Fourier transform cannot be used to calculate the spectrum of a non-equidistantly sampled signal. The power spectrum of such a signal must be estimated in a different way and this section will deal with this technique. In particular the SOC and the IHRS are described.

2.1. The spectrum of counts

A series of R-wave time points is represented by a series of delta pulses $\delta(t-t_i)$ at times t_i, $i=1,2,...N$ (figure 1e). These delta pulses form the signal:

$$p(t)=\sum_{i=1}^{N}\delta(t-t_i) \tag{1}$$

Several approaches to estimate the spectrum of this function have been proposed. One approach is to filter $p(t)$ with a low-pass filter with a cut-off frequency at about half the mean heart rate. The resulting time series is called the Low Pass Filtered Cardiac Event Series or LPFCES (Hyndman and Mohn, 1975). This is an equidistantly sampled series and from these samples the spectrum can be estimated with the use of a fast Fourier transform.

Another approach is given by Rompelman (1985). The spectrum P_C of the function $p(t)$ is:

$$P_C(f_k)=\frac{2}{T}\cdot X_C(f_k)\cdot X_C^*(f_k)$$

(Bendat and Piersol, 1986) with:

$$X_C(f_k) = \int_{-\infty}^{+\infty} p(t) \cdot e^{-2\pi j f_k t} dt = \sum_{i=1}^{N} e^{-2\pi j f_k t_i} \quad (2)$$

and $f_k = k/T$, $k = 0,1,2,...$, T is the total time of the record. The spectrum P_C of the function $p(t)$ is estimated by using the right part of equation (2). The spectrum P_C is called the spectrum of counts (SOC). This spectrum is based on non-equidistant sampling, the delta pulses are occurring at the R-wave occurrence times.

DC-correction can be performed by subtracting a sequence of N delta functions, placed at equal intervals I, from the original delta sequence. So the function $p(t)$ in (1) becomes:

$$p(t) = \sum_{i=1}^{N} \delta(t - t_i) - \sum_{i=1}^{N} \delta(t - i \cdot I)$$

From this function, the Fourier transform is calculated (Mulder, 1988).

2.2 The spectrum of a non-equidistantly sampled signal

The idea of non-equidistant sampling can be extended: other signals can be sampled at the R-wave occurrence times. At the detection times t_i of the R-waves, a sample is taken of another (cardiovascular) signal. For instance the diastolic blood pressure, the interbeat interval, or the respiration. In this way, a collection of data points on a beat-to-beat basis is obtained. Mulder (1988) gave a method to calculate the spectrum of these non-equidistantly sampled signals. This method is based on an approximation of the Fourier integral by a zero-order (rectangular) weighting of sample values. In the same way as is implicitely done in the equidistant discrete Fourier transform, each sample value is weighted with the sample interval duration. At times t_i (the R-waves occurrence times), the samples x_i, $i = 1,2,...,N$, of a signal are taken. The R-wave occurrence times at times t_i are represented by a series of delta pulses $\delta(t - t_i)$, these delta pulses have weights (and areas) equal to the sample x_i multiplied by the time-interval $t_i - t_{i-1}$ (figure 1f). The spectrum estimated from these data points is the spectrum of the function $p(t)$ consisting of all the weighted delta pulses:

$$p(t) = \sum_{i=1}^{N} x_i \cdot (t_i - t_{i-1}) \cdot \delta(t - t_i)$$

The spectrum P is defined by:

$$P(f_k) = \frac{2}{T} \cdot X(f_k) \cdot X^*(f_k)$$

with:

$$X(f_k) = \int_{-\infty}^{+\infty} p(t) \cdot e^{-2\pi j f_k t} dt = \sum_{i=1}^{N} x_i \cdot (t_i - t_{i-1}) \cdot e^{-2\pi j f_k t_i} \quad (3)$$

$f_k = k/T$, $k = 0,1,2,...$, and with T, the total sampling time. The spectrum P of the function $p(t)$ is estimated by using the right part of equation (3).

DC-correction is applied by subtracting a weighted mean of the samples x_i from the samples. This weighted mean has the form:

$$x_W = \frac{1}{T}\sum_{i=1}^{N} x_i \cdot (t_i - t_{i-1})$$

and (3) becomes:

$$X(f_k) = \sum_{i=1}^{N} (x_i - x_W) \cdot (t_i - t_{i-1}) \cdot e^{-2\pi j f_k t_i}$$

As mentioned before, other (cardiovascular) signals can be sampled at the R-wave occurrence times. Two special signals that can be sampled are the interbeat interval lengths and the inverses of the interval lengths. So at every R-wave occurrence time, the time that has passed since the last R-wave occurrence time is measured, and the interval I_i or the inverse $R_i = 1/I_i$ is the sampled value.

In section 2.3, the spectrum estimated from a series of non-equidistantly sampled interbeat intervals is described. This spectrum is called the interval spectrum. Mulder (1988) dealt with this spectrum in detail. The spectrum of a series of non-equidistant inverse interval lengths is described in section 2.4. This spectrum is called the instantaneous heart rate spectrum (IHRS).

2.3 The interval spectrum

At the R-wave occurrence times t_i, the interbeat intervals $I_i = t_i - t_{i-1}$ for $i = 1,2,...,N$, are sampled. The interval spectrum P_I is:

$$P_I(f_k) = \frac{2}{T} \cdot X_I(f_k) \cdot X_I^*(f_k)$$

in which $X_I(f_k)$ is defined in equation (3) with $x_i = I_i$ and $t_i - t_{i-1} = I_i$, i.e.:

$$X_I(f_k) = \sum_{i=1}^{N} I_i^2 \cdot e^{-2\pi j f_k t_i} \qquad (4)$$

where $f_k = k/T$, $k = 0,1,2,...$, and T is the total measuring time.

The DC-corrected form of (4) becomes:

$$X_I(f_k) = \sum_{i=1}^{N} (I_i - I_W) \cdot I_i \cdot e^{-2\pi j f_k t_i}$$

with

$$I_W = \frac{1}{T}\sum_{i=1}^{N} I_i \cdot (t_i - t_{i-1}) = \frac{1}{NI}\sum_{i=1}^{N} I_i^2,$$

and I is the mean interval length. I_W is the weighted mean of the interbeat interval lengths.

2.4 The instantaneous heart rate spectrum

At R-wave occurrence times t_i, the interbeat interval lengths $I_i = t_i - t_{i-1}$ for $i = 1, 2, ..., N$, are sampled. The power spectrum P_R of the IHRS approach is:

$$X_R(f_k) = \frac{2}{T} \cdot X_R(f_k) \cdot X_R^*(f_k)$$

with:

$$X_R(f_k) = \sum_{i=1}^{N} \frac{1}{I_i} \cdot I_i \cdot e^{-2\pi j f_k t_i} \tag{5}$$

where $f_k = k/T$, $k = 0, 1, 2, ...$, and T is the total measuring time. In this form, the IHRS is equivalent with the SOC (see (2)).

If DC-correction is applied, (5) becomes:

$$X_R(f_k) = \sum_{i=1}^{N} (R - R_W) \cdot I_i \cdot e^{-2\pi j f_k t_i}$$

with $R_i = 1/I_i$, and

$$R_W = \frac{1}{T} \sum_{i=1}^{N} R_i = N/T,$$

which is the weighted mean of the inverse interval lengths. This outcome is equivalent to the definition of mean heart rate as used in medicine: the number of beats divided by the measuring time. Equations (2) and (5) learn that the SOC and the IHRS are essentially equivalent. The main difference between the SOC and the IHRS is the method of DC-correction.

2.5 The IPFM-model

In our comparison of the IHRS with the SOC, extensive use has been made of the IPFM-model. The IPFM-model is used to simulate heart rate (for details: see Bayly (1968)). The model consists of an integrator, a comparator, and a reset-line (figure 2a). An input signal

$$m(t) = m_0 + m_1(t)$$

is integrated by the integrator. The integrated signal is compared by the comparator with a threshold R. As soon as the output becomes higher than the threshold, a unity pulse is generated. At the same time, the integrator is set to zero via the reset-line. The output of the model is a series of pulses $p(t)$ corresponding to a series of R-wave occurrence times.

The signal $m(t)$ is called the modulating input or signal and $f_0 = m_0/R$ is the mean (pulse) repetition rate or mean heart rate. Bayly (1968) gave an analytical

expression of the amplitude spectrum of the output pulse series $p(t)$ in case the modulating signal $m(t)$ is a sinusoid with phase θ:

$$m(t) = m_0 + m_1 \cdot \cos(2\pi f_m + \theta)$$

f_m is called the modulating frequency and $f_d = m_1/R$ is called the modulation depth.

The amplitude spectrum A consists of the following components (the pulses have unit area):

a) the DC-component:

$$A(0) = f_0;$$

b) components at f_m and $-f_m$:

$$A(f_m) = A(-f_m) = f_d/2;$$

c) components at $(k \cdot f_0 + n \cdot f_m)$ and $-(k \cdot f_0 + n \cdot f_m)$ for $k = 1, 2, \ldots$, and $n = \ldots, -2, -1, 0, 1, 2, \ldots$:

$$A(k \cdot f_0 + n \cdot f_m) = A(-k \cdot f_0 - n \cdot f_m) = f_0 \cdot \left(1 + \frac{n \cdot f_m}{k \cdot f_0}\right) \cdot J_n\left(\frac{k \cdot f_d}{f_m}\right)$$

J_n is the Bessel function of the first kind and of integral order n. An example of the amplitude spectrum of a signal produced by the IPFM-model is presented in figure 2b.

For the frequencies $f = 0$, $f = f_m$, and $f = k \cdot f_0 + n \cdot f_m$ the power spectral density (PSD) components are

$$S(f) = 2 \cdot T \cdot A^2(f),$$

where T is the duration of the function $p(t)$, and A is defined in a), b), and c). The harmonic frequencies of the mean heart rate are the frequencies $k \cdot f_0$ for $k = 1, 2, \ldots$, and the sidebands of the first harmonic are the frequencies $f_0 + n \cdot f_m$ for $n = \ldots, -2, -1, 0, 1, 2, \ldots$. These sidebands can give a noticable distortion in the signal components in the heart rate variability spectrum, i.e., the components at frequencies less than the Nyquist frequency (a.o. Bayly, 1968; Koenderink and Van Doorn, 1973; De Boer et al. 1985).

For a sequence of interbeat intervals $\{I_i, i = 1, 2, \ldots, N\}$ with mean interval length I, the sample frequency or mean repetition rate is defined by $f_S = 1/I$ and the Nyquist frequency is $f_N = f_S/2$. The SOC consists of the signal components in the frequency interval $[0, f_N]$, the harmonic components at multiplies $k \cdot f_S$ of the sample frequency, and the sideband components accompanying the harmonic components (Bayly, 1968). The huge amplitudes of the harmonic components in the SOC are due

to the applied DC-correction: the pulses of the subtracted delta sequence are placed at consecutive equal distances I, so the rate of the pulses is $f_S = 1/I$. The sidebands accompanying the harmonic components are spreading out at both sides of the harmonic components. These sidebands are not influenced by this method of DC-correction.

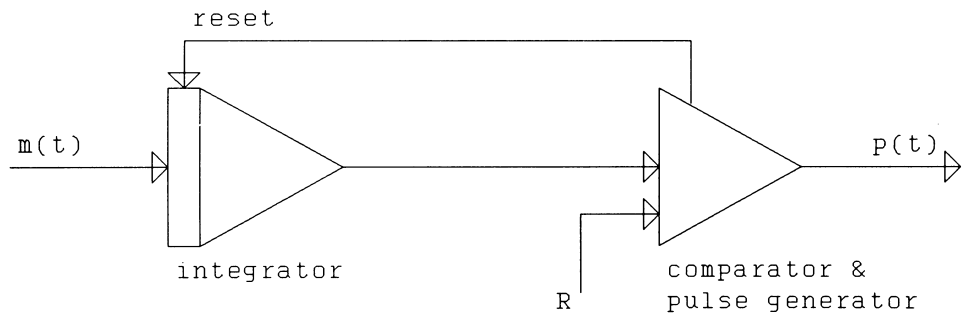

a

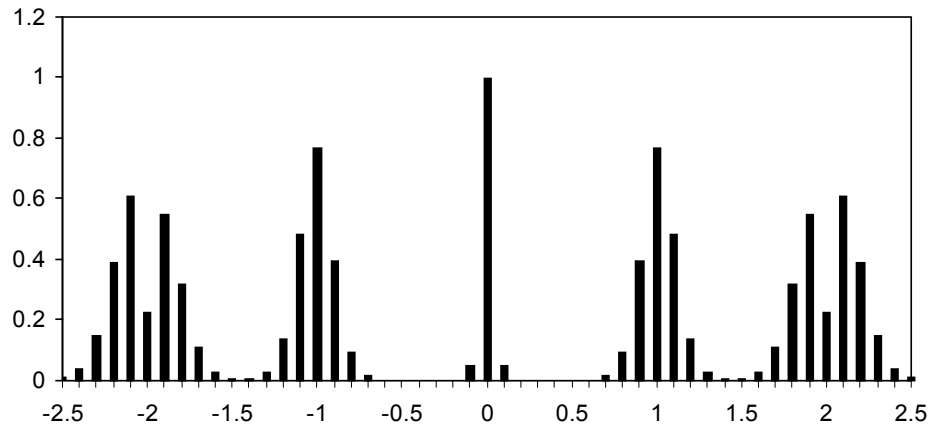

b

Figure 2

a) a: The IPFM-model, adapted from Rompelman (1985).

b) b: The amplitude spectrum of a signal produced by the IPFM-model: f_0 = 1.0 Hz, f_d = 0.1, f_m = 0.1 and R = 1.

Whenever the sidebands at the left sides of the harmonics of the sample frequency spread out into the frequency interval $[0, f_N]$, they will contaminate the signal components and they obscure the spectrum of the heart rate time series (Bayly, 1968). If there is such a distortion, it is most probably caused by the sidebands of the first harmonic.

DC-correction for the IHRS-spectrum as described in section 2.2 will, of course, make the DC-component zero, but also lower the amplitude of the harmonic components and its sidebands in the IHRS. This is in contrast to the DC-correction as defined for the SOC.

3 Methods

The Integral Pulse Frequency Modulation model (IPFM-model) was employed to quantify the power of the sidebands. The model was used to generate sequences of delta pulses for various choices of f_0, f_d, and f_m. Three values for the mean heart rate f_0 were chosen, i.e., f_0 = 0.8 Hz, 1.0 Hz, and 1.25 Hz. The modulation depth f_d varied from 0.02 to 0.3 in steps of 0.02 and the modulation frequency f_m varied from 0.05 Hz to the Nyquist frequency $f_N = f_0/2$ in steps of 0.05 Hz. For each combination of f_0, f_d, and f_m, the SOC and the IHRS were calculated and of each spectrum the sideband distortion was determined.

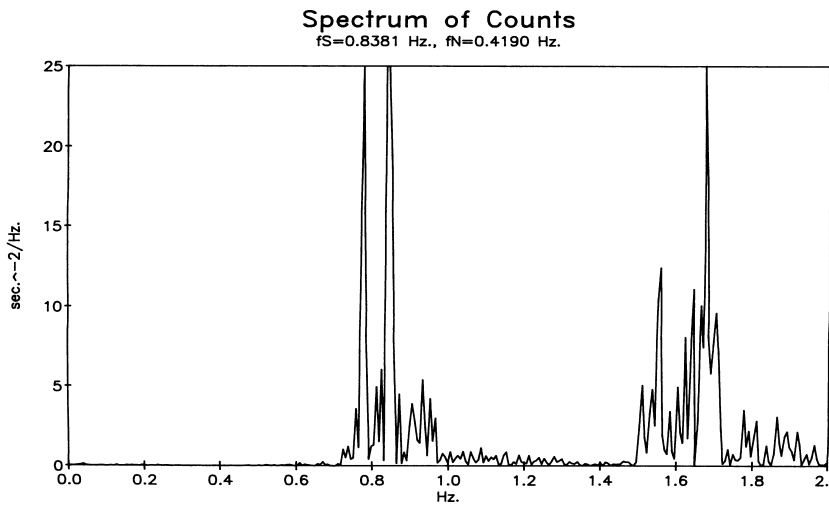

a

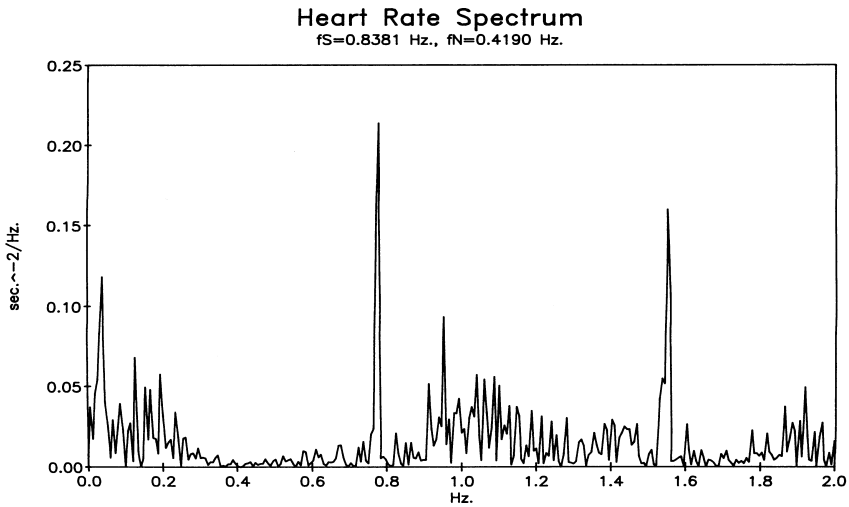

b

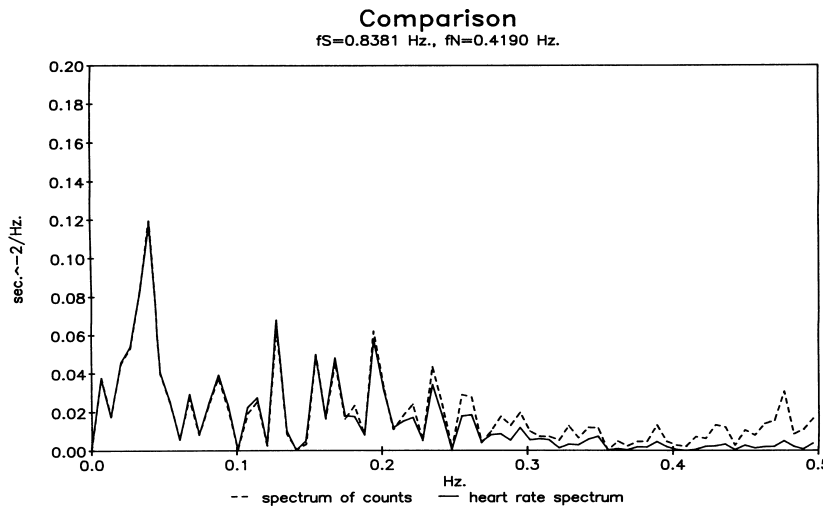

c

Figure 3: Power spectra of an interbeat interval series with f_S=0.8381 Hz and f_N=0.4190 Hz.

a) The spectrum of counts in the frequency region 0–2.0 Hz.

b) The instantaneous heart rate spectrum in the frequency region 0–2.0 Hz.

c) A comparison of the spectrum of counts (dashed) and the instantaneous heart rate spectrum (solid) in the frequency region 0–0.5 Hz.

The distortion due to the sideband components in the SOC or in the IHRS was measured by integrating the spectral components S(f) of the sideband frequencies of the first harmonic which are in the signal region of the spectrum, that is the region $0<f\leq f_N$. Thus, only those spectral components $S(f_0–n\cdot f_m)$ such that $0<f_0–n\cdot f_m\leq f_N$ were integrated. This yields the power of the sideband distortion in the SOC or in the IHRS. The powers of the individual sideband components were calculated, the power of the component at frequency $f_n = f_0 – n\cdot f_m$ is denoted by S_n, (n = 1,2,...). For each combination of f_0 and f_m the dominant sideband in the spectrum was determined. This sideband is the highest sideband, i.e., the sideband nearest to the heart rate frequency f_0, appearing in the spectra. In general, this sideband has the greatest contribution to the distortion. (Note that for a particular choice of f_0 and f_m, the dominant sideband is the same for varying f_d.)

4 Results

4.1 An example of the sideband distortion in the SOC and in the IHRS

An example of the sideband distortion is presented in figures 3a,b,c. An ECG-recording of a healthy male subject during a five minute period of rest was analyzed. The R-wave occurrence times were detected and the interbeat intervals were measured with an accuracy of 1 msec. The SOC and the IHRS were estimated. The mean interval length was I=1.1931 sec., so f_S=0.8381 Hz. This equals about 50 beats/minute. The Nyquist frequency was f_N=0.4190 Hz. In figure 3a, the SOC is presented in the frequency range from 0.0–2.0 Hz to show some harmonic components of the mean heart rate f_S and the accompanying sidebands. Figure 3b presents the IHRS, plotted in the same frequency range. As compared with the SOC, the harmonic components and the sidebands are considerably reduced in amplitude (notice the difference in scale of the y-axis, compared to the SOC). Therefore, the sidebands will cause less distortion in the signal components within the spectral area $[0,f_N]$. In figure 3c, the SOC and the IHRS are displayed in the frequency range from 0.0–0.5 Hz. The signal components in the frequency interval $[0,f_N]$ are reduced in amplitude in the IHRS as compared with the SOC. If no DC-correction is applied, the IHRS is equivalent with the SOC.

As expected, DC-correction applied to the SOC only affects the DC-component, which becomes zero. DC-correction applied to the IHRS also affects the harmonic and sideband components and reduces the amplitudes of these components.

4.2 Results of the simulation using the IPFM-model

For f_0 = 1.25 Hz, the sideband distortion of the SOC is presented in figure 4a, and the sideband distortion of the IHRS is presented in figure 4b. The power of the sideband distortion is plotted against the various choices of f_m and f_d. The results for f_0 = 0.8 Hz and f_0 = 1.0 Hz are comparable. Table 1 shows, for various choices of f_m, the sidebands S_n in the SOC, starting from the dominant sideband.

Figures 4a and 4b show that for constant f_m the power of the sidebands is increasing for increasing f_d, an increasing modulation depth causes a higher power of the sidebands. For f_0 = 1.25 Hz, the dominant sideband for f_m = 0.1 Hz is S_7: S_6, S_5, etc., do not occur in the spectra (Table 1). The dominant sideband for f_m = 0.2 Hz is S_4, for f_m = 0.25 Hz and 0.3 Hz the dominant sideband is S_3, and for f_m = 0.35 Hz, 0.4 Hz, and further, the dominant sideband is S_2. The component S_2 for f_m = 0.35 Hz is much larger than S_3 for f_m = 0.3 Hz (Table 1). This explains the jump in the figures at f_m = 0.35 Hz. For higher modulation frequencies f_m the component S_2 is decreasing, so in the region f_m > 0.35 Hz the sideband distortion is decreasing. This means that for modulation frequencies lower than 0.55 Hz the sideband distortion due to S_2 is decreasing (Table 1).

The sideband distortion in the IHRS is smaller than or equal to the sideband distortion in the SOC (compare figure 4a with figure 4b). The difference in sideband distortion is the largest in the sideband S_2 for f_m = 0.35 Hz and for f_m = 0.4 Hz. This sideband for both modulation frequencies is much smaller in the IHRS than in the SOC. For f_m = 0.35 Hz, the sideband S_2 is at frequency f_2 = 0.55 Hz, for f_m = 0.4 Hz, the sideband S_2 is at frequency f_2 = 0.45 Hz. So the difference in sideband distortion is the largest in this frequency region. Notice that the frequency f_2 of the sideband S_2 is dependent on both the modulation frequency f_m and the mean heart rate f_0. For f_0 = 0.8 Hz, the frequency region with the largest sideband distortion is between 0.2 and 0.3 Hz. For f_0 = 1.0 Hz, this region is between 0.3 and 0.4 Hz. This means that the sideband distortion is also dependent on the mean heart rate. The absolute values of the sideband distortion, as well as the difference in sideband distortion between the two methods, appeared to be largest in the frequency region between the lowest dominant sideband (f_2) and the Nyquist frequency f_N. The contribution of the sideband S_2 to the sideband distortion in the SOC and in the IHRS is visualized in figure 5 (MULDER, 1988). The figure shows the ratio of the S_2 component and the power of the modulation component, i.e., $S_2/S(f_m)$, for f_0 = 1.25 Hz and f_d = 0.3. At low modulation frequencies (0.35 Hz) the distortion in the SOC is about 1.5 times the distortion in the IHRS. At higher modulation frequencies (above 0.4 Hz) there is almost no difference between the two methods.

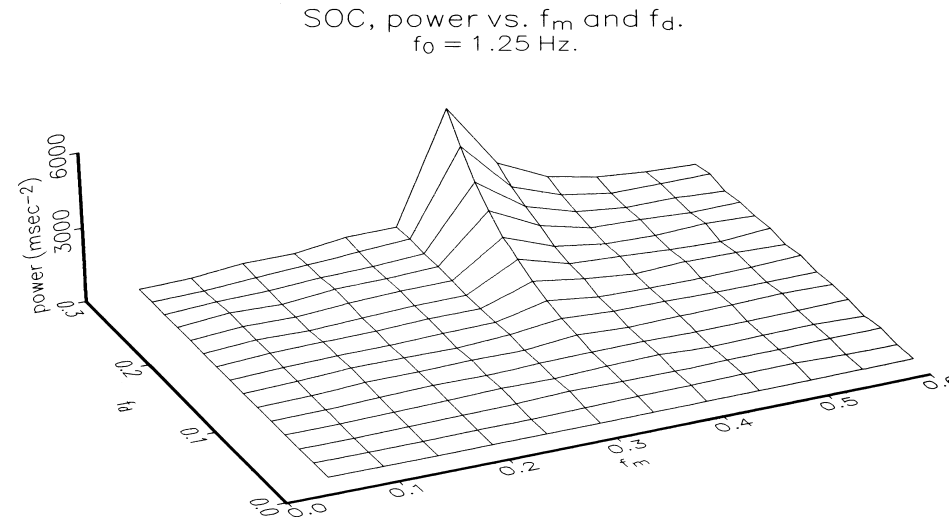

a

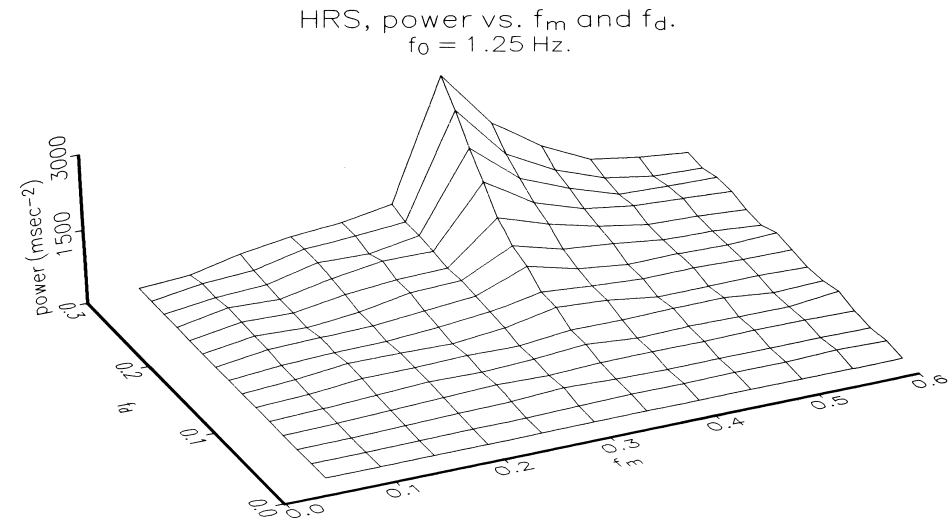

b

Figure 4: The power of the sideband components in the spectrum of counts (SOC) and the instantaneous heart rate spectrum (HRS) calculated on interbeat intervals generated by the IPFM-model for various choices of f_d and f_m.

a) f_0=1.25 Hz. SOC, power versus f_m and f_d.

b) f_0=1.25 Hz. IHRS, power versus f_m and f_d.

Note the difference in scaling.

f_m= (Hz) → f_n= (Hz) ↓	0.10	0.15	0.20	0.25	0.30	0.35	0.40	0.45	0.50	0.55	0.60
0.05		S_8 (0.06)	S_6 (0.04)		S_4 (0.02)		S_3 (0.10)				S_2 (0.21)
0.10		S_9 (0.15)						S_3 (0.01)			
0.15			S_7 (0.22)			S_4 (0.06)				S_2 (6.61)	
0.20		S_7 (0.08)				S_3 (2.41)					
0.25			S_5 (0.06)	S_4+S_6 (*)	S_5 (0.46)				S_2+S_3 (201)		
0.30											
0.35	S_9 (0.001)	S_6 (0.10)	S_8 (0.01)		S_3 (15.9)		S_4 (0.81)	S_2 (591)			
0.40										S_3 (0.10)	
0.45	S_8 (0.03)		S_4 (19.6)				S_2 (1469)				
0.50		S_5 (7.47)		S_3+S_7 (437)		S_5 (0.03)					
0.55	S_7 (1.32)		S_9 (0.02)		S_6 (0.02)	S_2 (4033)		S_4 (0.67)			S_3 (1.04)

Table 1: List of the sidebands in the SOC and their powers (in ms^{-2}) for various choices of f_m (f_0 = 1.25 Hz). For a particular f_m (horizontal), the list starts with the dominant sideband and ends with the lowest sideband present in the SOC (upto S_9). The sidebands are placed in the table at their sideband frequencies f_n (vertical). Sometimes the sidebands coincide, for instance S_2 and S_3 for f_m = 0.55 Hz. The listed power is the total power. Sidebands can coincide with the modulating frequency, for instance S_4 and S_6 coincide with f_m = 0.25 Hz (*).

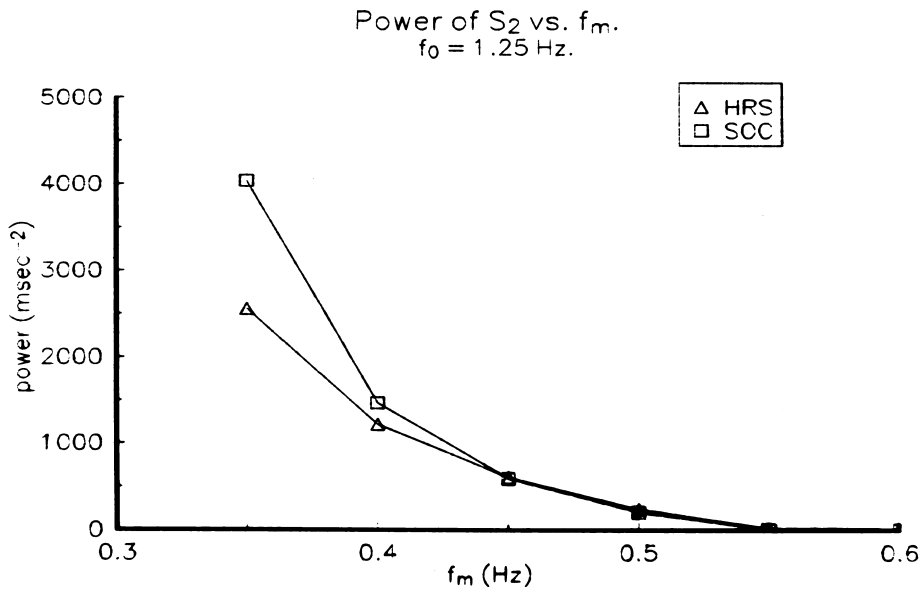

Figure 5: The powerratio of the sideband S_2 and the power of the modulation component $S(f_m)$ vs. the modulation frequency f_m (f_0 = 1.25 Hz) in the SOC and in the IHRS. It compares the distortion of the sideband S_2 in the SOC and in the IHRS.

The component S_3 is not taken into account in this comparison. For f_0 = 1.0 Hz, the distortion in the SOC around f_m = 0.25 Hz is about 3 times the distortion in the IHRS and decreases for higher f_m. For f_0 = 0.8 Hz, the distortion in the SOC around f_m = 0.25 Hz is about 6 times the distortion in the IHRS and decreases for higher f_m. These comparisons are dependent on the modulation depth f_d.

5 Discussion

Sideband distortion, occurring in heart rate variability spectra, has been studied previously. Koenderink and Van Doorn (1973) investigated the effects of the interference of the modulation signal with the sidebands, in other words, the coincidence of the modulation frequency with one of the sidebands of the mean heart rate. De Boer et al. (1985) compared three spectra: the SOC, the interval spectrum, and the heart rate spectrum. The interval spectrum and the heart rate spectrum were based on an equidistant Fourier transform (i.e., FFT). He described and compared the appearance of the sidebands of the mean heart rate in the SOC and the appearance of the harmonics of the modulation frequency in the SOC, the interval

spectrum, and the heart rate spectrum. Berger et al. (1986) used a method of interpolated inverse intervals and claimed that the SOC, the interval spectrum, and the heart rate spectrum were less influenced by the sidebands of the mean heart rate and were less influenced by the harmonics of the modulation frequency, compared to the results of De Boer. Mulder (1988) investigated the effects of the second and the third sideband (S_2 and S_3) in the interval spectrum and the SOC, based on his method (section 2.3). These two sidebands form the largest contribution to the total sideband distortion and he concluded that the distortion was larger in the interval spectrum than in the SOC. Bayly (1968) presented a simulation for the case that the main repetition rate was f_0 = 1.0 Hz and for three pairs of f_d and f_m, the modulation depth and the modulation frequency. His conclusion was that there was an increase in sideband distortion in case of increasing f_d and in case of increasing f_m. Our simulation shows that the dependency on f_d and f_m is much more complicated.

The sideband distortion was found to be less in the IHRS than in the SOC, due to the applied DC-correction, which caused the reduction of the sideband amplitudes in the IHRS. An increasing modulation depth caused a higher power of the sidebands. This was in agreement with the findings of Mulder (1988). The difference in sideband distortion was largest in the higher frequencies, i.e., the high frequency band (0.14–0.50 Hz) or higher. The frequency region, in which the difference is largest, was dependent on the mean heart rate. The lower frequencies, the low and the mid frequency band (< 0.14 Hz), were less affected or not affected. The dominant sideband in the spectrum was dependent on the modulation frequency. The larger the modulation frequency, the higher the dominant sideband. These high sidebands also had the largest effect on the sideband distortion.

In conclusion, in this paper we presented two methods to estimate the heart rate variability spectrum, based on non-equidistant sampling of the R-wave occurrence times. These methods have as advantage over methods using the FFT-algorithm, that for the calculation of the spectra any number of data points can be used, the spectra are functions of ‘cycles per second’, and no unwanted interpolation effects will occur.

Our simulations show that there are differences between the SOC and the IHRS regarding the sideband distortion:

1) the sideband distortion is less in the IHRS than in the SOC; and
2) sideband distortion is dependent on mean heart rate, the modulation depth, and the modulation frequency.

Acknowledgements

The authors would like to thank dr.ir. B.J. ten Voorde and dr.ir. Th.J.C. Faes of the Department of Medical Physics of the Free University in Amsterdam for their helpful suggestions regarding the preparation of this paper.

References

Akselrod S, Gordon D, Ubel FA, Shannon DC, and Cohen RJ. Power spectrum analysis of heart rate fluctuation: a quantitative probe of beat-to-beat cardiovascular control. Science 213:220-222, 1981.

Akselrod S, Gordon D, Madwed JB, Snidman NC, Shannon DC, and Cohen RJ: Hemodynamic regulation: investigation by spectral analysis. Am J Physiol 249:M867-M875, 1985.

Baselli G, Bolis D, Cerutti S, and Freschi C. Autoregressive modeling and power spectral estimate of R-R interval time series in arrhythmic patients. Comput Biomed Res 18:510-530, 1985.

Baselli G, Cerutti S, Civardi S, Liberati D, Lombardi F, Malliani A, and Pagani M. Spectral and cross-spectral analysis of heart rate and arterial blood pressure variability signals. Comput Biomed Res 19:520-534, 1986.

Bayly EJ. Spectral analysis of pulse frequency modulation in the nervous system. IEEE Trans Biomed Eng BME-15:257-265, 1968.

Bendat JS and Piersol AG. Random Data, Analysis and Measurements Procedures, 2nd edition. New York: John Wiley and Sons, Inc., 1986.

Berger RD, Akselrod S, Gordon D, and Cohen RJ. An efficient algorithm for spectral analysis of heart rate variability. IEEE Trans Biomed Eng BME-33:900-904, 1986.

Cooley JW and Tukey JW. An algorithm for the machine calculation of complex Fourier series. Math Comput 19: 297-301, 1965.

De Boer RW, Karemaker JM, and Strackee J. Comparing spectra of a series of point events, particularly for heart-rate variability spectra. IEEE Trans Biomed Eng BME-31:384-387, 1984.

De Boer RW, Karemaker JM, and Strackee J.. The spectrum of a series of point events, generated by the Integral Pulse Frequency Modulation model. Med Biol Eng Comput 23:138-142, 1985.

Hyndman BW, Kitney RI, and Sayers BMcA. Spontaneous rhythms in psysiological control systems. Nature 233:339-341, 1971.

Hyndman BW and Mohn RK. A model of the cardiac pacemaker and its use in decoding the information content of cardiac intervals. Automedica 1:239-252, 1975.

Koenderik JJ and Van Doorn AJ. Event train decoders with many inputs, pulse density versus momentaneous frequency. Kybernetik 13:215-222, 1973.

Luczak H and Laurig W. An analysis of heart rate variability. Ergonomics 16:85-97, 1973.

Mohn RK. Suggestions for the harmonic analysis of point process data. Comput Biomed Res 9:521-530, 1976.

Mulder, LJM. Assessment of cardiovascular reactivity by means of spectral analysis (Ph.D. Thesis). Groningen: University of Groningen, 1988.

Rompelman O. Spectral analysis of heart-rate variability. In: Psychophysiology of Cardiovascular Control. Orlebeke JF, Mulder G, Van Doornen LJP (eds). New York & London: Plenum Press pp:315-331, 1985.

Sayers BMcA. Analysis of heart rate variability. Ergonomics 16:17-32, 1973.

Sayers BMcA: Signal analysis of heart-rate variability In: The Study of Heart-Rate Variability. R.I. Kitney and O. Rompelman, Eds. Oxford: Clarendon Press, pp 27-58, 1980.

Womack BF. The analysis of respiratory sinus arrhythmia using spectral analysis and digital filtering. IEEE Trans Biomed Eng BME-18(6):399-409, 1971.

CHAPTER 4
QUANTIFICATION OF AUTONOMIC CARDIAC REGULATION IN PSYCHOPHARMACOLOGICAL RESEARCH

Measurement of heart rate and blood pressure variability in man. Methods, mechanisms and clinical applications of continuous finger blood pressure measurement. A.J. Man in 't Veld, G.A. van Montfrans, G.J. Langewouters, K.I. Lie, G. Mancia (eds.). Alphen aan den Rijn: Van Zuiden Communications BV, The Netherlands, 1995, chapter 8, pp:61-72

Joke H.M. Tulen[1,3], Hugo G. van Steenis[1], Lolke Pepplinkhuizen[1,3], Arie J. Man in 't Veld[2]

[1]Departments of Psychiatry, Erasmus University Rotterdam
[2]Department of Internal Medicine I, University Hospital Rotterdam Dijkzigt
[3]Section Pathophysiology of Behavior, Erasmus University Rotterdam

1 Introduction

Within human clinical psychopharmacological research, the growing interest in the assessment of autonomic cardiac regulation by means of spectral techniques finds its basis in the complex cardiovascular (side-)effects which may occur during treatment with the various types of psychoactive drugs (such as tricyclic antidepressants). Investigation of sympathetic and parasympathetic cardiovascular mechanisms by means of spectral analysis of beat-to-beat fluctuations of heart rate (HR) or blood pressure (BP) may provide new perspectives on defining the autonomic properties of psychoactive substances and their possible relationships with clinical characteristics.

Homeostatic cardiovascular regulation is thought to be effected for a large part through the interplay of sympathetic and vagal (parasympathetic) activity. Spectral analysis of the beat-to-beat changes in HR and BP has proved to be an adequate non-invasive tool to assess these changes in sympathetic and vagal modulation. The fluctuations in HR and BP are, within a time period of several minutes, usually characterized by three spectral peaks in a frequency range of 0.01 to 0.50 Hz:

- a low frequency peak around 0.04 Hz,
- a mid frequency peak around 0.1 Hz, and
- a high frequency peak between 0.20-0.35 Hz:

whereas all HR variations but particularly respiratory-related high frequency fluctuations of HR may reflect cardiac vagal (parasympathetic; cholinergic) tone, mid frequency fluctuations of HR and especially of BP may reflect baroreflex mediated sympathetic processes, and low frequency fluctuations may be of variable origin. In addition to spectral analysis, transfer function analysis can be utilized to describe the relationships between spontaneous fluctuations in cardiovascular time series in a particular frequency domain. On the basis of coherence and modulus (gain) functions of the cross spectra of systolic BP and interbeat interval (IBI) time series, non-invasive indices may be obtained of the arterial baroreflex control of the heart rate (Parati et al., 1995; Robbe et al., 1987).

Clinical psychopharmacological research sofar has focused on time domain measures of HR variability, respiratory sinus arrhythmia, and spectral analysis of HR variability. For instance, analysis of heart rate variability is presently employed to assess whether or not the new antidepressants (such as the selective serotonergic re-uptake inhibitors, SSRIs) differ from the classical tricyclic antidepressants regarding anticholinergic properties: the reduced HR variability or respiratory sinus

arrhythmia as observed in major depressive disorder and generalized anxiety disorder after treatment with imipramine or amitriptyline is interpreted as a decrease in cardiac vagal control, resulting from the strong anticholinergic properties of the tricyclic antidepressants. SSRIs such as fluoxetine or paroxetine may only cause miminal changes in heart rate variability. However, apart from the anticholinergic properties, most of these centrally active drugs have additional pharmacological characteristics which may influence hemodynamic parameters; these can only be evaluated reliably when BP variations are studied in relation to HR variations. Insight into the complex dynamics of short-term cardiovascular control may therefore necessitate the combined (spectral) analysis of HR and BP variations before and after treatment with psychoactive drugs, or after challenge tests with psychoactive drugs, in healthy subject and/or psychiatric patients. Additionally, (psycho)pharmaca may sometimes induce respiratory changes, either directly by means of their mechanism of action or indirectly by altering mood states. Irregularities in breathing pattern can have a major impact on cardiovascular variability (Saul et al., 1989). Although controlled breathing (i.e. breathing at a fixed frequency) is usually employed to standardize these respiratory-related effects, this procedure may induce an unnatural and sometimes even stressful situation. Within psychopharmacological and psychiatric research, spontaneous cardiovascular variations should preferably be studied, with separate control for the breathing pattern. The extent to which this approach may limit the usefulness of spectral techniques for the quantification of sympathetic and parasympathetic estimates of short-term autonomic cardiac control in psychiatric research remains to be established.

In this paper, we will compare the cardiovascular effects of several different types of centrally active drugs (clonidine, lorazepam, imipramine, mirtazapine) with those cardiovascular effects which may occur after infusions of norepinephrine or epinephrine:

a) infusions of norepinephrine or epinephrine were employed to describe the effects of peripheral sympathetic nervous system activity and adrenal medullary discharge on short-term cardiovascular variability,

b) clonidine, as α2-receptor agonist, was administered to analyze the complex central and peripheral, as well as pre- and post-synaptic α2-adrenergic mechanisms on sympathetic and vagal outflow as reflected in spectral analysis of cardiovascular variability,

c) animal research has shown that benzodiazepines can affect cardiac vagal tone by means of GABA-ergic inhibitory mechanisms, but the effects of benzodiazepines on autonomic cardiovascular control mechanisms in man have been studied primarily in

relation to sympathetic nervous system activity: lorazepam was administered to study the effects of a benzodiazepine on the non-invasive spectral estimates of both sympathetic and parasympathetic cardiovascular processes, and

d) the antidepressants imipramine and mirtazapine were employed to describe and compare the effects of two different types of antidepressants on cardiovascular variability. Imipramine, as a tricyclic antidepressant, may induce profound effects on HR and BP, resulting from its strong anticholinergic and alpha1-adrenergic properties. Mirtazapine (Org 3770, Remeron®) is a tetracyclic compound, characterized pharmacologically by blockade of presynaptic alpha2-receptors, enhancement of noradrenergic and serotonergic neurotransmission, weak 5-HT2 and 5-HT3-antiserotonergic and anticholinergic properties; present clinical data indicate a lack of cardiotoxicity, and minimal or absent effects on HR or BP.

Our data were collected from different experiments, employing the pharmaca either as challenge test (epinephrine, norepinephrine, clonidine, lorazepam: healthy subjects) or as chronic treatment (imipramine, mirtazapine: patients with a major depressive disorder). However, in all experiments simultaneous recordings of HR, BP, and respiration were obtained during a standardized situation of (supine/semi-recumbent) rest, which allowed us to describe and compare the effects of these (psycho)pharmaca on combined spectral analysis of spontaneous variations in HR and BP as well as the interrelationships between these cardiovascular time series, with a separate control for respiratory frequency. This approach provided the opportunity to determine some of the benefits and possible limitations of spectral techniques for the quantification of autonomic regulation in psychopharmacological and psychiatric research.

2 Methods

2.1 Subjects, pharmaca, design, and procedures

Details of the pharmacological experiments have been presented before (Tulen et al., 1993; 1994a,b, 1996). The studies were approved by the Medical Ethical Review Committee of the University Hospital Rotterdam Dijkzigt. All subjects gave informed consent prior to the start of the protocol.

a) Epinephrine and norepinephrine

10 normotensive healthy male volunteers (mean age: 23.6 years, range: 20-31 years) were subjected to either a 6 hour infusion of epinephrine (15 ng/kg/min: i.e. 82 pmol/kg/min), norepinephrine (30 ng/kg/min: i.e. 178 pmol/kg/min) or placebo (saline:

5.4 ml/h) in a random and double blind fashion. The 3 sessions were scheduled at least 10 days apart. Measurements were performed from 9.00 till 17.00 hrs, while the subjects were resting supine. The subjects were not allowed to eat, or drink: during all recordings they received a 5% dextrose solution infusion at a rate of 2 ml/min. The infusions were given from 10.00-16.00 hrs. During this period no specific requirements were made regarding physical or mental exertions; however, the subjects were requested to stay awake.

b) Clonidine

7 healthy male volunteers (mean age: 23.4 years; range 21-27 years) participated in 5 sessions each. In a randomized and double-blind manner, the following doses of clonidine were administered intravenously: 0 μg/kg, 0.25 μg/kg, 0.5 μg/kg, 1 μg/kg, or 2 μg/kg. Clonidine was diluted in 10 ml saline and injected slowly over a period of 10 min. The 5 sessions were recorded on separate days, at least 2 days apart. Each session was performed between 10.00-12.00 hrs. During this period, the subject rested comfortably in a semi-recumbent position in bed. After a baseline period of 20 min, clonidine was administered and the responses were monitored for a period of 1 hour.

c) Lorazepam

9 healthy male volunteers (mean age: 23.9 years; range 21-29 years) participated each in two sessions in a randomized and double blind study. During both sessions, the subjects performed on 5 consecutive occasions a mental effort task, with 10 min of rest between the tasks. During one session, an intravenous placebo injection (2.5 ml saline, slowly injected over 1 min) was administered 5 times, each time before the rest periods. During the other session, lorazepam was administered intravenously (in 2.5 ml saline, slowly injected over 1 min) before each rest period in increasing doses of 0.0, 0.0625, 0.125, 0.25, and 0.5 mg (total cumulative dose: 0.94 mg). The two sessions were recorded on separate days, 1 week apart. Each session lasted from 9.00-12.30 hrs. Measurements were obtained while the subjects were seated in a comfortable armchair. Only the data obtained during the rest periods will be presented here.

d) Imipramine and mirtazapine

20 hospitalized unipolar depressed patients (16 females, 4 males; mean age: 50.9 years, range: 29-64) participated in this study. The patients were diagnozed according to the criteria of the DSM-III/R (‘major depressive episode’). The patients received treatment with either imipramine (10 patients) or mirtazapine (10 patients) in a randomized and double-blind design. The patients were studied after a medication-

free baseline period and after four weeks of treatment with imipramine or mirtazapine (when stable therapeutic plasma levels were reached). Co-medication was avoided. During the recording sessions, the patients rested supine on a tilt-table; after a stabilization period (of at least 15 min), recordings were obtained during a 10 min period of supine rest and a 10 min orthostatic challenge test. Only the data of the supine rest period will be presented here.

In all experiments, during supine or semi-recumbent rest, the subjects were asked to relax and to breath regularly, not to speak, to move as little as possible, and to stay awake. Coffee and smoking were not allowed before or during the recordings.

2.2 Recordings and analysis

ECG (precordial lead), BP (Finapres device) and thoracic and abdominal respiration (impedance measurements) were recorded continuously during the sessions on a multichannel FM-type analogue recorder (Racal Store 14 DS) for off-line computer analyses. During the infusions of epinephrine and norepinephrine, intra-arterial blood pressure measurements were performed. The ECG, BP, and respiration signals were digitized at a sample frequence of 1024 Hz on a Personal Computer (Commodore PC 60-III) connected to an Analogue/Digital converter (Advantech PC-LabCard model PCL-718). R-R intervals in the ECG were detected with an accuracy of 1 ms and transposed to HR series. Systolic and diastolic BP (SBP, DBP) were defined per R-R interval of the ECG, with an accuracy of 0.1 mmHg. Time-series of IBI, SBP and DBP were scrutinized for stationarity, artifacts, and frequency of occurrence of supraventricular extra beats. If more than 5% of a time segment needed correction the segment was discarded from analysis. Consecutive periods of at least 2.5 min (maximal length: 5 min) of HR, SBP and DBP time series were subjected to a discrete Fourier transform, based on nonequidistant sampling of the R-wave incidences (CARSPAN program: Progamma, Groningen, The Netherlands; van Steenis et al., 1994), to yield power spectra of the rhythmic oscillations over a frequency range of 0.02-0.50 Hz, with a resolution of 0.01 Hz. For each time segment, the power was calculated for the total band (0.02-0.50 Hz), low frequency band (0.02-0.06 Hz), mid frequency band (0.07-0.14 Hz), and high frequency band (0.15-0.50 Hz), in addition to mean HR, SBP, and DBP, and variation coefficients of HR, SBP and DBP. Spectral power for each selected frequency band was expressed in relative terms, i.e. as fraction of the mean value of the considered signal (squared modulation index). If this measure is computed for the whole spectrum (0.01-0.50 Hz) it is directly comparable to the squared variation coefficient. The spectral power data were transformed to natural logarithmic (ln) values because of skewness of the

distributions. As an index of baroreflex sensitivity (BRS), we computed per time segment the gain (or modulus) in the mid frequency band between the SBP values and the R-R interval times, based on those frequency points within the 0.07-0.14 Hz range with a coherence between the two signals of greater than or equal to 0.35 (Robbe et al., 1987). Per time segment, samples of the respiratory signal were obtained at each incidence of the R-wave. Subsequently, these respiratory time series were subjected to spectral analysis, in a similar approach as described above and the dominant peak in the spectrum was assessed.

2.3 Statistical analysis

Spectral data were averaged to mean values per 10 or 15 min of (supine/ semirecumbent) rest (or hourly values in case of infusion of epinephrine and norepinephrine) to reduce a noise factor due to spontaneous segment to segment fluctuations, and to allow statistical analysis of the dose- or time-dependent changes within the experiments. If variability data of SBP and DBP showed similar effects, only spectral data of SBP will be presented. Within each experiment, the cardiovascular and respiratory responses after drug administration were compared with baseline or placebo data by means of multivariate analyses of variance (MANOVA) and/or Student's paired t-tests. A p-value of <0.05 was used to indicate a significant effect.

3 Results

3.1 Spontaneous cardiovascular fluctuations: some of the problems

When instructed to relax, not to speak, and to breath regularly, the power spectrum of the respiratory signal of a healthy subject normally shows a clearly defined (although broadband) peak at the dominant respiratory frequency. These (high band) respiratory frequencies are reflected in the spectrum of the HR time series, where they are clearly differentiated from the other (mid and low) frequency components (figure 1a). When an irregular breathing pattern (such as occurs during hyperventilation) dominates the respiratory time series (because the subject is anxious and can not relax, or breath regularly), interpretation of the HR (and BP) spectrum becomes more complicated. Multiple frequency components are present in the respiratory spectrum, whereas the HR (and BP) time series and spectra are dominated by regular low frequency oscillations as a result of the respiratory modulation (figure 1b, 1c). When no respiratory data are available, this may lead to

erronous conclusions regarding the meaning of the low and mid frequency fluctuations of HR and BP, particularly in clinical situations.

Cardiac arrhythmias may occasionally occur under drug-free conditions and may increasingly be present after treatment with some psychoactive drugs. Although isolated appearances of supraventricular beats may be corrected for by means of interpolation techniques, prolonged disturbances of the normal pattern leads to discarding the time segment for spectral analysis. Figure 1d shows an example where 4 weeks of treatment with imipramine in a depressed patient induced continuous (minor) rapid fluctuations in interbeat interval length, due to supraventricular (atrial) cardiac arrhythmias: the data of the subjects who showed this pattern were discarded from further analysis.

3.2 Cardiovascular effects of (psycho)pharmaca

a) Epinephrine

During infusion of epinephrine (plasma epinephrine levels increased 10 fold) mean HR increased significantly by 7% (mean±sem during infusion: 62.8±2.8 bpm), in comparison with placebo (58.8±1.9 bpm; figure 2; $p<0.05$). Low, mid and high frequency band ln power of HR were not influenced by infusion of epinephrine (figure 2). Infusion of epinephrine induced a small nonsignificant decrease of 4% in SBP (during infusion: 109.9±4.0 mmHg; placebo: 114.0±3.3 mmHg), whereas DBP significantly decreased by 9% (during infusion: 57.1±2.2 mmHg; placebo:63.4±2.1 mmHg; $p<0.01$). The ln power of the low frequency band of SBP during infusion of epinephrine was increased significantly by 5% (6.5±0.2; placebo: 6.3±0.2; $p<0.05$). The effects of epinephrine were present during the entire 6 hr infusion period and were stable over time. Epinephrine had no effect on mid and high frequency band fluctuations of SBP or DBP, nor did epinephrine influence baroreflex sensitivity or respiratory frequency (table 1).

b) Norepinephrine

Mean HR decreased by 4% during infusion of norepinephrine (during infusion: 56.7±1.7 bpm, placebo: 58.8±1.9 bpm) (plasma norepinephrine levels increased 5 fold). Low, mid, and high frequency band ln power of HR were not influenced significantly by infusion of norepinephrine, although for the mid frequency band of HR there was a trend towards a reduction during infusion of norepinephrine (3% decrease versus placebo; $p<0.08$; figure 2). Infusion of norepinephrine caused a small nonsignificant increase of 2% in SBP (during infusion: 116.0±4.3 mmHg; placebo: 114.0±3.3 mmHg) and a nonsignificant increase of 6% in DBP (during

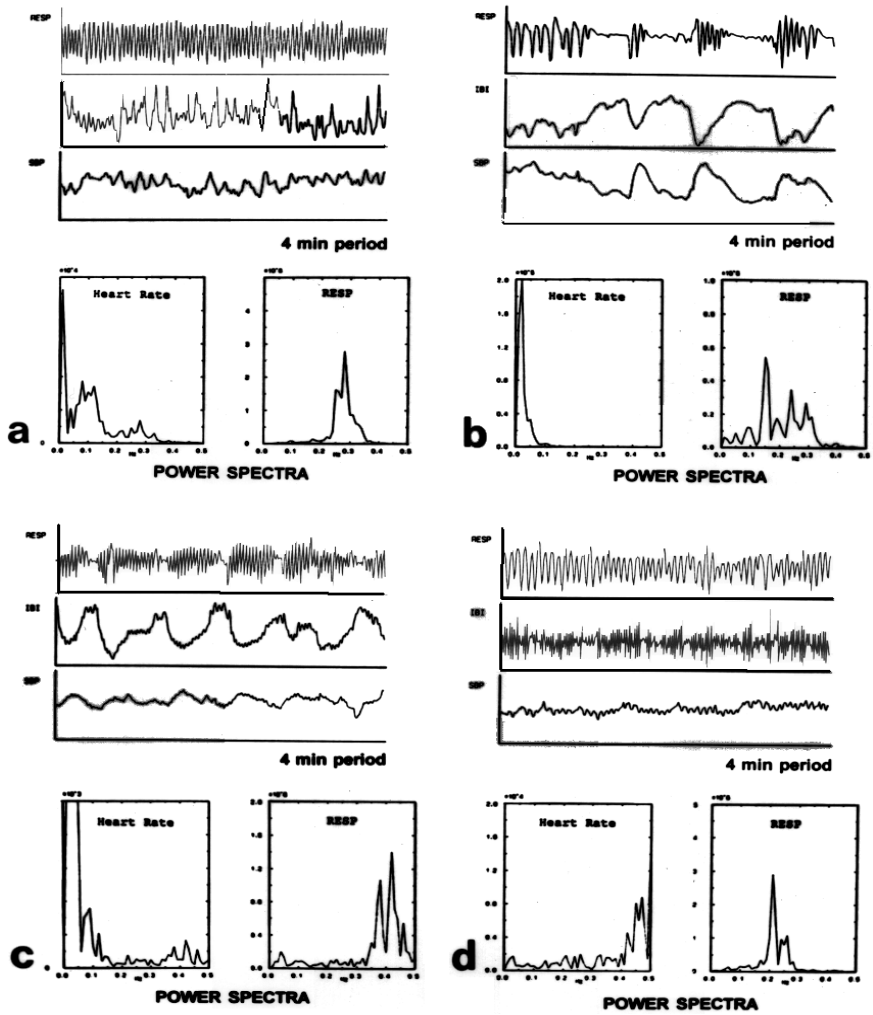

Figure 1: Examples of spontaneous fluctuations in respiration (RESP), interbeat interval (IBI), and systolic blood pressure (SBP) time series during a 4 min period of supine rest:

a) healthy subject,
b) depressed patient with hyperventilation,
c) depressed patient with hyperventilation,
d) depressed patient after 4 weeks of treatment with imipramine.

Power spectra of the heart rate and respiratory time series are presented below the cardiovascular time series.

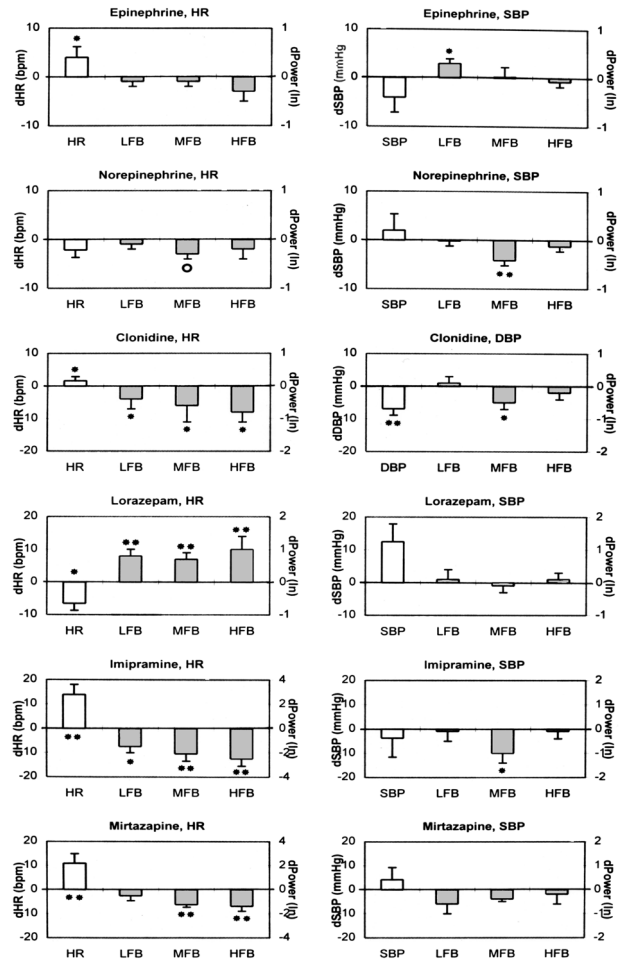

Figure 2: Effects of (psycho)pharmaca on heart rate (HR: bpm), blood pressure (BP: mmHg), and low, mid, and high frequency band fluctuations (LFB, MFB, HFB: ln power) of HR and BP. Delta responses (d) are presented as mean(+sem). o: $p<0.08$; *: $p<0.05$; **: $p<0.01$ (paired t-test: drug vs baseline, or drug vs placebo). Epinephrine and norepinephrine: responses of the averaged data during the 6 hr infusion period, versus placebo infusion. Clonidine: 15 min after infusion of 2 μg/kg, responses versus baseline. Lorazepam: responses versus baseline after a cumulative dose of 0.94 mg. Imipramine and mirtazapine: after 4 weeks of treatment: responses versus drug-free baseline.

infusion: 68.4±3.0 mmHg; placebo:63.4±2.1 mmHg). Mid frequency band ln power of SBP during infusion of norepinephrine was significantly reduced by 7% (during infusion: 5.2±0.1; placebo: 5.7±0.1; p<0.01). The effects of norepinephrine were present during the entire infusion period. Infusion of norepinephrine did not affect low or high frequency band fluctuations of BP, nor did it influence baroreflex sensitivity or respiratory frequency (table 1).

Table 1: Effects of (psycho)pharmaca on coherence, baroreflex sensitivity and respiratory cycle duration.

Mean (sd)		Coherence (ms/mmHg)	BRS (s)	Resp.cycle
Epinephrine	placebo	.60 (.1)	19 (6)	4.1 (.3)
(6 hrs)	15 ng/kg/min i.v.	.62 (.1)	17 (5)	3.9 (.6)
Norepinephrine	placebo	.60 (.1)	19 (6)	4.1 (.3)
(6 hrs)	30 ng/kg/min i.v.	.55 (.1)	20 (7)	3.9 (.3)
Clonidine	baseline	.55 (.1)	12 (4)	4.1 (.5)
(15 min)	2 µg/ kg i.v.	.63 (.1)	12 (11)	4.0 (.8)
Lorazepam	baseline	.64 (.1)	11 (6)	3.9 (.6)
(3 hrs)	0.94 mg i.v.	.63 (.1)	17 (6)*	3.9 (.6)
Imipramine	baseline	.53 (.2)	9 (5)	3.8 (.9)
(3 hrs)	289 (87) mg	.27 (.1)**	4 (3)	3.7 (.6)
Mirtazapine	baseline	.58 (.2)	15 (11)	3.8 (.3)
(4 wks)	69 (18) mg	.49 (.2)	8 (6)*	3.4 (.6)

*: p<0.05 (paired t-test: baseline vs. drug)

c) Clonidine

HR showed a small increase (3%) within 15 min after infusion of 0.5, 1, and 2 µg/kg clonidine (versus placebo: p<0.05; figure 2). This small increase in HR was followed by a gradual decline, which was no longer significantly different from placebo. After infusion of 2 µg/kg clonidine, low, mid, and high frequency band ln powers of HR were significantly reduced versus placebo, but only during the first 30 min after

infusion (figure 2, $p<0.05$). Clonidine induced a significant dose-dependent decrease in the SBP and DBP responses. Although the lowest dose of 0.25 µg/kg had no significant effect on SBP and DBP, the decrease in SBP and DBP 15 min after infusion of 2 µg/kg was significantly greater than the decrease observed after 1 or 0.5 µg/kg clonidine (SBP: 22%, 9%, 11% decrease, respectively); this effect remained present during the entire post-infusion period of 1 hr. Ln power of low and mid frequency bands of SBP were not significantly affected by clonidine. However, clonidine increased SBP high frequency band fluctuations: the increase versus baseline was significant 30 min after infusion of 2 µg/kg clonidine (ln power: 5.2±0.2 baseline to 5.6±0.2 post-infusion, $p<0.05$), and remained significant thereafter. Regarding DBP, clonidine did not affect low and high frequency band fluctuations, but ln power of the mid frequency band was significantly reduced after infusion of 2 µg/kg clonidine. The effect on mid frequency band ln power was strongest 15 min after infusion of 2 µg/kg (figure 2: 6.3±0.3 baseline vs 5.7±0.2 post-infusion), but for the whole post-infusion period the effect was significant versus placebo ($p<0.01$). Clonidine had no effect on baroreflex sensitivity or respiratory frequency (table 1).

d) Lorazepam: Lorazepam induced a dose-dependent decrease in HR, whereas low, mid, and high frequency band ln power of HR increased dose-dependently. After the highest cumulative dose of 0.94 mg lorazepam HR had decreased from 70.4±3.2 bpm (baseline) to 63.8±2.5 bpm ($p<0.05$), ln power of the low frequency band increased from 7.5±0.2 to 8.3±0.3 ($p<0.01$), ln power of the mid frequency band increased from 7.2±0.2 to 7.9±0.2 ($p<0.01$), whereas ln power of the high frequency band increased from 6.8±0.4 to 7.8±0.3 ($p<0.01$; figure 2). In comparison with placebo, cumulative doses of lorazepam did not induce significant changes in BP or BP variability, nor did it affect respiratory frequency (table 1). Baroreflex ratios increased dose-dependently after administration of lorazepam: after the highest cumulative dose level of 0.94 mg lorazepam, baroreflex sensitivity increased from 11±2 ms/mmHg (baseline) to 17±2 ms/mmHg ($p<0.05$; table 1).

e) Imipramine

When compared with the medication-free period, imipramine significantly increased HR (19%, drug-free: 74.6±4.1 bpm; treatment: 88.6±2.9 bpm; $p<0.01$), and decreased HR variability during supine rest (low frequency band ln power from 6.1±0.3 to 4.6±0.4: 25%, $p<0.01$; mid frequency band from 5.6±0.4 to 3.5±0.5: 38%, $p<0.01$; high frequency band 5.7±0.4 to 3.2±0.5: 44%, $p<0.01$) (figure 2). Imipramine had no effect on BP: SBP drug-free: 131.3±7.3 mmHg, SBP treatment: 127.5±7.2 mmHg; DBP drug-free: 69.4±3.5 mmHg, DBP treatment: 68.2±3.8 mmHg. Mid frequency band fluctuations of SBP were significantly reduced by imipramine (ln

power mid frequency band SBP: from 5.2±0.3 to 4.2±0.3, 19%, $p<0.05$). Imipramine significantly decreased the coherence between SBP and IBI in the mid frequency band (50% decline) (table 1). Due to the decline in coherence between SBP and IBI in the mid frequency band, assessment of the index of baroreflex sensitivity on the basis of coherence in the mid frequency band is not reliable during treatment with imipramine (a minimal coherence of 0.35 was required to compute the BRS). Imipramine did not influence respiratory frequency (table 1).

f) Mirtazapine

Compared with the medication-free period, mirtazapine increased HR (15%, drug-free: 66.4±5.2 bpm, treatment: 77.3±3.4, $p<0.05$) and decreased HR variability (ln power mid frequency band from 6.1±0.4 to 4.8±0.5, 21%, $p<0.001$; high frequency band from 6.5±0.6 to 5.1±0.6, 22%, $p<0.01$) during supine rest. Mirtazapine had no significant effect on BP or BP variability: SBP drug-free: 123.6±10.1 mmHG, SBP treatment: 127.8±7.0 mmHg; DBP drug-free: 67.2±5.4, DBP treatment: 64.9±3.0 mmHg. Mirtazapine had no significant effect on the coherence between SBP and IBI, but reduced the baroreflex sensitivity (50%) (table 1). Respiratory frequency did not change after 4 weeks of treatment with mirtazapine (table 1).

4 Discussion

Neural homeostatic cardiovascular regulation was evaluated by means of spectral analysis of fluctuations in HR, BP, and respiration, providing non-invasive estimates of sympathetic and parasympathetic activity. Specific and differential effects during supine/semi-recumbent rest could be detected in the spectral power of the different frequency components of HR and BP during or after infusion of epinephrine, norepinephrine, clonidine or lorazepam in healthy subjects, and after 4 weeks of treatment with imipramine or mirtazapine in patients suffering from major depressive disorder. The effects on HR and BP variability could not be attributed to significant changes in dominant respiratory frequency.

4.1 Epinephrine and norepinephrine

Increased plasma concentrations of epinephrine and norepinephrine within the high physiological range caused distinct but different hemodynamic effects, without affecting baroreflex sensitivity. Spectral analysis showed that low frequency fluctuations in BP after epinephrine and mid frequency fluctuations after norepinephrine changed in opposite directions. These effects were present from the first till the last hour of infusion and could not be explained by the effects of the

catecholamines on renin or aldosterone concentrations (Tulen et al., 1994a). The increased low frequency band fluctuations in BP during infusion of epinephrine may reflect increases in peripheral vasomotor fluctuations, due to effects of epinephrine on total peripheral resistance and stroke volume (Tulen et al., 1994a). Infusion of norepinephrine reduced mid frequency band fluctuations in BP probably due to a baroreflex mediated suppression of sympathetic activity, as also witnessed by a tendency of reduced mid frequency fluctuations in HR.

4.2 Clonidine

Within a dose-range of 0.25-2 µg/kg clonidine, significant effects could be detected for mean levels of SBP, DBP, and HR after 0.5 µg/kg or more, whereas spontaneous short-term fluctuations were influenced only after a dose of 2 µg/kg. Baroreflex sensitivity did not change after clonidine. Low and mid frequency band fluctuations of HR were reduced after 2 µg/kg clonidine, but only during the first 30 min following infusion, when the effects on BP were least; apart from a reduction in sympathetic outflow, these changes may reflect a parasympathetic effect due to a central vagal-mediated action of clonidine. DBP mid frequency band fluctuations were reduced after 2 µg/kg clonidine during the entire post-infusion period: these effects may reflect a reduced sympathetic outflow, which in this study coincided with a significant reduction in plasma norepinephrine concentrations (Tulen et al., 1993). SBP high frequency fluctuations were increased after 2 µg/kg clonidine, but only after 30 min post-infusion, which could be a consequence of alterations in both central vagal outflow and respiratory induced ‘mechanical’ alterations of intrathoracic pressure.

4.3 Lorazepam

During consecutive periods of rest, lorazepam induced a dose-dependent decrease in HR, and an increase in BRS and low, mid, and high frequency band fluctuations of HR, whereas no effects could be observed for BP, or BP variability. These data underline that benzodiazepines can exert an influence on cardiac vagal tone: in this experiment, lorazepam induced dose-dependent increases in cardiac vagal tone, resulting in decreased HR and increased HR variability during periods of rest. The increase in vagal tone observed after low doses of lorazepam was not related to diminished sympathetic activity as measured by BP or plasma catecholamines, altered respiration, or increased sedation (Tulen et al., 1994b).

4.4 Imipramine and mirtazapine (Tulen et al., 1996)

After four weeks of treatment, both imipramine and mirtazapine showed significant effects on HR (increase) and HR variability (decrease); the suppressing effect on mid and high-frequency fluctuations of HR was more pronounced for imipramine than for mirtazapine. The increase in HR and reduction in HR variability (especially of high-frequency band fluctuations) can probably be attributed to the anticholinergic properties of imipramine (strong) and mirtazapine (weak), resulting in in diminished cardiac vagal tone. Whereas mirtazapine had no effect on BP or BP variability, imipramine specifically reduced mid-frequency band fluctuations of BP. This specific decrease in mid-frequency band BP fluctuations during treatment with imipramine points to inhibition of sympathetic cardiovascular control mechanisms, however, in the absence of overt changes in overall BP levels. Animal research has shown that desipramine can suppress sympathetic nerve impulse activity due to action of desipramine within the central nervous system (decreased sympathetic outflow, suppression of noradrenaline release). These sympathetic nervous system processes may be reflected in the suppression of mid-frequency band fluctuations of BP. The reduction of mid frequency band fluctuations of BP can not totally explain the reduction of HR variations at this frequency range: the coherence between SBP and IBI time series in the mid frequency band was significantly reduced, indicating that separate mechanisms are active at this frequency range during treatment with imipramine. The reduction in the modulus (index of BRS) underlined a parasympathicolytic effect of mirtazapine; a decrease in BRS may be the result of parasympathetic inhibition.

4.5 Spontaneous cardiovascular fluctuations and respiratory modulation

Even during standardized situations of supine/semi-recumbent rest (without speaking), breathing patterns may reflect changes in respiratory frequency and amplitude, which both may vary as a function of time. Although in healthy subjects with a more or less regular breathing pattern (3 of the 4 experiments) the respiratory-related oscillations may be differentiated from the other (mid and low) frequency components in HR and BP variability, in clinical (psychiatric) populations it is essential to pay special attention to breathing abnormalities such as hyperventilation. The effects of these respiratory patterns may not be restricted to the high frequency area of HR and BP variability, but may influence or induce slower oscillations by means of complex nonlinear respiratory modulation of the autonomic nerves which control HR, the venous return to the heart and arterial blood pressure (Saul et al., 1989). Although the spectral effects of imipramine and mirtazapine were abundantly

clear, further attention needs to be paid to the quantification of changes in tidal volume in relation to respiratory frequency in order to assess the respiratory modulation of cardiovascular variability in clinical populations, before comprehensive studies are performed on the relationships between indices of autonomic cardiac control and clinical state.

5 Conclusions

Although our findings were restricted to situations of rest only, the following conclusions can be formulated on the basis of our experiments:

- Spectral analysis, in combination with transfer function analysis, of spontaneous fluctuations in heart rate and blood pressure offers a useful tool to assess the complex changes in cardiovascular control which may occur after administration of various types of (psycho)active substances.
- Spectral components of heart rate and blood pressure variations do not contain similar information regarding sympathetic and parasympathetic activity during situations of (supine/semi-recumbent) rest.
- It is essential to separate low from mid frequency fluctuations, because these bands may represent different components of homeostatic cardiovascular regulation.
- Whereas heart rate variations may be dominated by parasympathetic activity during supine/semi-recumbent rest, mid frequency fluctuations of blood pressure appear to reflect noradrenergic mediated sympathetic processes; the direction of the effect shows no unequivocal relationship with plasma concentrations of norepinephrine, but depends on reflex mechanisms and on the peripheral and/or central pharmacological properties of the drug.
- Particularly in clinical situations, control for respiratory variations is necessary to improve interpretation of spontaneous short-term cardiovascular variations.

Acknowledgements

The authors thank Jan Bruijn, Kommer Jan de Man, Frank Smeets, Ben van de Wetering, Peter Blankestijn (University Hospital Rotterdam - Dijkzigt), and Peter Moleman (Moleman Research BV) for their contributions to the (psycho)-pharmacological studies.

References

Parati G, Saul JP, Di Rienzo M, and Mancia G. Spectral analysis of blood pressure and heart rate variability in evaluating cardiovascular regulation. A critical appraisal. Hypertension 25:1276-1286, 1995.

Robbe HWJ, Mulder LJM, Ruddel H, Veldman JBP, Langewitz WA, and Mulder G. Assessment of baroreflex sensitivity by means of spectral analysis. Hypertension 10:538-543, 1987.

Saul JP, Kaplan DT, and Kitney RI. Nonlinear interactions between respiration and heart rate: classical physiology or entrained nonlinear oscillations. In: Proc Comp in Cardiology. Los Alamitos, Calif: IEEE Computer Society Press 15:299-302, 1989.

Tulen JHM, Smeets FML, Man in 't Veld AJ, van Steenis HG, van de Wetering BJM, and Moleman P. Cardiovascular variability after clonidine challenge: assessment of dose-dependent temporal effects by means of spectral analysis. J Cardiovasc Pharmacol 1993; 22:112-119.

Tulen JHM, Man in 't Veld AJ, van Roon AM, Moleman P, van Steenis HG, Blankestijn PJ, and Boomsma F. Spectral analysis of hemodynamics during infusions of epinephrine and norepinephrine in men. J Appl Physiol 76:1914-1921, 1994a.

Tulen JHM, Mulder G, Pepplinkhuizen L, Man in 't Veld AJ, van Steenis HG, and Moleman P. Effects of lorazepam on cardiac vagal tone during rest and mental stress: assessment by means of spectral analysis. Psychopharmacology 114:81-89, 1994b.

Tulen JHM, Bruijn JA, de Man KJ, Pepplinkhuizen L, van den Meiracker AH, and Man in 't Veld AJ. Cardiovascular variability in major depressive disorder and effects of imipramine and mirtazapine (Org 3770). J Clin Psychopharmacol 16:135-145, 1996.

Van Steenis HG, Tulen JHM, and Mulder LJM. Heart rate variability spectra based on nonequidistant sampling: the spectrum of counts and the instantaneous heart rate spectrum. Med Eng & Phys 16:355-362, 1994.

CHAPTER 5
EXAMINING NON-EQUIDISTANTLY SAMPLED CARDIOVASCULAR TIME SERIES BY MEANS OF THE WIGNER-VILLE DISTRIBUTION

Computers in psychology: applications, methods, and instrumentation. Maarse FJ, Akkerman AE, Brand AN, Mulder LJM, and Van der Stelt MJ (eds). Lisse: Swets & Zeitlinger chapter 13, pp:151-166, 1994. ISSN 0925-9244

H.G. van Steenis, J.H.M. Tulen

Departments of Clinical Neurophysiology and Psychiatry, University Hospital Rotterdam Dijkzigt

Spectral analysis of haemodynamic fluctuations can be employed to unravel the role of cardiovascular control mechanisms during various psychological processes. In addition to the traditional methods to compute power spectra over sequential time segments of 2-5 min, details of non-stationary time-frequency relationships may be emphasized in order to increase our insight into the dynamics of cardiovascular control mechanisms during situations of stress or mental load. Since traditional methods of spectral analysis assume the time series to be stationary, the Wigner-Ville distribution is presented here as an elegant technique to describe details of time-frequency relationships of non-equidistantly sampled cardiovascular time series, while allowing non-stationarities.

1 Introduction

Spectral analysis of fluctuations in haemodynamic parameters is an increasingly popular approach to quantify sympathetic, parasympathetic, and neurohumoral components of cardiovascular control mechanisms in psychophysiological studies. On a time scale of seconds to minutes, fluctuations of heart rate (HR) and blood pressure (BP) are characterized by three spectral peaks in a frequency range of 0.02 to 0.50 Hz:

1) a low-frequency peak around 0.04 Hz: for HR, this peak is associated with both parasympathetic and sympathetic activity, while low-frequency BP fluctuations are linked with variations in peripheral vasomotor activity due to thermoregulatory influences (Kitney, 1975) or renin-angiotensin system activity (Akselrod et al., 1985);

2) a mid-frequency peak with variations around 0.1 Hz: these fluctuations in BP with a period of approximately 10 seconds (Mayer waves) may be the results of oscillations or a resonance in the baroreflex control of peripheral resistance (Wesseling & Settels, 1985), while the HR fluctuations at these frequencies around 0.1 Hz represent a reflection of the baroreflex response. Malliani et al. (1990) proposed that fluctuations in this frequency range can be considered as a general marker of sympathetic modulation regardless of its mechanism; and

3) a high-frequency peak centered at the respiratory frequency, usually between 0.20-0.35 Hz: for HR, these fluctuations primarily reflect respiratory linked variations (respiratory sinus arrhythmia) as a result of centrally mediated vagal control. For BP, these fluctuations are proposed to be the result from the direct effect of centrally mediated HR fluctuations (Akselrod et al., 1985), although the mechanical effects of respiration may also contribute substantially to these fluctuations (Saul et al., 1991).

This means that spectral analysis can be employed to obtain non-invasive estimates of both sympathetic and parasympathetic activity within short-term cardiovascular control, and as such it may extend our knowledge of autonomic nervous system activity during various situations of rest, stress or anxiety, sustained attention and mental load (e.g. Mulder & Mulder, 1981).

Typically, spectral analysis is performed on consecutive time-segments, ranging from 2-5 min in segment length, during baselines and performance of mental or physical tasks. There are several reasons why this approach may not be sufficient to describe the dynamics of the cardiovascular control mechanisms:

1) even within a time-segment of 2-5 min, relevant changes in frequency components over short periods of time may occur which are not apparent in the overall power spectrum; and

2) the high segment-to-segment variation in the power of the different frequency components over time (Parati et al., 1990) also suggests that a more detailed analysis of time-frequency relationships is warranted.

Spontaneous cardiovascular fluctuations seldom appear to be completely stationary (Weber et al., 1992), not even in highly structured experimental situations, with or without controlled breathing and after removal of artifacts (due to body movements or errors in R-wave detection). Yet, an accurate description of these 'non-stationarities' may prove to be relevant for psychophysiological research. Based on the Fourier transform, spectral analysis only yields reliable information if the time series can be considered stationary. Therefore, a method is required that describes time-frequency relationships in detail, while allowing non-stationarities.

An exact time-frequency distribution (TFD) should reflect the signal properties in both the time and the frequency domain; these properties should not be lost by deriving the TFD. Therefore, a set of properties has been formulated which should apply to an ideal TFD (Cohen, 1989; Boashash, 1991; Kootsookos et al., 1992):

a) the TFD is real-valued and should be positive;

b) integration over both time and frequency yields the energy of the signal;

c) integration over time yields the spectral density of the signal;

d) integration over frequency yields the instantaneous power of the signal;

e) the instantaneous frequency and the group delay can be calculated directly from the TFD;

f) the TFD is zero outside the time and frequency regions in which the signal is present.

The short-time Fourier transform (STFT) as employed by Allen et al. (1977) only satisfies a). The Wigner-Ville distribution (WVD; Wigner, 1932; Ville, 1948), however,

comprises all the properties except positivity and therefore offers a more valid approach to describe time-frequency relationships accurately.

In this paper, we describe the WVD. We adapted this method in order to make it appropriate for the specific characteristics of cardiovascular time series. The method described below allows time-frequency analysis to be performed of HR time series based on non-equidistant sampling of the R-wave incidences of the ECG as described by Rompelman (1985). In addition, time-frequency analysis with the WVD also can be performed on different cardiovascular time series (such as BP or respiration), according to Mulder (1988).

After presentation of the method, the WVD is illustrated by presenting a WVD analysis during a situation of rest and during a stressful performance task, for HR, respiration, and systolic BP time series.

2 Theory

2.1 The Wigner-Ville distribution

The traditional method to estimate the power spectrum of an analytical stationary random process $z(t)$ is the calculation of the Fourier transform of the autocorrelation function (ACF) of $z(t)$:

$$S_z(f) = \int_{-\infty}^{+\infty} R_z(\tau) \cdot e^{-2\pi j f \tau} d\tau \qquad (1)$$

in which

$$R_z(\tau) = E\left[z^*(t) \cdot z(t+\tau) \right]$$

is the ACF of the analytical process $z(t)$ and $j = \sqrt{-1}$. In this context, an analytical signal is a signal without negative frequency components. It is the dual of causal signals in the time domain (Bendat & Piersol, 1986). For a stationary analytical process $z(t)$, the ACF $R_z(\tau)$ is only dependent on the time lag τ and is not dependent on time t. This property does not hold for non-stationary random processes. In that case, the ACF of an analytical process $z(t)$ becomes

$$R_z(t,\tau) = E\left[z\left(t+\frac{\tau}{2}\right) \cdot z^*\left(t-\frac{\tau}{2}\right) \right]$$

(Bendat & Piersol, 1986). Substituting this ACF in (1) yields a spectral representation of $z(t)$, given by:

$$S_z(t,f) = \int_{-\infty}^{+\infty} R_z(t,\tau) \cdot e^{-2\pi jf\tau} d\tau =$$

$$= E\left[\int_{-\infty}^{+\infty} z\left(t+\frac{\tau}{2}\right) \cdot z^*\left(t-\frac{\tau}{2}\right) \cdot e^{-2\pi jf\tau} d\tau \right] = E\left[W_z(t,f)\right]$$

in which:

$$W_z(t,f) = \int_{-\infty}^{+\infty} z\left(t+\frac{\tau}{2}\right) \cdot z^*\left(t-\frac{\tau}{2}\right) \cdot e^{-2\pi jf\tau} d\tau \qquad (2)$$

(Bendat & Piersol, 1986; Boashash, 1991). The function $W_z(t,f)$ is called the Wigner-Ville distribution (WVD) of the analytical random process $z(t)$ (Ville, 1948; Boashash, 1991). The expression

$$S_z(t,f) = E\left[W_z(t,f)\right]$$

is called the Wigner-Ville spectrum or the evolutive spectrum (Boashash, 1991).

The discrete Wigner-Ville distribution (DWVD) of a discrete analytical time series $\{z[n], n = 1,2,...,N\}$ of odd length $N = 2N_1 + 1$ is defined by:

$$W[n,k] = 2 \cdot \sum_{i=-L_1}^{i=L_1} v[i] \cdot z[n+i] \cdot v^*[-i] \cdot z^*[n-i] \cdot e^{-4\pi j \cdot \frac{ik}{L}} \qquad (3)$$

for $n = 1,2,...,N$, $k = 0,1,...,L-1$, $j = \sqrt{-1}$ (Claassen & Mecklenbräuker, 1980; Boashash & Black, 1987; Boashash, 1991). In this expression (3), $v[i]$ is a window function of odd length, $L = 2L_1 + 1$, non-zero for $-L_1 \le i \le L_1$, and zero outside this region (L can be equal to N). $v[i]$ can be a rectangular window or a taper like the Hanning or Hamming window. The discrete variables n, k, and i correspond to the continuous variables t, f, and τ in (2). The transformation of the continuous $\tau/2$ to the discrete variable i produces the factor 4 in the exponent and the factor 2 before the summation in (3).

There are two reasons to use the analytical form of a time series to compute the WVD:

1) real non-analytical signals can produce low-frequency artifacts which are a result of the interaction between positive and negative frequencies (Boashash, 1988). These interactions are comparable to the appearance of a 'ghost' curve between two positive frequency components, as explained below.

2) Real non-analytical signals have to be oversampled by at least four times the Nyquist frequency to avoid aliasing effects in the WVD. Aliasing is caused by the

overlap of positive and negative frequency components. The annihilation of the negative frequency components by forming the analytical form of the signal prevents this overlap. In fact, the sample frequency is doubled by producing an imaginary part to the real non-analytical signal in order to get the analytical form (Claassen and Mecklenbräuker, 1980; Boashash, 1988).

A limitation of the WVD is the appearence of spectral cross terms, or 'ghost' curves in the time-frequency domain. These cross terms are artifacts, which are due to the bilinear nature of the WVD (2) (Cohen, 1989; Boashash, 1991). To clarify this phenomenon, we describe the WVD of the sum of two pure sine waves:

$$z(t) = A_1 \cdot e^{2\pi j f_1} + A_2 \cdot e^{2\pi j f_2}$$

The WVD is:

$$W(t,f) = A_1^2 \cdot \delta(f - f_1) + A_2^2 \cdot \delta(f - f_2) +$$

$$+ 2A_1A_2 \cdot \delta\left(f - \frac{f_1 + f_2}{2}\right) \cdot \cos\left(2\pi(f_2 - f_1)t\right) \qquad (4)$$

($\delta(\cdot)$ is the Dirac delta function). The first two terms on the right hand side of (4) are the auto-terms; they are the expected components in the time-frequency plane at the frequencies f_1 and f_2 of the sine waves. Compare this with the spectrum of a sine wave. The third term is a cross term. It is located halfway the two auto-terms and the form of the cross term is sinusoidal. The cross terms in the WVD of a signal can also occur at the position of the auto-terms; they then obscure the true TFD and they hamper the interpretation of the distribution. Because the cross terms are sinusoidal, smoothing the WVD will lower the amplitudes of the sine waves. A two-dimensional smoothing-filter in the time-frequency domain can be used to diminish the effects of these cross terms in the WVD (Boashash, 1991).

The DWVD (3) can be implemented in a computer program using a standard discrete Fourier transform. For each n, the kernel

$$\left\{v[i] \cdot z[n+i] \cdot v^*[-i] \cdot z^*[n-i],\ i = -L_1, ..., L_1\right\}$$

is input of the discrete Fourier transform. In order to transform an odd number of data the chirp Z-transform (Oppenheim & Schafer, 1975) can be used. The implementation of the DWVD is further descibed in appendix A.1. Boashash and Black (1987) also gave a method to calculate the DWVD.

2.2 The discrete Wigner-Ville distribution of a cardiovascular time series based on non-equidistant sampling

A well known way to estimate a heart rate variablity spectrum is to calculate the interbeat intervals (IBIs) between the R-wave incidences, place them equidistantly as a function of interval number and calculate the spectrum using the fast Fourier transform.

An other approach is introduced by Rompelman (1985). This method is based on the non-equidistant sampling of the R-wave occurence times. The sampled occurence times are represented by delta functions, placed non-equidistantly in time at the detection times. The Fourier transform of this series of delta functions is calculated to estimate the heart rate spectrum. At the R-wave occurence times, samples of other cardiovascular signals can be obtained: the systolic or diastolic BP can be determined, the IBI since the last R-wave occurence time can be calculated, a sample of the respiration signal can be taken. The delta functions at the R-wave detection times now have weights according to these sample values. This series of delta functions is a function of time and it is not a function of interval number as described above. Again, the Fourier transform of this series of delta functions can be taken to estimate the spectrum of this cardiovascular time series (Mulder, 1988; appendix A.2).

A cardiovascular time series in this form is a non-equidistantly sampled signal. To calculate the DWVD of a non-equidistant time series, this series has to be transformed in an equidistant series. Firstly, the complex Fourier transform is calculated of the cardiovascular time series. This results in an equidistant series in the frequency domain. Then, this series in the frequency domain is transformed back to the time domain by a standard discrete inverse Fourier transform. The DWVD can be calculated of the resulting equidistant cardiovascular time series.

Concluding, the WVD in this form can be computed from different kinds of cardiovascular time series, such as heart rate, interbeat intervals, blood pressure, or respiration. The changes in signal frequency can be visualized graphically as a function of time by means of contour plots or three-dimensional surface plots. In the contour plots, the amplitude of the WVD can be visualized by means of colours.

Our program of the WVD is written in Microsoft Fortran. For the graphical display of the TFDs, we employed GSS*CGI routines and drivers. Because of the complexity and quantity of the analyses, a powerful personal computer (minimal 80386 plus FPU) is essential for implementation of the technique. Calculation of the WVD of a time series with a length of several hours is possible.

3 Applications

The WVD can be employed to analyze time series such as HR, BP or respiration, in order to characterize details of time-frequency relationships which may prove relevant for psychophysiological research.

3.1 Data collection and analysis

The following examples are based on data of healthy subjects during situations of rest and mental stress (the Stroop Color Word Test, CWT). The CWT consists of four words (red, green, blue and yellow) which are presented on videotape, one word at a time, in four different colors (red, green, blue and yellow). The stimulus presentation and the interstimulus interval last about 1.5-2.0 sec. The subject has to indicate the color of the word on an answer sheet, with the specific request to do their very best and make as few errors as possible. Spontaneous fluctuations in ECG, BP, and respiration during rest and CWT were recorded on a multichannel FM-type analogue recorder (Racal Store 14 DS) for off-line computer analyses. The ECG was derived using a precordial lead, amplified by a polygraph (Nihon Kohden). BP was monitored and recorded by means of a servo-plethysmo-manometer for continuous, non-invasive measurement of finger arterial blood pressure (Finapres 2300 NIBP monitor, Ohmeda). Thoracic respiration was measured by means of a Nihon Kohden impedance plethysmograph. ECG, BP, and respiration were digitized at a sample frequency of 1024 Hz on a Personal Computer (Commodore PC 60-III) connected to a PC-LabCard A/D converter. IBIs were detected with an accuracy of 1 msec. Systolic BP was defined per R-R interval of the ECG with an accuracy of 0.1 mmHg. At the incidence of the R-waves in the ECG, a sample was also obtained of the respiratory signal. Thus, beat-to-beat time series of IBI, SBP and respiration were further processed to obtain WVDs per period of rest or CWT. A two dimensional rectangular smoothfilter has been applied to reduce the disturbance of the cross terms. The length of the smoothfilter in the time-direction was 4 time points and the length in the frequency-direction was 3 frequency points. The changes in amplitude within a WVD contour plot are presented in black or grey in our examples. The amplitude of the WVD can, however, be better reflected in colour contour plots.

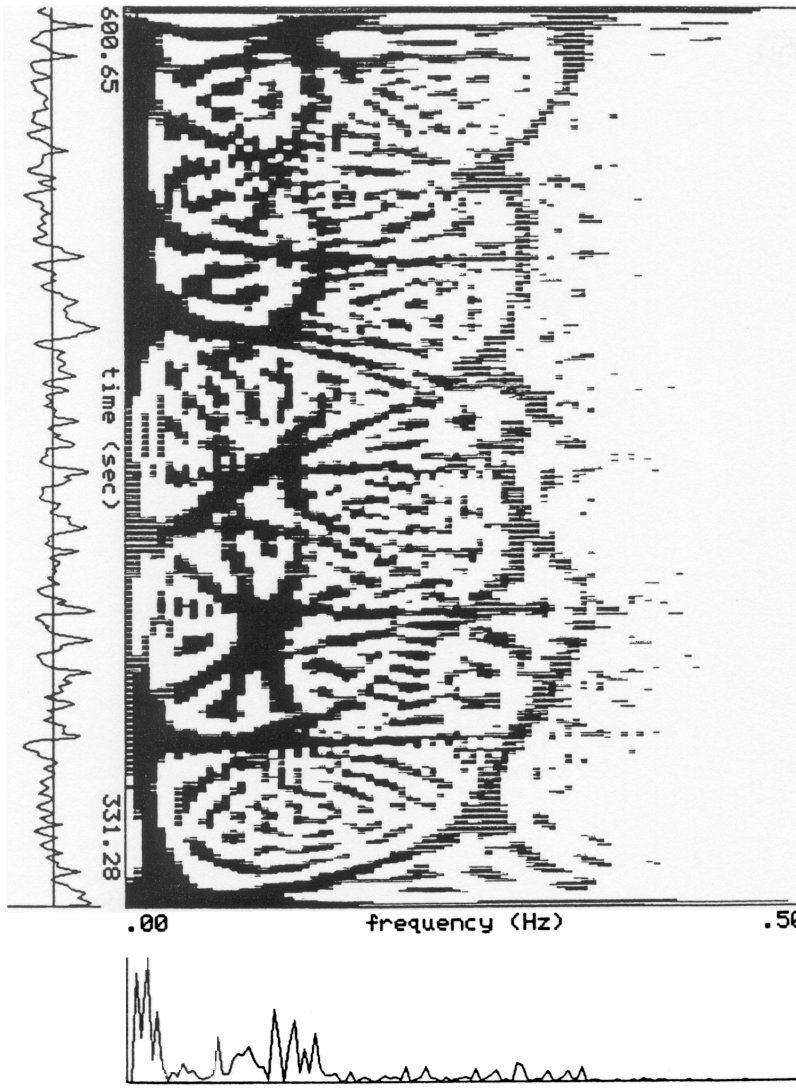

Figure 1: Contour plot of the WVD of a non-equidistantly sampled IBI-series (230 secs in length) of a healthy female during a situation of supine rest (mean HR is 89.75 bpm). The abcisses represents the frequency axis, while the ordinate shows the time axis. The frequency resolution of the WVD is 5.89 mHz. Along the abcisses, below the WVD distribution, the squared magnitude of the Fourier transform of the whole time period is presented. Along the ordinate, the raw IBI-series is shown in the time domain. In this contour plot, the black parts indicate higher amplitude than the grey parts.

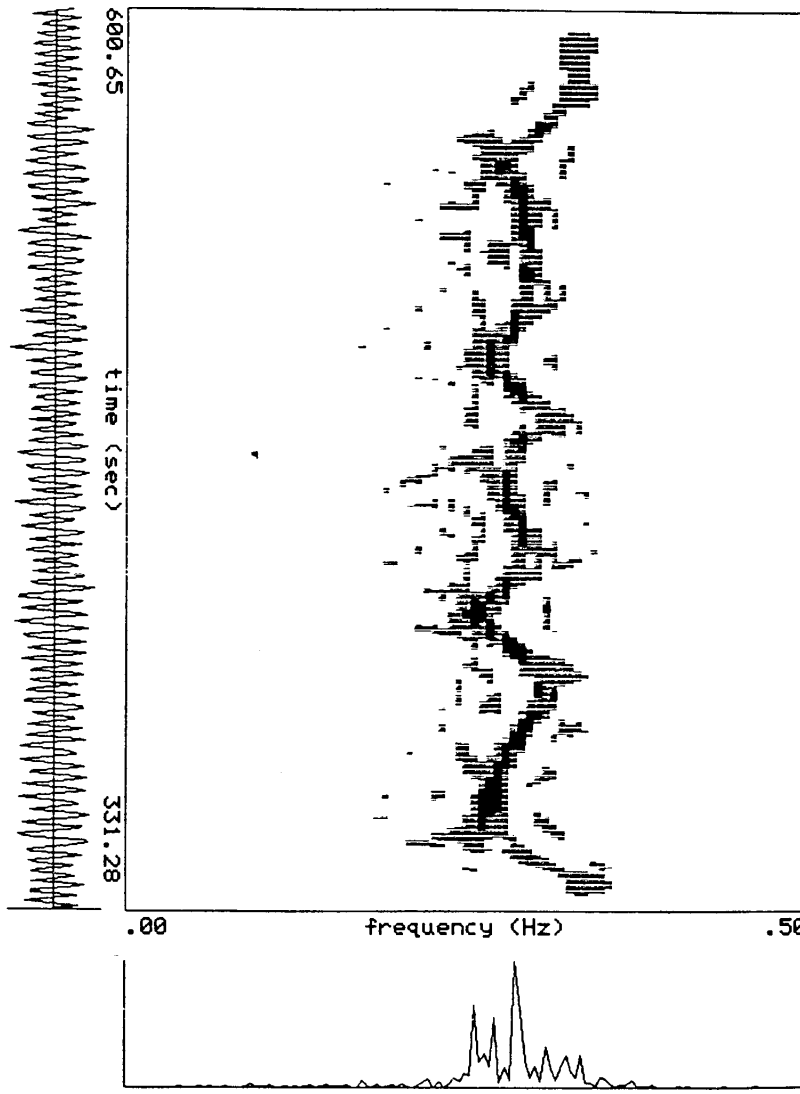

Figure 2: Contour plot of the WVD of a non-equidistantly sampled respiratory time series, of the same subject and time segment as shown in figure 1 (see for explanation of abcisses and ordinate: figure 1.)

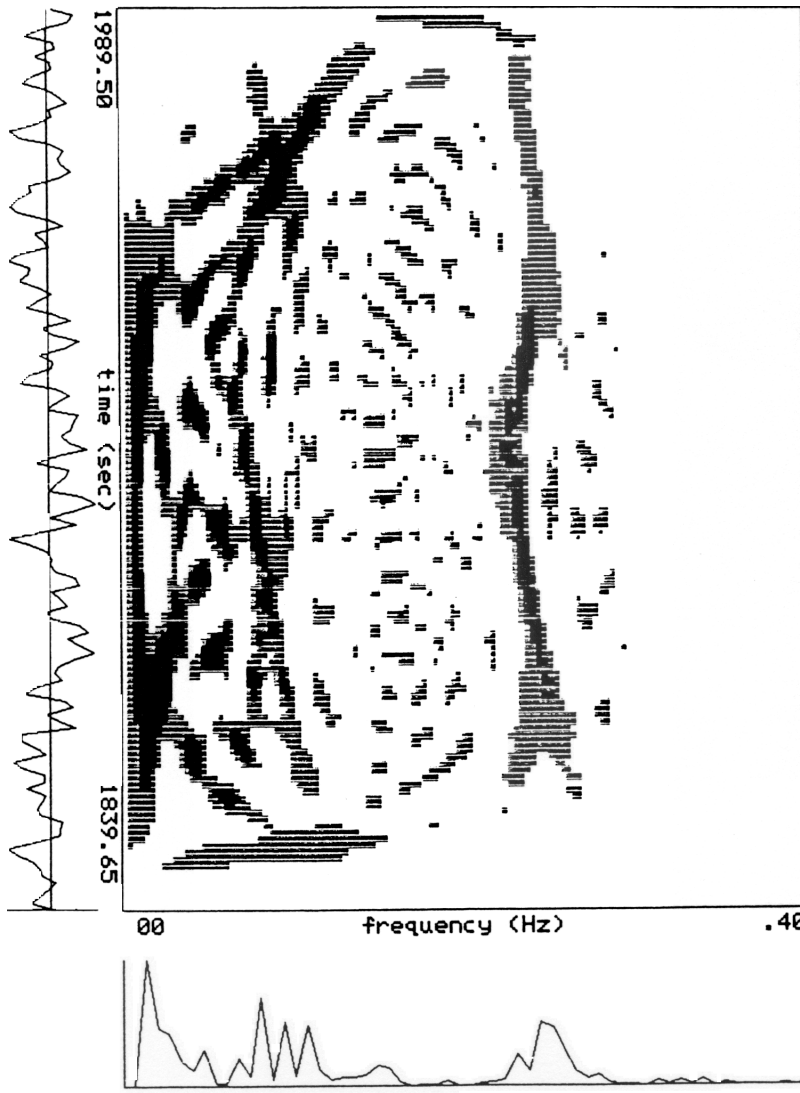

Figure 3: Contour plot of the WVD of a non-equidistantly sampled IBI-series of a healthy male during a situation of rest (sitting position; time segment length 150 sec). The frequency resolution is 3.34 mHz. (See for explanation of abcisses and ordinate: figure 1.)

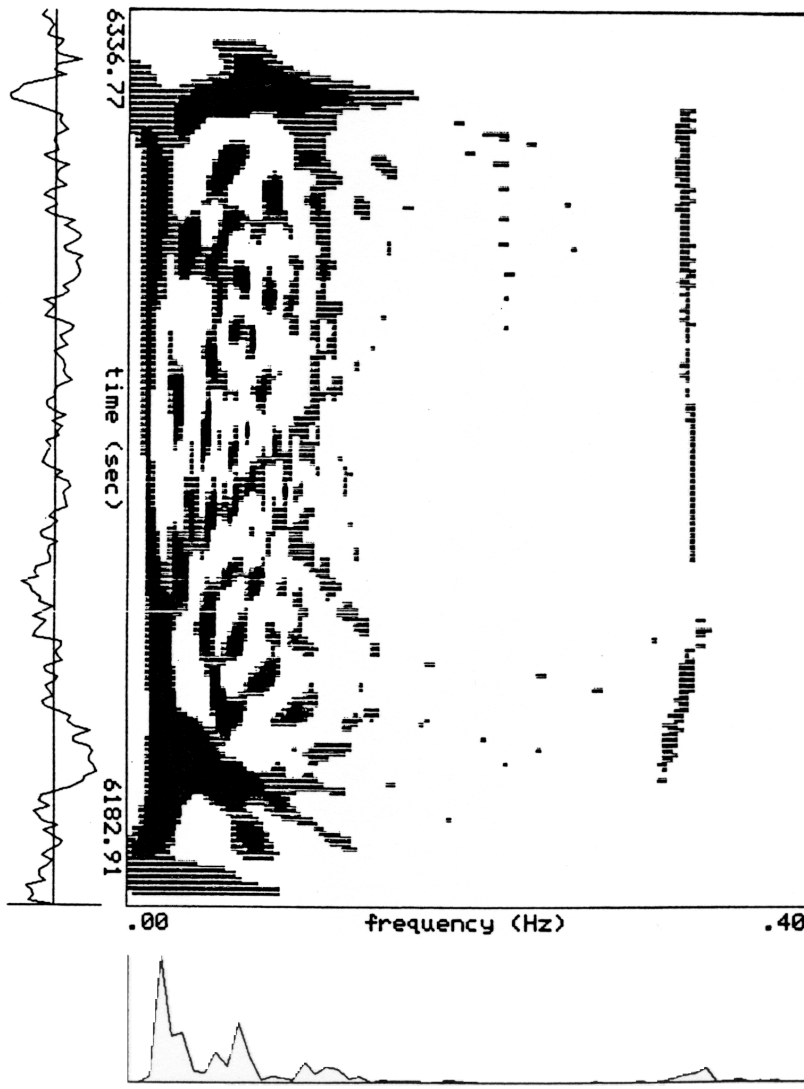

Figure 4: Contour plot of the WVD of a non-equidistantly sampled IBI-series of the same subject as described in figure 3, during performance of the CWT (time segment length 150 sec). The frequency resolution is 3.25 mHz. (See for explanation of abcisses and ordinate: figure 1.)

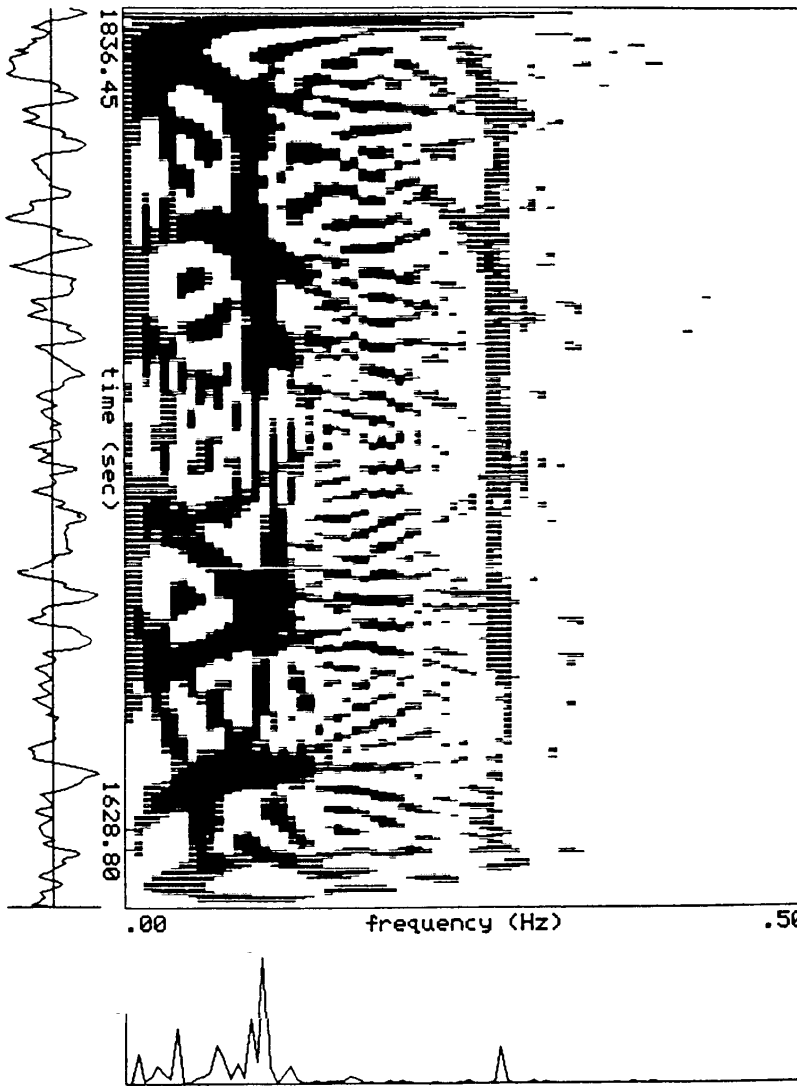

Figure 5: Contour plot of the WVD of a non-equidistantly sampled systolic BP time series of a healthy female during a situation of supine rest. The frequency resolution is 6.62 mHz. (See for explanation of abcisses and ordinate: figure 1.)

3.2 Example 1, rest situation

A typical WVD of an IBI-series of healthy young female during a situation of supine rest (figure 1) clearly shows the low, mid, and high frequency fluctuations as defined in the introduction. The low frequencies (<0.06 Hz) are fluctuating in amplitude over time; the mid frequency fluctuations (around 0.1 Hz) are also not stationary present throughout the time series. These fluctuations appear to come in bursts: several concentrations are visible. The high frequency fluctuations (related to respiratory modulation) also show non-stationarities over time. Figure 2 shows that these non-stationarities in the high frequency fluctuations as presented in figure 1 are indeed related to changes in respiration. Both figure 1 and 2 illustrate that the different frequency components within cardiovascular signals show complex changes, even within a short time period of 230 sec and during a situation of supine rest.

3.3 Example 2, mental stress

During performance of a mental stress task, HR and HR variability can change dramatically. In our example, the heart rate of a young male increased from 53.25 bpm (variation coefficient: 2.67%) during rest (figure 3), to 69.78 bpm (vc: 4.64%) during performance of the CWT (figure 4). Figure 3 and 4 visualize the changes that occur in time-frequency fluctuations during rest and during performance of the CWT. Both figures show the time course of the relevant frequency fluctuations. During the CWT, respiration rate increases and becomes very regular, causing a shift in the WVD of the respiratory related fluctuations in the IBI series to a higher frequency, which appears very stationary but only after about 30-40 sec. The other frequency components also show that initial changes in cardiovascular fluctuations during performance of a mental stress task may differ from the changes that occur during the later part of the task. These examples indicate that the WVD may help to unravel the relevance of initial time-frequency changes versus sustained changes in the understanding of cardiovascular control mechanisms during mental stress.

3.4 Example 3, cross terms

The non-stationary and discontinuous pattern (or bursts) of the mid frequency fluctuations around 0.1 Hz is also observed in the WVD of systolic BP. This is clearly visible in figure 5. However, figure 5 also shows a ‘regular’ discontinuous pattern at about 0.2 Hz. At the same frequency in the squared magnitude of the Fourier transform of this signal, there is almost no activity present. Figure 5 is presented here

as an illustration of the phenomenon of cross terms in the WVD. Smoothing helps to reduce the disturbance of these 'ghost' curves (section 2.1).

4 Conclusion

The Wigner-Ville distribution offers a promising approach to study details of time-frequency relationships of cardiovascular time series within psychophysiological research. The fact that no assumptions need to be made on the stationarity of the data, makes the method preferable to other spectral methods when analyzing spontaneous cardiovascular fluctuations over time. Two-dimensional presentation of the frequency related amplitude changes over time by means of WVD contour plots offers an elegant approach to study cardiovascular fluctuations during rest and task situations. Analysis of cardiovascular fluctuations by means of this method may further extend our knowledge on the mechanisms of cardiovascular control during situations of rest and mental stress.

Appendix

A.1 Implementation of the discrete Wigner-Ville distribution

Let $\{x[n], n = 1,2,...,N\}$ be an equidistantly sampled time series of odd length, $N = 2N_1 + 1$, and $\{v[i], i = -L_1,...,L_1\}$ a window function of odd length, $L = 2L_1 + 1$. T is the total measuring time of the time series and $\Delta t = T/N$ is the sample interval. T' is the duration of the window function, i.e., $T' = L\Delta t$. Calculate the analytical form $z[n]$ of $x[n]$ and define

$$k_n[i] = v[i] \cdot z[n+i] \cdot v^*[-i] \cdot z^*[n-i]$$

for $n = 1,2,...,N$, $i = -L_1,...,L_1$. The DWVD (3) becomes:

$$W[n,k] = 2 \cdot \sum_{i=-L_1}^{L_1} k_n[i] \cdot e^{-4\pi j \cdot \frac{ik}{L}} \qquad \text{(A1)}$$

for $n = 1,2,...,N$, $N = 2N_1 + 1$, $k = 0,1,...,L-1$. Define $k' = k/2$ and rewrite (A1):

$$W[n,k'] = W[n,k/2] = 2C_k \cdot \sum_{m=0}^{L-1} k_n[m - L_1] \cdot e^{-2\pi j \cdot \frac{mk}{L}} =$$

$$= 2C_k \cdot \mathrm{DFT}\{k_n[i], i = -L_1,...,L_1\} \qquad \text{(A2)}$$

in which

$$C_k = e^{2\pi j \cdot \frac{kL_1}{L}}$$

(Boashash & Black, 1987; Boashash, 1991). DFT in (A2) is a standard discrete Fourier transform of the points $\{k_n[i], i=-L_1,...,L_1\}$. The negative frequency components are zero as a consequence of the fact that $z[n]$ is analytical. So, the frequency resolution is doubled: instead of L_1+1 positive frequency components at $f_k = k/T'$, $k=0,1,...,L_1$, there are L positive frequency components at the frequency point $f_{k'} = k'/2T'$, $k'=0,1,...,L-1$. Compare this with the frequency resolution of the spectrum of $x[n]$, which is defined at the positive frequency points f_k, $k=0,1,...,N_1$. If the window length equals half the number of time points, i.e., $L=N_1+1$, the frequency resolution of the DWVD equals the frequency resolution of the spectrum.

In conclusion, the DWVD can be calculated using a standard discrete Fourier transform. An efficient routine to calculate the DFT of an arbitrary number of data is the chirp Z-transform (CZT) (Oppenheim & Schafer, 1975).

A.2 Heart rate variability spectra based on non-equidistant sampling

The methods of Rompelman (1985) and Mulder (1988), to estimate spectra of (cardiovascular) time series based on non-equidistant sampling of the R-wave occurence times, are as follows.

At the detection times t_i of the R-waves, samples x_i, $i=1,2,...,N$, are taken of a cardiovascular signal. These samples are represented by a series of delta pulses:

$$p(t) = \sum_{i=1}^{N} x_i \Delta t_i \delta(t - t_i) \tag{A3}$$

with $\Delta t_i = t_i - t_{i-1}$. This is called a cardiovascular time series. The Fourier transform of the function $p(t)$ is:

$$X(f_k) = \int_{-\infty}^{+\infty} p(t) \cdot e^{-2\pi j f_k t} dt = \sum_{i=1}^{N} x_i \Delta t_i \cdot e^{-2\pi j f_k t_i} \tag{A4}$$

with $f_k = k/T$, $k=0,1,2,...$, and T is the total measuring time (Mulder, 1988). The spectrum P of the function $p(t)$ is calculated from (A4) by:

$$P(f_k) = 2X(f_k)X^*(f_k)/T$$

(Bendat & Piersol, 1986).

In case the time series is a heart rate time series, we take $x_i \Delta t_i = 1$ in (A4) (Rompelman, 1985).

References

Akselrod, S., Gordon, D., Madwed, J.B., Snidman, N.C., Shannon, D.C., and Cohen, R.J. (1985). Hemodynamic regulation: investigation by spectral analysis. Am. J. Physiol., 249, H867-H875.

Allen, J.B. and Rabiner, L.R. (1977). A unified approach to short-time Fourier analysis and synthesis. Proc. IEEE, 65, 1558-1564.

Bendat, J.S., and Piersol, A.G. (1986). Random data, analysis and measurement procedures (2nd edition). John Wiley and Sons, Inc., New York.

Boashash, B. (1988). Note on the use of the Wigner distribution for time-frequency signal analysis. IEEE Trans. ASSP-36, 1518-1521.

Boashash, B. (1991). Time-Frequency Signal Analysis. In: Haykin, S. (Ed.): Advances in Spectrum Analysis and Array Processing, Volume I (pp. 418-517). Prentice Hall, Englewood Cliffs, New Jersey.

Boashash, B., and Black, P.J. (1987). An efficient real-time implementation of the Wigner-Ville distribution. IEEE Trans. ASSP-33, 1611-1618.

Claassen, T.A.C.M., and Mecklenbräuker, W.F.G. (1980). The Wigner distribution - A tool for time-frequency signal analysis. Part II: Discrete-time signals. Philips Res. J., 35, 276-300.

Cohen, L. (1989). Time-frequency distributions - a review. Proc. IEEE., 77, 941-981.

Kitney, R.I. (1975). Entrainment of the human RR interval by thermal stimuli. J. Physiol. Lond., 252, 37P-38P.

Kootsookos, P.J., Lovell, B.C., and Boashash, B. (1992). A unified approach to the STFT, TFDs and instantaneous frequency. IEEE Trans. Signal Processing, 40, 1971-1982.

Malliani, A., Lombardi, F., Pagani, M., and Cerutti, S. (1990). The neural regulation of circulation explored in the frequency domain. J. Auton. Nerv. Syst., 30, S103-S108.

Mulder, G., and Mulder, L.J.M. (1981). Information processing and cardiovascular control. Psychophysiology, 14, 392-402.

Mulder, L.J.M. (1988). Assessment of cardiovascular reactivity by means of spectral analysis. Ph.D. Thesis, Groningen: University of Groningen.

Oppenheim, A.V., and Schafer, R.W. (1975). Digital signal processing. Prentice-Hall, Inc., Englewood Cliffs, New Jersey.

Parati, G., Castiglioni, P., Di Renzo, M., Omboni, S., Pedotti, A., and Mancia, G. (1990). Sequential spectral analysis of 24-hour blood pressure and pulse interval in humans. Hypertension, 16, 414-421.

Rompelman, O. (1985). Spectral analysis of heart-rate variability. In: Orlebeke, J.F., Mulder, G., and Van Doornen, L.J.P. (Eds.): Psychophysiology of cardiovascular control (pp:315-331). Plenum Press, New York & London.

Saul, J.P., Berger, R.D., Albracht, P., Stein, S.P., Chen, M.H., and Cohen, R.J. (1991). Transfer function analysis of the circulation: unique insights into cardiovascular regulation. Am. J. Physiol., 261, H1231-H1245.

Ville, J. (1948). Théorie et applications de la notion de signal analytique. Cables et Transmission, 2^{e}A, 1, 61-74.

Weber, E.J.M., Molenaar, P.C.M., and Van der Molen, M.W. (1992). A nonstationarity test for the spectral analysis of physiological time series with an application to respiratory sinus arrhythmia. Psychophysiology, 29, 55-65.

Wesseling, K.H., and Settels, J.J. (1985). Baromodulation explains short-term blood pressure variability. In: Orlebeke, J.F., Mulder, G., van Doornen, L.J.P. (Eds.): Psychophysiology of cardiovascular control (pp:69-97). Models, methods and data. New York: Plenum Press.

Wigner, E. (1932). On the quantum correction for thermodynamic equilibrium. Phys. Rev., 40, 749-759.

CHAPTER 6
THE EXPONENTIAL DISTRIBUTION APPLIED TO NON-EQUIDISTANTLY SAMPLED CARDIOVASCULAR TIME SERIES

Computers and Biomedical Research 29:174-193, 1996

H.G. van Steenis, J.H.M. Tulen

Department of Psychiatry, Erasmus University Rotterdam

Beat-to-beat fluctuations in cardiovascular time series comprise different frequency components which can be employed to describe autonomic regulatory processes. The exponential distribution (ED) is presented here as a specific time-frequency distribution which has the potential to describe the time-related changes in the frequency content of these cardiovascular fluctuations. The ED has as advantage that it gives a good suppression of the cross terms, a characteristic feature of bilinear time-frequency distributions. An implementation to apply the ED to non-equidistantly sampled cardiovascular time series is provided. Applications of the ED to various clinical and experimental human cardiovascular time series show that the ED can be an important aid to describe and interprete time-varying frequency components of cardiovascular signals such as heart rate, interbeat interval, blood pressure and respiration.

1 Introduction

The conventional method to study the dynamics of cardiovascular control mechanisms is to estimate the variability spectra of the beat-to-beat fluctuations in heart rate (HR) and blood pressure (BP). These fluctuations in HR and BP are usually characterized by three spectral peaks in a frequency range of 0.01 to 0.50 Hz:

- a low frequency peak around 0.04 Hz,
- a mid frequency peak around 0.1 Hz, and
- a high frequency peak between 0.20-0.35 Hz.

These peaks are believed to contain differential information related to either sympathetic and/or parasympathetic processes within the cardiovascular control system [1-4]: whereas respiratory-related high frequency fluctuations in HR particularly reflect cardiac vagal (parasympathetic) tone, low and mid frequency fluctuations in HR and especially BP may reflect sympathetic processes.

To estimate HR spectra and spectra of other cardiovascular signals, several methods have been developed. Most of these methods are based on equidistant sampling of the cardiovascular signals, in order to produce various time series of cardiovascular quantities such as interbeat intervals or systolic BP (SBP). Spectra can then be calculated using a fast Fourier transform. However, HR is a frequency modulated signal [5], whereas SBP and diastolic BP (DBP) are frequency and amplitude modulated signals [6]. We recently presented a method to compute spectra of cardiovascular time series by means of non-equidistant sampling of the R-waves [7] based on the assumptions of Rompelman [5] and Mulder [6]. Non-

equidistant sampling of the HR signal or other cardiovascular signals guarantees that whenever time relationships between signals have to be studied (such as between HR and SBP), there are no relative time shifts between the time series or the relative time shifts are constant over time. Computation of variability spectra and cross-spectra by means of non-equidistant sampling of the cardiovascular time series have the advantage that these methods take into account both the frequency and amplitude modulation properties of these signals.

Spectral analysis is usually performed on consecutive time-segments ranging from 2–5 min, under the assumption that these time-segments can be considered stationary. But even on this time-scale, the spontaneous cardiovascular fluctuations are, in general, not completely stationary. This makes the spectra of the consecutive segments less appropriate to examine changes in frequency components over time. For each segment, the time-varying frequency components will accumulate into wide frequency bands within the overall power spectrum. Furthermore, the high segment-to-segment variations in the power of the different frequency components over time [8] suggest that a more detailed analysis of time-frequency relationships is warranted. These relationships can be described with a (joint) time-frequency distribution (TFD). A TFD describes the frequency changes of the signal as a function of time, while allowing non-stationarities. At each instant of time, a TFD shows the frequencies that exist at that time. A well-known TFD is the Wigner-Ville Distribution (WVD; [9-14]). Novak & Novak [15] were the first to apply the WVD to cardiovascular time series. In this paper, we will explore the possibilities of the exponential distribution (ED; [16]) to describe time-frequency relationships of various cardiovascular time series. The ED is a modified WVD, which diminishes the effects of the so-called cross terms. These cross terms are artefacts in a TFD due to the bilinearity of the TFD; cross terms are considered to be a drawback of the WVD.

Our aim of this paper is to apply the exponential distribution to non-equidistantly sampled cardiovascular time series. The implementation of the method into a computer program is provided. Furthermore, the applicability of the method to study details of cardiovascular time-frequency relationships is illustrated on both clinical and experimental human data.

2 Theory

2.1 Spectral analysis of non-equidistant cardiovascular time-series

The estimation of HR variability (HRV) spectra based on non-equidistant sampling of the R-wave incidences was first introduced by Rompelman [5]. The R-waves are detected and represented by Dirac delta pulses $\delta(t-t_i)$ at the incidence times t_i, $i=1,2,...,N$. These delta pulses form the signal:

$$p(t)=\sum_{i=1}^{N}\delta(t-t_i) \tag{1}$$

Such a series of consecutive R-wave incidences is called a HR signal or HR time series.

The Fourier transform of the function $p(t)$ is:

$$X_C(f_k)=\int_{-\infty}^{+\infty}p(t)\cdot e^{-2\pi jf_kt}dt=\sum_{i=1}^{N}e^{-2\pi jf_kt_i} \tag{2}$$

in which $f_k=k/T$, $k=0,1,...,$ and T is the total record time. The spectrum P_C of the function $p(t)$ is [17]:

$$P_C(f_k)=\frac{2}{T}\cdot X_C(f_k)\cdot X_C^*(f_k) \tag{3}$$

and is estimated using the right part of equation (2). This spectrum is based on non-equidistant sampling, the delta pulses are occurring at the R-wave incidences. The spectrum P_C is called the spectrum of counts (SOC).

Let $p(t)$ be a HR time series of consecutive R-wave incidences at times t_i, $i=1,2,...,N$. The time-intervals Δt_i between the R-waves or interbeat intervals I_i (IBIs) are defined by $I_i = \Delta t_i = t_i - t_{i-1}$ for $i=1,2,...,N$ (the first interval starts at R-wave incidence t_0). The total record time T is

$$T=\sum_{i=1}^{N}\Delta t_i\ .$$

The mean sample interval Δt or mean IBI I is T/N. The 'sample frequency' is defined by $f_S = 1/I = N/T$ (this is also called the 'mean HR') The 'Nyquist frequency' is defined by $f_N=f_S/2$. The frequency resolution is $\Delta f=1/T$.

Prior to the calculation of the spectrum of a time series, it is customary to subtract the DC of the time series. In case of an HR signal, DC-correction is performed by subtracting a sequence of N delta functions from the original delta series $p(t)$ in equation (1). These delta functions are placed at equal intervals I, the mean IBI. The function $p(t)$ then becomes [6]:

$$p(t)=\sum_{i=1}^{N}\delta(t-t_i)-\sum_{i=1}^{N}\delta(t-i\cdot I)$$

At the R-wave incidences, samples of other cardiovascular signals can be obtained: the SBP or DBP can be determined, the IBI since the last R-wave incidence can be calculated, or a sample of the respiration (RSP) signal can be taken. In this way, a collection of data points on a beat-to-beat basis is obtained. Such a series is called a cardiovascular time series. Mulder [6] introduced a method to calculate the spectrum of these non-equidistantly sampled signals (see also Van Steenis et al., [7]).

Let x_i, $i = 1, 2, ..., N$ be the samples of a cardiovascular signal taken at the R-wave incidences t_i, $i = 1, 2, ..., N$. The R-wave incidences are again represented by the delta functions $\delta(t - t_i)$, but now they have weights $x_i \Delta t_i$ in which Δt_i is the time interval $t_i - t_{i-1}$. Together they form the function $p(t)$:

$$p(t) = \sum_{i=1}^{N} x_i \Delta t_i \cdot \delta(t - t_i)$$

The Fourier transform of the function $p(t)$ is:

$$X(f_k) = \int_{-\infty}^{+\infty} p(t) \cdot e^{-2\pi j f_k t} dt = \sum_{i=1}^{N} x_i \Delta t_i \cdot e^{-2\pi j f_k t_i} \quad (4)$$

The spectrum P of the function $p(t)$ is:

$$P(f_k) = \frac{2}{T} \cdot X(f_k) \cdot X^*(f_k) \quad (5)$$

and is estimated using the right part of equation (4).

DC-correction is applied by subtracting a weighted mean of the samples x_i from each sample. This weighted mean has the form:

$$x_W = \frac{1}{T} \sum_{i=1}^{N} x_i \Delta t_i$$

and (4) becomes:

$$X(f_k) = \sum_{i=1}^{N} (x_i - x_W) \Delta t_i \cdot e^{-2\pi j f_k t_i} \quad (6)$$

2.2 The Wigner-Ville distribution

The traditional method to estimate the power spectrum of a stationary stochastic process $x(t)$ is the calculation of the Fourier transform of the autocorrelation function (ACF) of $x(t)$:

$$S_x(f) = \int_{-\infty}^{+\infty} R_x(\tau) e^{-2\pi j f \tau} d\tau \quad (7)$$

in which

$$R_x(\tau) = E\left[x^*(t) \cdot x(t + \tau) \right]$$

is the ACF of the process $x(t)$ (* denotes the complex conjugate) [17]. For a stationary process $x(t)$, the ACF $R_x(\tau)$ is only dependent on the time lag τ and is not dependent on time t. This property does not hold for non-stationary stochastic processes. In that case, the ACF of a stochastic process $x(t)$ becomes [17]:

$$R_x(t,\tau) = E\left[x(t+\tau/2)\cdot x^*(t-\tau/2)\right].$$

Substituting this ACF in (7) yields a time-dependent spectral representation of $x(t)$, given by:

$$S_x(t,f) = \int_{-\infty}^{+\infty} R_x(t,\tau)e^{-2\pi jf\tau}d\tau$$

it follows that:

$$S_x(t,f) = E\left[\int_{-\infty}^{+\infty} x\left(t+\frac{\tau}{2}\right)x^*\left(t-\frac{\tau}{2}\right)\cdot e^{-2\pi jf\tau}d\tau\right] = E\left[W_x(t,f)\right]$$

in which [13,17]:

$$W_x(t,f) = \int_{-\infty}^{+\infty} x\left(t+\frac{\tau}{2}\right)x^*\left(t-\frac{\tau}{2}\right)\cdot e^{-2\pi jf\tau}d\tau\,. \qquad (8)$$

The function $W_x(t,f)$ is called the Wigner distribution (WD) of the stochastic process $x(t)$ [9,11,13].

The discrete time equivalent of (8) for a random process $x(t)$ is [18]:

$$W_x(n\Delta t,f) = 2\Delta t\sum_{i=-\infty}^{\infty} x(n\Delta t+i\Delta t)\,x^*(n\Delta t-i\Delta t)\cdot e^{-4\pi j\cdot i\Delta t\cdot f}$$

($n = ...,-2,-1,0,1,2,...$), in which Δt is the sample interval. $f_S = 1/\Delta t$ is the sample frequency. This function is periodic, with period $f_1 = 1/2\Delta t = f_S/2$. This means that frequency components of the signal outside the frequency range $[-f_1/2, f_1/2]$ will be folded within this region, i.e., aliasing will occur. There are two methods to avoid this [12,19]:

1) make sure that the frequency components outside $[-f_1/2, f_1/2]$ are zero; this can be done by oversampling the signal by, at least, a factor four of the Nyquist frequency, which is the highest frequency in the signal, i.e., $f_1/2 \geq f_N$ and $f_S \geq 4f_N$; or

2) make sure that the negative frequency components are zero; in this case the frequency components in the region $[f_1/2, f_1]$ are zero and cannot disturb the frequency components in the region $[0, f_1/2]$; this can be done by using analytical signals.

An analytical signal is a signal without negative frequency components. It is the dual of causal signals in the time domain [17]. Analytical signals can be sampled at a rate which is at least twice the Nyquist frequency, i.e., $f_S \geq 2f_N$. In fact, the sample

frequency is doubled by producing an imaginary part to the real non-analytical signal in order to get the analytical form [19]. For an analytical stochastic process z(t), the function $W_z(t,f)$ is called the Wigner-Ville distribution (WVD; [10,11,13]):

$$W_z(t,f) = \int_{-\infty}^{+\infty} z\left(t+\frac{\tau}{2}\right) z^*\left(t-\frac{\tau}{2}\right) \cdot e^{-2\pi jf\tau} d\tau \qquad (9)$$

There is a second reason to use analytical signals [19]: real non-analytical signals can produce low-frequency artefacts in the Wigner distribution. These are a result of interactions between positive and negative frequency components. Annihilation of the negative frequency components by using the analytical form of a real signal prevents these interactions. The interactions between positive and negative frequencies are comparable to the appearance of 'ghost' curves between two positive components.

2.3 Properties of TFDs

A TFD should reflect the energy distribution of the signal, both over time and frequency. Therefore, a set of properties has been formulated which should apply to an ideal TFD [13,14,20]:

P1: the TFD is real-valued;
P2: integration over both time and frequency yields the total energy of the signal;
P3: integration over time yields the spectral density of the signal;
P4: integration over frequency yields the instantaneous power of the signal;
P5: averaging over frequency yields the instantaneous frequency;
P6: averaging over time yields the group delay;
P7: the TFD satisfies the weak finite time support: if the signal is zero outside a time segment, then the TFD is zero outside this time segment;
P8: the TFD satisfies the weak finite frequency support: if the signal is zero outside a frequency segment, then the TFD is zero outside this frequency segment;
P9: the TFD is positive.

The short-time Fourier transform (STFT; [21]) only satisfies P1 and P9; the WVD satisfies all except P9 [13,14].

2.4 Cross terms and the exponential distribution

A limitation of the WVD is the appearence of spectral cross terms, or 'ghost' curves in the time-frequency domain. These cross terms are artefacts, which are due to the bilinear nature of the WVD (equation (9)) [13,14]. To understand this notion we work out the WVD of the sum of two pure sine waves [14]:

$$z(t) = A_1 e^{2\pi j f_1 t} + A_2 e^{2\pi j f_2 t}$$

The WVD of this analytical function consists of two autoterms and a cross term ($\delta(\bullet)$ is the Dirac delta function):

$$W(t,f) = A_1^2 \delta(f - f_1) + A_2^2 \delta(f - f_2) + \text{cross term} \tag{10}$$

The cross term has the following form:

$$\text{cross term} = 2A_1 A_2 \cdot \delta\left(f - \frac{(f_1 + f_2)}{2}\right) \cdot \cos\left(2\pi(f_2 - f_1)t\right) \tag{11}$$

The first two terms on the right hand side of (10) are the autoterms, they are the expected components in the time-frequency plane at the frequencies f_1 and f_2 of the sine waves (compare this with the power spectrum of a sine wave). The resulting cross term, given in (11), is located halfway the two autoterms and the form of the cross term is sinusoidal. The cross terms in the WVD of a signal can also occur at the position of the autoterms; they obscure the true time-frequency distribution and they hamper the interpretation of the distribution.

An approach to diminish the cross terms is the use of the exponential distribution (ED), or Choi-Williams distribution, introduced by Choi & Williams [16]. In comparison to the WVD, the ED has lower cross terms amplitudes, but it contains the same information in the autoterms as the WVD [13]. This is achieved by convoluting the function $z(t+\tau/2) \cdot z^*(t-\tau/2)$ in (9), as a function of t, with an exponential kernel which has the form:

$$K_\sigma(t,\tau) = \sqrt{\frac{\sigma}{4\pi\tau^2}} \cdot e^{-\sigma t^2/4\tau^2},$$

in which σ is a parameter. For an analytical stochastic process $z(t)$ the ED has the form [16]:

$$E_z(t,f) = \int_{-\infty}^{+\infty} \left\{ \int_{-\infty}^{+\infty} K_\sigma(u-t,\tau) \cdot z\left(u + \frac{\tau}{2}\right) z^*\left(u - \frac{\tau}{2}\right) du \right\} \cdot e^{-2\pi j f \tau} d\tau$$

For large σ, the ED is almost equal to the WVD. Smaller values of σ will suppress the cross terms. $\sigma = 2$ has been found to be a good compromise for our applications. The ED satisfies the properties P1 through P6 (section 2.3). If σ is sufficiently large, the ED will also satisfy P7 and P8 [13,14,16].

2.5 The discrete exponential distribution

The discrete exponential distribution (DED) of a discrete analytical time series $z[n]$, $n = 1,2,...,N$ is defined by [13,16]:

$$E[n,k] = 2\sum_{i=-L_1}^{L_1}\left\{\sum_{m=-M_1}^{M_1}\sqrt{\frac{\sigma}{4\pi i^2}}\cdot e^{-\sigma m^2/4i^2}\cdot k[n+m,i]\right\}\cdot e^{-4\pi j\cdot ik/L} \tag{12}$$

in which the kernelfunction $k[n,i]$ is defined by:

$$k[n,k] = v[i]\cdot z[n+i]\cdot v^*[-i]\cdot z^*[n-i] \tag{13}$$

for $n = 1,2,...,N$, $k = 0,1,...,L-1$ and $L = 2L_1+1$, L must be odd. L can be equal to N. $v[i]$ is a window function of odd length L. $v[i]$ is zero outside the segment $[-L_1, L_1]$. σ is a parameter. $M = 2M_1+1$, M must be odd, and M can be equal to L. The factor 4 in the exponent and the factor 2 before the summation in equation (12) are the result of the transformation of the continuous $\tau/2$ into the discrete variable i.

3 Methods

3.1 Implementation of the exponential distribution

The ED can only be applied to equidistantly sampled analytical signals. HR time series and cardiovascular time series are non-equidistant time series (both series will be called cardiovascular time series from now on). In order to calculate the DED of a cardiovascular time series, this series has to be transformed into an equidistant analytical time series. Let $p(t)$ be a cardiovascular time series, according to section 2.1. The first step is to calculate the complex Fourier transform, using equation (2) or (6), of this $p(t)$. This results in an equidistant complex series in the frequency domain. This series can be transformed back to the time domain with the well-known inverse discrete Fourier transform (DFT). The number of R-waves in $p(t)$ and accordingly the number of complex data in the frequency domain is generally not a power of two. Furthermore, it can be an odd number. Therefore, a fast Fourier transform (FFT) cannot be used here. An efficient method to calculate the DFT or the inverse DFT of an arbitrary number of data is the chirp Z-transform (CZT) resp. inverse chirp Z-transform [22]. So, the second step is to apply the inverse CZT to the complex series in the frequency domain in order to get the desired equidistant time series in the time domain. It guarantees the same time resolution as the original time series. And the power spectrum of the equidistant series, calculated with the DFT, will be equal to the power spectrum of the non-equidistant series, calculated with

equation (3) or (5). The next step is to calculate the analytical form of the resulting equidistant cardiovascular time series. One method, using the DFT, in this case the CZT, is described by Boashash & Reilly [23]. In short, this method calculates the complex Fourier transform of the time series, annihilates the negative frequency components and multiplies the positive frequency components by two, and transforms the result back to the time domain. An alternative way to produce the analytical form is to use the Hilbert transform [17]. A FIR filter implementation of the Hilbert transform is discussed by Boashash & Black [18]. The DED of the resulting equidistant analytical cardiovascular time series can be calculated as follows. Let $z[n]$, $n=1,2,...,N$ be a discrete equidistant analytical cardiovascular time series and $v[i]$, $i=-L_1,...,L_1$ a window function of odd length $L=2L_1+1$. T is the total measuring time and $\Delta t=T/N$ is the sample interval. T' is the duration of the window function, i.e., $T'=L\Delta t$. Define:

$$k_n[i]=\sum_{m=-M_1}^{M_1}\sqrt{\frac{\sigma}{4\pi i^2}}\cdot e^{-\sigma m^2/4i^2}\cdot k[n+m,i]$$

(see equation (13)) and

$$C_L[\alpha]=e^{2\pi j\frac{\alpha L_1}{L}}$$

Define $k'=k/2$ and rewrite (12):

$$E[n,k']=E[n,k/2]=2C_L[k]\cdot\sum_{l=0}^{L_1}k_n[l-L_1]\cdot e^{-2\pi j\cdot ik/L}$$

for $k'=0,1,...,L-1$. Thus, the DED consists of the DFTs of the series $k_n[i]$, $i=-L_1,...,L_1$ for each $n=1,2,...,N$:

$$E[n,k']=2C_L[k]\cdot \mathrm{DFT}\{\mathrm{k_n}[i],i=-L_1,...,L_1\} \tag{14}$$

The negative frequency components are zero as a consequence of the fact that $z[n]$ is analytical; thus, the frequency resolution is doubled: instead of L_1+1 positive frequency components at $f_k=k/T'$, $k=0,1,...,L_1$, there are L positive frequency components at the frequency points $f_{k'}=k'/2T'$, $k'=0,1,...,L-1$, i.e., the frequency resolution of the DED is $\Delta f'=1/2T'$. Note that the spectrum of the original time series $x[n]$ is defined at the frequency points $f_k=k/T$, $k=0,1,...,N/2$, i.e., the frequency resolution is $\Delta f=1/T$.

Equation (14) can easily be implemented in a computer program. One can use the CZT to calculate the DFT of the odd number of data in (14). Our CZT-routine comes from MicroWay (387FFT, version 1.00, MicroWay Inc.). Equation (14) has to be calculated for each n. Together the results form the DED of the equidistant analytical

cardiovascular time series. The DED can visualized graphically as a function of time and frequency by means of contour plots or three-dimensional surface plots.

3.2 Data acquisition

The applications presented in the next section were selected from several experiments in which cardiovascular parameters were studied during situations of supine rest, orthostatic stress, and controlled breathing, in healthy subjects, patients with major depressive disorder [24], and patients with autonomic dysfunctions [25]. ECG, BP, and RSP were recorded continuously during supine rest (10 min), controlled breathing by means of a metronome (3 min; 16 cls/min), orthostatic stress (8 min; passive 60° head-up tilt), controlled breathing (16 cls/min) during the 60° head-up tilt (3 min) and a 10 min-period of post-orthostatic supine rest. The ECG was derived using a precordial lead, amplified by means of a polygraph (Nihon Kohden, Tokyo, Japan). BP was measured with a servoplethysmographic finger transducer (Finapres 2300 NIBP monitor, Ohmeda, Englewood, CO, USA). Thoracic RSP was measured with an impedance plethysmograph (Nihon Kohden, Tokyo, Japan). The signals were digitized on an IBM compatible Personal Computer (Commodore PC 60-III) equipped with an A/D converter (Advantech PC-LabCard model PCL-718). The sampling rate was 1024 Hz per channel. R-wave moments and R-R intervals were detected with an accuracy of 1 ms; per R-R interval the SBP and DBP were detected with an accuracy of 0.1 mmHg; and at each R-wave moment a sample of the RSP signal was taken as explained in section 2.1, these samples form the RSP time series. The time series were divided in periods of 3 to 5 minutes corresponding to the above mentioned experimental procedures. Of each period, the power spectrum and the DED, according to sections 2.1 and 3.1, were calculated.

4 Applications

4.1 Spontaneous cardiovascular fluctuations during supine rest

Figures 1, 2, and 3 present typical DEDs, computed from the corresponding HR, SBP, and RSP time series of a healthy subject during a 5 min period of supine rest (mean HR= 65.43 bpm, variation coefficient of the interbeat intervals: vc= 5.75%; mean SBP: 100.1 mmHg, vc= 4.57%). The overall spectra of HR and SBP (figures 1 and 2) illustrate the three relevant frequency components around 0.04 Hz (low), 0.1 Hz (mid), and around the dominant respiratory frequency at 0.30 Hz (high). The low frequencies (<0.06 Hz) of the DED of the HR and SBP time series show non-

stationary fluctuations in both amplitude and frequency (figures 1 and 2). The mid frequency fluctuations around 0.1 Hz of the DED of both the HR and SBP time series are very irregular in appearance; some isolated areas of increased activity at corresponding time points are apparent, reflecting the coherence between HR and BP fluctuations in the mid frequency range. The non-stationary fluctuations of the DED of the RSP signal (figure 3) are reflected at the corresponding frequencies of the DEDs of the HR and SBP time series (figures 1 and 2, respectively) due to the respiratory modulation of vagal-mediated cardiac control (HR) and/or due to the mechanical effects of breathing (SBP). The DEDs of the HR, SBP and RSP time series nicely reflect the different frequency components within short-term cardiovascular fluctuations, but they also illustrate that even within a period of several minutes and during a 'stationary' situation of supine rest, complex time-related changes do occur.

4.2 Clinical example illustrating interference and correction of cross terms

The necessity to correct for cross terms in order to interprete time-frequency relationships accurately is illustrated by an example of a patient with pure autonomic failure (PAF). Patients with PAF suffer from a complete or almost complete failure of both the sympathetic and the parasympathetic nervous system, resulting in dramatic reductions of both HR and BP variability [25]. Figure 4 presents the uncorrected discrete WVD (DWVD), based on an IBI sequence of a patient with PAF during a 5 min period of supine rest (mean HR=67.3 bpm, vc= 0.66%). Although the total power of the overall spectrum of the IBI sequence is low (figure 4), two frequency bands still are apparent: one peaks at about 0.03 Hz, the other peaks at the respiratory frequency at about 0.2 Hz. The fluctuations at about 0.4 Hz are harmonic frequencies of the respiratory frequency. Frequencies at 0.1 Hz are completely absent, due to the strongly diminished sympathetic tone in these patients. The DWVD does show the frequencies at 0.03, 0.2 and 0.4 Hz, but halfway the low and respiratory peaks and halfway the respiratory peak and the peak of the harmonic frequencies, two highly irregular bands are visible: the ghost curves or cross terms (section 2.4). Notice that there is no activity at the corresponding frequencies in the overall spectrum.

Figure 5 presents the DED computed from the same IBI sequence: most of the cross terms are disappeared due to the procedures as described in section 2.4. The relevant frequency bands are now clearly represented in the time-frequency distribution. Especially in subjects with autonomic failure, where evaluation of minimal fluctuations in cardiovascular signals may have clinical relevance, adequate suppression of cross terms is an essential feature of a time-frequency distribution.

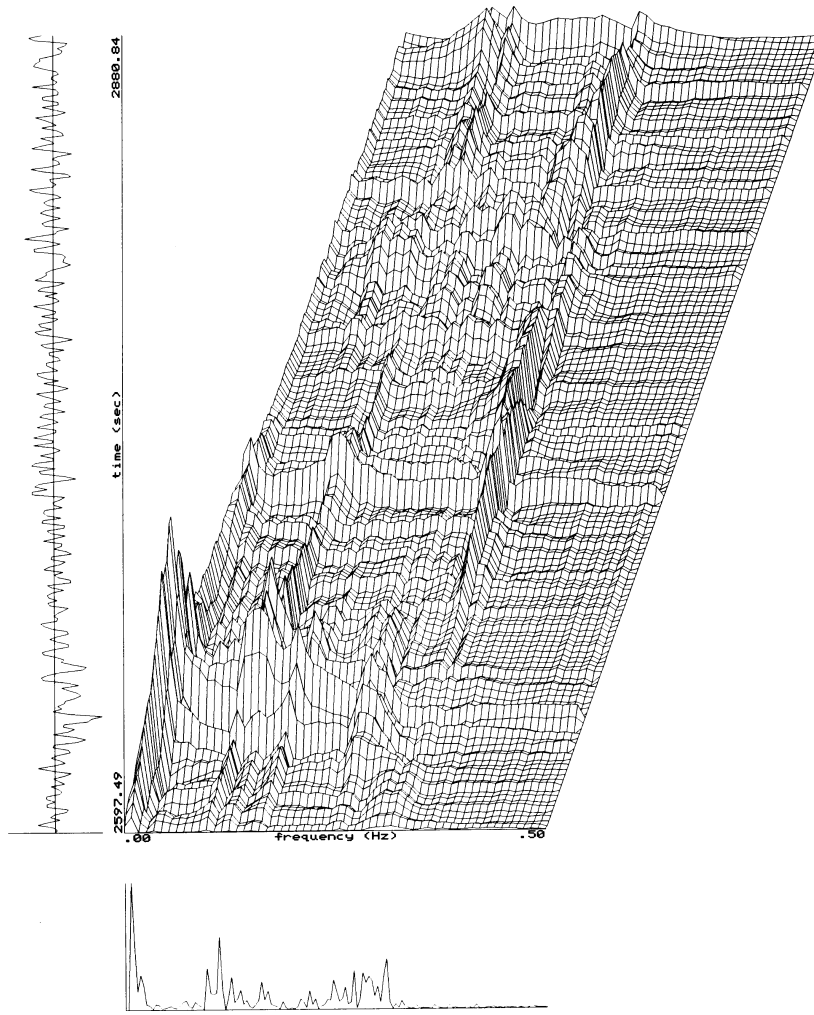

Figure 1: DED of a non-equidistantly sampled HR time series (300 sec in length) of a healthy subject during supine rest. The abcisses is the frequency axis and the ordinate is the time axis. Along the ordinate, the raw IBI-series is shown in the time domain. Along the abcisses, the power spectral density (spectrum) of the whole time series is presented. The scale of the spectrum, in this figure and the next figures, is always equal to the maximal component in the spectrum; in this case the scale is 0.12 sec^{-2}/Hz.

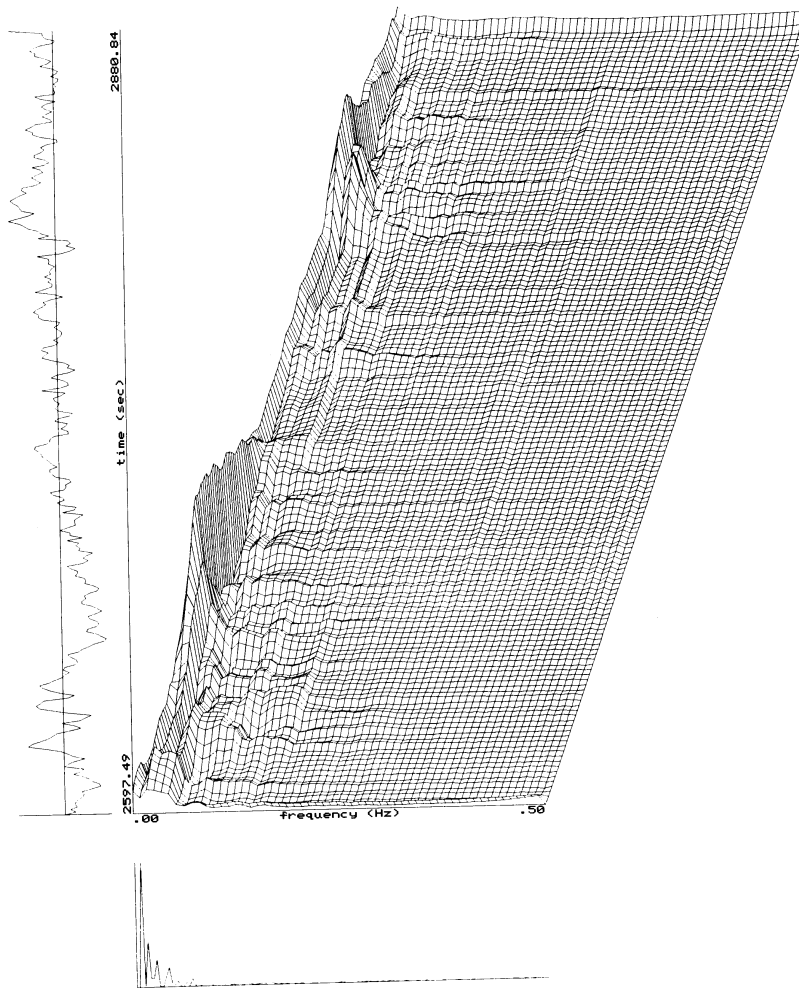

Figure 2: DED of a non-equidistantly sampled SBP time series for the same subject and time segment as presented in figure 1 (see figure 1 for explanation of abcisses and ordinate). The scale of the spectrum is 2167.89 $mmHg^2/Hz$.

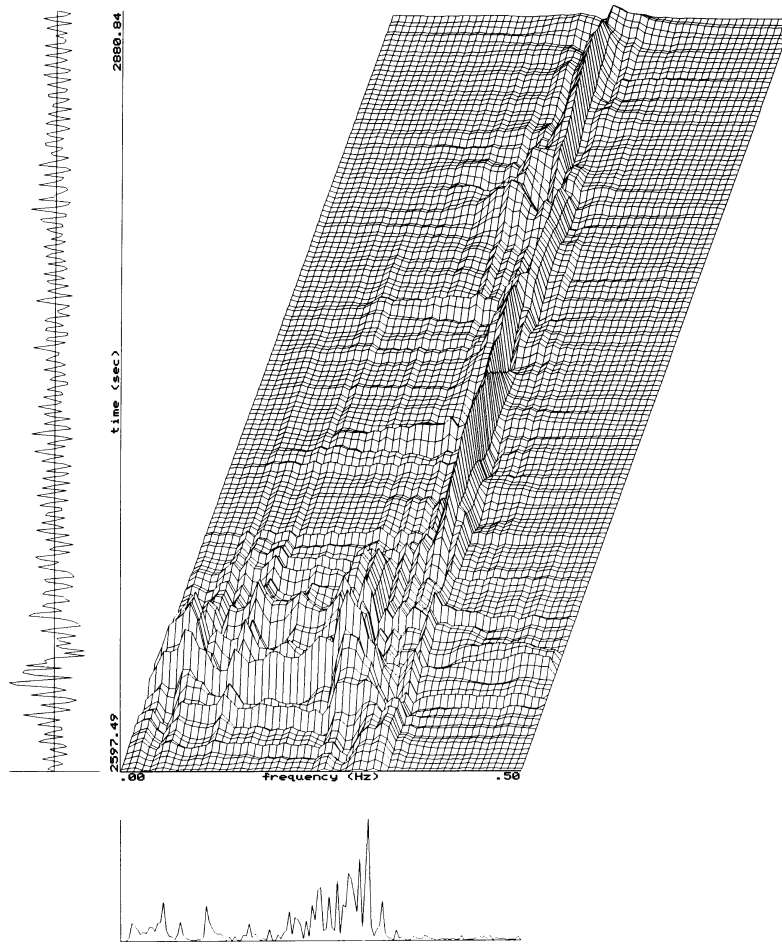

Figure 3: DED of a non-equidistantly sampled RSP time series of the same subject and time segment as presented in figure 1.

4.3 Specific examples of non-stationary time-frequency relationships

1a) Respiratory modulation of HR variability

In certain situations, interpretation of overall spectra of HR (and BP) variability may lead to erroneous conclusions if there is no information available of the respiratory signal. Figures 6 and 7 illustrate the DEDs from corresponding HR and RSP time series of a depressed patient during a 4 min period of supine rest. The overall spectrum of the HR time series (figure 6; mean HR=68.38 bpm, vc=13.1%) shows two clear broad-band frequencies: one around 0.1 Hz, a possible reflection of sympathetic-mediated processes, and one around 0.25 Hz, reflecting respiratory-linked variations due to vagal-mediated cardiac control. The corresponding DED illustrates a sudden shift from slow to faster frequencies, suggesting a dramatic change in sympathetic modulation. However, as can be observed in figure 7, the corresponding respiratory signal shows a change from a slow breathing frequency (about 0.1 Hz) to a faster breathing frequency (0.18-0.22 Hz). This time-related change is evident in the DED, whereas the overall spectrum shows the two broad-band peaks corresponding to the change in breathing frequency. Therefore, in this example, both peaks in the HR spectrum primarily reflect respiratory-linked vagal activity.

1b) Cardiac arrhythmias

The DED of an IBI sequence of a depressed patient treated with the tricyclic antidepressant imipramine is presented in figure 8 (mean HR=79.74 bpm, vc=2.7%). The IBI sequence was derived from a 4 min period of supine rest and reflects a brief episode of supraventricular cardiac arrhythmias. This brief period of arrhythmias affects all frequency components in the DED due to the rapid fluctuations in the successive IBI lengths. Furthermore, there appears a high peak around the Nyquist frequency in the DED. This peak is also visible in the overall spectrum of the IBI sequence, and interferes greatly with the respiratory-related high frequencies. Just before and during the arrhythmic period, there is a slow trend in the IBI sequence. In the DED, this trend appears as a high peak in the low frequency range. In the spectrum, the low frequency peak is primarily caused by this temporary change. Notice the effect of the isolated arrhythmic artefacts later on in the IBI sequence. The delta-like peaks affect all frequency components in the DED. At the crosspoints with the respiratory-related frequencies, the two components are superponated. Cardiac arrhythmias have a major impact on homeostatic cardiovascular processes as reflected in HR and BP variability; this example illustrates the extent to which isolated grouped arrhythmias disturb time-frequency distributions.

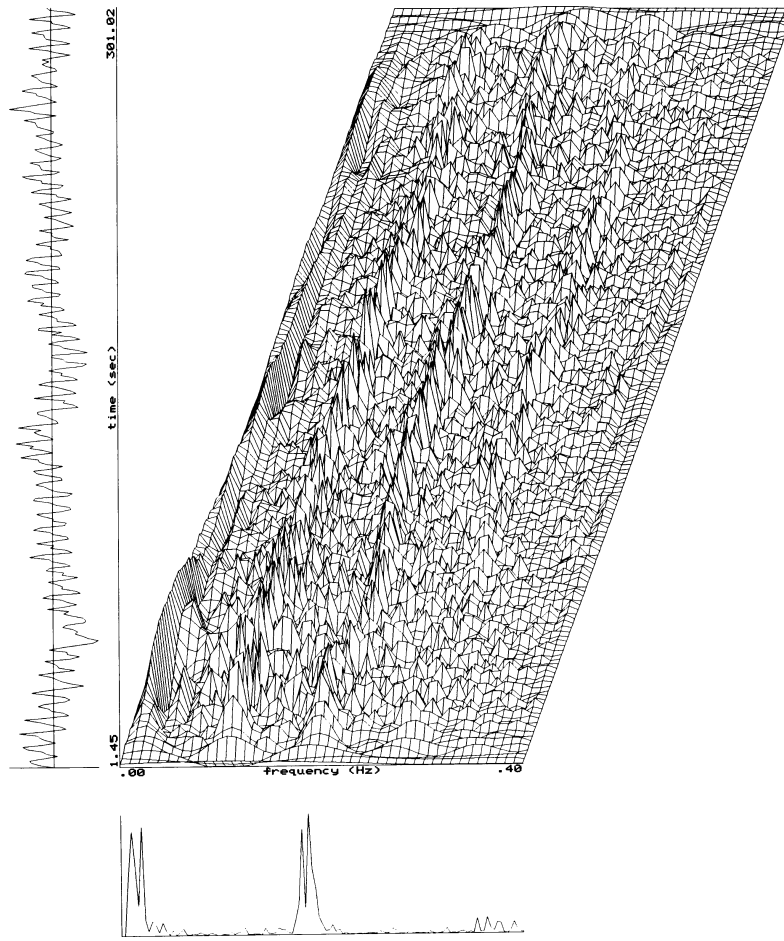

Figure 4: DWVD of a non-equidistantly sampled IBI time series of a patient with PAF during 5 min of supine rest. The scale of the spectrum is 0.0011 sec^2/Hz. The figure is very irregular due to the cross terms. Note the two striking cross term bands.

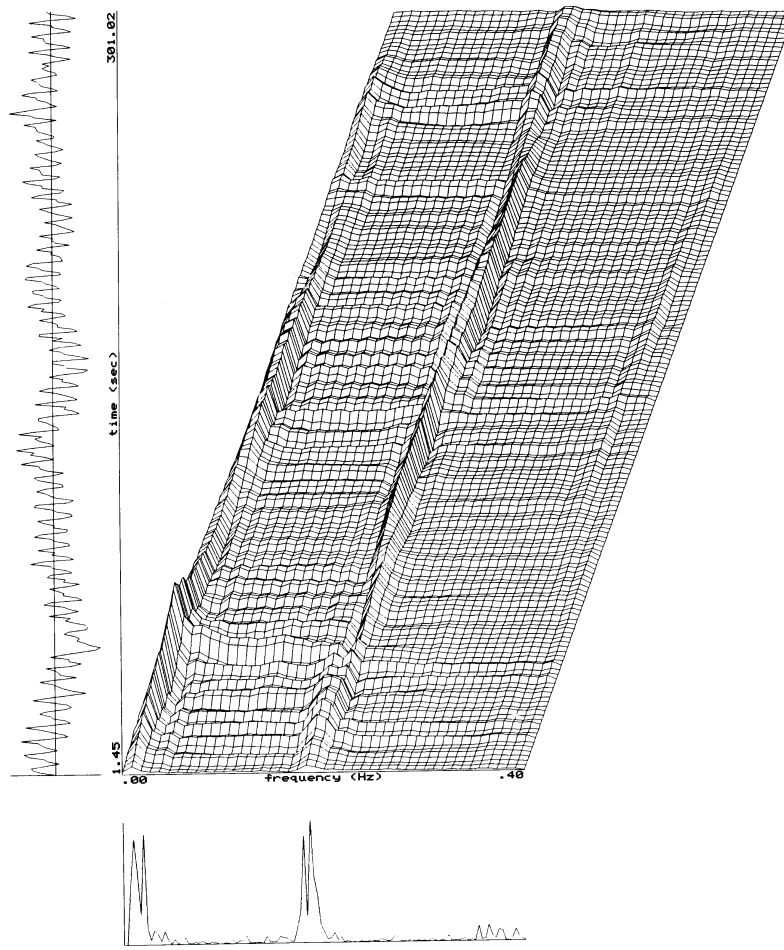

Figure 5: DED of the same IBI time series as in figure 4. The cross terms are almost disappeared due to the smoothing effect of the ED.

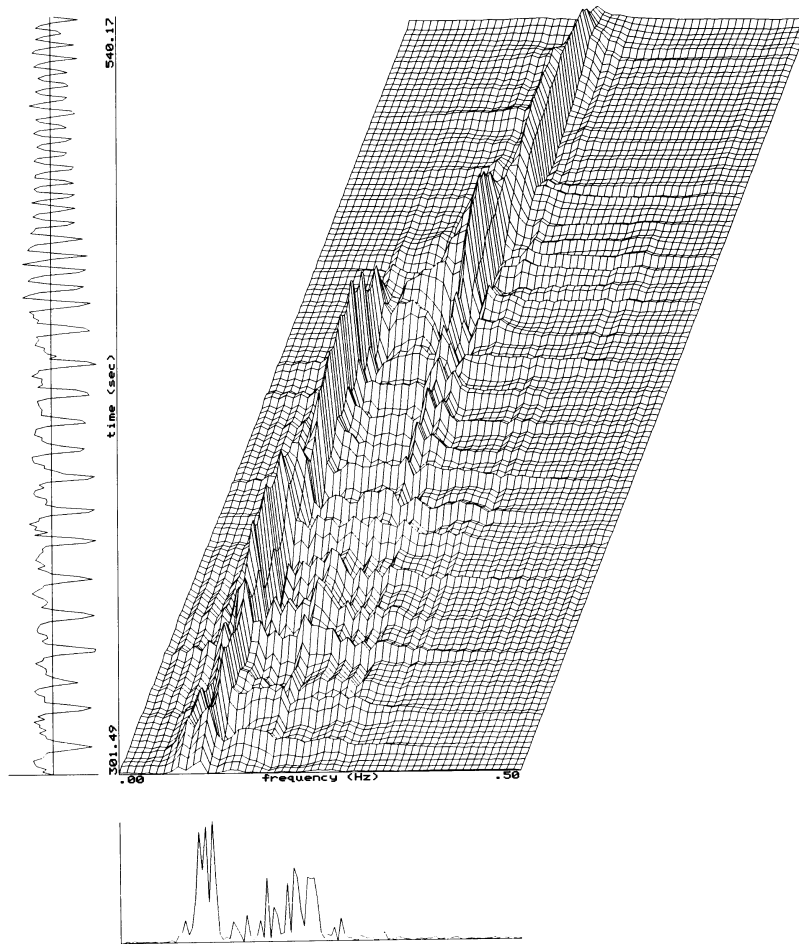

Figure 6: DED of a non-equidistantly sampled HR time series of a depressed patient during 4 min of supine rest. The scale of the spectrum is 0.49 sec^{-2}/Hz.

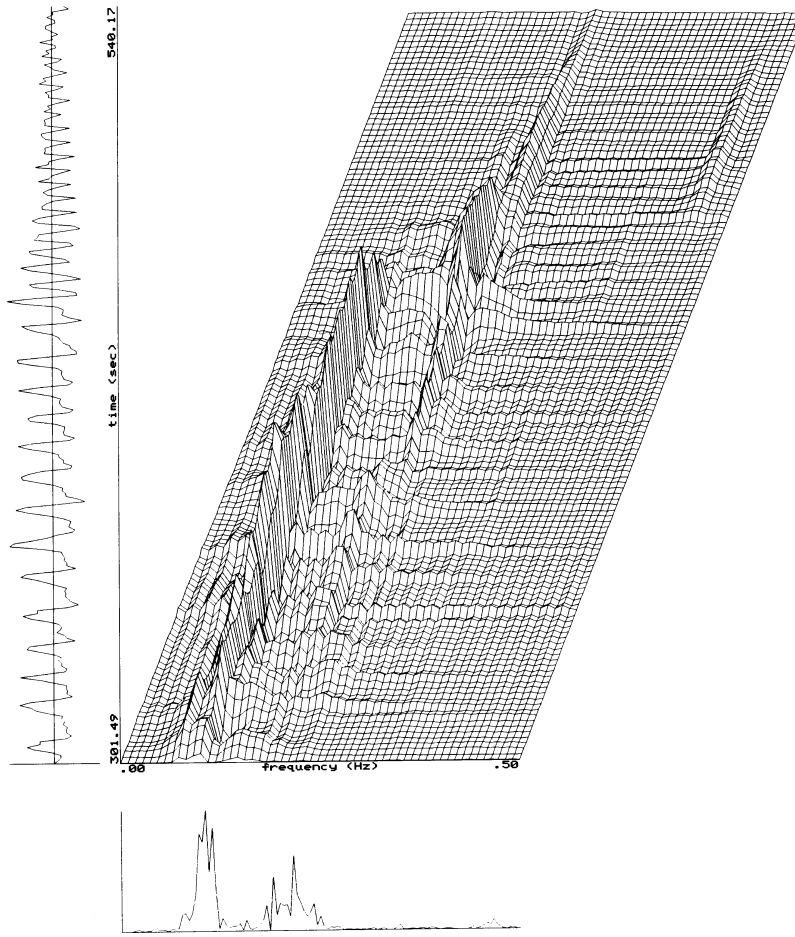

Figure 7: DED of the RSP time series of the same subject and time segment as presented in figure 6. Note the sudden shift from slow to faster frequencies.

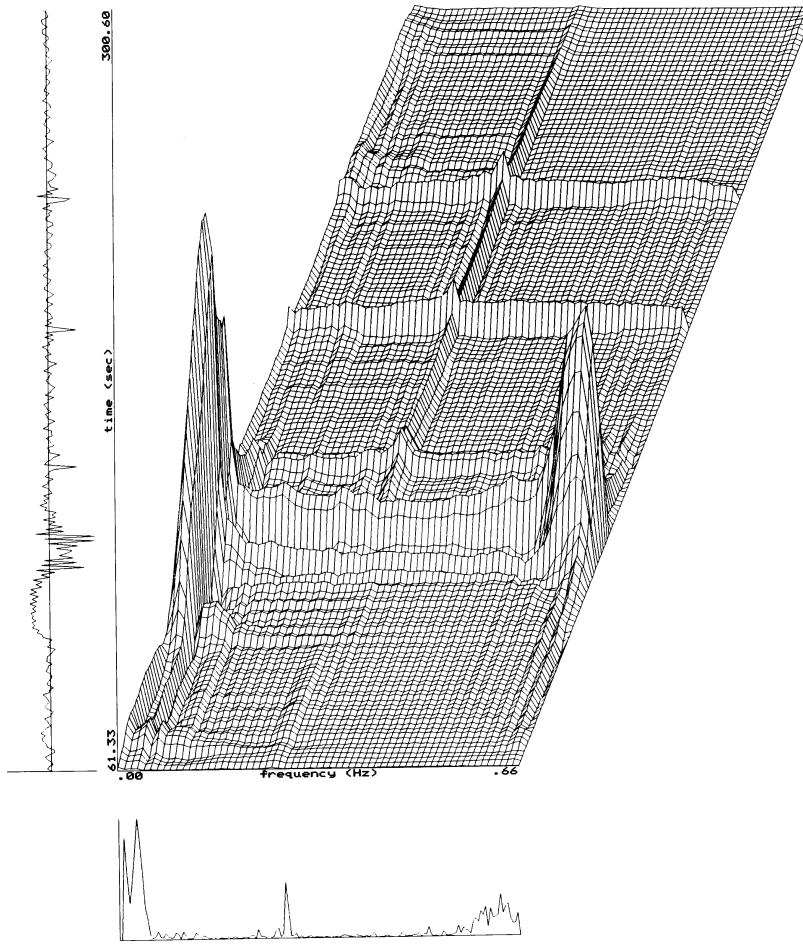

Figure 8: DED of an IBI time series of a depressed patient during 4 min of supine rest. The scale of the spectrum is 0.0095 sec^2/Hz.

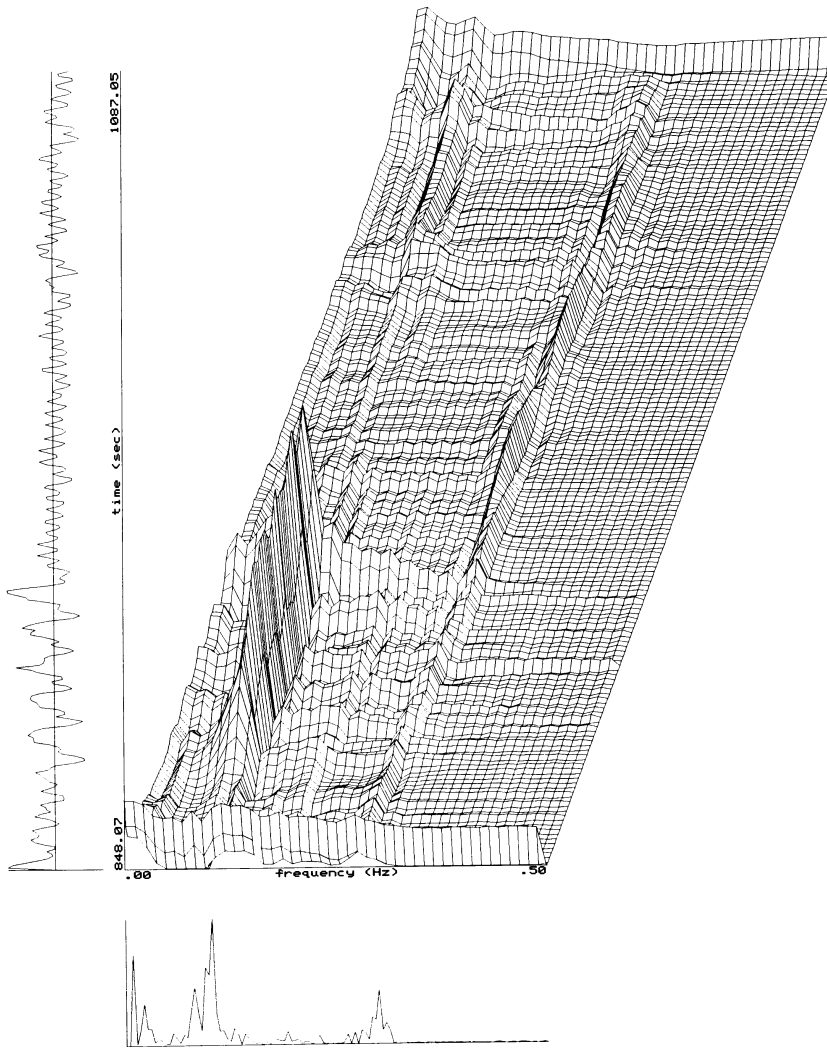

Figure 9: DED of a SBP time series of a depressed patient dureing 4 min of head up tilt. The scale of the spectrum is 767.11 $mmHg^2$/Hz. The initial cardiovascular reaction to the head up tilt is most prominent in the frequency components around 0.1 Hz.

1c) Adjustments to sudden situational changes

In figure 9, the SBP sequence of a depressed subject reflects the initial cardiovascular reaction to the 60° head-up tilt procedure (mean SBP= 127.2 mmHg, vc= 4.20%). In the DED, the respiratory-related high frequencies are apparent throughout the entire procedure. However, the transition from supine posture to passive standing causes a momentary increase in activity around 0.1 Hz, as an indication of an increase in sympathetic tone, which is evident also in the DED. However, its reflection in the overall spectrum erroneously suggests a sustained presence of these periodicities during the entire period. The DED illustrates that the patient gets accustomed to the standing position: the activity around 0.1 Hz diminishes rapidly and after that the DED shows some isolated moments of activity at these frequencies. This example shows that initial cardiovascular adjustments to sudden situational changes can be visualized in detail by means of a DED.

5 Discussion

In this paper, an implementation to apply the exponential distribution to non-equidistantly sampled cardiovascular time series has been given. We used the methods of Rompelman [5] and Mulder [6] to transform the non-equidistantly sampled cardiovascular time series into equidistant time series. This enabled us to calculate the DED of HR as well as IBI time series. Furthermore, using the CZT enabled us to calculate the Fourier transform of time series with lengths not necessarily equal to a power of two.

The ED is a modified WVD. Implementations of the DWVD and/or DED have been discussed previously by Martin & Flandrin [26], Chester [27], Boashash & Black [18], Sun et al. [28], Boashash & Reilly [23]. A method to suppress cross terms in a DWVD has been discussed by Martin & Flandrin [26]. They used a symmetric normalized time window and a time smoothing function. The effect of the time window is smoothing of the WVD in the frequency direction; thus, it will also spread out the autoterms. The effect of the smoothing function is a reduction of the cross terms, but it has also a smoothing effect on the autoterms in the time direction. Therefore, the implementation of the DWVD by Martin & Flandrin does not satisfy the properties P3-P8 (section 2.3). Novak & Novak [15] applied the DWVD, using FFT techniques, to IBI, SBP, DBP, and RSP time series, each time series linearly interpolated to an equidistant time series. They implemented the method of Martin & Flandrin to correct for cross terms, using a computation algorithm of Peyrin & Prost [29]. We employed the ED because it has certain advantages over the forementioned

method: the ED satisfies the advocated properties P1-P6 (section 2.3) for TFDs, for all values of σ. When the smoothing effect is too large, i.e. small σ ($\sigma \leq 1$; [16]), the autoterms and the components in the time direction will be spread noticeably. Thus, P7 and P8 will not be satisfied. If σ is sufficiently large ($\sigma > 1$) then the ED will approximately satisfy properties P7 and P8 [14]. Furthermore, for increasing σ, the ED will become approximately equal to the WVD. According to Choi & Williams, a good choice of σ will be found between 0.1 and 10. Our DED examples of cardiovascular time series, with $\sigma = 2$, show that the cross term suppression by the ED is satisfactory without disturbing the autoterms too much.

Our applications illustrated the potential of the ED to study time-frequency relationships of and between cardiovascular time series. Complex time-varying aspects of the relevant cardiovascular frequency components of HR, IBI, BP, and RSP time series could be made visible by means of the ED. Therefore, the ED can be an important aid to describe and interprete the complex dynamics of autonomic regulatory processes.

References

[1] Sayers BMcA. Analysis of heart rate variability. Ergonomics 16: 17-32, 1973.

[2] Akselrod S, Gordon D, Madwed JB, Snidman NC, Shannon DC, and Cohen RJ. Hemodynamic regulation: investigation by spectral analysis. Am J Physiol 249: M867-M875, 1985.

[3] Tulen JHM, Smeets FML, Man in 't Veld AJ, Van Steenis HG, Van de Wetering BJM, and Moleman P. Cardiovascular variability after clonidine challenge: assessment of dose-dependent temporal effects by means of spectral analysis. Journal of Cardiovascular Pharmacology, 22: 112-119, 1993.

[4] Tulen JHM, Man in 't Veld AJ, AM van Roon, Moleman P, Van Steenis HG, Blankestijn PJ, and Boomsma F. Spectral analysis of hemodynamics during infusions of epinephrine or norepinephrine in men. Journal of Applied Physiology, 76(5): 1914-1921, 1994.

[5] Rompelman O. Spectral analysis of heart-rate variability. In: Psychophysiology of Cardiovascular Control. Orlebeke JF, Mulder G, Van Doornen LJP (eds). New York & London: Plenum Press, pp:315-331, 1985.

[6] Mulder LJM. Assessment of cardiovascular reactivity by means of spectral analysis (Ph.D. Thesis). Groningen: University of Groningen, 1988.

[7] Van Steenis HG, Tulen JHM, and Mulder LJM. Heart rate variability spectra based on non-equidistant sampling: the spectrum of counts and the

instantaneous heart rate spectrum. Medical Engineering and Physics 16:355-362, 1994.

[8] Parati G, Castiglioni P, di Renzo M, Omboni S, Pedotti A, and Mancia G: Sequential spectral analysis of 24-hour blood pressure and pulse interval in humans. Hypertension 16: 414-421, 1990.

[9] Wigner E. On the quantum correction for thermodynamic equilibrium. Phys Rev 40: 749-759, 1932.

[10] Ville J. Théorie et application de la notion de signal analytique. Cables et Transmissions 2A(1): 61-74, 1948.

[11] Claassen TACM and Mecklenbräuker WFG. The Wigner distribution - a tool for time-frequency signal analysis, part I: continuous-time signals. Philips Res J 35: 217-250, 1980.

[12] Claassen TACM and Mecklenbräuker WFG. The Wigner distribution - a tool for time-frequency signal analysis, part II: discrete-time signals. Philips Res J 35: 276-300, 1980.

[13] Boashash B. Time-frequency signal analysis. In: Advances in Spectrum Analysis and Array Processing, Vol. 1. S. Haykin, Ed. Englewood Cliffs, NJ: Prentice Hall, pp:418-517, 1991.

[14] Cohen L. Time-Frequency Analysis. Englewood Cliffs, NJ: Prentice Hall Inc, 1995.

[15] Novak P and Novak V. Time/frequency mapping of the heart rate, blood pressure and respiratory signals. Medical & Biological Engineering & Computing 31(2): 103-110, 1993.

[16] Choi HI and Williams WJ. Improved time-frequency representation of multicomponent signals using exponential kernels. IEEE Trans Acoust Speech Signal Proc ASSP-37: 862-871, 1989.

[17] Bendat JS and Piersol AG. Random Data, Analysis and Measurements Procedures, 2nd edition. New York: John Wiley and Sons, Inc., 1986.

[18] Boashash B and Black PJ. An efficient real-time implementation of the Wigner-Ville distribution. IEEE Trans Acoust Speech Signal Proc ASSP-33: 1611-1618, 1987.

[19] Boashash B. Note on the use of the Wigner distribution for time-frequency signal analysis. IEEE Trans Acoust Speech Signal Proc ASSP-36: 1518-1521, 1988.

[20] Kootsookos PJ, Lovell BC, and Boashash B. A unified approach to the STFT, TFDs and instantaneous frequency. IEEE Trans. Signal Processing 40: 1971-1982, 1992.

[21] Allen JB and Rabiner LR. A unified approach to short-time Fourier analysis and synthesis. Proc IEEE 65: 1558-1564, 1977.

[22] Oppemheim AV and Schafer RW. Digital signal processing. Englewood Cliffs, NJ: Prentice-Hall Inc, 1975.

[23] Boashash B and Reilly A. Algorithms for time-frequency signal analysis. In: Time Frequency Signal Analysis – Methods and Applications, chapter 7. B. Boashash, Ed. Longman Cheshire, pp:163-181, 1992.

[24] Tulen JHM, Bruijn JA, De Man KJ, Pepplinkhuizen L, Van den Meiracker AH, and Man in 't Veld AJ. Cardiovascular variability in major depressive disorder and effects of imipramine or mirtazapine (org 3770). Journal of Clinical Psychopharmacology 16: 135-145, 1996.

[25] Van den Meiracker AH, Tulen JHM, Man in 't Veld AJ, Balk AHMM, Van Steenis HG, and Schalekamp MADH. Blood pressure and heart rate variability in clinical models of cardiac denervation, sympathicolysis and sympathico- and parasympathicolysis. J Hypertension, 11(suppl 5): S152-S153, 1993.

[26] Martin W and Flandrin P. Wigner-ville spectral analysis of nonstationary processes. IEEE Trans Acoust Speech Signal Proc ASSP-33(6): 1461-1470, 1985.

[27] Chester D. Discrete Wigner implementations. 1986 Int Symp Circuit and Syst Proc San Jose, 38-41, 1986.

[28] Sun M, Li CC, Sekhar LN, and Sclabassi RJ. Efficient computation of the discrete pseudo-Wigner distribution. IEEE Trans Acoust Speech Signal Proc ASSP-37: 1735-1742, 1989.

[29] Peyrin F and Prost RA. A unified definition for the discrete-time, discrete-frequency and discrete-time/frequency Wigner distribution. IEEE Trans Acoust Speech Signal Proc ASSP-34: 858-867, 1986.

CHAPTER 7
QUANTIFICATION OF THE DYNAMIC BEHAVIOR OVER TIME OF NARROW-BAND COMPONENTS PRESENT IN HEART RATE VARIABILITY BY MEANS OF THE INSTANTANEOUS AMPLITUDE AND FREQUENCY

Submitted

H.G. van Steenis[1], W.L.J. Martens[2], J.H.M. Tulen[1]

[1]Department of Psychiatry, Erasmus Medical Center Rotterdam
[2]PhyVision b.v., Gemert

Variability in heart rate sometimes shows oscillatory, sine-wave-like, or 'deterministic' properties whereas under different circumstances the signals look 'noisy' or 'irregular'. Three oscillatory narrow-band components have been postulated to occur in spontaneous variability of heart rate within a time-scale of several minutes: low (0.02-0.07 Hz), mid (0.07-0.15 Hz), and high (0.15-0.50 Hz). Reduction of these oscillations in disease states has been shown to be a powerful predictor of future clinical events and mortality.

By applying Fourier transforms to quantify these three components, an observation interval (or time window) of 2-5 minutes is usually chosen as a compromise to achieve an appropriate frequency-resolution. However, in this observation interval, the signal may be 'non-stationary', meaning that the statistical properties of the signals may change over time.

Given the fact of the three narrow-band components, this paper describes a method to derive the shortest possible observation interval for each of these components, which is inversely related to the bandwidth of these three components as given by the uncertainty principle of Gabor. For the high-frequency component, if a bandwidth of 0.35 Hz is postulated, such minimal observation interval σ_t translates into a time-resolution Δt of about 2.25 sec in the discrete time-domain. For the mid-frequency component, with a bandwidth of 0.08 Hz, this yields about 7.75 sec, respectively. If signal properties, such as amplitude (or envelope) and frequency, are computed at such proper and optimal time-resolution, adjacent points in time are independent in a statistical sense, that means that these properties then are instantaneous. In that case the amplitude and the frequency are called instantaneous amplitude and frequency. Computations over a shorter time interval yield adjacently dependent points in time; if computed over a longer time interval, properties will be averaged, i.e., smeared over time (as with Fourier analysis). This means that the presented method does not introduce redundancy (by interpolation) nor smearing over time, so the instantaneous properties then can be related to the underlying physiological model that reacts on (non) stationary internal and external circumstances.

Recalling that cardiovascular signals may show waxing and waning of oscillatory 'deterministic' and noisy 'irregular' properties in time, especially the oscillatory periods in time may be related to autonomic cardiac control processes. In this paper, in addition to the computation of the instantaneous amplitude and frequency, a method is introduced to compute an index of the instantaneous bandwidth for the narrow-band components as a means to separate the oscillatory and irregular periods in time.

1 Introduction

Heart rate variability is controlled by the autonomic nervous system and affected by external and internal factors, such as physical activities and locomotion, circadian rhythm and psychological influences. Furthermore, heart rate variability is altered in a variety of disease states; reduced variability has repeatedly been shown to be a powerful predictor of clinical events and mortality [e.g., 1,2].

The oscillatory sine-wave-like narrow-band fluctuations that occur in short-term heart rate variations originate from various sources in the autonomic cardiovascular control system. We mention three [3-12].

1) Fluctuations in peripheral vasomotor tone related to thermoregulation, renin-angiotensin system activity, or other processes. The period length of these fluctuations varies between 14-50 sec.

2) Oscillations due to the baroreflex control of peripheral resistance, with a period length of about 10 sec; these oscillations may reflect sympathetic processes. And

3) respiratory-related fluctuations, possibly reflecting cardiac parasympathetic (vagal) nervous activity; the period length of these fluctuations is about 3 sec.

These oscillatory fluctuations are called short-term fluctuations. Spectral analysis aims at characterizing such oscillations in the frequency domain; three spectral ranges or peaks can be discerned in:

1) the low-frequency range: 0.02-0.07 Hz;
2) the mid-frequency range: 0.07-0.15 Hz; and
3) the high-frequency range: 0.15-0.50 Hz.

The conventional observation interval or time window over which spectral analysis of short-term fluctuations is performed varies between 2-5 min, i.e., intervals long enough to measure the slow fluctuations of the low-frequency range. But even in a time interval as short as 2-5 min, the frequency content of heart rate varies considerably [13]. Apparently, the spontaneous fluctuations are too rapid to be captured in observation intervals, even as short as a few minutes.

In general, heart rate variability is a dynamic ‘non-stationary’ signal [14]. We use the term ‘non-stationary signal’ in the sense of statistical properties of the signal changing over time. This means that the characteristic spectral peaks, low, mid, and high, vary in time in their position on the frequency axis (frequency), energy (or amplitude), as well as in the spread or width of their peak (bandwidth). One can imagine an ‘instantaneous spectrum’ [15,16] at each instant in time. These ‘instantaneous spectra’ visualize the time-varying characteristics of a signal. One way to obtain these is by means of a time-frequency distribution, such as the Wigner-Ville

distribution [15,17] or the Exponential Distribution [18,19]. In this paper, we provide a method to compute the time-varying 'instantaneous spectrum' quantitatively by means of the instantaneous amplitude (IA), frequency (IF), and the instantaneous bandwidth (IB). The method only applies to monocomponent signals of which the energy is concentrated in one spectral peak. To approximate a monocomponent signal, as close as possible, we decompose the heart rate variability signal with a three zero-phase band-pass filters into the three spectral peaks of interest: low, mid, or high. The time-varying properties of each of the three components can now be described by means of the IA and the IF. The squared IA is a measure of the instantaneous power or energy per unit time. The IF defines the frequency location of the spectral peak. The spread of the spectral peak is measured by means of the IB, being the associated standard deviation of the average IF. In our case, the so-called instantaneous bandwidth coefficient (IBC) is computed as an index for the IB. The IBC may serve as a time-varying segmentator of oscillatory versus irregular periods: low values indicate oscillatory properties, high values indicate irregularities.

Our method was developed to gain information on the functioning of the sympathetic and parasympathetic processes within the cardiovascular control system on the highest possible time-resolution as given by the uncertainty principle of Gabor. This time-resolution is different for the low-, mid-, and high-frequency components, that is, it is inversely related to the bandwidth of these three components. It means that the method does not introduce redundancy (by interpolation) or smearing over time. Hence the parameters IA and IF of the fluctuations in low-, mid-, and high-frequency bands can now be totally related to external and internal time-varying processes. For instance, under ambulatory conditions, the fluctuations can be related to body posture (lying, sitting, standing) and physical activities (walking), whereby also the time-varying spectral details of transitions between postures and activities can be examined. In the case of measurements in a controlled laboratory environment, the fluctuations can be related to the effects of psychological, physical, or pharmacological challenge tests. In addition, a detailed description of IA and IF, in relation to the IBC, in disease states associated with altered heart rate variability will contribute to an increased understanding of the processes involved in the triggering of clinical events or mortality.

In this paper we limit ourselves to the application of the method to the mid- and high-frequency band of heart rate variability time series. However, the method was developed to be applied to the three narrow-band (low-, mid-, and high-frequency) components of cardiovascular time series and also to respiratory signals.

2 Theory of instantaneous properties of narrow-band signals

In a first approximation, the instantaneous amplitude or envelope and instantaneous frequency of a narrow-band oscillatory signal can be computed by rectification followed by smoothing and by zero-crossing techniques respectively. The undistorted envelope, that is the removal of the carrier oscillation frequency, can only be accomplished via complex demodulation which is based on the so-called complex analytical signal. This is explained in the next section.

2.1 Analytical signals and the instantaneous frequency

The (complex) analytical signal $\hat{s}(t)$ [20] associated with a real signal $s(t)$ allows us to define the instantaneous amplitude, phase, and frequency of the real signal $s(t)$. The real part of the analytical signal $\hat{s}(t)$ equals the original real signal $s(t)$. The imaginary part is obtained from the real signal by means of the Hilbert transform [16,20,21]. The envelope or IA $a(t)$ and the instantaneous phase (IP) $\varphi(t)$ are defined as the modulus and the argument of the complex number $\hat{s}(t)$, respectively. The analytical signal can now be written in polar form $\hat{s}(t) = a(t)e^{j\varphi(t)}$ and visualized as a moving vector in the complex plane. Furthermore, the IF can be defined as the rate of change of the phase angle $\varphi(t)$ [15,16,21]:

$$f_i(t) = \frac{1}{2\pi}\frac{d\varphi}{dt}(t). \tag{1}$$

If the spectrum of $a(t)$ is contained in a frequency region $-\omega_1 < \omega < \omega_1$ and the spectrum of $\cos\varphi(t)$ is zero for $\omega \le \omega_1$, i.e., reflecting a slowly varying amplitude modulation and a fast phase modulation, it can be proven that the analytical signal $\hat{s}(t)$ is a reliable and natural representation of the real signal $s(t)$ [16,21]. This means that $a(t)$, $\varphi(t)$, and $f_i(t)$ represent the IA, IP, and IF, respectively, of the real signal $s(t)$. Furthermore, Rihaczek [22] proved that under the same conditions, the time-varying signal's energy is in frequency concentrated in a single narrow frequency range at the IF $f = f_i(t)$. See appendix A.1 for a further explanation of the analytical signal and the Hilbert transform.

Suppose that locally (in time) the analytical signal $\hat{s}(t)$ is 'multicomponent' [16,18,21]. This means that the signal's energy is locally distributed in two or more frequency peaks. In that case the IF has no physical meaning. Cohen [21 p.40] mentioned a few inconsistencies that may occur. For instance, the computed IF may not be in the signal's spectral region, even if the signal is band-limited. It may become negative, though the signal is analytical. Therefore, the IF has only meaning for 'monocomponent' signals, for which there is only one time-varying spectral

concentration. The IF has no meaning for multicomponent signals with more than one spectral concentration. See appendix A.3 for a further description of the concepts multicomponent and monocomponent.

Concluding, our model signal is a band-limited, monocomponent, and analytical signal. Of this signal the IF can be computed reliably and is meaningful. Furthermore, the spectral peak is concentrated at the IF on the frequency axis.

2.2 The Wigner-Ville distribution and the instantaneous frequency

A means to study the time-varying energy content and the time-varying IF is the Wigner-Ville distribution. Ville introduced the Wigner-Ville distribution of an analytical signal $\hat{s}(t) = a(t)e^{j\varphi(t)}$ [15,17,21,23,24,25]:

$$W(t,f) = \int_{-\infty}^{+\infty} \hat{s}\left(t + \frac{\tau}{2}\right) \cdot \hat{s}^*\left(t - \frac{\tau}{2}\right) \cdot e^{-2\pi j f \tau} d\tau .$$

The Wigner-Ville distribution is a joint time-frequency distribution of an analytical signal $\hat{s}(t)$, which gives insight in the signal's frequency distribution at every instant t. The Wigner-Ville distribution can help to analyze the structure of the components of $\hat{s}(t)$. If the signal is multicomponent, the multiple components will cause cross terms in the Wigner-Ville distribution [21,23]. In our case the signal is monocomponent and band-limited, so there is only one component in the time-frequency plane.

At each instant t, the frequency distribution $W(t,f)$ constitutes an 'instantaneous spectrum' [15,16]. The area of $W(t,f)$ at time t is the instantaneous power or energy per unit time and equals the squared IA [21,23]:

$$a^2(t) = \int_{-\infty}^{+\infty} W(t,f)\, df .$$

The IF of an analytical signal $\hat{s}(t)$ is defined as the derivative of the IP $\varphi(t)$ (equation (1)). For a sinusoidal signal, this definition is unambiguous. The sinusoid is a sharp delta peak in the time-frequency plane at the IF and has no spread, i.e., there is only one frequency present, namely at the IF. If the signal has (locally) a stochastic component, this definition becomes harder to interpret because the frequency content is not concentrated in one delta peak. However, Ville showed that the conditional average $\langle f \rangle_t$ of the existing frequency components at a certain time t equals the derivative of the phase at that time, i.e., the IF at time t is the first conditional moment of the Wigner-Ville distribution with respect to frequency at time t [15,21,23]:

$$\langle f \rangle_t = \frac{\int_{-\infty}^{+\infty} f \cdot W(t,f)\, df}{\int_{-\infty}^{+\infty} W(t,f)\, df} = \frac{1}{2\pi}\varphi'(t) = f_i(t) \qquad (2)$$

The IF of a signal with a stochastic component can now be defined unambiguously as the first conditional moment of the Wigner-Ville distribution. The IF of this signal will have a spread due to the stochastic component. The width (in the frequency direction) of the spread is called the instantaneous bandwidth (IB). To say this in other words: the conditional standard deviation $\sigma_{f|t}$ or spread of the conditional average $\langle f \rangle_t = f_i(t)$, can be interpreted as the IB at time t, and is defined by the second conditional moment [16,21,23,26]:

$$\sigma_{f|t}^2 = \frac{\int_{-\infty}^{+\infty} (f - f_i(t))^2 \cdot W(t,f)\, df}{\int_{-\infty}^{+\infty} W(t,f)\, df} \tag{3}$$

Equations (2) and (3) are valid for other joint time-frequency distributions [e.g., 21]. However, the result $\sigma_{f|t}$ is dependent on the time-frequency distribution used [21]. In case of the Wigner-Ville distribution of $\hat{s}(t) = a(t)e^{j\varphi(t)}$, equation (3) results in [21,26]:

$$\sigma_{f|t}^2 = \frac{1}{8\pi^2} \cdot \left(\frac{a'(t)}{a(t)} \right)^2 - \frac{1}{8\pi^2} \cdot \frac{a''(t)}{a(t)}.$$

This result is unsatisfactory because it can become negative. Cohen and Lee [26] presented an expression for the IB of a complex signal $z(t) = a(t)e^{j\varphi(t)}$ that depends only on the IA $a(t)$:

$$B_i^2(t) = \frac{1}{4\pi^2} \cdot \left(\frac{a'(t)}{a(t)} \right)^2. \tag{4}$$

They provided several arguments that this is a reasonable measure of the conditional standard deviation of the IF, i.e., $\sigma_{f|t}^2 = B_i^2(t)$. If there is no amplitude modulation ($a(t) = c$) at time t, then there exists only one frequency at that time and the IB is zero, i.e., no spread. Amplitude modulation ($a'(t) \neq 0$) at time t will result in a spread $B_i(t)$ of frequencies and the average of this spread is the IF $f_i(t)$ [24,26].

2.3 The local autocorrelation function

The local autocorrelation function of an analytical signal $\hat{s}(t) = a(t)e^{j\varphi(t)}$ is defined by [21 p.137, 25 p.948, e.g., 27 p.445]:

$$R_{\hat{s}\hat{s}l}(t,\tau) = \hat{s}\left(t + \frac{\tau}{2} \right) \cdot \hat{s}^*\left(t - \frac{\tau}{2} \right). \tag{5}$$

(Note that this definition is in general valid for complex signals $z(t) = a(t)e^{j\varphi(t)}$, but we restrict ourselves to analytical signals.) The instantaneous spectrum is the Fourier

transform of the local autocorrelation function; they are linked with each other by means of the Wiener-Khinchine theorem [27].

Both the IF $f_i(t)$ and the IB $B_i(t)$ of $\hat{s}(t)$ can be written in terms of the local autocorrelation function. In case of the IF, an approximation for $f_i(t)$ is obtained by substituting $\hat{s}(t) = a(t)e^{j\varphi(t)}$ in $R_{\hat{s}\hat{s}l}(t,\tau)$ for $\tau = h$:

$$R_{\hat{s}\hat{s}l}(t,h) = a\left(t+\frac{h}{2}\right)a\left(t-\frac{h}{2}\right)\cdot e^{j\left(\varphi\left(t+\frac{h}{2}\right)-\varphi\left(t-\frac{h}{2}\right)\right)}$$

The argument of $R_{\hat{s}\hat{s}i}(t,h)$ is:

$$\arg R_{\hat{s}\hat{s}l}(t,h) = \varphi\left(t+\frac{h}{2}\right)-\varphi\left(t-\frac{h}{2}\right) \approx h\cdot\varphi'(t).$$

Using equation (1) it follows that [28-31]:

$$f_i(t) \approx \frac{1}{2\pi}\arg\ R_{\hat{s}\hat{s}l}(t,1) \tag{6}$$

Phase-shifts of $\pm 2\pi$ due to the ambiguity of the inverse tangent do not occur in (6) because the phase-shifts are canceled in the difference of the phases in the multiplication of the right-hand complex conjugated product factors in (5).

In case of the IB, expanding $R_{\hat{s}\hat{s}l}(t,h)$ gives us also an approximation for $B_i(t)$, using the fact that $a(t) \geq 0$:

$$1-\frac{\left|R_{\hat{s}\hat{s}l}(t,h)\right|}{\left|R_{\hat{s}\hat{s}l}(t,0)\right|} = 1-\frac{a\left(t+\frac{h}{2}\right)a\left(t-\frac{h}{2}\right)}{a(t)^2} \approx$$

$$\frac{a(t)^2-\left(a(t)+\frac{h}{2}\cdot a'(t)\right)\left(a(t)-\frac{h}{2}\cdot a'(t)\right)}{a(t)^2} = \frac{h^2}{4}\cdot\frac{a'(t)^2}{a(t)^2} \text{ (for small } h\text{).}$$

Comparing this result with equation (4), it follows that:

$$B_i^2(t) \approx \frac{1}{\pi^2}\left[1-\frac{\left|R_{\hat{s}\hat{s}l}(t,1)\right|}{\left|R_{\hat{s}\hat{s}l}(t,0)\right|}\right] \tag{7}$$

The right-hand expressions of (6) and (7) are estimates of the IF and the IB respectively. In practice, these estimates can lead to unsatisfactory results. Due to superimposed noise, the estimate of $f_i(t)$ can make unpredictably large 'jumps'. Furthermore, it is not guaranteed that the estimate of $B_i(t)$ will always be positive,

especially if the signal becomes small. Substituting (5) in (7) will result in discontinuities whenever the IA $a(t)$ has zeros. Therefore, in the next section 2.4 another autocorrelation function will be defined that can be used in (6) and (7) instead of the local autocorrelation function to give better results.

2.4 The pseudo autocorrelation function

Returning to the Wigner-Ville distribution: if a lower frequency-resolution is acceptable, it is computationally more efficient to apply a time window to the signal. Let $w(\tau)$ be a time window, with $w(\tau)=0$ for $|\tau|>T_w/2$. By applying this window to the analytical signal $\hat{s}(t)$ at time τ, a windowed signal is obtained: $\hat{s}_w(t)=\hat{s}(t)\cdot w(t-\tau)$. The resulting Wigner-Ville distribution is called the pseudo Wigner-Ville distribution [23 p.456]:

$$W_w(t,f)=\int_{-\infty}^{+\infty}\hat{s}_w\left(t+\frac{\tau}{2}\right)\cdot\hat{s}_w^*\left(t-\frac{\tau}{2}\right)\cdot e^{-2\pi jf\tau}d\tau\,.$$

In analogy with the Wiener-Khinchine theorem [27] we use the pseudo Wigner-Ville distribution $W_w(t,f)$ to define an autocorrelation function which can be used in (6) and (7). For that purpose we need the squared envelope of each time-slice of the pseudo Wigner-Ville distribution. For a fixed time t, take the time-slice $W_{w,t}(f)$ at time t: $W_{w,t}(f)=W_w(t,f)$ for all f. Compute the analytical time-slice using the Hilbert transform (see appendix A.1):

$$\hat{W}_{w,t}(f)=W_{w,t}(f)+jHW_{w,t}(f).$$

According the Wiener-Khinchine theorem, the inverse Fourier tranform of the squared envelope of the time-slice $W_{w,t}(f)$:

$$R_{\hat{s}\hat{s}w}(t,\tau)=F_{f\to\tau}^{-1}\left|\hat{W}_{w,t}(f)\right|^2 \tag{8}$$

is an autocorrelation function, called the pseudo autocorrelation function (the notation of equation (8) is explained in appendix A.4). The Wiener-Khinchine theorem states that the autospectral density function $S_{xx}(f)$ and the autocorrelation function $R_{xx}(\tau)$ of a signal $x(t)$ are a Fourier pair: $R_{xx}(\tau)=F_{f\to\tau}^{-1}S_{xx}(f)$. The Wigner-Ville distribution is not a true density, because it can become negative, so the squared modulus of the analytical time-slice is taken, in analogy with the autospectral density function $S_{xx}(f)$, which in turn is the squared modulus of the Fourier transform of $x(t)$.

Subsequently, the pseudo autocorrelation function $R_{\hat{s}\hat{s}w}(t,\tau)$ is used in the equations (6) and (7) to define the following estimates of the IF and the IB:

$$f_w(t) = \frac{1}{2\pi} \arg R_{\hat{s}\hat{s}w}(t,1), \tag{9}$$

$$B_w^2(t) = \frac{1}{\pi^2}\left[1 - \frac{\left|R_{\hat{s}\hat{s}w}(t,1)\right|}{\left|R_{\hat{s}\hat{s}w}(t,0)\right|}\right]. \tag{10}$$

Due to the applied window, the pseudo autocorrelation function $R_{\hat{s}\hat{s}w}(t,\tau)$ is not an instantaneous value and therefore (9) and (10) are not instantaneous measures: they are 'local estimators of the instantaneous frequency and the instantaneous bandwidth'. The 'smoothing' effect of the window is apparent. The use of a windowed signal diminishes the effect of noise and stabilizes $f_w(t)$. However, under certain conditions imposed on the signal and the time window, the estimates will be instantaneous. Sections 3.2, 3.3, and 3.4 describe the combination of a band-pass filter, which is used to make the signal band-limited, and a time window chosen according to the uncertainty principle of Gabor, which will make $R_{\hat{s}\hat{s}w}(t,\tau)$ instantaneous. Using this instantaneous pseudo autocorrelation function, the estimates $f_w(t)$ and $B_w(t)$ are well-behaving instantaneous measures of the IF and IB.

3 Method

Under certain assumptions, the theory of section 2 can be applied to heart rate variability. Our model signal is a band-limited, monocomponent, and analytical signal. It is expected that on the basis of this model the time-varying IA, IF, and IB can be derived accurately, because the model signal corresponds sufficiently to the quadrature model signal (see appendix A.1).

First, the design of the zero-phase band-pass FIR-filters is described in the next section 3.2. These filters correspond to the mid- and high-frequency ranges of interest as mentioned in the Introduction. Then a time window has to be selected according to the uncertainty principle of Gabor to compute the pseudo Wigner-Ville distribution. The length of this time window is dependent on the bandwidth of the applied filter. This is described in sections 3.2, 3.3, and 3.4. After that we have to sequentially perform the following steps to compute the estimates of the IA, IF, and IB:

- Compute an equidistantly sampled heart rate variability time series from the detected R-waves in the electrocardiogram (section 3.1).
- Decompose the heart rate variability time series into narrow-band mid- and high-frequency components by zero-phase band-pass FIR-filtering.

- The analytical signal is computed by means of a Hilbert transform FIR-filter (see appendix A.2).
- This yields the IAs for the narrow-band mid- and high-frequency components.
- The pseudo Wigner-Ville distribution is computed, using a time window as described in sections 3.2, 3.3, and 3.4.
- The time-slices of the pseudo Wigner-Ville distribution are made analytical by means of the Hilbert transform based on the discrete Fourier transform (see appendix A.1).
- And the discrete inverse Fourier transform of the squared envelope of each time-slice is used to compute the pseudo autocorrelation function.
- The final step is to derive the estimates of the IF and the IB for each of the narrow-band components from the pseudo autocorrelation function (section 3.5).

3.1 The computation of an equidistantly sampled analytical heart rate variability time series

Heart rate variability time series are obtained by detecting the R-waves from the electrocardiogram with a resolution of 1 ms and subsequently generating a pulse train consisting of Dirac pulses at the R-wave occurrence times. This pulse train is demodulated by means of a low-pass filter with cutoff frequency of 0.5 Hz [32,33]. The output signal of the filter is called the 'low-pass filtered cardiac event series', and can be sampled regularly [33,34,35]. In our case, the filtered event series is sampled with a sample interval $t_s = 0.25$ sec, i.e., the sample frequency is $F_s = 1/t_s = 4$ Hz. The resulting discrete real heart rate variability time series is denoted by $s[n]$, $n = 0,...,N-1$.

The time series $s[n]$ is filtered with a zero-phase band-pass FIR-filter corresponding to one of the frequency ranges of interest, i.e., mid- or high-range. The filtered time series is subsequently filtered with a zero-phase Hilbert transform FIR-filter to obtain the analytical time series (see appendix A.1). The resulting analytical, band-limited, and monocomponent time series is denoted by $\hat{s}[n]$, $n = 0,...,N-1$. Each complex number $\hat{s}[n]$ can be presented in polar form: $\hat{s}[n] = a[n]e^{j\varphi[n]}$, with non-negative envelope or IA $a[n]$ and IP $\varphi[n]$.

3.2 Filter bandwidth and duration of the impulse response according to Gabor

We designed the band-pass filters for the mid- and high-frequency components of the HRV-signal based on the requirements of an optimal resolution in the time-domain, unity-gain, and a minimal overlap between consecutive band-pass filters.

To find the best possible resolution in time, we started from the uncertainty principle of Gabor [20]. Gabor stated that, for a given filter, the product of the width in the time-domain and the width in the frequency-domain is greater than or equal to $1/4\pi$. In equation:

$$\sigma_t \cdot \sigma_f \geq \frac{1}{4\pi} \tag{11}$$

This means that, the wider (or narrower) the bandwidth of a filter is, the shorter (or longer) the corresponding impulse response is in the time-domain. The minimal product in the above equation (11) is reached for a normal distribution, that is a Gaussian shaped filter. Any other filter shape will deviate from a minimal product in (11).

In the above equation, σ_t and σ_f are expressed in a statistical sense to describe the width of a distribution as the second moment – or the standard deviation – of such a distribution:

$$\sigma_t^2 = \frac{1}{E}\int_{-\infty}^{+\infty} t^2 \cdot \left|h(t)\right|^2 dt \tag{12}$$

and

$$\sigma_f^2 = \frac{1}{E}\int_{-\infty}^{+\infty} f^2 \cdot \left|H(f)\right|^2 df \tag{13}$$

where $H(f)$ constitutes the filter transfer function in the frequency domain and $h(t)$ its corresponding impulse response in the time domain. E is the power of both $h(t)$ and $H(f)$:

$$E = \int_{-\infty}^{+\infty} \left|h(t)\right|^2 dt = \int_{-\infty}^{+\infty} \left|H(f)\right|^2 df .$$

Note that the expressions (12) and (13) are invariant for the localization of the filter on the frequency axis. So, for a given low-pass filter, the same product $\sigma_t \cdot \sigma_f$ holds true if this low-pass filter is translated over the frequency axis.

In the case of band-pass filters for the mid- and high-frequency components of the HRV-signal, the width in the frequency-domain is defined by the characteristic frequency ranges of HRV. The corresponding width in the time-domain then is determined by the duration of the impulse response expressed in terms of its standard deviation. On its turn, this standard deviation yields a measure for the resolution in time, i.e., spacing of points in time that are statistically independent; this will be explained below.

Long-tailed Gaussian shaped filters are incompatible with the unity-gain requirement. To be as close as possible to Gabor's optimum, we used 'squared cosine shaped' filters instead. Because in our case consecutive filters have a wider

bandwidth, the slopes of the filters need to be asymmetrical. The trailing slope is twice the length of the leading slope, but the trailing and leading slope of consecutive band-pass filters are equal (see figure 1); this yields the desired unity-gain filter-bank. A discrete zero-phase band-pass FIR-filter is designed by defining the cutoff frequencies (in our case the –6 dB points) f_{c1} and f_{c2}, and the transition bands $[f_{b1}, f_{t1}]$ and $[f_{t2}, f_{b2}]$ (see figure 2). The pass-band is the interval $[f_{c1}, f_{c2}]$ between the cutoff frequencies. The filter-basis is the interval $[f_{b1}, f_{b2}]$, i.e. the pass-band plus the two transition bands. The center frequency is the midpoint of the base: $f_0 = (f_{b1} + f_{b2})/2$.

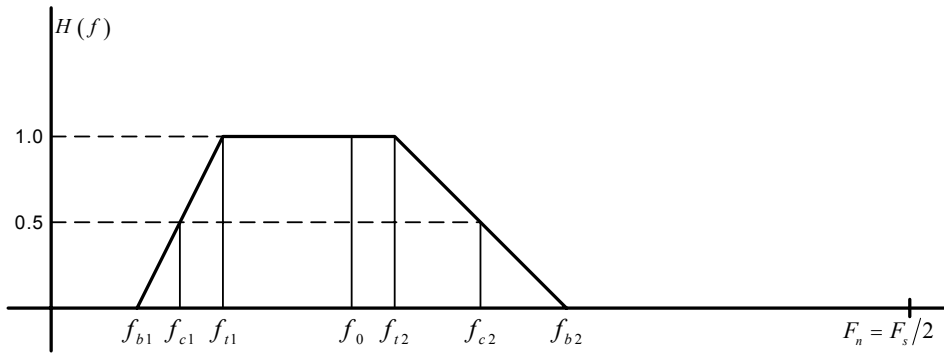

Figure 1. The set of consecutive band-pass filters for the low-, mid-, and high-frequency components constitutes a unity-gain filter-bank. The slopes are 'squared cosine shaped'.

We computed the product of σ_t and σ_f for the squared cosine shaped mid-en high-range band-pass filters and compared this product to the minimal product of Gabor's Gaussian shaped filter. For the mid-range filter:

$\sigma_t = 4.6512$ sec, $\sigma_f = 0.0204$ Hz, and $\sigma_t \cdot \sigma_f = 1.19/4\pi$ (14)

For the high-range filter:

$\sigma_t = 1.3960$ sec, $\sigma_f = 0.0952$ Hz, and $\sigma_t \cdot \sigma_f = 1.67/4\pi$ (15)

The replacement of Gaussian shaped filters by squared cosine shaped filters to accomplish unity gain has only a small impact on the product of width in frequency- and time-domain, and is close to optimal.

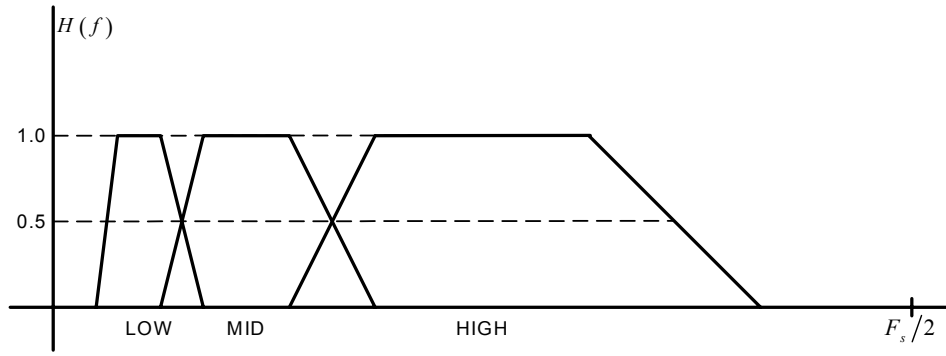

Figure 2. The design of a band-pass FIR-filter. The pass-band is the frequency interval $[f_{c1}, f_{c2}]$, defined by the two cutoff frequencies, in our case –6 dB points, f_{c1} and f_{c2}. The filter-basis is the interval $[f_{b1}, f_{b2}]$. The two transition bands $[f_{b1}, f_{t1}]$ and $[f_{t2}, f_{b2}]$, are 'squared cosine shaped' slopes. The trailing slope is made twice as long as of the leading slope. The center frequency f_0 is the midpoint of the basis: $f_0 = (f_{b1} + f_{b2})/2$. The signal to be filtered is analytical, therefore there is no pass-band at the negative frequencies.

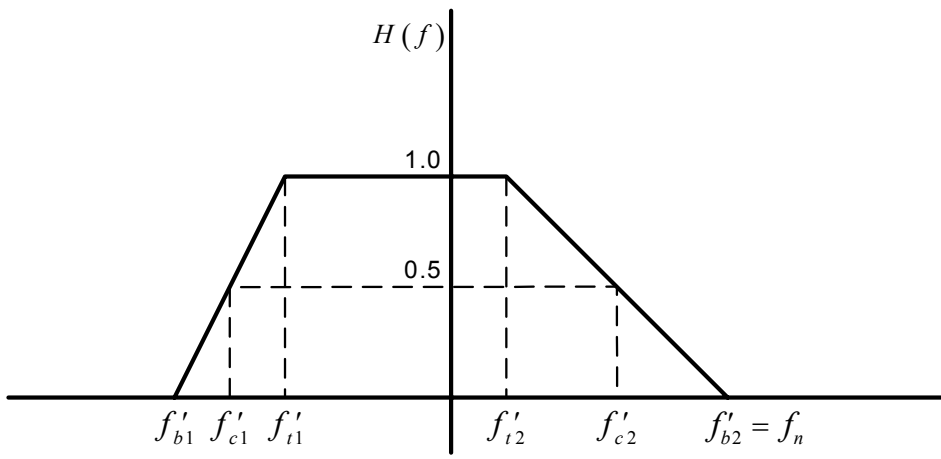

Figure 3. The filter-basis of the band-pass filter of figure 2 is translated over a range f_0 towards the origin. This basis of this filter lies symmetrical around the zero frequency. After demodulation of the signal with frequency f_0, it is sufficient to sample the filtered signal with sample rate $2 \cdot f'_{b2}$.

3.3 Low-pass equivalent and dependency between adjacent points in time

The center frequency of a given band-filter is the midpoint of the base: $f_0 = (f_{b1} + f_{b2})/2$. Suppose we translate the frequency response of the filter towards the zero frequency over a range f_0. It follows that: $f'_{b1} = f_{b1} - f_0 = -f_{b2} + f_0 = -f'_{b2}$, i.e., the basis of this filter lies symmetrical around the zero frequency (figure 3). Therefore, after demodulation of the signal with frequency f_0, it is sufficient to sample the filtered signal with sample rate $2 \cdot f'_{b2}$ [27]. This means that, in case of an ideal rectangular band-pass filter, the application of the translated low-pass filter in combination with complex demodulation will result in an over-sampled demodulated signal and the 'over-sampling ratio' is:

$$n_{\mathrm{DF}} = \frac{F_s}{f_{b2} - f_{b1}}.$$

In fact, we could decimate or downsample the time series with a 'decimation factor' n_{DF} and still retain the same information. In this downsampled situation, the adjacent points in time are uncorrelated, so independent in a statistical sense. That means that parameters computed at this resolution then are instantaneous. In that case the amplitude and the frequency are called instantaneous amplitude and frequency. Computations over a shorter time-interval yield adjacently dependent points in time; if computed over a longer time-interval, properties will be averaged, i.e., smeared over time (as with Fourier analysis). The decimation factor n_{DF} depends on the sample frequency F_s and the width of the filter at the basis. In our case of a 4 Hz sampled HRV time series and our design of the band-pass filters, the decimation factor for the mid-range filter is 31, and the decimation factor for the high-range filter is 9.

However, instead of downsampling, we utilize all the original n_{DF} points within a window to compute a pseudo Wigner-Ville 'time-slice' (see sections 2.4 and 3.5) and this is repeated for all the adjacent and disjoint intervals of n_{DF} points. Hence the consecutive time-slices of the pseudo Wigner-Ville distribution will be independent. This will make the pseudo autocorrelation function $R_{\hat{s}\hat{s}w}(t,\tau)$ and consequently the estimates of the IF and the IB also instantaneous. This design of the time-window will be used in the following section 3.5. However, to provide smooth IF and IB time series, we shift the window of n_{DF} points point by point.

In our case, we do not use rectangular band-pass filters, but band-pass filters with squared cosine shaped transition bands to achieve smoother time-domain behavior according to Gabor. This means that, using the same window length n_{DF} that we derived for the rectangular filter, the consecutive time-slices of the pseudo Wigner-Ville distribution are not truly independent. But the consequential dependency

of consecutive estimates of the IF and the IB is minimal; and therefore we claim that we can consider the estimates of the IF and the IB to be instantaneous.

3.4 Time-resolution and instantaneous properties of mid- and high-frequency components

To investigate the maximal discrete resolution Δt in time that we can accomplish with the postulated asymmetrical band-pass filters, we computed the envelope $|h(t)|$ of the impulse response $h(t)$ of the demodulated band-pass filter $H(f-f_0)$, i.e., $h(t)$ is the inverse Fourier transform of the frequency response $H(f-f_0)$. The frequency response $H(f-f_0)$ is the low-pass analogy of the band-pass filter after demodulation with f_0. The frequency f_0 is the center frequency of the band-pass filter (see sections 3.2 and 3.3). In case of the mid-range band-pass filter, the center frequency is $f_0 = 0.1230$ Hz. To determine the discrete instantaneous value Δt in the time domain, the Nyquist frequency of the demodulated band-pass filter was determined to be

$$f_n = \frac{F_s/2}{n_{DF}} = f'_{b2}$$

(section 3.3 and figure 3), i.e., $f_n = 2/31 = 0.0645$ Hz, to allow for perfect signal integrity, whilst minimizing sidelobes in the filter impulse response and therefore dependency between adjacent points in time. The numerical values of $|h(t)|$ around $t = 0$ are:

$$0.03 \quad 0.05 \quad 0.26 \quad 0.58\,(t=0) \quad 0.26 \quad 0.05 \quad 0.03 \tag{16}$$

with $\Delta t = 7.75$ sec (= 31 samples) (17)

and $\Delta t = 1.6662\,\sigma_t$

(see equation (14)). These results mean the following. If, after filtering with the mid-range band-pass filter, consecutive Wigner-Ville time-slices are computed over $\Delta t = 7.75$ sec (= 31 samples), these consecutive time-slices and the computed estimates of IF and IB are not truly independent, so not truly instantaneous. They still show a minimal dependency over (mainly) 3 data points as given by (16).

In case of the high-range band-pass filter, $f_0 = 0.3447$ Hz, $f_n = 2/9 = 0.2222$ Hz, and the numerical values of $|h(t)|$ around $t = 0$ are:

$$0.05 \quad 0.12 \quad 0.21 \quad 0.75\,(t=0) \quad 0.21 \quad 0.12 \quad 0.05 \tag{18}$$

with $\Delta t = 2.25$ sec (= 9 samples) (19)

and $\Delta t = 1.6117\,\sigma_t$

(see equation (15)). Also in this case there is a dependency over (mainly) 5 data points as given by (18).

For the remainder of this article, 'instantaneous' is referred to as consecutive points in time only showing a minimal dependency in time as given by (16) and (18) and spaced over Δt as given by (17) and (19) for the mid- and high-range band-pass filter, respectively.

3.5 The discrete pseudo autocorrelation function

Let $\hat{s}[n]$, $n = 0,...,N-1$ be a filtered analytical heart rate variability time series, i.e., mid- or high-range. A real-valued discrete time window $w[i], i = 0,...,M-1$ of length $M = n_{DF}$ is chosen. Conform sections 3.3 and 3.4, this length is chosen to make the estimates of the IF and the IB instantaneous. The discrete pseudo Wigner-Ville distribution is defined by [23 p.456]:

$$W_w[n,k] = \sum_{i=-M_1}^{M_1} w[i]\hat{s}[n+i]w^*[i]\hat{s}^*[n-i]\cdot e^{-4\pi j\cdot ik/M}, \tag{20}$$

with $M_1 = M/2$, for $n = 0,...,N-1$ and $k = 0,...,M-1$. We use the algorithm of Boashash and Reilly [36] to compute the discrete pseudo Wigner-Ville distribution.

The next step is the computation of the discrete pseudo autocorrelation function (DPACF). For each time index n take the time-slice $W_{w,n}[k] = W_w[n,k]$, for $k = 0,...,M-1$, of the discrete pseudo Wigner-Ville distribution $W_w[n,k]$. This is a real data series in the frequency domain. Since the discrete pseudo Wigner-Ville distribution also contains negative values (it is not a true density), we will start to determine the squared envelope of each time-slice. To accomplish this, compute the discrete analytical data series:

$$\hat{W}_{w,n}[k] = W_{w,n}[k] + jHW_{w,n}[k].$$

This method constitutes in fact a band-pass filtering of the positive times and a zeroing of the negative times (see appendix A.1 and A.2). After that, the squared modulus of the analytical time-slice is taken to yield the squared envelope of the time-slice. The procedure of computing the envelope of the time-slice can be seen as a smearing function of this data series in the frequency domain. It follows that the inverse Fourier transform of the envelope constitutes a particular real weighting

function in the τ-domain, with a maximum value at $\tau = 0$. We now compute the inverse discrete Fourier transform of the squared envelope of the time-slice $W_{w,n}[k]$, in the index k:

$$R_{\hat{s}\hat{s}w}[n,l] = F_{k\to l}^{-1}\left|\hat{W}_{w,n}[k]\right|^2, \text{ for } l = 0,...,M-1. \tag{21}$$

(See appendix A.4). The resultant $R_{\hat{s}\hat{s}w}[n,l]$ is called the DPACF. (Equation (21) corresponds with equation (8) of section 2.4.)

The computation of the discrete estimator $f_w[n]$ of the IF and the squared estimator $B_w^2[n]$ of the IB are now straightforward using the expressions:

$$f_w[n] = \frac{F_s/2}{2\pi}\cdot\arctan\left(\frac{\text{Im } R_{\hat{s}\hat{s}w}[n,1]}{\text{Re } R_{\hat{s}\hat{s}w}[n,1]}\right) \tag{22}$$

and

$$B_w^2[n] = 1 - \frac{\left|R_{\hat{s}\hat{s}w}[n,1]\right|}{\left|R_{\hat{s}\hat{s}w}[n,0]\right|}, \tag{23}$$

corresponding with equations (9) and (10). These estimates are instantaneous conform section 3.4. Concerning equation (22), the value $R_{\hat{s}\hat{s}w}[n,1]$ is an estimate of the local autocorrelation function $R_{\hat{s}\hat{s}l}(t,\tau)$ at $\tau = 1$, therefore, phase-shifts of $\pm 2\pi$ due to the ambiguity of the inverse tangent do not occur, as explained in section 2.3, and unwrapping is not necessary. Concerning equation (23), zero divisions cannot occur because the maximum of the series $R_{\hat{s}\hat{s}w}[n,l], l = 0,...,M-1$ is at $l = 0$, and this data series can only be identical to zero if the time series $\hat{s}[n]$ is locally identical to zero (see section 2.3).

At this point it is recalled that the DPACF $R_{\hat{s}\hat{s}w}[n,l]$ is weighted or multiplied with a real weighting function that resulted from the calculation of the envelope of the time-slice in the frequency domain. Because $R_{\hat{s}\hat{s}w}[n,l]$ has been weighted, $B_w^2[n]$ is a biased squared estimator of the (squared) IB. The index $B_w^2[n]$, however, is useful as an indicator of noise or interference due to other signal components. Therefore, this index is called the instantaneous bandwidth coefficient (IBC). The IBC $B_w^2[n]$ is a qualitative index and is chosen in such a way that it will always have a value between 0 and 1 (note the absence of the factor $1/\pi^2$ in equation (23), e.g., equation (10)). Value 0 means that there is no amplitude modulation, so the signal is purely frequency modulated (see section 2.2); value 1 means that the signal is a noise signal. The estimator $f_w[n]$ is useful to calculate the IF and is not biased because

both real and imaginary part of $R_{\hat{s}\hat{s}w}[n,1]$ have been multiplied by the same real factor of the weighting function.

3.6 The circular mean direction

Finally, we describe the computation of the circular mean direction. The circular mean direction is an estimate of the IF. In the next section 4, we make a comparison between this estimate and our estimate of the IF.
Again, let $\hat{s}[n]$, $n = 0,...,N-1$ be a filtered analytical heart rate variability time series. A real-valued discrete time window $w[i], i = 0,...,M-1$, is chosen. This window may be relatively long, for instance $M = 100$. The discrete pseudo Wigner-Ville distribution $W_w[n,k]$ is computed using equation (20). The discrete first moment [37]:

$$f_i[n] = \frac{F_s}{M} \cdot \frac{\sum_{k=0}^{M-1} k \cdot W_w[n,k]}{\sum_{k=0}^{M-1} W_w[n,k]}$$

is an estimate of the IF, corresponding with equation (2). However, the discrete pseudo Wigner-Ville distribution is periodical, therefore this estimate is biased [23 p.463]. A better estimate is the circular mean direction [23,38,39]:

$$f_i[n] = \frac{F_s/2}{2\pi} \cdot \arg \sum_{k=0}^{M-1} W_w[n,k] \cdot e^{2\pi j \cdot k/M}, \qquad (24)$$

which takes the periodical character of the data into account.
The estimation of the discrete IB using the discrete second moment, corresponding with equation (3), as well as using the circular standard deviation [38], gives unsatisfactory results, see also section 2.2.

4 Application and discussion

4.1 Mid- and high frequency components, the IA

Figure 4 presents an illustration of the application of the method to a heart rate variability time series in the mid-frequency range (0.07-0.15 Hz) and the high-frequency range (0.15-0.50 Hz). The upper graph of A is an example of a heart rate variability time series, sampled with 4 Hz. The result of the mid-range filter applied to the heart rate variability time series is shown in B (mf), and the result of the high-range filter is shown in E (hf). The result of a combined (zero-phase) MID+HIGH-range FIR-filter (0.07-0.50 Hz) is shown in the lower graph of A (mf&hf). Adding the mid- and the high-frequency heart rate variability time series in B and E, respectively,

results in exactly the same MID+HIGH-frequency heart rate variability time series. This is the case because the FIR-filters are zero-phase and have compensating overlap in the transition bands, i.e., they constitute a unity-gain filter-bank (section 3.2).

The envelope or IA of the mid-frequency heart rate variability time series is presented in B. It is apparent that the IA is fluctuating slowly with respect to the mid-frequency heart rate variability time series. This is in agreement with the conditions mentioned in section 2.1. (I.e., to be able to compute a meaningful IF, the spectra of the envelope and the phase have to be disjoint, whereby the envelope has to be lower in frequency than the phase; see also conditions 1) and 2) of appendix A.1.) The same applies to the IA of the high-frequency heart rate variability time series in E.

4.2 The IF and the IBC

Figure C shows the estimators $f_w[n]$ of the IF and $B_w^2[n]$ of the IBC of the mid-frequency heart rate variability time series in B. Notice the instants in time where the IBC is high. These high values correspond with:

a) low, almost zero, values of the IA in B;
b) phase-shifts of the mid-frequency heart rate variability time series, see B;
c) irregularities in the IF in this figure (some peaks are deflected); and
d) fast changes in the circular mean direction in figure D.

At these points of high valued IBC, the signal may not fulfill the requirements of our model signal. This means that locally the signal may not be monocomponent, causing phase-shifts at low amplitudes. Or the high values may be due to random phase-shifts. This will be explained below by adding two sinusoids. The same remarks can be made with respect to the estimators $f_w[n]$ of the IF and $B_w^2[n]$ of the IBC, presented in figure F, of the high-frequency heart rate variability time series in E.

Figure D shows the discrete IF of the mid-frequency heart rate variability time series, estimated with the circular mean direction (24). Notice the peaks that stretch out of the mid-frequency range and some peaks even become negative. The estimation of the accessory discrete IB using the discrete second moment, corresponding with equation (3), as well as using the circular standard deviation [38], give unsatisfactory results, as mentioned in section 3.6, making these methods unsuitable for practical use. As mentioned in section 2.1, the estimate of the IF of a multicomponent signal can shift out of the signal's spectral region, and this is what we see in figure D. Notice the resemblance of the circular mean direction in D and the IF in C. Except for the periods of high IBC, these two estimators are almost equal

numerically. This indicates that the estimate of the IF is reliable, although the DPACF itself is biased (section 3.5).

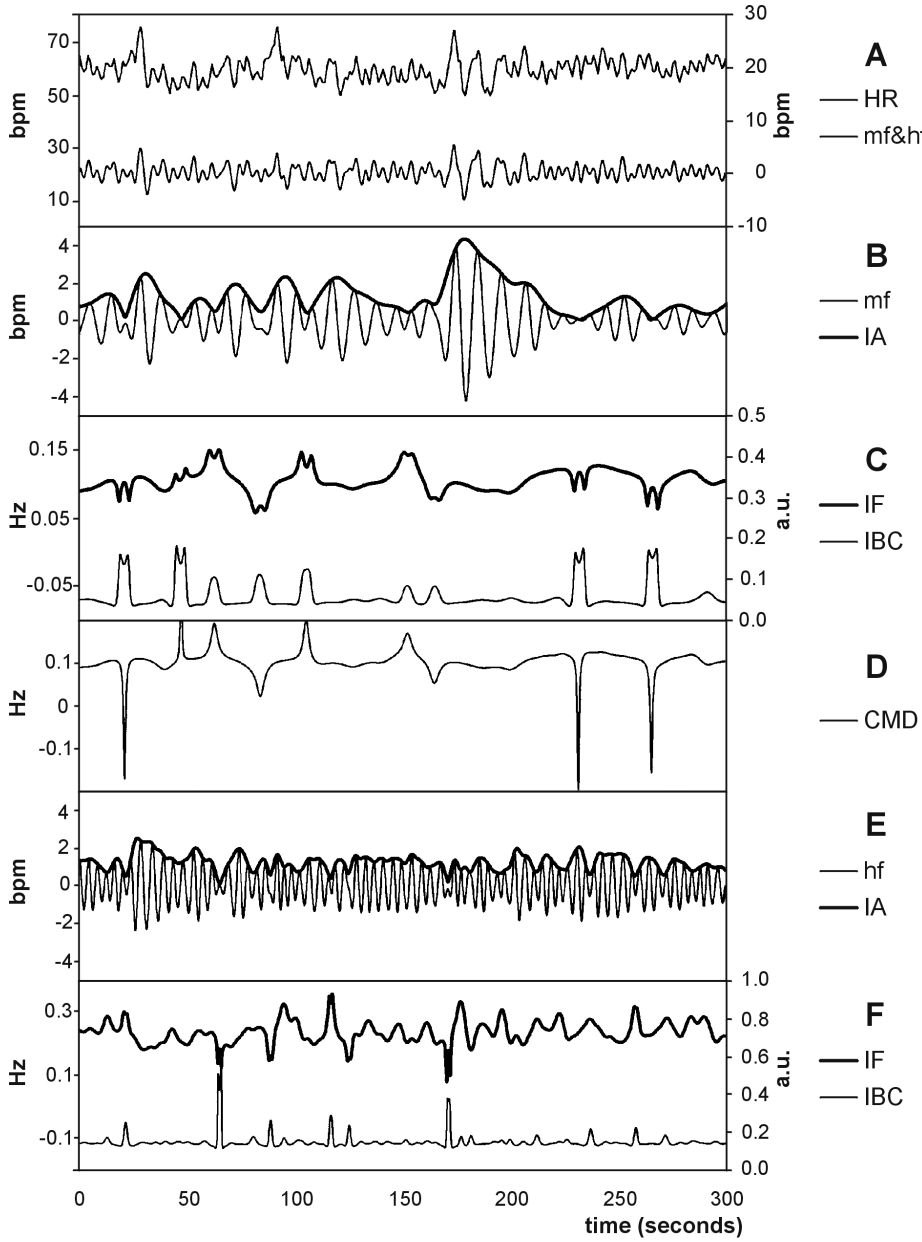

Figure 4. Spontaneous fluctuations in heart rate and the estimated instantaneous amplitude, frequency, and bandwidth coefficient of the MID and HIGH frequency bands, during a period of 300 sec.
A: The upper graph presents the original unfiltered 4 Hz heart rate time series (HR), the scale in beats per minute (bpm) is on the left side. The lower graph (mf&hf) is the result the combined MID+HIGH filter applied to the heart rate. The scale in bpm is on the right side.
B: The thin line (mf) presents the MID frequency HR time series. The bold line (IA) is the instantaneous amplitude or envelope of this time series. Both graphs are scaled in bpm.
C: The estimated instantaneous frequency (IF, upper bold graph) and the instantaneous bandwidth coefficient (IBC, lower thin graph) of the MID frequency HR time series as presented in B. The scale of the IF in Hz is on the left side, the scale of the IBC in arbitrary units (a.u.) is on the right side.
D: The instantaneous frequency (CMD) estimated by means of the circular mean direction, of the same MID frequency HR time series as presented in B. The scale is in Hz.
E: The thin line (hf) presents the HIGH frequency HR time series. The bold line (IA) is the instantaneous amplitude of this time series. Both graphs are scaled in bpm.
F: The estimated instantaneous frequency (IF, upper bold graph, scale in Hz on the left side) and the instantaneous bandwidth coefficient (IBC, lower thin graph, scale in a.u. on the right side) of the HIGH frequency HR time series as presented in E.

4.3 The behavior of the IF and the IBC

The irregularities in the IF at points of high valued IBC, 1) when the signal is locally, i.e., for a short period in time, not monocomponent, or, 2) due to random phase fluctuations in the original signal, may be explained as follows.
1) A signal is locally multicomponent ([16,18,21,23], see also appendix A.3) in the frequency band of interest if there is locally more than one spectral concentration present in the time-varying ‘instantaneous spectrum’. For instance, a signal may locally become multicomponent if harmonic or sub-harmonic components arise due to non-sinusoidal shape of waveforms. For multicomponent signals, the IF has no

meaning [21]. The effect is that phase-shifts at low amplitudes cause discontinuities in the IF and the IBC. For instance, suppose $\hat{s}(t)$ consists of two sinusoids with different frequencies $f_2 > f_1$ [39]:

$$\hat{s}(t) = e^{2\pi j f_1 t} + e^{2\pi j f_2 t} = 2\left|\cos(2\pi f_d t)\right| e^{2\pi j f_h t + \pi j \cdot \mathrm{sign}(\cos(2\pi f_d t))}$$

in which $f_d = (f_2 - f_1)/2$ and $f_h = (f_1 + f_2)/2$. The signal $\hat{s}(t)$ is a complex analytical signal and the IA is $a(t) = 2\left|\cos(2\pi f_d t)\right|$. The double sinusoid shows phase-shifts of $\pm 2\pi$ at each time the cosine function $\cos(2\pi f_d t)$ of the IA changes sign. Phase-shifts cause discontinuities in the IF, because the IF is the derivative (1) of the phase. It follows from equation (4) that the IBC is approximated by:

$$B_i^2(t) = \pi^2 f_d^2 \tan^2(2\pi f_d t).$$

Therefore, there are high peaks in the IBC at times where the cosine function $\cos(2\pi f_d t)$ changes sign. The deflections in the IF and the IBC are due to aliasing because the sample frequency is too low to catch the slope of the peaks.

2) Random phase fluctuations may have various origins. It may be quantization noise due to small R-wave detection errors. It may also be physiological noise originating from stochastic components of the underlying physiological system. Under pure noise conditions, neighbouring samples in time are uncorrelated. If noise is present on the signal, this may result in 'sudden' phase-shifts. 'Sudden' phase-shifts, in turn, may result in discontinuities in the IF, as explained above. Also, the autocorrelation function at $\tau = 1$ of a noisy signal is zero in expectation, but varies randomly. Therefore, the IBC (7,23) of a noisy signal varies randomly and will show outlier peaks. By nature, the IBC is peaked at all phase-shifts. Deflections in IF and IBC originate in the same way as explained in 1), see figures C and F.

5 Conclusion

In this paper, we have provided methods to compute estimators of the instantaneous amplitude, frequency, and bandwidth coefficient of certain narrow-band components present within heart rate variability time series; these components are separated using predefined zero-phase band-pass FIR-filters. The estimators offer a quantitative description of the time-varying spectral energy of the heart rate variability signal within each frequency band. At every instant in time, the IA offers an estimate of the signal's instantaneous power, while the IF estimates the time-varying frequency location of the spectral peak. Together they provide a time-frequency description of the energy in a particular frequency band. A comparison with the

circular mean direction gives an indication of the reliability of the estimate of the IF computed with our method.

The IBC may serve as a time-dependent indicator of oscillatory and irregular periods. Oscillatory fragments with low IBC can be used in further analysis, irregular fragments of high IBC can be excluded or otherwise processed.

At periods of high IBC, the interaction of other signal components may be investigated, for instance with cross-correlation techniques. In addition, the IF in both mid- and high-frequency band may show possible harmonic relationships at those periods in time where the components are coupled by phase locking. A non-sinusoidal waveform in the mid-frequency band may show a clear harmonic component in the high-frequency band. Otherwise, respiration components may produce sub-harmonic components in the mid-frequency band. Phase locking may be revealed by means of cross-correlation.

The traditional approach of short-term Fourier spectral analysis is based on time windows of 2-5 min to yield an appropriate frequency-resolution. The resolution in time of the described method is in the order of several seconds, inversely related to the width of the band-pass filter. This optimal resolution in time reveals the highly dynamic nature of the various components in the heart rate, comprising the, sometimes antagonistic, waxing and waning in time of the mid- and high-frequency components. This dynamic behavior is smeared over time and thus hidden when using traditional time-averaged spectral analysis techniques.

The presented method provides instantaneous information of time-varying changes in heart rate variability, with an optimal time-resolution. Therefore, this method may contribute to a more detailed description of the time-varying dynamics of the autonomic regulatory processes within the cardiovascular control system under normal or pathological conditions.

Appendix

A.1 Analytical signals

Given a complex signal $z(t)$, the envelope or instantaneous amplitude $a(t)$ and the instantaneous phase $\varphi(t)$ are defined as the modulus and the argument of the complex number $z(t)$. The signal $z(t)$ can subsequently be written in polar form $z(t) = a(t)e^{j\varphi(t)}$ and visualized as a moving vector in the complex plane. Furthermore, the instantaneous frequency $f_i(t)$ may now be defined as the rate of change of the phase: $f_i(t) = \varphi'(t)/2\pi$. To compute the instantaneous amplitude, phase, and

frequency of a real signal, we need a complex representation that represents the real signal in a 'natural' way.

There is a unique way to represent a simple harmonic oscillation $s(t) = a \cdot \cos \omega t$ as a rotating vector in the complex plane. Namely, by adding the imaginary quadrature component $jQs(t) = ja \cdot \sin \omega t$. The resulting complex vector is $z(t) = a \cdot e^{j\omega t}$. More generally, the natural complex representation of $s(t) = a(t)\cos\varphi(t)$ as a complex vector is $z(t) = a(t)e^{j\varphi(t)}$, in which the imaginary quadrature component is $jQs(t) = ja(t)\sin\varphi(t)$ [20].

Constructing a unique natural complex representation of a real signal $s(t)$ by first writing the real signal in the form $s(t) = a(t)\cos\varphi(t)$ and subsequently adding the imaginary quadrature component is called the quadrature operation. The real signal is represented as a moving vector in the complex plane and the real part of the complex signal is equal to the original real signal. The resulting complex signal is called the quadrature model signal. The quadrature model signal is assumed to be the natural complex representation of a real signal and the instantaneous amplitude $a(t)$ and phase $\varphi(t)$ represent the instantaneous amplitude and phase of the original real signal [21 p.36].

In that respect, one needs the quadrature model signal of a real signal to be able to compute the instantaneous amplitude and phase of this signal. However, there is no unique way to write a real signal $s(t)$ in the form $s(t) = a(t)\cos\varphi(t)$, and so there is no unique way to construct a complex representation of a general real signal by means of the quadature operation [16,21].

To overcome this problem, Gabor [20] introduced the analytical signal of a real signal $s(t)$. The construction is as follows. Another real signal $Hs(t)$ is constructed by replacing each component $a \cdot \cos \omega t$ of $s(t)$ with $a \cdot \sin \omega t$ and each component $b \cdot \sin \omega t$ with $-b \cdot \cos \omega t$. Consequently, the complex signal

$$\hat{s}(t) = s(t) + jHs(t)$$

consists of components $a \cdot e^{j\omega t}$ (replacing each component $a \cdot \cos \omega t$) and components $-jb \cdot e^{j\omega t}$ (replacing each component $b \cdot \sin \omega t$). This signal $\hat{s}(t)$ is called the analytical signal. The real signal $Hs(t)$ is called the Hilbert transform of $s(t)$. It follows that $Hs(t)$ can be considered as the output of a filter with frequency response $H(f)$ defined by $H(f) = 1$ for $f > 0$; $H(0) = 0$; and $H(f) = -1$ for $f < 0$ [27]. In the time domain, the impulse response of $H(f)$ is

$$h(t) = F^{-1}_{f \to t} H(f) = 1/\pi t$$

and the Hilbert transform is the convolution $s(t)*h(t)$. The mathematical form of the Hilbert transform is

$$Hs(t) = p.v.\int_{-\infty}^{+\infty} \frac{s(\tau)}{\pi(t-\tau)} d\tau$$

[20,21,27]. (P.v. means that Cauchy's principle value of the integral has to be taken.) The resulting analytical signal is a complex signal and has two properties:

a) The amplitudes of the positive frequency components of the analytical signal equal the amplitudes of the positive frequency components of the original real signal multiplied by two, but the negative frequency components are eliminated; and

b) the real part of the complex analytical signal equals the real signal.

With respect to these two properties, the construction of the analytical signal of a real signal is unique [16 p.523].

The analytical signal is meaningful if it is equal to, or an approximation of, the quadrature model signal because then the instantaneous amplitude and phase are meaningful, as explained above. However, the analytical signal is not always equal to the quadrature model signal. If there is a leakage of positive frequency components into the negative spectral region, then the analytical signal will not correspond to the quadrature model signal, because the Hilbert transform eliminates the negative frequency components.

Consider the real signal $s(t) = a(t)\cos\varphi(t)$. Suppose:

1) the spectrum of $a(t)$ is contained in a frequency region $-\omega_1 < \omega < \omega_1$; and

2) the spectrum of $\cos\varphi(t)$ is zero for $-\omega_1 \le \omega \le \omega_1$.

Under these conditions, it can be proved that

$$a(t)\cos\varphi(t) + jH\left[a(t)\cos\varphi(t)\right] = a(t)e^{j\varphi(t)},$$

meaning that the analytical signal and the quadrature model signal coincide [16,21]. Therefore, the analytical signal $\hat{s}(t) = a(t)e^{j\varphi(t)}$ of a real signal $s(t)$ equals the quadrature model signal, if $a(t)$ and $\varphi(t)$ satisfies 1) and 2), i.e., under these conditions, the instantaneous amplitude and phase are meaningful. In general, for a narrow-band real signal, the analytical signal approximates the quadrature model signal because there is little or no leakage of the positive frequency components into the negative spectral region.

Under the same conditions 1) and 2), reflecting a slowly varying amplitude modulation and a fast phase modulation, the instantaneous amplitude $a(t)$ and the instantaneous phase $\varphi(t)$ can be treated as independent signals [16]. Furthermore,

Rihaczek [22] proved that the time-varying signal's energy is in frequency concentrated in a single narrow frequency range at $f = f_i(t)$.

A.2 Discrete analytical time series

Based on the above description, there are two methods to compute the discrete analytical signal:

1) Use the fact that the negative frequency components must be zero and the positive frequency components are twice the positive frequency components of the original real signal. Let $x[i], i = 0,...,N-1$ be a discrete time series and $X[k], k = 0,...,N-1$ the discrete Fourier transform of $x[i]$. For N is odd, define $M = N/2$ and $\hat{X}[0] = X[0]$, $\hat{X}[k] = 2 \cdot X[k]$ for $1 \le k \le M$, and $X[k] = 0$ for $M+1 \le k \le N-1$. For N is even, define $M = (N/2)-1$ and $\hat{X}[0] = X[0]$, $\hat{X}[k] = 2 \cdot X[k]$ for $1 \le k \le M$, $\hat{X}[N/2] = X[N/2]$, and $X[k] = 0$ for $M+2 \le k \le N-1$. The inverse discrete Fourier transform of $\hat{X}[k]$ produces the discrete analytical signal $\hat{x}[i], i = 0,...,N-1$ [23 p.458].

2) In the time domain, the discrete impulse response of the Hilbert transform $H(f)$ can be used to filter the real signal $x[i]$, $i = 0,...,L$ to obtain the imaginary part of the discrete analytical signal [36,40]. The discrete frequency response $H[k], k = -N/2,...,N/2$ is defined by $H[k] = -1$ for $k < 0$; $H[0] = 0$; and $H[k] = 1$ for $k > 0$ (see figure 5). The discrete impulse response $h[n]$ is the inverse Fourier transform of the discrete frequency response $H[k]$ of the Hilbert transform. The theoretical impulse response is [36,40]:

$$h[n] = \frac{2}{n\pi} \cdot \sin^2\left(\frac{n\pi}{2}\right)$$

if $n \neq 0$, $h[0] = 0$. Better results are obtained by constructing two 'squared cosine shaped' transition bands, at $k = 0$ and at $k = \pm N/2$, in the frequency response $H[k]$. Or, in other words, squared cosine shaped transition bands at $f = 0$ and $f = \pm F_n = \pm F_s/2$. In figure 6, the pass-bands and the transition bands of the Hilbert transform are drawn. The squared cosine shaped transition band at $f = 0$ is $[-f_{a1}, f_{a1}]$. The transition band at $f = \pm F_n$ has to be contiguous after periodical extension of the frequency response. This means that we can imagine the squared cosine shaped transition band at $f = \pm F_n$, to be the interval $[f_{a2}, f_{a1} + F_n]$, see figure 6. The resulting frequency response will give a shorter impulse response and smaller 'ripples' in the transfer function.

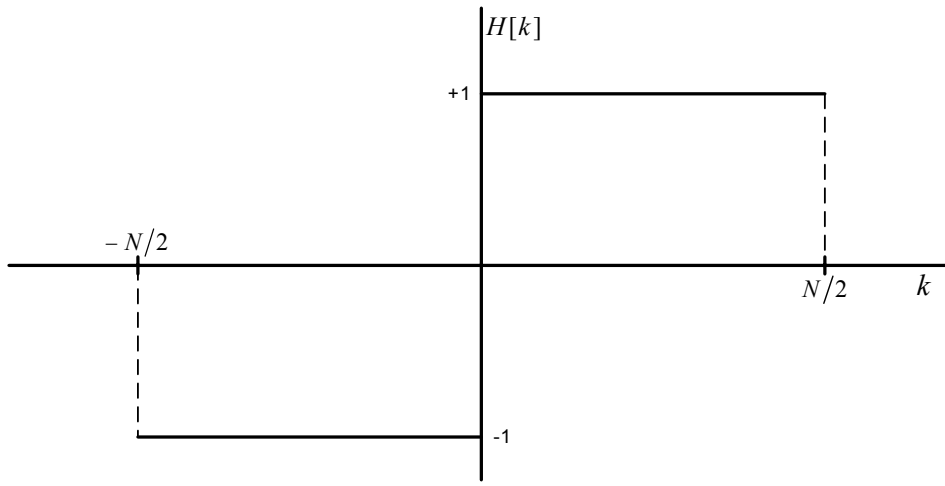

Figure 5. The discrete frequency response $H[k]$, $k=-N/2,...,N/2$ of the discrete Hilbert transform, defined by $H[k]=-1$ for $k<0$; $H[0]=0$; and $H[k]=1$ for $k>0$.

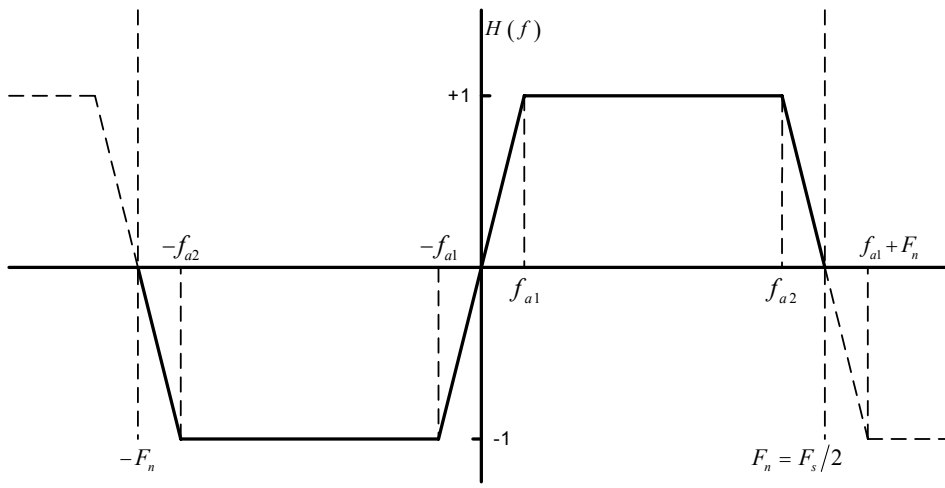

Figure 6. Design of a Hilbert transform FIR-filter. The transition bands $[-f_{a1}, f_{a1}]$ and $[f_{a2}, f_{a1}+F_n]$ at $f=0$ and $f=\pm F_n=\pm F_s/2$, respectively, are 'squared cosine shaped' slopes (after periodical extension of the frequency response).

Applying $h[n]$ as a FIR-filter to the original signal $x[i]$ by computing the discrete convolution $x[i]*h[i]$, this filter produces the imaginary component $Hx[i], i = 0,...,L$ of the discrete analytical signal: $\hat{x}[i] = x[i] + jHx[i]$. $h[n]$ is called the Hilbert transform FIR-filter.

In both cases, 1) and 2), the methods perform badly for frequencies near zero and near half the sample frequency. Therefore, a band-pass filter has to be applied to the data before applying method 1) or the Hilbert transform FIR-filter (method 2). In our case we use the mid- or high-range band-pass filter. The design of the Hilbert transform filter has to be adapted to the band-pass filter in the following way. The pass-bands of the Hilbert transform are $[f_{a1}, f_{a2}]$ and $[-f_{a2}, -f_{a1}]$, see figure 6. Only in these pass-bands there is an analytical relationship. Comparing figure 1 and figure 6, this means that the basis $[f_{b1}, f_{b2}]$ of the band-pass filter must lie totally within the pass-band $[f_{a1}, f_{a2}]$ of the Hilbert transform, i.e., $f_{a1} \le f_{b1}$ and $f_{b2} \le f_{a2}$, see figure 7. Only then a correct analytical signal is guaranteed.

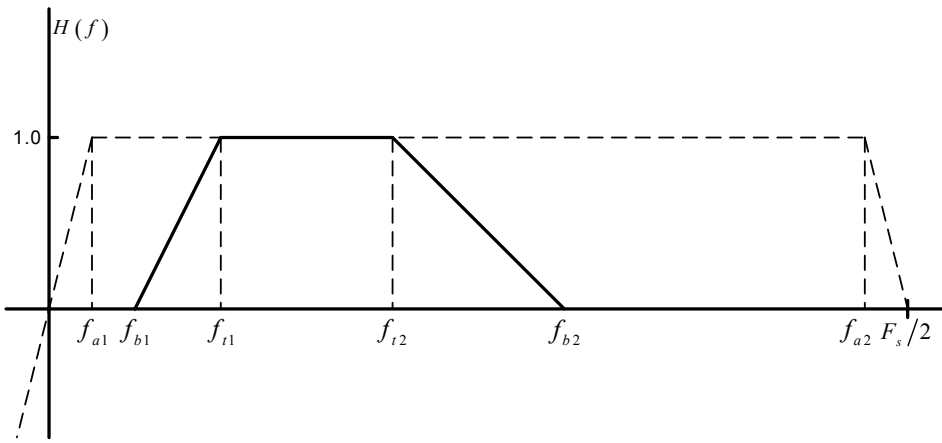

Figure 7. The design of the Hilbert transform filter has to be adapted to the band-pass filter to be used. The basis $[f_{b1}, f_{b2}]$ of the band-pass filter must lie totally within the pass-band $[f_{a1}, f_{a2}]$ of the Hilbert transform, i.e., $f_{a1} \le f_{b1}$ and $f_{b2} \le f_{a2}$.

Method 1) is only used for very short data series because, in general, method 2) gives better results for data series longer than one or two times the length of the Hilbert transform FIR-filter [36].

A.3 Multicomponent signals [16,18,21,23]

Suppose an analytical signal $z(t)$ is locally (in time) a composition of analytical signals $z_k(t)$, i.e.,

$$z(t)=\sum_{k=1}^{K} z_k(t);$$

and each $z_k(t)$ is characterized by a peak in the time-frequency plane localized at the IF of $z_k(t)$ and the width of its peak (the conditional standard deviation in the frequency direction) is the IB of $z_k(t)$. Suppose, furthermore, that the peaks are locally mutually disjoint at the frequency-bases of the peaks, i.e., the peaks $z_k(t)$ are locally well delineated in the time-frequency plane; in that case the analytical signal $z(t)$ is called multicomponent (in frequency, i.e., in the frequency direction) [21 p.182]. Note that this is not a global but a local condition. The decomposition of a multicomponent signal may not be unique. If $K=1$, $z(t)$ is called monocomponent (in frequency), but in this case the width of the peak must also be limited, i.e., $z(t)$ must also lie in a well delineated region of the time-frequency plane.

A.4 Notation

We use the following notations for the Fourier transform and the inverse Fourier transform. The Fourier transform

$X(f)=\int_{-\infty}^{+\infty} x(t)e^{-2\pi j\cdot ft}dt$ is denoted by $X(f)=F_{t\to f}x(t)$;

the inverse Fourier transform

$x(t)=\int_{-\infty}^{+\infty} X(f)e^{2\pi j\cdot tf}df$ by $x(t)=F_{f\to t}^{-1}X(f)$.

In the discrete case, the discrete Fourier transform

$X[k]=\frac{1}{N}\sum_{n=0}^{N-1} x[n]\cdot e^{-2\pi j\cdot nk/N}$ is denoted by $X[k]=F_{n\to k}x[n]$;

the discrete inverse Fourier transform

$x[n]=\sum_{k=0}^{N-1} X[k]\cdot e^{2\pi j\cdot kn/N}$ by $x[n]=F_{k\to n}^{-1}X[k]$.

References

[1] A. Stys and T. Stys, “Current clinical applications of heart rate variability,” Clin. Cardiol., vol. 21, pp. 719-724, 1998.

[2] H. Tsuji, M.G. Larson, F.J. Venditti, E.S. Manders, J.C. Evans, C.L. Feldman, and D. Levy, “Impact of reduced heart rate variability on risk for cardiac events, the Framingham heart study,” Circulation, vol. 94, pp.2850-2855, 1996.

[3] B.McA. Sayers, “Analysis of heart rate variability,” Ergonomics, vol. 16, pp. 17-32, 1973.

[4] B.McA. Sayers, “Signal analysis of heart-rate variability,” in: The study of heart-rate variability, R.I. Kitney, O. Rompelman (eds). Clarendon Press, Oxford. pp: 27-58,1980.

[5] R.I. Kitney and O. Rompelman, The Study of Heart-Rate Variability. Oxford Medical Engineering Series, Clarendon Press, Oxford, 1980.

[6] R.I. Kitney, “Beat-by-beat interrelationships between heart rate, blood pressure and respiration,” in: Beat-to-beat investigation of cardiovascular function, R.I. Kitney, O. Rompelman (eds). Oxford University Press, Oxford. pp: 146-178,1985.

[7] S. Akselrod, D. Gordon, J.B. Madwed, N.C. Snidman, D.C. Shannon, and R.J. Cohen, “Hemodynamic regulation: investigation by spectral analysis,” Am. J. Physiol., vol. 249, pp. M867-M875, 1985.

[8] G. Baselli, S. Cerutti, S. Civardi, A. Malliani, and M. Pagani, “Cardiovascular variability signals: towards the identification of a closed-loop model of the neural control mechanisms,” IEEE Trans. Biomed. Eng., vol. 35, pp. 1033-1046, 1988.

[9] J.P. Saul, R.D. Berger, P. Albracht, S.P. Stein, M.H. Chen, and R.J. Cohen, “Transfer function analysis of the circulation: unique insights into cardiovascular regulation,” Am. J. Physiol., vol. 261, pp. H1231-H1245, 1991.

[10] J.H.M. Tulen, A.J. Man in 't Veld, A.M. van Roon, P. Moleman, H.G. van Steenis, P.J. Blankestijn, and F. Boomsma, “Spectral analysis of hemodynamics during infusions of epinephrine and norepinephrine in men,” J. Appl. Physiol., vol. 76(5), pp. 1914-1921, 1994.

[11] J.H.M. Tulen, J.A. Bruijn, K.J. de Man, L. Pepplinkhuizen, A.H. van den Meiracker, and A.J. Man in 't Veld, “Cardiovascular variability in major depressive disorder and effects of imipramine or mirtazapine (Org 3770),” J. of Clin. Psychopharmacol., vol. 16(2), pp. 135-145, april 1996.

[12] J.H.M. Tulen, F. Boomsma, and A.J. Man in 't Veld, “Cardiovascular control and plasma catecholemines during rest and mental stress: effects of posture,” Clinical Science, vol. 96, pp. 567-576, 1999.

[13] G. Parati, P. Castiglioni, M. di Renzo, S. Omboni, A. Pedotti, and G. Mancia, “Sequential spectral analysis of 24-hour blood pressure and pulse interval in humans,“ Hypertension, vol. 16, pp. 414-421, 1990.

[14] E.J.M. Weber, P.C.M. Molenaar, and M.W. van der Molen, “A nonstationary test for the spectral analysis of physiological time series with an application to respiratory sinus arrhythmia,” Psychophysiology, vol. 29, pp. 55-65, 1992.

[15] J. Ville, “Théorie et application de la notion de signal analytique,” Cables et Transmissions, vol. 2A(1), pp. 61-74, Paris, France, 1948.

[16] B. Boashash, “Estimating and interpreting the instantaneous frequency of a signal – part 1: fundamentals,” Proc. IEEE, vol. 80, no. 4, pp. 520-538, April 1992.

[17] E. Wigner, “On the quantum correction for thermodynamic equilibrium,” Phys. Rev., 40, 749-759, 1932.

[18] H.I. Choi and W.J. Williams, “Improved time-frequency representation of multicomponent signals using exponential kernels,” IEEE Trans. Acoust., Speech, Signal Processing, ASSP-37, 862-871, 1989.

[19] H.G. van Steenis and J.H.M. Tulen, “The exponential distribution applied to nonequidistantly sampled cardiovascular time series,” Computers and Biomed. Res., vol. 29, pp. 174-193, 1996.

[20] D. Gabor, “Theory of communication,” Proc. IEE, vol. 93 (III), pp. 429-457, 1946.

[21] L. Cohen, Time-Frequency Analysis. Englewood Cliffs, NJ, Prentice Hall, 1995.

[22] A.Rihaczek, “Signal energy distribution in time and frequency,” IEEE Trans. Inform. Theory, vol. IT-14, pp. 369-374, 1968.

[23] B. Boashash, “Time-frequency signal analysis,” in Advances in Spectrum Analysis and Array Processing, Vol. 1, S. Haykin, Ed., Englewood Cliffs, NJ: Prentice Hall, 1991, pp. 418-517.

[24] L. Cohen, “Introduction: A primer on time-frequency analysis,” in Time Frequency Signal Analysis – Methods and Applications, chapter 1. B. Boashash, Ed., Longman Cheshire, 1992.

[25] L. Cohen, “Time-frequency distributions – a review,” Proc IEEE, vol. 77, no. 7, pp. 941-981, July 1992.

[26] L. Cohen and C. Lee, “Instantaneous bandwidth,” in Time Frequency Signal Analysis – Methods and Applications, chapter 4. B. Boashash, Ed., Longman Cheshire, 1992.

[27] J.S. Bendat and A.G. Piersol, Random Data, Analysis and Measurements Procedures, 2nd edition. New York, John Wiley and Sons, Inc., 1986.

[28] B. A. J. Angelsen, “Instantaneous frequency, mean frequency and variance of mean frequency estimatores for ultrasonic blood velocity doppler signals,” IEEE Trans Biomed. Eng., vol. BME-28, pp. 733-741, Nov. 1981.

[29] B.A.J. Angelsen and K. Kristoffersen, “Discrete time estimation of the mean Doppler frequency in ultrasonic blood velocity measurements,” IEEE Trans Biomed. Eng., vol. BME-30, pp.207-214, April 1983.

[30] W.L.J. Martens, “The fast time frequency transform (F.T.F.T.): a novel on-line approach to the instantaneous spectrum,” 14th International Conference of the IEEE Engineering in medicine and Biology Society, 1992, Paris.

[31] W.L.J. Martens, “Segmentation of ‘rhythmic’ and ‘noisy’ components of sleep EEG, heart rate and respiratory signals based on instantaneous amplitude, frequency, bandwidth and phase,” Abstract submitted to 1st joint BMES/EMBS conference 1999, Atlanta.

[32] E.J. Bayly, “Spectral analysis of pulse frequency modulation in the nervous system,” IEEE Trans Biomed Eng, 15:257-265, October 1968.

[33] B.W. Hyndman, R.K. Mohn, “A model of the cardiac pacemaker and its use in decoding the information content of cardiac intervals,” Automedica, 1:239-252, 1975.

[34] O. Rompelman, “The assessment of fluctuations in heart rate, “ in: The study of heart rate variability, R.I. Kitney, O. Rompelman (eds). Clarendon Press, Oxford, 1980, pp:59-77.

[35] O. Rompelman, “Spectral analysis of heart-rate variability,” in: Psychophysiology of cardiovascular control, J.F. Orlebeke, G. Mulder, L.J.P. van Doornen (eds). Plenum Press, New York, 1985, pp:315-331.

[36] B. Boashash and A. Reilly, “Algorithms for time-frequency signal analysis,“ in Time Frequency Signal Analysis – Methods and Applications, chapter 7. B. Boashash, Ed., Longman Cheshire, 1992.

[37] Kootsookos, B.C. Lovell, and B. Boashash, “A unified approach to the STFT, TFDs, and instantaneous frequency,” IEEE Trans. Signal Processing, vol. 40, no. 8, pp. 1971-1982, 1992.

[38] K.V. Mardia, Statistics of Directional Data. London UK, Academic Press, 1972.

[39] P. Flandrin, Time-frequency / time-scale analysis. Academic Press, San Diego, 1999.

[40] A.V. Oppenheim, R.W. Schafer, and J.R. Buck, Discrete-Time Signal Processing, 2nd edition. Englewood Cliffs, NJ, Prentice Hall, 1999.

CHAPTER 8
THE INSTANTANEOUS FREQUENCY OF CARDIOVASCULAR TIME SERIES: A COMPARISON OF METHODS

Computer Methods and Programs in Biomedicine, accepted

H.G. van Steenis[1], W.L.J. Martens[2], J.H.M. Tulen[1]

[1]Department of Psychiatry, Erasmus Medical Center Rotterdam
[2]PhyVision b.v., Gemert

The instantaneous frequency of cardiovascular time series is used to describe the time-varying spectral contents of the characteristic frequency bands that are of interest for psychophysiological and cardiovascular research. Four methods to compute the instantaneous frequency of band-limited, monocomponent, and analytical cardiovascular time series were compared by means of simulated time series contaminated with additive noise. These four methods are: the method using the inverse Fourier transform of uncorrelated time-slices of the Wigner-Ville distribution, the discrete time-frequency transform, the circular mean direction of the time-slices of the Wigner-Ville distribution, and the central finite difference of the phase. The time-resolution of the estimates is optimal and is inversely related to the bandwidth of the frequency components, as given by the uncertainty principle of Gabor. At periods in time where the signal fulfills the requirements of the model signal, the four estimates of the instantaneous frequency are numerically equal, only the circular mean direction showed a slight deviation from the other estimates. Although the estimates of the instantaneous frequency differ at sudden phase-shifts at low amplitude, i.e., at points where the signal locally does not comply with the requirements of the model signal, overall the four methods produce comparable estimates of the instantaneous frequency of a cardiovascular time series at an optimal time-resolution.

1 Introduction

Short-term beat-to-beat variations in heart rate and blood pressure may reflect periodicities with a time-period ranging from about 2 seconds to about a minute, i.e., the frequency range of the fluctuations varies between 0.02-0.50 Hz. The heart rate and blood pressure fluctuations in this frequency range are believed to reflect sympathetic and parasympathetic processes within the cardiovascular control system. Usually, on the basis of spectral analysis, these fluctuations are divided into three characteristic spectral regions [1-4]:

1) the low-frequency range: 0.02-0.07 Hz;
2) the mid-frequency range: 0.07-0.15 Hz; and
3) the high-frequency range: 0.15-0.50 Hz.

Cardiovascular time series may be ‘non-stationary’, meaning that the statistical properties of the signals may change over time [5]. The consequence is that, in general, the conventional method of spectral analysis of consecutive or isolated time-windows of 2-5 min is not detailed enough to capture the variations over time of the characteristic spectral peaks: low, mid, and high [6]. However, for monocomponent

time series, i.e., time series with only one spectral peak, the time-varying energy and frequency location of the peak can be described more refined by means of the instantaneous amplitude (IA) and frequency (IF), respectively. To approximate a monocomponent time series, the cardiovascular time series need to be filtered with a band-pass filter that corresponds to one of the spectral ranges of interest: low-, mid-, or high-frequency range, before computing the IA and IF. The IA is simply the envelope of the filtered time series. There are several methods to compute the IF of a monocomponent time series:

1) using the discrete pseudo autocorrelation function (ACF), calculated by means of the inverse Fourier transform, of each time-slice of the discrete pseudo Wigner-Ville distribution (WVD); the discrete pseudo WVD has to consist of uncorrelated time-slices (UTS-method);

2) by means of the discrete time frequency transform (DTFT); this algorithm is the computational heavier but general applicable version of the fast time frequency transform introduced by Martens [7,8];

3) the circular mean direction (CMD) used as an estimator of the first moment of each time-slice of the discrete Wigner-Ville distribution (WVD) of the time series [9,10]; and

4) the central finite difference (CFD) of the phase of the time series, i.e., the first derivative of the phase angle [9,11]. The time-resolution of the resulting IF-estimates of the four methods and of the IA corresponds with the width of the characteristic frequency band under analysis.

The purpose of this paper is to compare these four methods to establish the reliability of the UTS- and the new DTFT-method. The methods are described and compared by means of simulated cardiovascular time series contaminated with additive noise. Cardiovascular time series can be amplitude modulated (AM) and/or frequency modulated (FM). Therefore, both AM time series with noise added to the amplitude and FM time series with noise added to the phase will be simulated. The methods will be performed on the simulations within the mid-frequency range of cardiovascular variations. The resulting IF-estimates will be compared in three ways:

1) the deviation from the expected mean of the IF-estimates as a function of increasing noise;

2) the deviation from the noise-free IF-estimate as a function of increasing noise; and

3) comparison of the distinct IF-estimates: the deviation from each other as a function of increasing noise.

The mathematical theory of the UTS-method has been presented in the previous chapter.

The algorithms were implemented on a Pentium based PC using Microsoft C++ version 1.52c.

2 Methods

2.1 Model signal

For a complex signal $z(t) = a(t)e^{j\varphi(t)}$, the instantaneous frequency (IF) is defined as the rate of change of the phase angle or instantaneous phase $\varphi(t)$ [9,13,14,15]:

$$f_i(t) = \frac{1}{2\pi}\frac{d\varphi}{dt}(t). \quad (1)$$

Throughout this paper, our model signal is an analytical, band-limited, and monocomponent signal with:

a) a slowly varying amplitude modulation; and

b) a fast phase modulation.

For a continuous-time real-valued signal $s(t)$, the complex analytical signal [16] is denoted by:

$$\hat{s}(t) = a(t)e^{j\varphi(t)}.$$

The function $a(t)$ is the envelope or instantaneous amplitude (IA). The model signal is analytical and band-limited because in that case the analytical signal approximates the quadrature model signal [13,15]; this is assumed to be the natural complex representation of a real signal for which the phase is defined and consequently the IF can be derived [15]. For monocomponent signals the IF is meaningful because there is only one spectral concentration [13]. The conditions a) and b) imply that the spectral concentration is positioned in a narrow frequency range at the IF [17]. Furthermore, the same conditions guarantee that the IA $a(t)$ and the IF $f_i(t)$ can be treated as independent signals [13].

The methods described in this paper are applied to heart rate time series but can also be applied to other cardiovascular time series, such as systolic or diastolic blood pressure.

Heart rate variability time series are obtained by detecting the R-waves from the electrocardiogram with a resolution of 1 ms and subsequently generating a pulse train consisting of Dirac pulses at the R-wave occurrence times. This pulse train is demodulated by means of a low-pass filter with cutoff frequency of 0.5 Hz [18,19].

The output signal of the filter is called the 'low-pass filtered cardiac event series', and can be sampled regularly [19,20,21]. In our case, the filtered event series is sampled with a sample interval $t_s = 0.25$ sec, i.e., the sample frequency is $F_s = 1/t_s = 4$ Hz. The other cardiovascular signals are sampled non-equidistantly at R-wave occurrence times and linearly interpolated to an equidistantly sampled cardiovascular time series with interpolation interval $t_s = 0.25$ sec. The discrete heart rate or cardiovascular real time series is denoted by $s[n], n = 0,...,N-1$.

The time series $s[n]$ is filtered with a zero-phase band-pass FIR-filter corresponding to one of the frequency ranges of interest, i.e., low-, mid-, or high-frequency range. This results in a band-limited and monocomponent time series. The filtered time series is subsequently filtered with a zero-phase Hilbert transform FIR-filter to obtain the analytical time series. The resulting analytical and band-limited time series is denoted by $\hat{s}[n], n = 0,...,N-1$. Each complex number $\hat{s}[n]$ can be presented in polar form:

$$\hat{s}[n] = a[n]e^{j\varphi[n]}, \tag{2}$$

with non-negative envelope or IA $a[n]$ and instantaneous phase $\varphi[n]$.

2.2 Band-pass filter design

A discrete zero-phase band-pass FIR-filter is designed by defining the cutoff frequencies (in our case the –6 dB points) and the transition bands. The pass-band is the interval between the cutoff frequencies. The filter-basis spans the pass-band plus the two transition bands. The uncertainty principle of Gabor [16] states that, for a given filter, the product of the width σ_f in the frequency-domain and the width σ_t in the time-domain is greater than or equal to $1/4\pi$. The minimal product is reached for a Gaussian shaped filter. In our application, we want to have minimal interference between consecutive band-pass filters (low-, mid-, and high-range), so the tails of the Gaussian filter should be truncated at some point. In addition, the bank of consecutive band-pass filters should have unity-gain. Therefore, in stead of truncated Gaussian shaped filters, we designed transition bands with 'tail-free squared cosine shaped' slopes in such a manner that the consecutive band-pass filters form a unity-gain filter-bank. Also, our filters are asymmetrical: the trailing slope is twice the length of the leading slope, but the trailing and leading slope of consecutive filters are equal. For these filters, the product of width in time and frequency is close to optimal, for our mid-range filter we computed: $\sigma_t \cdot \sigma_f = 1.19/4\pi$, and for our high-range filter: $\sigma_t \cdot \sigma_f = 1.67/4\pi$.

Suppose the length of the filter-basis is $2 \cdot f_b$ and the midpoint of the filter-basis is the center frequency f_0. Complex demodulation of the signal with frequency f_0 constitutes a translation of the filter transfer function towards the zero frequency over a range of f_0, and the segment $[-f_b, f_b]$ becomes the filter-base. Therefore, after demodulation with frequency f_0, it is sufficient to sample the signal with sample rate $2 \cdot f_b$. This means that, in the case of an ideal rectangular band-pass filter, the application of the translated low-pass filter in combination with complex demodulation will result in an over-sampled signal and the 'over-sampling ratio' or 'decimation factor' n_{DF} is: $n_{\mathrm{DF}} = F_s / (2 \cdot f_b)$. In fact, we could decimate or down-sample the time series with a factor n_{DF} and still retain the same information. In this down-sampled situation, the adjacent points in time are uncorrelated. In our case we do not have ideal rectangular band-pass filters, but band-pass filters with squared cosine shaped transition bands. This means that adjacent points are not truly independent. Examining the impulse response of the demodulated mid-range band-pass filter, we found that there remains a minimal dependency over 3 data points in the down-sampled demodulated time series. In the case of the high-range filter there remains a minimal dependency of 5 data points. The decimation factor n_{DF} depends on the sample frequency F_s and the width of the filter-basis. The decimation factor n_{DF} of our mid-range filter is 31. This leads to an optimal time-resolution of the IF-estimates (each method) of $\Delta t = n_{\mathrm{DF}} \cdot t_s = 7.75$ sec (= 31 samples) for the mid-frequency component. This means that computations over a shorter time-interval yield adjacently dependent results. Or, down-sampling with a factor smaller than 31 yields interpolation. Computations over a longer time-interval yield averaged results ('smearing'). Or, down-sampling with a factor larger than 31 yields aliasing. In the case of our high-range band-pass filter the decimation factor n_{DF} is 9. The optimal time-resolution is $\Delta t = 2.25$ sec (= 9 samples).

In conclusion, we refer to 'instantaneous' as consecutive points in time spaced over $\Delta t = n_{\mathrm{DF}} \cdot t_s$ and only showing a minimal dependency in time. For our mid-range filter, consecutive points are spaced over $\Delta t = 7.75$ sec with a dependency of 3 points. For our high-range filter, consecutive points are spaced over $\Delta t = 2.25$ sec with a dependency of 5 points.

2.3 The discrete Wigner-Ville distribution (WVD)

The time-varying energy contents of an analytical time series $\hat{s}[n], n = 0, ..., N-1$ can be studied by means of the discrete WVD [9,15]. For computational reasons the signal is often windowed with a real-valued discrete window $w[i], i = 0, ..., M-1$. The discrete windowed or pseudo WVD is defined by [9]:

$$W_w[n,k] = \sum_{i=-M_1}^{M_1} w[i]\hat{s}[n+i]w^*[i]\hat{s}^*[n-i]\cdot e^{-4\pi j\cdot ik/M} \quad (3)$$

with $M_1 = M/2$, for $n = 0,...,N-1$ and $k = 0,...,M-1$. We use the algorithm of Boashash and Reilly [22] to compute the discrete pseudo WVD. A time-slice $W_{w,n} = \{W_{w,n}[k], k = 0,...,M-1\}$ at time-index n of the discrete pseudo WVD $W_w[n,k]$ is defined by: $W_{w,n}[k] = W_w[n,k]$, for $k = 0,...,M-1$. The discrete pseudo WVD $W_w[n,k]$ consists of a collection of concatenated time-slices $W_{w,n}$, $n = 0,...,N-1$, each of length M. Each time-slice $W_{w,n}$ can be considered as an 'instantaneous spectrum [13]' reflecting the time-varying energy contents of the time series at each instant in time.

2.4 The local autocorrelation function (ACF)

The local ACF of a continuous-time analytical signal $\hat{s}(t)$, is defined by:

$$R_{\hat{s}\hat{s}l}(t,\tau) = \hat{s}\left(t+\frac{\tau}{2}\right)\cdot\hat{s}^*\left(t-\frac{\tau}{2}\right). \quad (4)$$

The discrete-time analogy is the discrete local ACF of an analytical time series $\hat{s}[n]$, given by:

$$R_{\hat{s}\hat{s}l}[n,l] = \hat{s}\left[n+\frac{l}{2}\right]\cdot\hat{s}^*\left[n-\frac{l}{2}\right],\ n = 0,...,N-1. \quad (5)$$

2.5 IF-estimate: the Circular Mean Direction (CMD)

The discrete first moment of each time-slice $W_{w,n}$ of the discrete pseudo WVD $W_w[n,k]$ (3) yields an estimate of the IF at each time-index n [9,15,23]:

$$f_i[n] = \frac{F_s}{M}\cdot\frac{\sum_{k=0}^{M-1} k\cdot W_{w,n}[k]}{\sum_{k=0}^{M-1} W_{w,n}[k]}.$$

However, the discrete pseudo WVD is periodical, therefore this estimate is biased [9]. A better estimate, which takes the periodical character of the data into account, is the circular mean direction [9,10,23]:

$$f_i^{\mathrm{CMD}}[n] = \frac{F_s/2}{2\pi}\cdot\arg\sum_{k=0}^{M-1} W_{w,n}[k]\cdot e^{2\pi j\cdot k/M},\ n = 0,...,N-1. \quad (6)$$

2.6 IF-estimate: the Central Finite Difference (CFD)

A discrete estimator of the IF is, in analogy with equation (1), the discrete derivative of the phase $\varphi[n]$ of the analytical time series $\hat{s}[n] = a[n]e^{j\varphi[n]}$. The argument of $\hat{s}[n]$ is the discrete instantaneous phase:

$$\varphi[n] = \arg \hat{s}[n] = \arctan\left(\frac{\operatorname{Im} \hat{s}[n]}{\operatorname{Re} \hat{s}[n]}\right).$$

'Unwrapping the phase' resolves possible phase-shifts of $\pm 2\pi$ due to the ambiguity of the inverse tangent (arctan). However, this method may deteriorate with increasing noise. The estimator of the IF is the symmetrical discrete derivative:

$$f_i^{\mathrm{CFD}}[n] = \frac{1}{2\pi} \cdot \left(\frac{\varphi\left[n + \frac{n_{\mathrm{DF}}}{2}\right] - \varphi\left[n - \frac{n_{\mathrm{DF}}}{2}\right]}{n_{\mathrm{DF}} t_s} \right), \tag{7}$$

at each time-index n ($n = 0,...,N-1$) and is called the central finite difference (CFD). Notice that discrete differentiation of $\varphi[n]$ must be obtained by subtracting phases at uncorrelated points:

$$\varphi\left[n + \frac{n_{\mathrm{DF}}}{2}\right] \text{ and } \varphi\left[n - \frac{n_{\mathrm{DF}}}{2}\right],$$

i.e., n_{DF} points apart.

The CFD was introduced as the symmetrical sum of the phases of neighbouring points, i.e., put $n_{\mathrm{DF}}/2 = 1$ in equation (7) [9,11,23]. Boashash [9] and Kootsookos et al. [24] proved that the CMD and this particular CFD (from now on abbreviated with CFD1) are equal: $f_i^{\mathrm{CFD1}}[n] = f_i^{\mathrm{CMD}}[n]$. For band-limited signals, the neighbouring points used in the CFD1-method are correlated, in contrary to the CFD-method, which takes the symmetrical difference of the phases of neighbouring uncorrelated points. This means that for band-limited signals the CFD1-method is biased. Furthermore, because of the equivalence of the CMD-method and the CFD1-method, the CMD-method is biased.

2.7 IF-estimate: the Discrete Time Frequency Transform (DTFT, [7,8])

The DTFT produces an estimator of the IF of a discrete analytical, band-limited and monocomponent time series. Its algorithm is based on the local ACF. It is easy to see that the argument of the complex valued local ACF (4) approximates the IF [7,8,25], i.e., using:

$$\arg R_{\hat{s}\hat{s}l}(t,h) \approx h \cdot \varphi'(t) \tag{8}$$

it follows that:

$$f_i(t) \approx \frac{1}{2\pi} \arg R_{\hat{s}\hat{s}l}(t,1). \tag{9}$$

After filtering with one of the band-pass FIR-filters of interest, low-, mid-, or high-frequency band, the analytical and band-limited time series $\hat{s}[n], n = 0,...,N-1$ is complex demodulated with the center frequency f_0 of the used FIR-filter (section 2.2):

$$\hat{s}_d[n] = \hat{s}[n] e^{-2\pi j \cdot n t_s f_0}. \tag{10}$$

The complex demodulation is followed by the computation of the discrete local ACF of $\hat{s}_d[n]$ (section 2.4) using a lag of n_{DF} points, corresponding with the lag $\tau = 1$ in equation (9):

$$R_{\hat{s}_d\hat{s}_d l}[n, n_{\mathrm{DF}}] = \hat{s}_d\left[n + \frac{n_{\mathrm{DF}}}{2}\right] \cdot \hat{s}_d^*\left[n - \frac{n_{\mathrm{DF}}}{2}\right]. \tag{11}$$

Finally, the estimator of the IF is:

$$f_i^{\mathrm{DTFT}}[n] = f_0 + \frac{F_s}{n_{\mathrm{DF}}} \cdot \frac{1}{2\pi} \cdot \arg R_{\hat{s}_d\hat{s}_d l}[n, n_{\mathrm{DF}}], \tag{12}$$

for $n = 0,...,N-1$. Notice the addition of f_0, which has to be added to neutralize the frequency shift of the complex demodulation. The division factor n_{DF} compensates the lag $h = n_{\mathrm{DF}}$ in equation (8). The factor F_s guarantees that the scale is related to the sample frequency. This explains the factor F_s / n_{DF} in equation (12).

Phase-shifts of $\pm 2\pi$ due to the ambiguity of the inverse tangent do not occur in the computation of the argument of the discrete local ACF (12) because these phase-shifts are canceled in the difference of the phases in the multiplication of the right-hand complex conjugated product factors of equation (11). Therefore, in contrast to the CFD-method in section 2.6, no phase unwrapping is necessary. However, irregular or sudden phase-shifts may occur due to random phase fluctuations or at points where the signal locally does not comply with the requirements of our model signal. These sudden phase-shifts cause irregularities or discontinuities in the IF-estimates of all four methods.

2.8 UTS-method: using Uncorrelated Time-Slices of the discrete pseudo WVD

Similar to the DTFT, this method uses equation (9) to estimate the IF. However, this algorithm uses the 'uncorrelated' time-slices (UTS) of the discrete pseudo WVD to estimate the local ACF $R_{\hat{s}\hat{s}l}(t,\tau)$ in equation (9). Band-pass filtering results in an oversampled time series in which neighbouring points are correlated. The decimation factor n_{DF} of the filter determines the number of adjacent correlated points (section 2.2). In stead of down-sampling the time series with a factor n_{DF}, we use all the original (correlated) points in time. After filtering with one of the band-pass FIR-filters of interest, the discrete pseudo WVD (3) of the filtered time series $\hat{s}[n], n = 0,...,N-1$ is computed. A time-window $w[i], i = 0,...,M-1$ is used which only includes correlated points, i.e., $M = n_{\mathrm{DF}}$. This means that time-slices $W_{w,n}$ of the discrete pseudo WVD only includes correlated points. In the ideal case, consecutive time-slices computed of consecutive disjoint time-windows will be independent. However, in our case using our band-pass filters, there will remain a minimal dependency between consecutive time-slices. Each time-slice is used to compute an estimate of the IF, i.e., the computation of an estimate is spaced over $\Delta t = n_{\mathrm{DF}} \cdot t_s$ sec ($\Delta t = 7.75$ sec and a dependency over 3 time-slices in the case of our mid-range filter and $\Delta t = 2.25$ sec and a dependency over 5 time-slices for our high-range filter). Therefore, in view of section 2.2, the computed IF is instantaneous. In our case we do not use disjoint time-windows, but to provide a smooth IF, the time-window is shifted point by point.

For each time-index $n = 0,...,N-1$, take the time-slice $W_{w,n} = \{W_{w,n}[k], k = 0,...,M-1\}$ of the discrete pseudo WVD (section 2.5). This is a real data series in the frequency-domain. The envelope of each time-slice is determined by computing the modulus of the discrete analytical form $\hat{W}_{w,n}[k] = W_{w,n}[k] + jHW_{w,n}[k]$, in which H is the Hilbert transform. After that, the inverse discrete Fourier transform of the envelope is computed in the index k:

$$R_{\hat{s}\hat{s}w}[n,l] = F_{k\to l}^{-1}\left|\hat{W}_{w,n}[k]\right|^2, \text{ for } l = 0,...,M-1. \tag{13}$$

We call the resultant $R_{\hat{s}\hat{s}w}[n,l]$ discrete pseudo ACF. This estimate (13) of the local ACF is now used for the computation of the discrete instantaneous estimator $f_i^{UTS}[n]$ of the IF:

$$f_i^{\mathrm{UTS}}[n] = \frac{F_s/2}{2\pi} \cdot \arctan\left(\frac{\mathrm{Im}\, R_{\hat{s}\hat{s}w}[n,1]}{\mathrm{Re}\, R_{\hat{s}\hat{s}w}[n,1]}\right), \text{ for } n = 0,...,N-1.$$

As for the DTFT-method of section 2.7, there are no phase-shifts due to the ambiguity of the inverse tangent.

The UTS-method simultaneously produces an instantaneous index $B_i^2[n]$ of the instantaneous bandwidth, called the instantaneous bandwidth coefficient (IBC), by means of [12]:

$$B_{i,\mathrm{UTS}}^2[n] = 1 - \frac{\left|R_{\hat{s}\hat{s}w}[n,1]\right|}{\left|R_{\hat{s}\hat{s}w}[n,0]\right|}. \tag{14}$$

2.9 Simulations

The described methods (UTS, DTFT, CMD, and CFD) are compared by means of simulated amplitude modulated (AM) and frequency modulated (FM) time series. The AM and FM time series are computed with:

$$s_{\mathrm{AM}}[n] = \left[1 + \left(m + r[n]\right) \cdot \cos\left(2\pi f_m \cdot nt_s\right)\right] \cdot \cos\left(2\pi f_c \cdot nt_s\right),$$

and:

$$s_{\mathrm{FM}}[n] = \cos 2\pi\left[f_c \cdot nt_s + k \cdot \cos 2\pi\left(f_m \cdot nt_s + r[n]\right)\right],$$

respectively. The carrier frequency f_c is chosen to be 0.1 Hz, so the simulations will be in the mid-frequency range. The 'message' frequency f_m is 0.01 Hz. In case of AM, the modulation depth m is 0.2. In case of FM, the sensitivity k is chosen in such a way that the modulation depth m is 0.1, using the relation

$$k = \frac{mf_c}{2\pi f_m}.$$

Gaussian noise $r[n]$ is added to the amplitude or to the phase, respectively. The length of each simulated time series is 10 min.

In each case (AM and FM), a number of time series were computed by choosing a variation of standard deviations of the Gaussian noise $r[n]$, including a time series with $r[n] = 0$, i.e., no noise added. With increasing standard deviation, the signal-to-noise ratio (S/N ratio) will be decreasing. The infinite S/N ratio of the noise-free time series will be marked in the figures with $S/N = 999$. Subsequently, we applied the four methods to the resulting AM and FM time series in the mid-frequency range, i.e., using the mid-frequency band-pass filter (section 2.1), to compute and compare the IF-estimates $f_i^{\mathrm{UTS}}[n]$, $f_i^{\mathrm{DTFT}}[n]$, $f_i^{\mathrm{CMD}}[n]$, and $f_i^{\mathrm{CFD}}[n]$. The noise-free estimates are denoted by $\bar{f}_i^{a}[n]$ (a =UTS, DTFT, CMD, and CFD).

If $r[n] = 0$ (no noise), the theoretical IF (denoted with $\hat{f}_i[n]$) of the AM time series is constant:

$$\hat{f}_i[n] = f_c, \tag{15}$$

and the theoretical IF of the FM time series is a sinusoid with amplitude mf_c:

$$\hat{f}_i[n] = f_c \cdot \left(1 - m \cdot \sin\left(2\pi f_m \cdot nt_s\right)\right). \tag{16}$$

For each resulting estimate $f_i^a[n]$ (a=UTS, DTFT, CMD, and CFD) the time average and standard deviation is computed. Next, means and standard deviations of the differences $f_i^a[n] - \bar{f}_i^a[n]$ are computed, except for the noise-free case; in the latter case we compute the means and standard deviations of the differences $\bar{f}_i^a[n] - \hat{f}_i[n]$, using equation (15) for AM, and equation (16) for FM simulations, respectively. Finally, means and standard deviations of differences $f_i^a[n] - f_i^b[n]$ between distinct IF-estimates are computed (a, b =UTS, DTFT, CMD, and CFD).

3 Results and discussion

3.1 Comparing the CFD and the DTFT

All simulations showed that the IF-estimates $f_i^{\mathrm{CFD}}[n]$ and $f_i^{\mathrm{DTFT}}[n]$ of the CFD-method and the DTFT-method, respectively, are numerically equal. In fact, it can be proven readily that the DTFT and the CFD are equivalent. Simple algebra learns that, using equations (11), (10), and (5):

$$R_{\hat{s}_d\hat{s}_d i}[n, n_{\mathrm{DF}}] = R_{\hat{s}\hat{s}i}[n, n_{\mathrm{DF}}] \cdot e^{-2\pi j \cdot n_{\mathrm{DF}} t_s f_0}. \tag{17}$$

Using equations (5) and (2) it follows that:

$$\arg R_{\hat{s}\hat{s}i}[n, n_{\mathrm{DF}}] = \varphi\left[n + \frac{n_{\mathrm{DF}}}{2}\right] - \varphi\left[n - \frac{n_{\mathrm{DF}}}{2}\right]. \tag{18}$$

And finally, using equations (12), (17), (18), (7), and $F_s = 1/t_s$:

$$f_i^{\mathrm{DTFT}}[n] = f_0 + \frac{F_s}{2\pi n_{\mathrm{DF}}} \cdot \left(\arg R_{\hat{s}\hat{s}i}[n, n_{\mathrm{DF}}] - 2\pi n_{\mathrm{DF}} t_s f_0\right) = \frac{1}{2\pi n_{\mathrm{DF}} t_s} \cdot \arg R_{\hat{s}\hat{s}i}[n, n_{\mathrm{DF}}] = f_i^{\mathrm{CFD}}[n],$$

for $n = 0, \ldots, N-1$. Therefore, in the following, the comparison of the CFD-method with the other methods will be omitted, and we will only compare the IF-estimates of the UTS-method, the DTFT-method, and the CMD-method.

3.2 AM Simulations

The effects of increasing noise will be quantified by means of a series of AM-simulations with modulation depth 0.2 and described in the next sections.

3.2.1 Deviation from the expected mean

The means and standard deviations of the IF-estimates $f_i^a[n]$ (a=UTS, DTFT, and CMD) are presented in figures 1A and B as functions of S/N-ratio. For high S/N ratio ($S/N > 3.41$), including the noise-free simulation, the three IF-estimates equal the expected IF, being f_c. For low S/N ratio ($S/N \leq 3.41$), means and standard deviations are increasing. Increasing noise causes more frequent sudden phase-shifts in the phase of the filtered time series at low (instantaneous) amplitudes (see figure 2A). As already mentioned in section 2.7, these sudden phase-shifts cause discontinuities in the IF-estimates $f_i^{\mathrm{UTS}}[n]$, $f_i^{\mathrm{DTFT}}[n]$, and $f_i^{\mathrm{CMD}}[n]$ (figure 2B, C, and D, respectively). Consequently, increasing noise leads to increasing standard deviations of the IF-estimates. Increasing noise also has a tendency to increase the means of the IF-estimates. Due to the asymmetrical filter design, low-frequency components of the noise are slightly more attenuated than the high-frequency components, thereby driving the mean value of the IF-estimate upwards (see figure 1A for low S/N).

The appearance of the discontinuities causes the differences in the standard deviations (figure 1B). In case of the CMD-method, points with low IA coincide with isolated points of low WVD-amplitude in the WVD. At these points the sudden phase-shifts cause high and sharp peaks in the IF-estimate (equation (6), figure 2D). Therefore, the standard deviations of the CMD-method are larger than the standard deviations of the other two methods. In fact, the CMD-method is biased (see section 2.6), this is apparent from the prominent sharp peaks in the IF of the CMD-method, which can extend outside the signal's spectral region and even become negative (see figure 2D).

3.2.2 Deviation from the noise-free IF-estimate

Figures 1C and D present the means and standard deviations of the differences $f_i^a[n] - \bar{f}_i^a[n]$, i.e., the difference of the IF-estimate with respect to the noise-free IF-estimate, for a=UTS, DTFT, and CMD. However, in case of the noise-free simulations ($S/N = 999$), the means and standard deviations of the differences $\bar{f}_i^a[n] - \hat{f}_i[n]$ are computed, i.e., the difference between the noise-free estimate with the theoretical IF (15). In this latter case, it follows from the means and standard deviations that the IF-estimates of the noise-free simulations equal the theoretical IF. For high S/N ratio ($S/N > 3.41$), the means and standard deviations demonstrate that the IF-estimates are fluctuating moderately around the expected IF, being f_c. For low S/N ratio ($S/N \leq 3.41$), the discontinuities in the IF-estimates cause large deviations from the expected IF f_c, and therefore the means and standard deviations are increasing with decreasing S/N ratio. Furthermore, the prominent high and sharp

peaks in the IF-estimate of the CMD-method are the reason that this estimate is deviating more from the expected IF than the IF-estimates of the UTS-method and the DTFT-method.

3.2.3 Comparison of the distinct IF-estimates

Means and standard deviations of differences $f_i^a[n] - f_i^b[n]$ between distinct estimates (a, b =UTS, DTFT, and CMD) are presented in figures 1E and F. For high S/N ratio ($S/N > 3.41$), there are no discontinuities in the IF-estimates, and from the means and standard deviations it follows that the IF-estimates are almost equal. Because the CMD-method is biased, there is a very small deviation of the CMD-method versus the UTS-method and the DTFT-method. For low S/N ratio ($S/N \leq 3.41$), again the discontinuities cause the differences between the IF-estimates. The appearance of the discontinuities causes the large values of the means in figure 1E. The sharp peaks of the IF-estimates of the CMD-method cause the larger standard deviations of the differences $f_i^{\mathrm{UTS}}[n] - f_i^{\mathrm{CMD}}[n]$ and $f_i^{\mathrm{DTFT}}[n] - f_i^{\mathrm{CMD}}[n]$, compared to the standard deviations of the differences $f_i^{\mathrm{UTS}}[n] - f_i^{\mathrm{DTFT}}[n]$ (figure 1F). Therefore, the IF-estimates of the UTS-method and the DTFT-method resemble each other more than the IF-estimates of the UTS-method and the CMD-method or the IF-estimates of the DTFT-method and the CMD-method, respectively.

3.3 FM Simulations

FM-simulations will be performed with a low modulation depth of 0.1. Due to this low modulation depth, the instantaneous frequency stays within a limited frequency range, i.e., no sudden phase-shifts occur, even with increasing contamination with noise. A higher modulation depth, however, may induce sudden phase-shifts more easily, even with moderate noise level.

3.3.1 Deviation from the expected mean of the IF-estimates

Figures 3A and B present the means and standard deviations of the IF-estimates $f_i^a[n]$ (a =UTS, DTFT, and CMD). Figure 3A illustrates that the means of the sinusoidal IF-estimates of all methods fluctuate around the carrier frequency f_c as expected (notice the very small range of the z-axis of figure 3A). From figure 3B it follows that the standard deviations of the noise-free estimates ($S/N = 999$) are almost equal to the expected standard deviation, namely $m \cdot f_c / \sqrt{2}\ (\approx 0.007071)$, which is the standard deviation of the theoretical IF (16).

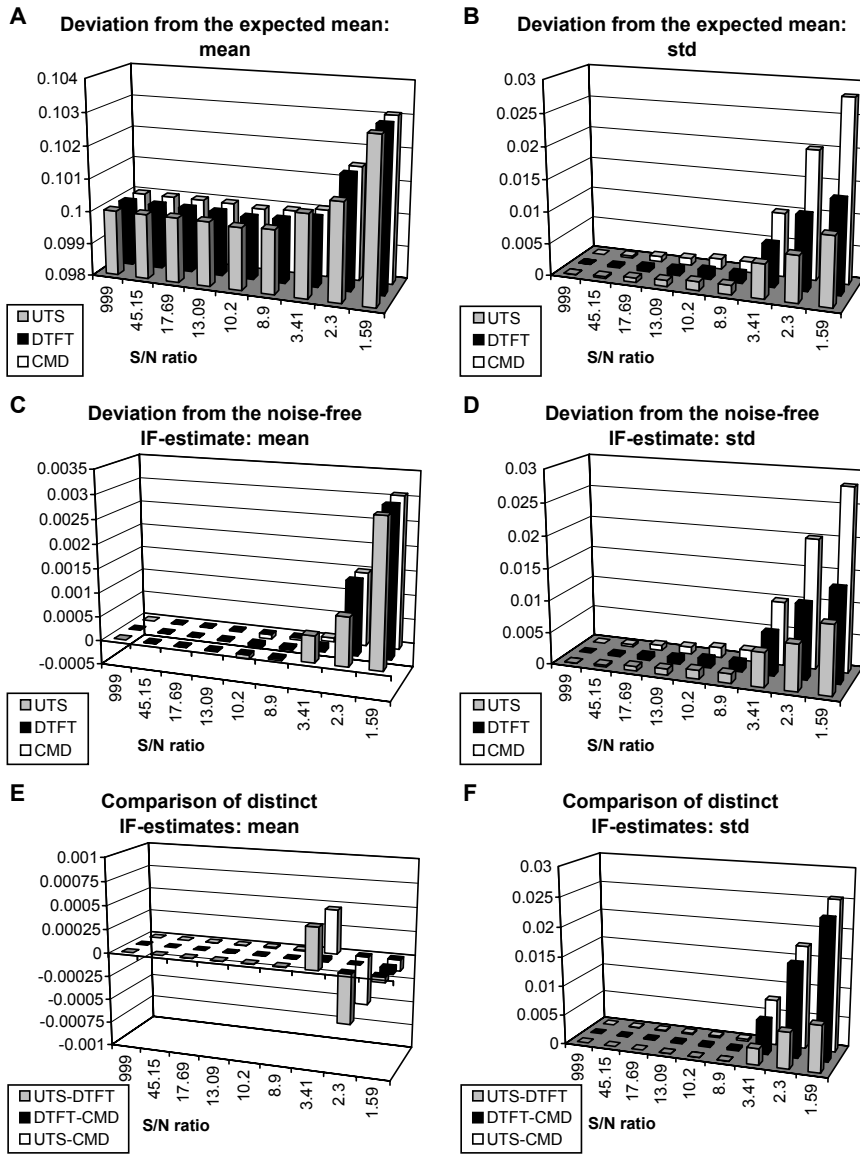

Figure 1. Means and standard deviations of the estimates of the instantaneous frequency of the AM-simulations, as a function of S/N-ratio (modulation depth is 0.2). The scale of the z-axis is in Hz. UTS: method of uncorrelated time-slices; DTFT: discrete time-frequency transform; CMD: circular mean direction.

A and B: deviation from the expected mean.

C and D: deviation from the noise-free IF-estimate.

E and F: comparison of distinct IF-estimates.

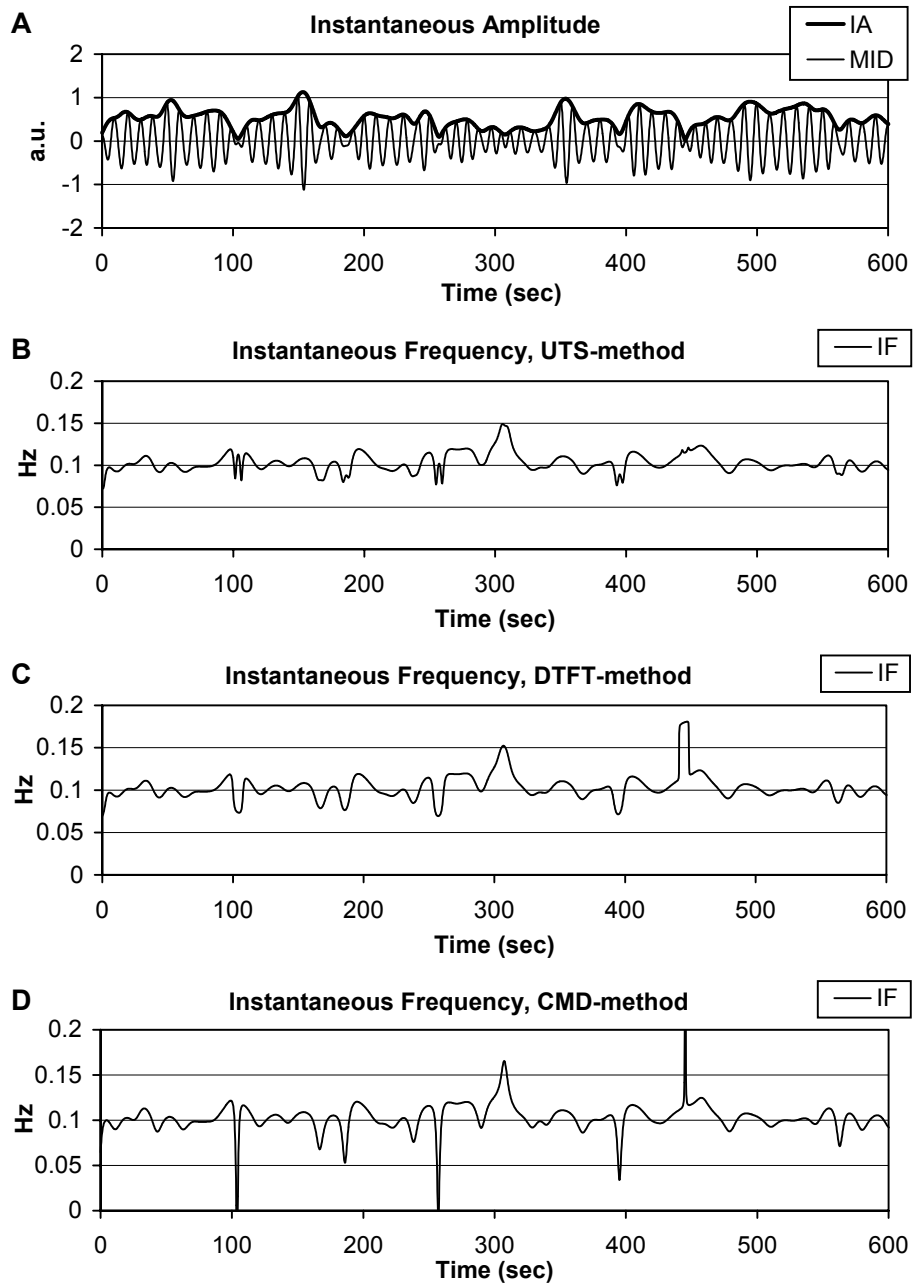

Figure 2. An example of an AM-simulation (modulation depth is 0.2, S/N ratio is 1.59). A: the filtered output of the mid-range filter and the instantaneous amplitude; B, C, and D: the IF-estimates of the UTS-, DTFT, and CMD-method, respectively.

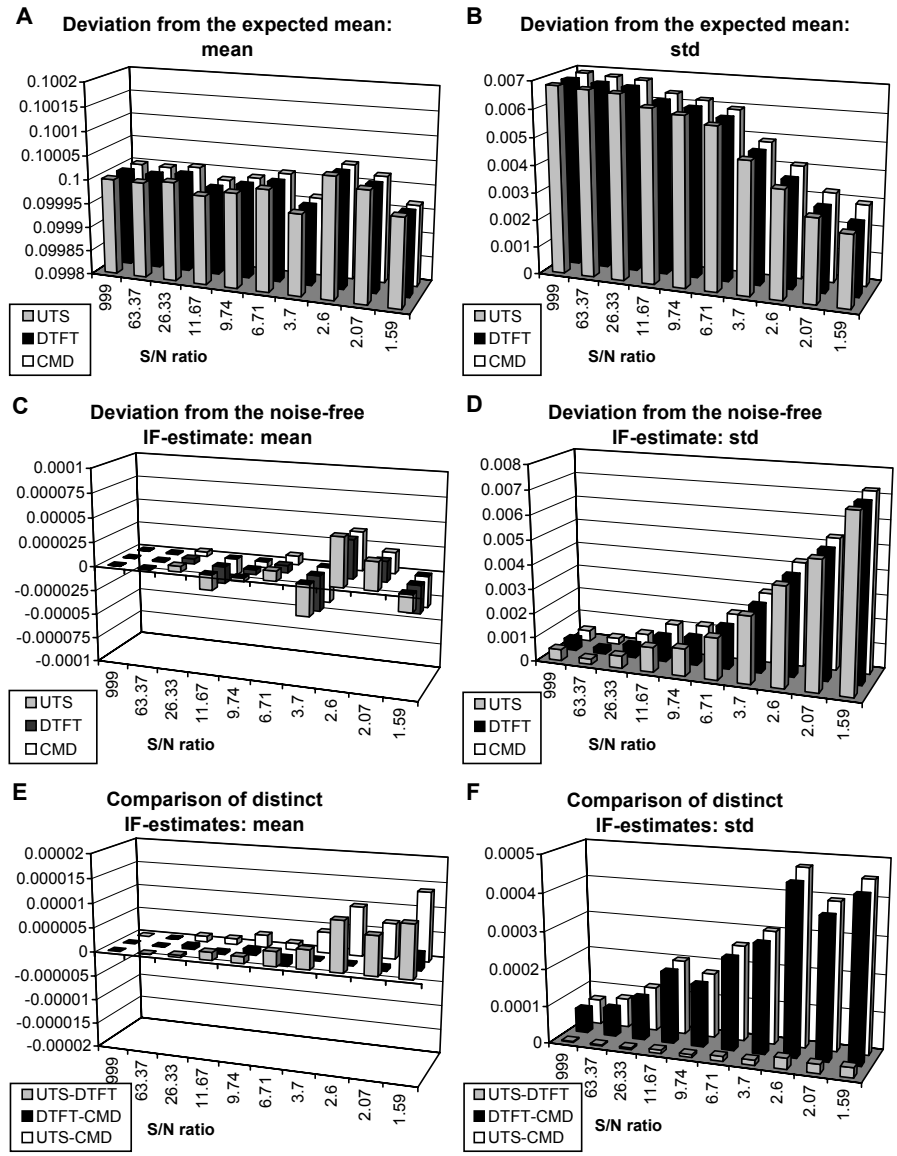

Figure 3. Means and standard deviations of the IF-estimates of the FM-simulations, as a function of S/N-ratio (modulation depth is 0.1). The scale of the z-axis is in Hz. UTS: method of uncorrelated time-slices; DTFT: discrete time-frequency transform; CMD: circular mean direction.

A and B: deviation from the expected mean.

C and D: deviation from the noise-free IF-estimate.

E and F: comparison of distinct IF-estimates.

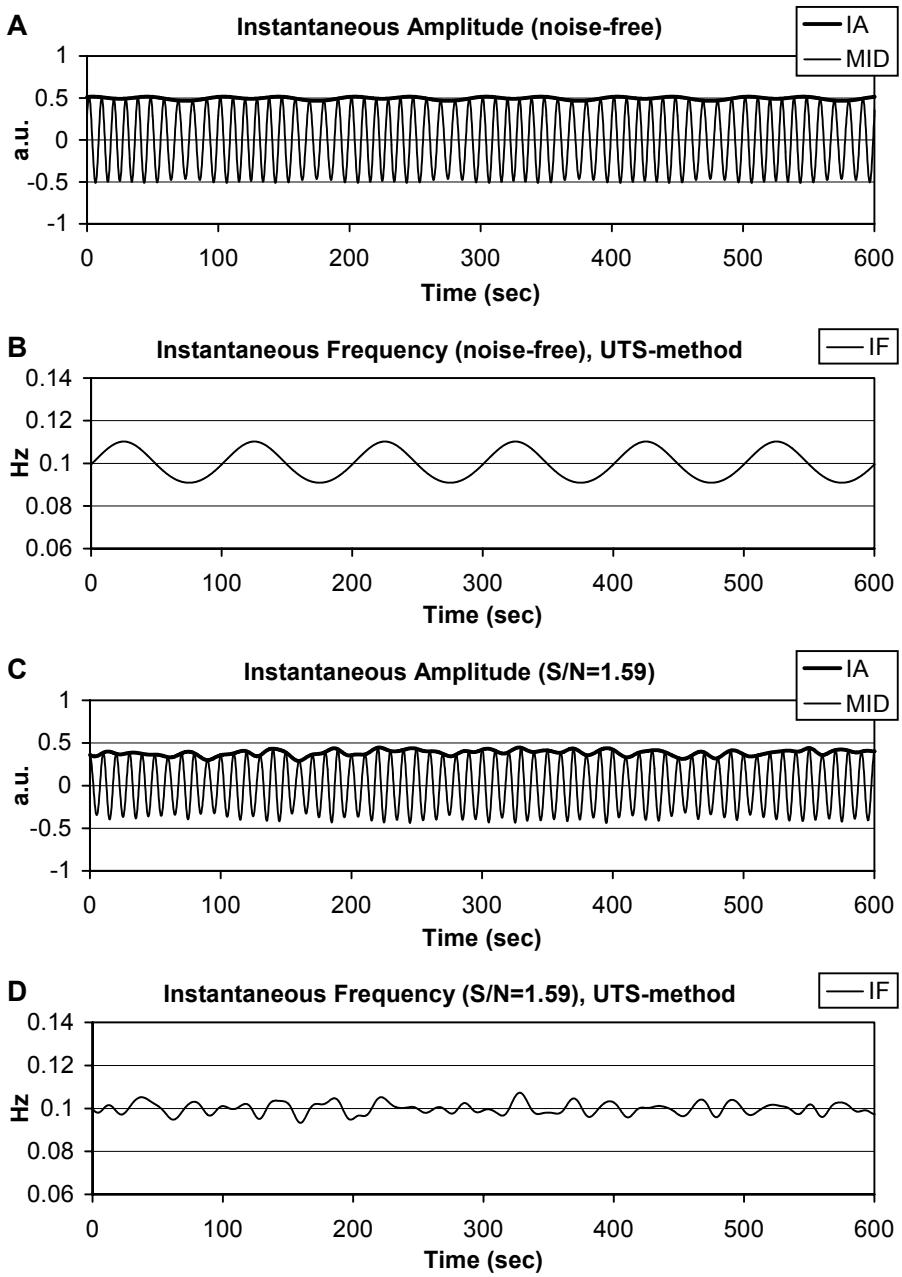

Figure 4. Two examples of FM-simulation (modulation depth is 0.1). A and B: noise-free; C and D: with noise added to the 'message' frequency (S/N ratio is 1.59). A and C: the filtered output of the mid-range filter and the instantaneous amplitude; B and D: the IF-estimate of the UTS-method.

The sinusoidal noise-free IF-estimate of the UTS-method is presented in figure 4B, the noise-free filtered time series and the IA are shown in figure 4A. Note the ripple on the IA in figure 4A: although kept constant, the IA is influenced by the IF.

An example of a FM simulation with noise ($S/N = 1.59$) is presented in figure 4: the IA and the filtered time series in figure 4C and the IF-estimate of the UTS-method in figure 4D. No sudden phase-shifts occur in the phase of the filtered time series and thus no associated discontinuities are present in the IF-estimates. The reason is that the modulation depth $m = 0.1$ is too small to cause sudden phase-shifts.

Figure 3B shows that the standard deviations of the IF-estimates are monotonically decreasing with decreasing S/N ratio. The noise causes the fluctuations of the IF-estimates to collapse, as can be seen in figure 4D. Compare the IF-estimate of figure 4D with the sinusoidal noise-free IF-estimate of figure 4B. The standard deviations are therefore decreasing with increasing noise. The monotonicity of the decrease is due to the absence of discontinuities in the IF-estimates. Also, due to the lack of discontinuities, the effect of increasing noise on the IF-estimates is the same for all methods.

3.3.2 Deviation from the noise-free IF-estimate

Figures 3C and D show the means and standard deviations of the differences $\bar{f}_i^a[n] - \hat{f}_i[n]$ ($S/N = 999$) and the differences $f_i^a[n] - \bar{f}_i^a[n]$ for decreasing S/N ratio, for a=UTS, DTFT, and CMD. The figures demonstrate that the noise-free IF-estimates are all numerically almost equal to the theoretical IF (16). The minor differences, reflected by the standard deviations, are due to effects of the applied asymmetrical mid-range filter (low frequencies are more attenuated than higher frequencies) . For decreasing S/N ratio, the means of the differences $f_i^a[n] - \bar{f}_i^a[n]$ stay close to zero, because the means of both the IF-estimates of the noise-free simulation and the IF-estimates of the simulations with noise are almost the expected mean f_c, as we concluded from figure 3A. (Notice the very small range of the z-axis of figure 3C.) The associated standard deviations of the differences are increasing with decreasing S/N ratio, because the amplitudes and the standard deviations of the IF-estimates are decreasing with increasing noise (see figure 3B) and thus the IF-estimates become more deviated from the noise-free IF-estimate. The monotonicity of the increase is due to the absence of discontinuities in the IF-estimates. Furthermore, because of the absence of discontinuities the effect of increasing noise is the same for all methods (see section 3.3.1).

3.3.3 Comparison of the distinct IF-estimates

Means and standard deviations of differences $f_i^a[n] - f_i^b[n]$ between distinct estimates (a, b =UTS, DTFT, and CMD) are presented in figures 3E and F. The IF-estimates of all methods are almost equal for all simulations (see figure 3E, notice the very small range of the z-axis). The small distinction in the means is due to the fact that the differences $f_i^{\mathrm{DTFT}}[n] - f_i^{\mathrm{CMD}}[n]$ lie more symmetrical around zero than the differences $f_i^{\mathrm{UTS}}[n] - f_i^{\mathrm{CMD}}[n]$ and the differences $f_i^{\mathrm{UTS}}[n] - f_i^{\mathrm{DTFT}}[n]$. The CMD-method is slightly deviating from the UTS-method and the DTFT-method, especially for low S/N ratio, even when there are no discontinuities in the IF-estimates (see figure 3F). The IF-estimates of the UTS-method and the DTFT-method are more similar to each other than the CMD-method to the UTS-method or to the DTFT-method. The reason is that the CMD-method is biased. The standard deviations increase with increasing noise because of the increasing effects of the noise on the amplitude of the IF-estimates.

3.3.4 The effects of increasing modulation depth

The chosen modulation depth of $m = 0.1$ is too small to cause sudden phase-shifts in the phase of the filtered time series and associated discontinuities in the IF-estimates, as already mentioned in section 3.3.1. However, larger modulation depths do rapidly cause frequent sudden phase-shifts and associated discontinuities in the IF-estimates. The effects of the discontinuities on the means and standard deviations are comparable to the effects of the discontinuities in case of AM simulations. As in AM, the appearance of the discontinuities in the IF-estimates will cause the differences between the IF-estimates of the distinct methods.

In addition, it must be noted that increasing the modulation depth m will cause distortion of the IF because eventually the fluctuations of the IF may fall outside the frequency range of the pass-band of the mid-range filter.

4 Concluding remarks

Four methods (UTS, DTFT, CFD, and CMD) to compute the IF of cardiovascular time series were described and compared by means of AM- and FM-simulations of cardiovascular variability. The CFD-method was shown to be analytically equivalent to the DTFT-method. The disadvantage of the CFD-method is the necessity of phase unwrapping, which may rapidly fail for noisy signals. Therefore, the CFD-method was left out of the comparisons between the IF-methods. Furthermore, in comparing the CMD- with the CFD-method, the CMD-method proved to be biased.

The methods were tested on simulated cardiovascular time series (AM and FM) which were contaminated with additive noise. Noise-free simulations showed that the three IF-estimated were almost equal to the theoretical IF, thus the methods produced reliable IF-estimates.

The simulations showed that there were differences between the three IF-estimates due to the aspect of handling sudden phase-shifts at low amplitude, suggesting that the signal locally may not fulfill the requirements of our one-component model signal. Noise or another signal component may be interfering and may cause these sudden phase-shifts and consequently discontinuities in the IF-estimates. The appearances of the discontinuities in the IF-estimates differ between the distinct IF-estimates. Therefore, if there are discontinuities in the IF-estimates, these discontinuities cause large differences between the IF-estimates, as was shown for the AM-simulations with low S/N ratio. These periods with sudden phase-shifts may be submitted to other analysis, such as intra-cross-correlation between different frequency bands (of one specific cardiovascular time series), to investigate possible dependencies between frequency bands, for instance, harmonic relationships.

At time-periods without sudden phase-shifts, i.e., at periods where the signal locally complies with the requirements of our model signal, both the AM-simulations (with high S/N ratio) and the FM-simulations showed that the IF-estimates of the UTS- and the DTFT-methods were numerically identical. The simulations only showed a small deviation of the IF-estimate of the CMD-method from the IF-estimates of the UTS-method and the DTFT-method, due to the bias of the CMD-method.

A practical advantage of the DTFT-algorithm is that it is suitable for very fast computer implementation: the fast time-frequency transform [7,8]. But the DTFT-method is broader applicable than the fast time-frequency transform, because there is more flexibility in choosing interesting frequency regions and associated filters. The UTS-method is computational heavier than the DTFT-method, but the advantage of the UTS-method above the other methods is that it simultaneously can produce an index (14) of the instantaneous bandwidth, called the instantaneous bandwidth coefficient (IBC). The IBC may serve as a time-dependent indicator of irregularities: high values indicate either random phase fluctuations or the interference of other signal components. The above findings make that the IBC can serve as a discriminator between ‘good’ or oscillatory and ‘poor’ or noisy fragments of the signal. The IBC may serve as an indicator for intra-band dependencies.

In conclusion, although the estimates of the IF differ at discontinuities caused by sudden phase-shifts, the four methods overall produced comparable and reliable estimates of the IF of cardiovascular time series. Contrary to the sequential spectral analysis, they provide instantaneous information of time-varying cardiovascular changes with an optimal time-resolution according to Gabor's principle and corresponding to the width of the band-pass filter (low-, mid-, or high-range).

References

[1] S. Akselrod, D. Gordon, J.B. Madwed, N.C. Snidman, D.C. Shannon, R.J. Cohen, Hemodynamic regulation: investigation by spectral analysis, Am. J. Physiol., 249 (1985) M867-M875.

[2] J.P. Saul, R.D. Berger, P. Albracht, S.P. Stein, M.H. Chen, R.J. Cohen, Transfer function analysis of the circulation: unique insights into cardiovascular regulation, Am. J. Physiol., 261 (1991) H1231-H1245.

[3] J.H.M. Tulen, A.J. Man in 't Veld, A.M. van Roon, P. Moleman, H.G. van Steenis, P.J. Blankestijn, F. Boomsma, Spectral analysis of hemodynamics during infusions of epinephrine and norepinephrine in men, J. Appl. Physiol., 76(5) (1994) 1914-1921.

[4] J.H.M. Tulen, F. Boomsma, A.J. Man in 't Veld, Cardiovascular control and plasma catecholamines during rest and mental stress: effects of posture, Clinical Science, 96 (1999) 567-576.

[5] E.J.M. Weber, P.C.M. Molenaar, M.W. van der Molen, A nonstationary test for the spectral analysis of physiological time series with an application to respiratory sinus arrhythmia, Psychophysiology, 29 (1992) 55-65.

[6] G. Parati, P. Castiglioni, M. di Renzo, S. Omboni, A. Pedotti, G. Mancia, Sequential spectral analysis of 24-hour blood pressure and pulse interval in humans, Hypertension, 16 (1990) 414-421.

[7] W.L.J. Martens, The fast time frequency transform (F.T.F.T.): a novel on-line approach to the instantaneous spectrum, 14th International Conference of the IEEE Engineering in medicine and Biology Society (Paris, 1992).

[8] W.L.J. Martens, Segmentation of 'rhythmic' and 'noisy' components of sleep EEG, heart rate and respiratory signals based on instantaneous amplitude, frequency, bandwidth and phase, 1st joint BMES/EMBS conference (Atlanta, 1999).

[9] B. Boashash, Time-frequency signal analysis, in Advances in Spectrum Analysis and Array Processing, Vol. 1, ed. S. Haykin, pp. 418-517 (Prentice Hall, Englewood Cliffs NJ, 1991).

[10] K.V. Mardia, Statistics of Directional Data (Academic Press, London UK 1972).

[11] T.A.C.M. Claasen, W.F.G. Mecklenbräuker, The Wigner distribution – a tool for time-frequency signal analysis – part II: discrete-time signals, Philips Res. J., 35 (1980) 276-300.

[12] H.G. van Steenis, W.L.J. Martens, J.H.M. Tulen, Quantification of the dynamic behaviour over time of narrow-band components present in heart rate variability by means of the instantaneous amplitude and frequency, submitted.

[13] B. Boashash, Estimating and interpreting the instantaneous frequency of a signal – part 1: fundamentals, Proc. IEEE, 80(4) (1992) 520-538.

[14] B. Boashash, G. Jones, Instantaneous frequency and time frequency distributions, in Time Frequency Signal Analysis – Methods and Applications, chapter 2, ed. B. Boashash (Cheshire, Longman, 1992).

[15] L. Cohen, Time-Frequency Analysis (Prentice Hall, Englewood Cliffs NJ, 1995).

[16] D. Gabor, Theory of communication, Proc. IEE, 93 (III) (1946) 429-457.

[17] A. Rihaczek, Signal energy distribution in time and frequency, IEEE Trans. Inform. Theory, IT-14 (1968) 369-374.

[18] E.J. Bayly, Spectral analysis of pulse frequency modulation in the nervous system, IEEE Trans. Biomed. Eng., BME-15 (1968) 257-265.

[19] B.W. Hyndman, R.K. Mohn, A model of the cardiac pacemaker and its use in decoding the information content of cardiac intervals, Automedica, 1 (1975) 239-252.

[20] O. Rompelman, The assessment of fluctuations in heart rate, in The study of heart rate variability, eds. R.I. Kitney and O. Rompelman, 59-77 (Clarendon Press, Oxford, 1980).

[21] O. Rompelman, Spectral analysis of heart-rate variability, in Psychophysiology of cardiovascular control, eds. J.F. Orlebeke, G. Mulder, and L.J.P. van Doornen, 315-331 (Plenum Press, New York, 1985).

[22] B. Boashash, A. Reilly, Algorithms for time-frequency signal analysis, in Time Frequency Signal Analysis – Methods and Applications, chapter 7, ed. B. Boashash (Cheshire, Longman, 1992).

[23] B. Boashash, Estimating and interpreting the instantaneous frequency of a signal – part 2: algorithms and applications, Proc. IEEE, 80(4) (1992) 539-568.

[24] Kootsookos, B.C. Lovell, B. Boashash, A unified approach to the STFT, TFDs, and instantaneous frequency, IEEE Trans. Signal Processing, 40(8) (1992), 1971-1982.

[25] B.A.J. Angelsen, Instantaneous frequency, mean frequency and variance of mean frequency estimatores for ultrasonic blood velocity doppler signals, IEEE Trans. Biomed. Eng., BME-28 (1981) 733-741.

CHAPTER 9
TIME-FREQUENCY PARAMETERS OF HEART RATE VARIABILITY – USING INSTANTANEOUS AMPLITUDE AND FREQUENCY TO UNRAVEL THE DYNAMICS OF CARDIOVASCULAR CONTROL PROCESSES

IEEE Engineering in Medicine and Biology Magazine, in press

H.G. van Steenis[1], W.L.J. Martens[2], J.H.M. Tulen[1]

[1]Department of Psychiatry, Erasmus Medical Center Rotterdam
[2]PhyVision b.v., Gemert

The statistical properties in both time- and frequency-domain of heart rate variability are known to vary over time. Three narrow-band components have been postulated to appear within short-term heart rate variability: low (0.02-0.07 Hz), mid (0.07-0.15 Hz), and high (0.15-0.50 Hz). The time-varying spectral contents of a frequency component can be described by means of the instantaneous amplitude and frequency. The instantaneous frequency of a frequency component may show oscillatory periods in time, but also noisy or irregular periods. This 'deterministic' versus 'stochastic' behavior can be described by means of the instantaneous bandwidth.

In the present paper, we explore the time-frequency characteristics of heart rate variability, i.e., the instantaneous amplitude and frequency and the distribution of oscillatory and irregular periods in time.

Methods are presented to compute the instantaneous amplitude and frequency at an optimal time resolution and to compute two indices of the instantaneous bandwidth to discriminate between oscillatory and irregular periods in time and to correct the instantaneous amplitude and frequency for irregular periods. A number of time-frequency parameters are defined to describe the corrected time-varying spectral contents and the time-varying characteristics of the irregular periods. We applied these parameters to heart rate data obtained from 39 healthy volunteers during steady state situations of supine rest and orthostatic challenge.

Both in mid- and high-frequency band, the instantaneous amplitude and frequency, total duration of the irregular periods and mean duration of oscillatory periods, changed significantly from supine to standing. In the mid-frequency band about 77% of the total time during supine rest could be considered oscillatory, and about 84% during standing. In the high-frequency band about 77% of the total time during supine rest could be considered oscillatory, and about 73% during standing.

The time-frequency parameters, as well as the characteristics of the oscillatory and irregular periods, discrimated differentially between supine rest and orthostatic challenge. Time-frequency parameters may be relevant to quantify to unravel the dynamic nature of homeostatic cardiovascular control processes in time.

1 Introduction

In recent years heart rate variability has become a topic of major clinical interest subsequent to pioneering investigations [e.g., 1-4]. Since Kobayashi [5] we know that long term (24 hour) heart rate variability has an 1/f spectrum with a frequency range from as low as 10^{-5} Hz to about 0.5 Hz.

In physiological and in clinical research, however, most attention has gone to the higher frequencies in the 1/f spectrum. Specifically, the respiratory related fluctuations (around 0.20 - 0.35 Hz), which may reflect parasympathetic activity, the 'ten-second rhythm' band (between 0.07 - 0.15 Hz), which may reflect sympathetic and parasympathetic activity, and frequencies around 0.04 Hz (between 0.02 - 0.07 Hz) which may be of variable origin, have been attended to [1,3,6,7,8,9,10]. It has been shown that the ratio of the power in the first two bands may be indicative of the sympathovagal balance.

To visualize and quantify the variability in these bands, Fourier analysis, wavelet analysis, and time-frequency representations such as the Wigner-Ville distribution and the short-time Fourier transform have been employed. With these techniques it was demonstrated, that oscillations in these bands were unstable in amplitude and in frequency to the extend that they cannot be captured in time windows even as short as 2-5 min [e.g., 11]. Given this instability, it would be of interest to know at any instant what the time-varying amplitude and frequency of these oscillations are, rather than having to satisfy oneself with statistical averages over epochs. Fourier analysis is severely limited in this respect, since frequency and time resolution are inversely linked: time resolution improves when frequency resolution deteriorates. This trade-off is also a drawback of the short-time Fourier transform: using the short-time Fourier transform to compute the instantaneous frequency with a reliable resolution is not possible without a priori knowledge of the instantaneous frequency [12,13]. Wavelet analysis has delivered a form of instantaneous amplitude but has as yet not been used to provide instantaneous frequency. Wigner-Ville techniques can be used to obtain the instantaneous frequency of band-limited heart rate variability signals. However, the technique breaks down at instants that the instantaneous amplitude is low or when there appear to be phase shifts [14,15]. At these instants, discontinuities in the instantaneous frequency occur, making it difficult to quantify results.

Recently, a new method was presented to compute the instantaneous amplitude and frequency of band-limited heart rate variability signals [14]. This method offers a view on the instantaneous frequency of the oscillations with an optimal resolution in time (seconds rather than minutes), based on the uncertainty principle of Gabor [16]. This method is also able to indicate the locations of irregularities or discontinuities in the instantaneous frequency and reject these. This technique was compared to other methods to asses its reliability [15]. In the present paper, we apply this extended method to heart rate variability data, obtained from healthy subjects during supine rest and orthostatic load. We explore, for the first time,

the time-frequency characteristics, i.e., the instantaneous amplitude and frequency and the distribution of oscillatory and irregular periods in time, during steady state situations of supine rest and standing.

2 Methods

Three oscillatory narrow-band components of interest have been postulated in the literature to appear within short-term heart rate variability signals:

1) the low-frequency range: 0.02-0.07 Hz;
2) the mid-frequency range: 0.07-0.15 Hz; and
3) the high-frequency range: 0.15-0.50 Hz.

Heart rate variability is a dynamic signal: the statistical properties change in time. This means that the characteristic spectral peaks, low, mid, and high, vary in time. They vary in frequency (location on the frequency axis), amplitude (energy), and bandwidth (the width or spread of the peak). One can imagine an 'instantaneous spectrum' [12,17] at each instant in time to visualize these time-varying characteristics. One way to obtain 'instantaneous spectra' in time is by means of the Wigner-Ville distribution [13,17,18,19].

The time-varying properties of the spectral peaks can be described by means of the squared instantaneous amplitude, which is a measure of the instantaneous power or energy per unit time [13], and the instantaneous frequency, which defines the frequency location of the spectral peak in time. The spread of the spectral peak is measured by means of the instantaneous bandwidth. A method to compute the instantaneous amplitude and frequency is presented and an index for the instantaneous bandwidth, called the instantaneous bandwidth coefficient, is computed. This index serves as a time-varying segmentator of oscillatory versus irregular periods in the instantaneous frequency. The time resolution of the computed instantaneous amplitude, frequency, and bandwidth coefficient is optimal and is inversely related to the bandwidth of the frequency components, as given by the uncertainty principle of Gabor [16].

The mathematical theory of the method has been presented in a previous paper [14]. In Van Steenis, et al. [14] analytical and monocomponent signals are discussed and the design of the band-pass and Hilbert transform FIR-filters are described in detail. Also a comprehensive justification of the resolution in time, based on the uncertainty principle of Gabor was provided.

In this paper we limit ourselves to the application of the method to the mid- and high-frequency band of heart rate variability time series. However, the method

was developed to be applied to the three narrow-band (low-, mid-, and high-frequency) components of various cardiovascular time series and also to respiratory time series.

Our model signal is an analytical, monocomponent, and band-limited signal, as will be explained in the next sections.

2.1 Prerequisites

The (complex) analytical signal $\hat{s}(t)$ [16] associated with a real signal $s(t)$ allows us to define the instantaneous amplitude, phase, and frequency of the real signal. The analytical signal $\hat{s}(t)$ is, under certain conditions, a natural complex representation of the real signal $s(t)$ and has two properties:

a) the amplitudes of the positive frequency components of the analytical signal $\hat{s}(t)$ equal the amplitudes of the positive frequency components of the original real signal $s(t)$ multiplied by two, but the negative frequency components are eliminated; and

b) the real part of the complex analytical signal $\hat{s}(t)$ equals the real signal $s(t)$. The analytical signal can be obtained from the original real signal by means of the Fourier transform [19,20] or by means of the Hilbert transform [12,13,16,20,21].

The analytical signal can now be written in polar form $\hat{s}(t) = a(t)e^{j\varphi(t)}$ and visualized as a moving vector in the complex plane. The envelope or instantaneous amplitude (IA) $a(t)$ and the instantaneous phase (IP) $\varphi(t)$ are defined as the modulus and the argument of the complex number $\hat{s}(t)$, respectively. Furthermore, the instantaneous frequency (IF) can be defined as the rate of change of the phase angle $\varphi(t)$ [12,13,17]:

$$f_i(t) = \frac{1}{2\pi}\frac{d\varphi}{dt}(t). \tag{1}$$

If the spectrum of the envelope $a(t)$ lies in a frequency region $(-\omega_1, \omega_1)$ and the spectrum of $e^{j\varphi(t)}$ lies above this region, i.e., $\hat{s}(t)$ has a slow amplitude modulation and a fast phase modulation, it can be proven that:

1) the analytical signal is a reliable and natural complex representation of the real signal $s(t)$. Therefore, the IA $a(t)$, IP $\varphi(t)$, and IF $f_i(t)$ represent the IA, IP, and IF of the original real signal [13]; and

2) the time-varying signal's energy is in frequency concentrated in a single narrow frequency range at the IF $f = f_i(t)$ [22].

Suppose that locally (in time) the signal's energy is distributed in two or more frequency peaks; this is called 'multicomponent' [12,13,19,23]. In that case the IF has no physical meaning. Cohen [13] mentioned a few inconsistencies that may occur. Therefore, the IF has only meaning for 'monocomponent' signals, for which there is

only one time-varying spectral concentration. A means to study the time-varying energy content of an analytical signal is in the time-frequency plane by means of a time-frequency distribution [13,19], for instance the Wigner-Ville distribution. A time-slice T_t at time t of a time-frequency distribution $T(t,f)$ is defined by $T_t = \{T_t(f), \text{all } f\}$ and $T_t(f) = T(t,f)$. Each time-slice can be viewed as an 'instantaneous spectrum'. Thus, one can imagine a time-frequency distribution as a concatenation of 'instantaneous spectra'. In our case the signal is monocomponent and band-limited, so our signal has only one time-varying component in the time-frequency plane. Therefore, each time-slice or 'instantaneous spectrum' contains only one spectral peak of limited width.

The IF of an analytical signal $\hat{s}(t)$ is defined as the derivative of the IP $\varphi(t)$ (equation (1)). For a sinusoidal signal, this definition is unambiguous. The sinusoid is a sharp delta peak in the time-frequency plane at the IF and has no spread, i.e., there is only one frequency present, namely at the IF. If the signal has (locally) a stochastic component, this definition becomes harder to interpret because the frequency content is not concentrated in one delta peak. However, in the case of the Wigner-Ville distribution $W(t,f)$, Ville [17] showed that the IF at time t equals the first conditional moment of the Wigner-Ville distribution $W(t,f)$ with respect to frequency, i.e., the IF at time t is the conditional average $\langle f \rangle_t$ of the frequency components in the time-slice W_t at a time t [e.g., 12,13,17]. The IF of a signal with a stochastic component can now be defined unambiguously as the first conditional moment of the Wigner-Ville distribution. Cohen [13] defined a large class of time-frequency distributions for which this is also valid. The IF of this signal will have a spread due to the stochastic component. The width (in the frequency direction) of the spread is called the instantaneous bandwidth (IB). To say this in other words: the conditional standard deviation $\sigma_{f|t}$ or spread of the conditional average $\langle f \rangle_t = f_i(t)$, can be interpreted as the IB at time t, and is defined by the second conditional moment [12,13,19,24]. However, the second conditional moment of the Wigner-Ville distribution may become negative and therefore this is not a good measure of the IB [13,19].

Cohen and Lee [24] presented an expression for the IB that does not depend on the time-frequency distribution but depends only on the IA $a(t)$:

$$B_i^2(t) = \frac{1}{4\pi^2} \cdot \left(\frac{a'(t)}{a(t)} \right)^2 \tag{2}$$

[e.g., 13]. They provided several arguments that this is a reasonable measure of the conditional standard deviation of the IF, i.e., $\sigma_{f|t} = B_i(t)$. If there is no amplitude

modulation ($a(t)=c$) at time t, then there exists only one frequency at that time and the IB is zero, i.e., no spread. Amplitude modulation ($a'(t)\neq 0$) at time t will result in a spread $B_i(t)$ of frequencies and the average of this spread is the IF $f_i(t)$ [24].

A time-slice W_t of the Wigner-Ville distribution $W(t,f)$ can be considered as an 'instantaneous spectrum'. In analogy with the Wiener-Khinchine theorem [25], the inverse Fourier transform $R_t(\tau)$ of $W_t(f)$ can be considered as an autocorrelation function. We use this autocorrelation function, to define the following estimates of the IF [26,27,28] and the IB:

$$\overline{f}_i(t)=\frac{1}{2\pi}\arg R_t(1) \tag{3}$$

and

$$\overline{B}_i^2(t)=\frac{1}{\pi^2}\left[1-\frac{|R_t(1)|}{|R_t(0)|}\right] \tag{4}$$

It can be proven that $\overline{f}_i(t)$ is an approximation of the IF $f_i(t)$ of equation (1), and that $\overline{B}_i$ approximates the IB B_i of equation (2) [14]. In the next sections, the equations (3) and (4) will be implemented to compute instantaneous estimates of the IF and the IB. Due to this construction by means of the autocorrelation function, there will be no phase shifts of $\pm 2\pi$ due to the ambiguity of the inverse tangent in equation (3). Zero division in equation (4) will only occur if the heart rate variability signal $\hat{s}(t)$ is locally identical to zero.

2.2 Implementation, part 1

Heart rate variability time series are obtained by detecting the R-waves from the electrocardiogram (ECG). In our studies, the ECG is measured and digitized at a sample frequency of 1024 Hz. The R-waves are detected with an resolution of 1 ms. These R-waves can be represented as a pulse train consisting of Dirac pulses placed in time at the R-wave occurrence times. The pulse train is demodulated by means of a low-pass filter with cutoff frequency of 0.5 Hz [29,30]. The output signal of the filter is called the 'low-pass filtered cardiac event series', and can be sampled regularly [30,31,32]. In our case, the filtered event series is sampled with a sample interval $t_s=0.25$ sec, i.e., the sample frequency is $F_s=1/t_s=4$ Hz.

The resulting discrete real heart rate variability time series is filtered with a zero-phase band-pass FIR-filter corresponding to one of the frequency ranges of interest, i.e., mid- or high-frequency range. The filtered time series is subsequently filtered with a zero-phase Hilbert transform FIR-filter [20,21], to obtain the analytical time series. The resulting analytical, band-limited, and monocomponent time series is

denoted by $\hat{s}[n]$, $n = 0,...,N-1$. Each complex number $\hat{s}[n]$ can be presented in polar form: $\hat{s}[n] = a[n]e^{j\varphi[n]}$, with non-negative envelope or IA $a[n]$ and IP $\varphi[n]$. This means that the IA is the modulus of the complex number $\hat{s}[n]$.

The next step is to choose a real-valued discrete time window $w[i]$, $i = 0,...,M-1$ of length M (see the next two sections). This window is used to compute the discrete pseudo Wigner-Ville distribution [19] of the filtered analytical heart rate variability time series $\hat{s}[n]$:

$$W_w[n,k] = \sum_{i=-M_1}^{M_1} w[i]\hat{s}[n+i]w^*[i]\hat{s}^*[n-i]\cdot e^{-4\pi j\cdot ik/M}$$

with $M_1 = M/2$, for $n = 0,...,N-1$ and $k = 0,...,M-1$. We use the algorithm of Boashash and Reilly [20] to compute the discrete pseudo Wigner-Ville distribution. The discrete pseudo Wigner-Ville distribution $W_w[n,k]$ can be considered as a concatenation of N time-slices $W_{w,n} = \{W_{w,n}[k],\ k = 0,...,M-1\}$ for $n = 0,...,N-1$ defined by $W_{w,n}[k] = W_w[n,k]$, i.e., a time-slice of length M at each time point n.

2.3 Band-pass filtering

A discrete zero-phase band-pass FIR-filter is designed by defining the cutoff frequencies (in our case the –6 dB points) and the transition bands. The pass-band is the interval between the cutoff frequencies. The filter-basis is the pass-band plus the two transition bands (see figure 1A). The uncertainty principle of Gabor [16] states that, for a given filter, the product of the width σ_f in the frequency domain and the width σ_t in the time domain is greater than or equal to $1/4\pi$. In practice it means that, the wider (narrower) the bandwidth of a filter is, the shorter (longer) the corresponding impulse response is in the time domain. The minimal product is reached for a Gaussian shaped filter. In our application, we want to have minimal interference between consecutive mid- and high-range band-pass filters, so the tails of the Gaussian filter should be truncated at some point. In addition, the bank of consecutive band-pass filters should have unity-gain. Therefore, in stead of applying truncated Gaussian shaped band-pass filters, we used transition bands with 'tail-free squared cosine shaped' slopes, designed in such a manner that they form a unity-gain filter-bank (figure 1B). Our filters are asymmetrical: the trailing slope is twice the length of the leading slope, but the trailing and leading slope of consecutive band-pass filters are equal ('semi constant Q'). For these filters, the product of width in time and frequency is close to optimal, for our mid-range filter we computed: $\sigma_t \cdot \sigma_f = 1.19/4\pi$, and for our high-range filter: $\sigma_t \cdot \sigma_f = 1.67/4\pi$.

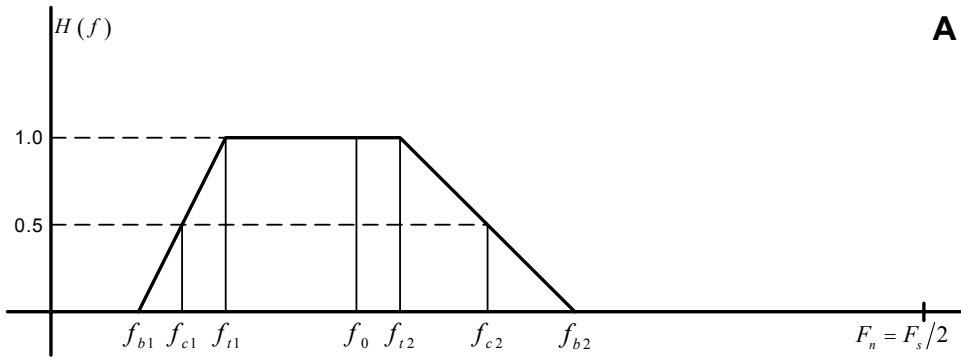

Figure1A. The design of a band-pass FIR-filter. The pass-band is the frequency interval $[f_{c1}, f_{c2}]$, defined by the two cutoff frequencies, in our case –6 dB points, f_{c1} and f_{c2}. The filter-basis is the interval $[f_{b1}, f_{b2}]$. The two transition bands $[f_{b1}, f_{t1}]$ and $[f_{t2}, f_{b2}]$, are 'squared cosine shaped' slopes. The trailing slope is made twice as long as of the leading slope. The center frequency f_0 is the midpoint of the basis: $f_0 = (f_{b1} + f_{b2})/2$. The signal to be filtered is analytical, therefore there is no pass-band at the negative frequencies.

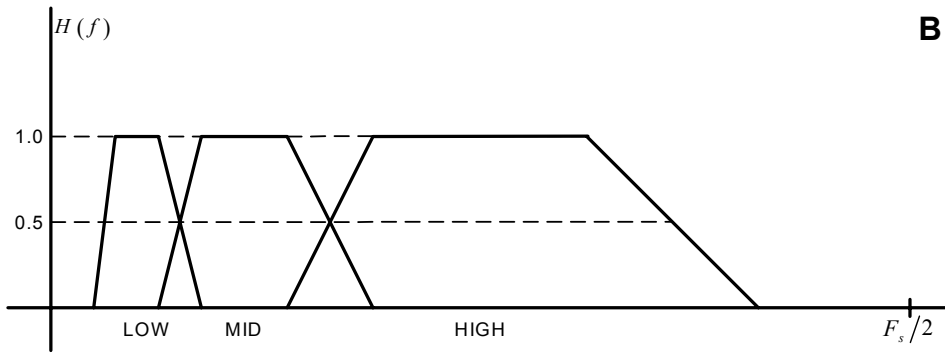

Figure 1B. The set of consecutive band-pass filters for the low-, mid-, and high-frequency components constitutes a unity-gain filter-bank. Trailing and leading slopes of consecutive band-pass filter are equal.

The center frequency f_0 is the midpoint of the filter-basis. Suppose we translate the center frequency to the zero frequency, then the filter-basis lies symmetrical around the zero frequency. Suppose the width of the filter-basis is B Hz. Then the new Nyquist frequency will be $f_n = \frac{1}{2}B$ (figure 1C). Therefore, after demodulation of the signal with frequency f_0, it is sufficient to sample the filtered

signal with sample rate B Hz. This means that, in the case of an ideal rectangular band-pass filter, the application of the translated low-pass filter in combination with complex demodulation will result in an over-sampled signal and the 'over-sampling ratio' or 'decimation factor' n_{DF} is $n_{\mathrm{DF}} = F_s / B$. In fact, we could decimate or down-sample the time series with a factor n_{DF} and still retain the same information. In this down-sampled situation, the adjacent points in time are uncorrelated. In our case we do not have ideal rectangular band-pass filters, but band-pass filters with squared cosine shaped transition bands. This means that adjacent points are not truly independent.

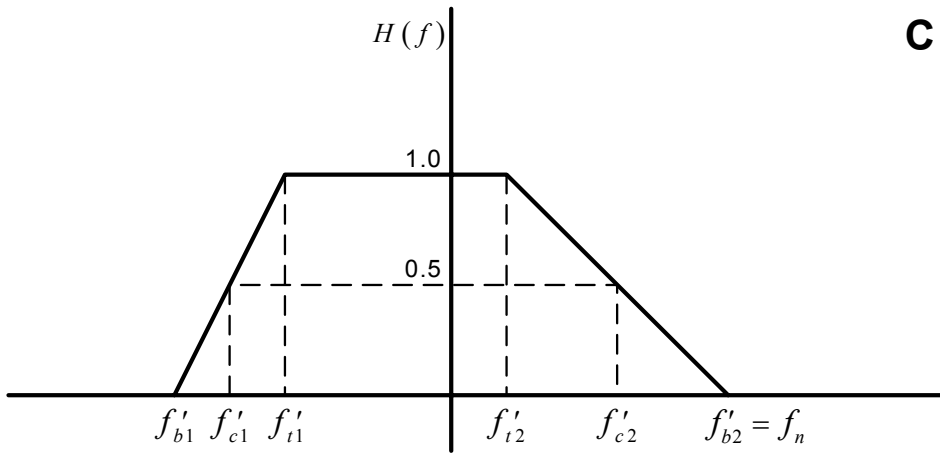

Figure 1C. The filter-basis of the band-pass filter of figure 1A is translated over a range f_0 towards the origin, $f'_{b1} = f_{b1} - f_0$, $f'_{b2} = f_{b2} - f_0$, etc. This basis of this filter lies symmetrical around the zero frequency. After demodulation of the signal with frequency f_0, it is sufficient to sample the filtered signal with sample rate $2 \cdot f'_{b2}$.

The decimation factor n_{DF} depends on the sample frequency F_s and the width of the filter-basis. The decimation factor n_{DF} of our mid-range filter is 31. To determine the maximal discrete resolution Δt in time, the Nyquist frequency of the demodulated band-pass filter was determined to be

$$f_n = \frac{F_s/2}{n_{DF}} = \frac{2}{31} = 0.0645 \text{ Hz},$$

to allow for perfect signal integrity, whilst minimizing dependency between adjacent points in time. This leads to an optimal time resolution of $\Delta t = 1/2 f_n = 7.75$ sec (= 31 samples). This means that computations over a shorter time interval yield adjacently dependent results. Or, down-sampling with a factor smaller than 31 yields interpolation. Computations over a longer time interval yield averaged results

('smearing'). Or, down-sampling with a factor larger than 31 yields aliasing. Examining the impulse response of the demodulated mid-range band-pass filter, we found that there is a minimal dependency in the down-sampled demodulated time series over 3 data points (see chapter 7).

We now choose the window length M of the time window of the discrete pseudo Wigner-Ville distribution to be $n_{\mathrm{DF}} = 31$ points, in the case of the mid-range band-pass filter. This means that consecutive Wigner-Ville time-slices are computed over $\Delta t = 7.75$ sec. A shorter window leads to adjacently dependent time-slices, a longer window results in smearing. But in the case of the ideal length of 31 points, the adjacent time-slices are not truly independent, they show a minimal dependency over 3 slices (see chapter 7).

In the case of our high-range band-pass filter we found that the decimation factor n_{DF} is 9 and the Nyquist frequency is $f_n = 2/9 = 0.2222$ Hz. The optimal time resolution is $\Delta t = 2.25$ sec (= 9 samples). We now choose the window length M of the discrete pseudo Wigner-Ville distribution to be $n_{\mathrm{DF}} = 9$ points, and in this case there is a minimal dependency between adjacent time-slices of 5 slices.

In conclusion, for the remainder of this article, 'instantaneous' is referred to as consecutive points in time only showing a minimal dependency in time. For our mid-range filter, consecutive points are spaced over $\Delta t = 7.75$ sec with a dependency of 3 points. For our high-range filter, consecutive points are spaced over $\Delta t = 2.25$ sec with a dependency of 5 points.

2.4 Implementation, part 2

The length M of the time window of the discrete pseudo Wigner-Ville distribution is chosen to be n_{DF}, the decimation factor belonging to the mid- or high-range band-pass filter. For each time index n, we take the time-slice $W_{w,n}$ of the discrete pseudo Wigner-Ville distribution $W_w[n,k]$. This is a real data series in the frequency domain. It can be considered as an 'instantaneous spectrum', as mentioned above, but it is not a true density, because it may contain negative values. Therefore, we determine the squared envelope of each time-slice by computing the discrete analytical data series:

$$\hat{W}_{w,n}[k] = W_{w,n}[k] + jHW_{w,n}[k]$$

and its squared modulus. We now compute the inverse discrete Fourier transform of the squared modulus in the index k:

$$R_{\hat{s}\hat{s}w}[n,l] = F_{k\to l}^{-1}\left|\hat{W}_{w,n}[k]\right|^2$$

for $l = 0,...,M-1$. We call the resultant $R_{\hat{s}\hat{s}w}[n,l]$ the discrete pseudo autocorrelation function (DPACF).

The computation of the discrete estimator $f_w[n]$ of the IF and the squared estimator $B_w^2[n]$ of the IB are now straightforward using the expressions:

$$f_w[n] = \frac{F_s/2}{2\pi} \cdot \arctan\left(\frac{\text{Im } R_{\hat{s}\hat{s}w}[n,1]}{\text{Re } R_{\hat{s}\hat{s}w}[n,1]}\right) \tag{5}$$

and

$$B_w^2[n] = 1 - \frac{|R_{\hat{s}\hat{s}w}[n,1]|}{|R_{\hat{s}\hat{s}w}[n,0]|} \tag{6}$$

corresponding with equations (3) and (4). These estimates are instantaneous conform the former section. As mentioned in the first Methods-section 'Prerequisites', phase unwrapping is not necessary in the computation of equation (5) and zero division in equation (6) cannot occur in case of non-zero signals.

The procedure of computing the envelope of the time-slice $W_{w,n}$ can be seen as a smearing function in the frequency domain, i.e., convolution with an averaging filter. It follows that in the τ-domain the inverse Fourier transform is weighted, i.e., the DPACF is multiplied with a weighting function. But this means that $B_w^2[n]$ is a biased squared estimator of the squared IB. The index $B_w^2[n]$, however, is useful as an indicator of irregularities or interference due to other signal components, as will be demonstrated in the next sections. Therefore, this index is called the instantaneous bandwidth coefficient (IBC). The IBC $B_w^2[n]$ is a qualitative index and is chosen in such a way that it will always have a value between 0 and 1 (note the absence of the factor $1/\pi^2$ in equation (6), e.g., equation (4)). Value 0 means that there is no amplitude modulation, so the signal is purely frequency modulated (see the Methods-section 'Prerequisites'); value 1 means that the signal is a noise signal. The estimator $f_w[n]$ is useful to calculate the IF and is not biased because both real and imaginary part of $R_{\hat{s}\hat{s}w}[n,1]$ have been multiplied by the same real factor of the weighting function.

2.5 The behavior of the IF and the IBC

In this section we describe the behavior of the IF and the IBC: 1) when the signal is locally, i.e., for a short period in time, not monocomponent, or, 2) due to the presence of noise or random phase fluctuations in the original signal.

1) A signal is locally multicomponent [12,13,19,23] in the frequency band of interest if there is locally more than one spectral concentration present in the time-varying 'instantaneous spectrum'. For instance, a signal may locally become multicomponent if harmonic or sub-harmonic components arise due to non-sinusoidal shape of waveforms. For multicomponent signals, the IF has no meaning [13]. The effect is

that phase shifts at low amplitudes cause discontinuities in the IF and the IBC. For instance, suppose $\hat{s}(t)$ consists of two sinusoids with different frequencies $f_2 > f_1$ [33]:

$$\hat{s}(t) = e^{2\pi j f_1 t} + e^{2\pi j f_2 t} = 2\left|\cos(2\pi f_d t)\right| e^{2\pi j f_h t + \pi j \cdot \mathrm{sign}(\cos(2\pi f_d t))}$$

in which $f_d = (f_2 - f_1)/2$ and $f_h = (f_1 + f_2)/2$. The signal $\hat{s}(t)$ is a complex analytical signal and the IA is $a(t) = 2\left|\cos(2\pi f_d t)\right|$. The double sinusoid shows phase shifts of $\pm 2\pi$ at each time the cosine function $\cos(2\pi f_d t)$ of the IA changes sign. Phase shifts cause discontinuities in the IF, because the IF is the derivative (1) of the phase. It follows from equation (2) that the IBC is approximated by $B_i^2(t) = \pi^2 f_d^2 \tan^2(2\pi f_d t)$. Therefore, there are high peaks in the IBC at times where the cosine function $\cos(2\pi f_d t)$ changes sign.

2) Random phase fluctuations may have various origins. It may be quantization noise due to R-wave detection errors. It may also be physiological noise originating from stochastic components of the underlying physiological system. Under pure noise conditions, neighbouring samples in time are uncorrelated. If noise is present in the signal, this may result in 'sudden' phase shifts. 'Sudden' phase shifts, in turn, may result in discontinuities in the IF, as explained above. Also, the autocorrelation function at $\tau = 1$ of a noisy signal is zero in expectation, but varies randomly. Therefore, the IBC (see equations (4) and (6)) of a noisy signal varies randomly and will show outlier peaks. By nature, the IBC is peaked at all phase shifts.

An illustration of the peaks in the IBC is provided in figure 2B. The middle and lower graph present the IF and the IBC derived from a mid-frequency range heart rate variability time series. High peaks in the IBC coincide with discontinuities in the IF. The deflections in the IF and the IBC are due to aliasing because the sample frequency is too low to catch the slope of the peaks.

2.6 How to use the IBC?

The IBC may be used to locate irregularities or discontinuities in the IF due to (sudden) phase shifts. The IBC is an index between 0 and 1. A suitable threshold can be chosen such that IBC-values above this threshold indicate discontinuities in the IF; corresponding segments in time of the IF can be excluded from further analysis and the time-frequency parameters can now be computed.

However, the IF of a noisy or irregular signal may sometimes behave 'regular'. In that case, the IBC cannot discriminate between a 'regular' IF of an irregular time segment and an oscillatory time segment of a signal. In general, we assume the IA of an irregular time segment of a signal to be low-valued in our frequency bands of

interest. It is therefore that an alternative index is defined that involves both the IA and the IBC to discriminate between irregular and oscillatory time segments and, simultaneously, to exclude discontinuities in the IF. This signal is called the 'amplitude-corrected instantaneous bandwidth coefficient (ACIBC)' and is defined by:

$$\mathrm{ACIBC}(t) = \frac{\mathrm{IA}(t)}{\mathrm{IA}(t) + \mathrm{IBC}(t)}$$

This is an index between 1 and 0. If the IA is high-valued, the ACIBC is high (close to 1). If the signal is irregular, i.e., has a low-valued IA, the ACIBC is low-valued (close to 0). Upward peaks in the IBC correspond to downward peaks (close to 0) in the ACIBC. Therefore, low ACIBC-values mean that the signal is locally irregular and downward peaks indicate discontinuities in the IF. A threshold can be chosen such that ACIBC-values under this threshold indicate irregularities and downward peaks under this threshold indicate discontinuities in the IF. Figure 2B presents an ACIBC time series (upper graph) associated with the IBC (lower graph) and the IF (middle graph) derived from a heart rate variability time series in the mid-frequency band. The original heart rate variability time series, the mid-frequency heart rate variability, and the IA are presented in figure 2A.

In this manner, the IBC and the ACIBC are used to exclude or reject certain short periods of time in the signal under analysis. The rejected periods in time define corresponding samples of the IF and the IA, which are to be removed from further analysis. The IBC is used to remove discontinuities from the IF, whereas the ACIBC is used for the simultaneous removal of discontinuities from the IF and irregular parts from the IA. Threshold levels determine the rejected periods. A threshold level of, for instance, 0.25 or 25% means that samples with corresponding IBC-values higher than 0.25 are rejected or, when using the ACIBC, that samples with corresponding ACIBC-values lower than 0.75 are rejected. In both cases, a lower threshold level means that, in general, more samples will be rejected and will result in larger rejected periods. When a number (≥ 1) of adjacent samples is detected for rejection, then at each side this group is supplemented with $n_{DF}/2$ adjacent samples. Together they form the rejected period. Thus a rejected period is at least n_{DF} samples wide. This widening is done to also remove the slopes of a discontinuity in the IF. In figure 3A,B the rejected periods are shown as windows spanning the discontinuities in the IF including the slopes of the discontinuities. The complementary accepted samples are also grouped in accepted periods (of length ≥ 1 samples).

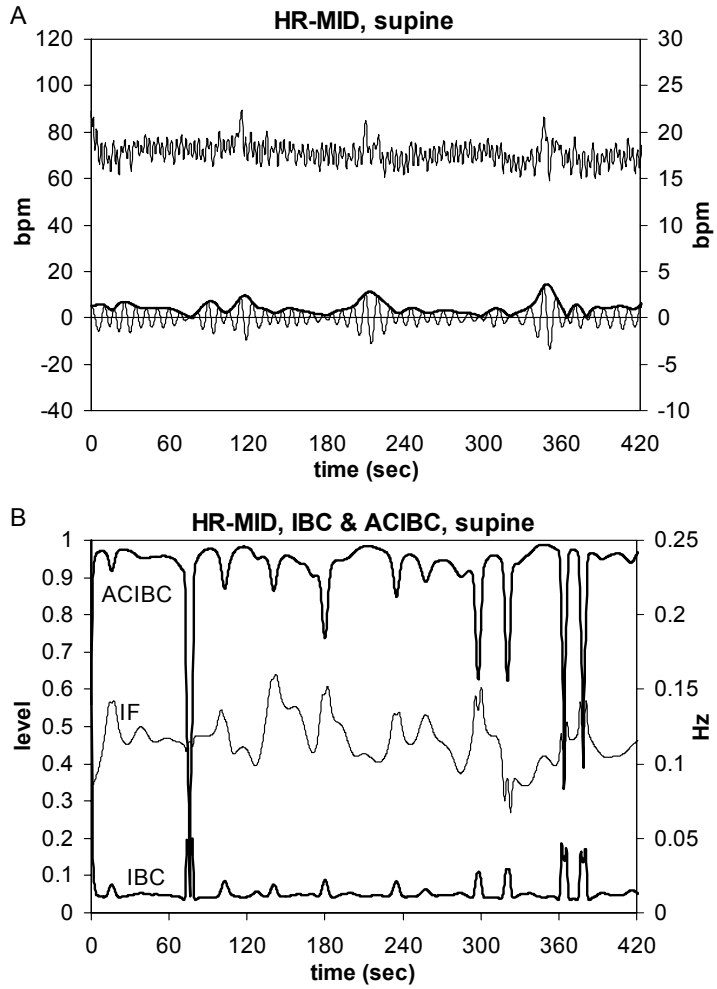

Figure 2. An IBC and ACIBC time series derived from a mid-frequency band heart rate variability time series.

A: spontaneous heart rate, the mid-frequency (filtered) heart rate, and the IA of the mid-frequency component during supine rest (mean heart rate is 71 bpm, mean IA is 1.4 bpm, and the SD of the mid-frequency heart rate is 1.0 bpm). The scale of the original and unfiltered heart rate in bpm is on the left side and the scale of the filtered heart rate and the IA in bpm on the right side of the graph.

B: the IF (middle), the IBC (lower), and the associated ACIBC (upper graph). Note the deflections in the IBC and the IF. The scale of the y-axis on the right side is the threshold level of IBC and ACIBC, the scale of the IF in Hz is on the right side of the graph.

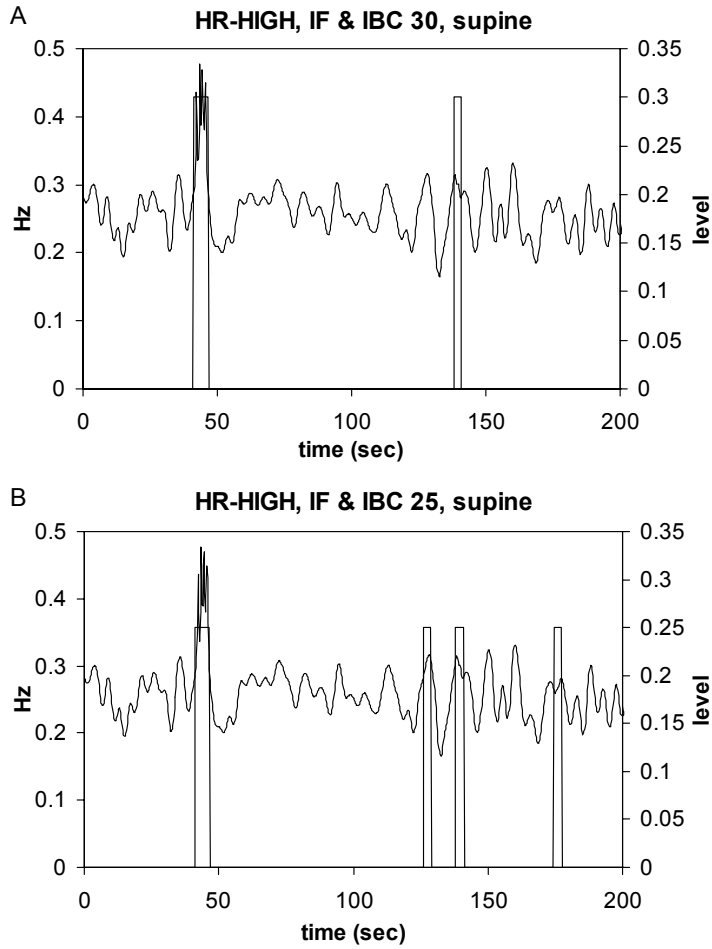

Figure 3. IBC threshold levels: the graphs A and B show the same IF of a high-frequency band heart rate variability time series and the effects of different threshold levels. The scale of the IF in Hz is on the left side and the threshold level of the IBC is on the right side of the graph. The IBC is used to locate discontinuities in the IF and the rejected periods are marked with windows. Rejected periods in graph A are determined by means of an IBC threshold level of 30%. The rejected fraction is 3.4%. The IBC threshold level of graph B is 25%, yielding a rejected fraction of 8.1%.

2.7 Definition of the time-frequency parameters

This section defines several time-frequency parameters for each IA and IF time series of the mid- and high-frequency band. These parameters take into account the periods that are accepted or rejected by means of the IBC or the ACIBC. Assume that the time segment under analysis consists of N samples, the total time of the time segment is $T = N \cdot t_s$, because the sample interval is t_s. The IBC and the ACIBC are used to exclude or reject certain parts or periods within the time segment. This leads to rejecting a total number N_{rej} of samples in the rejected periods. Then the total duration of the rejected periods is $T_{rej} = N_{rej} \cdot t_s$. A complementary number of samples $N_{acc} = N - N_{rej}$ is accepted. The duration of the accepted periods is

$T_{acc} = N_{acc} \cdot t_s = T - T_{rej}$.

2.7.1 Time parameters

- The Rejected Fraction is the fraction of the time segment that is rejected:

$\mathrm{RF} = \left(T_{rej} / T\right) \times 100\,\%$.

- The Accepted Fraction is the complementary fraction of the time segment that is accepted:

$\mathrm{AF} = \left(T_{acc} / T\right) \times 100\,\%$.

2.7.2 IF and IA parameters

- The Mean Instantaneous Amplitude is computed with:

$$\left\langle \mathrm{IA} \right\rangle = \left(1 / N_{acc}\right) \sum_{n \in N_{acc}} \mathrm{IA}\left[n\right]$$

after removing the rejected samples from the IF and/or the IA time series: $n \in N_{acc}$ means that only accepted samples are used.

- The Mean Square Instantaneous Amplitude is computed in the same way:

$$\left\langle \mathrm{IA}^2 \right\rangle = \left(1 / N_{acc}\right) \sum_{n \in N_{acc}} \mathrm{IA}\left[n\right]^2$$

The mean square instantaneous amplitude is a measure of the spectral power of the signal in the frequency band of interest.

- The Mean Instantaneous Frequency in the time segment is computed with:

$$\left\langle \mathrm{IF} \right\rangle = \left(1 / N_{acc}\right) \sum_{n \in N_{acc}} \mathrm{IF}\left[n\right]$$

- The Mean Frequency is the weighed mean IF using the square IA as weight. It is computed with:

$$\langle f \rangle = \sum_{n \in N_{acc}} \mathrm{IF}[n] \cdot \mathrm{IA}[n]^2 \Big/ \sum_{n \in N_{acc}} \mathrm{IA}[n]^2$$

The mean frequency has the following meaning: the Fourier transform of the filtered analytical signal $\hat{s}(t) = a(t)e^{j\varphi(t)}$ is denoted by $\hat{S}(f) = F_{t \to f}\hat{s}(t)$. The total power of the signal is given by

$$E_{\hat{s}} = \int_{-\infty}^{+\infty} \left|\hat{S}(f)\right|^2 df ,$$

i.e., this is the power of the signal $\hat{s}(t)$ in the frequency band of interest. Furthermore, the mean frequency of the signal in the frequency band is given by

$$\langle f \rangle = \int_{-\infty}^{+\infty} f \left|\hat{S}(f)\right|^2 df \Big/ E_{\hat{s}} .$$

It can be shown that the mean frequency $\langle f \rangle$ is equal to the average over time of the IF $f_i(t)$ weighted with the square IA [13]:

$$\langle f \rangle = \int_{-\infty}^{+\infty} f_i(t) \cdot a(t)^2 \, dt \Big/ E_{\hat{s}} .$$

Therefore, the mean frequency as defined above can be used as a measure of the mean frequency of the signal in the frequency band.

2.7.3 Fragmentation parameters, reflecting patterns of rejected periods in time

- The Rejection Index is the ratio n_{rej}/T_{rej} of the number n_{rej} of rejected periods and the total duration T_{rej} of the rejected periods. The more rejected periods there are, the higher the fragmentation of the time segment is, and the higher the rejection index is.
- The Acceptation Index is defined in the same way as the ratio n_{acc}/T_{acc} of the number of accepted periods n_{acc} and the total duration T_{acc} of the accepted periods. If there are few rejected periods and the accepted periods are long then the acceptation index is small.
- The Fragmentation Length is the mean duration of the accepted periods, see figure 4. Only periods that lie completely within the time segment are averaged. Accepted periods at the beginning or at the end of the time segment are not counted, because they possibly reach outside the time segment.
- Finally, the Interburst Interval Length is the mean distance between accepted periods. To compute the interburst interval length, the centers of all the accepted periods, which lie completely within the time segment, are determined. The time intervals between consecutive centers are computed and averaged, see figure 4. The mean duration is called the interburst interval length. It measures the occurrence frequency of accepted periods, or 'bursts'. If the accepted periods are long and only intersected by short rejected periods then the interburst interval length will be long,

i.e., the occurrence frequency of accepted periods is low. But, the more rejected periods there are, the shorter the interburst interval length will be.

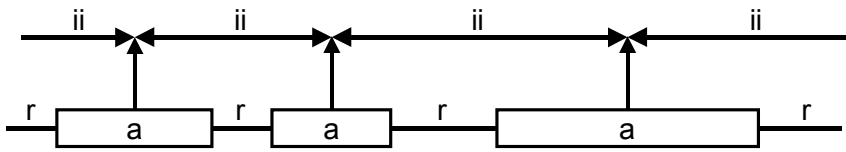

Figure 4. The definition of the fragmentation length and the interburst interval length. The rejected periods of a time segment are marked with r. The mean duration of the accepted periods (a) is the fragmentation length. Interburst intervals are the time intervals between the centers of two consecutive accepted periods a, they are marked with ii. Each interburst interval spans a rejected period r. The mean duration of the interburst intervals is the interburst interval length.

3 Application

3.1 Quantification of duration and number of irregular periods for obtaining time-frequency parameters

To quantify (and correct the IA and IF time series of the mid- and high-frequency band for) the duration and number of (rejected) periods of irregularities, the following approach was used. Based on the instantaneous bandwidth coefficient (IBC) and the amplitude-corrected instantaneous bandwidth coefficient (ACIBC), several threshold levels were defined and evaluated for their effectiveness in indicating and removing the sequential periods of irregularities from IA and IF time series. These threshold levels were chosen based on visual inspection by two researchers of the original heart rate variability time series and the corresponding IA and IF time series of 10 min periods of supine rest and orthostatic challenge of 10 healthy subjects and 10 patients with autonomic dysfunction showing abnormal mid- and high-frequency fluctuations (cardiac transplant recipients; autonomic failure). Figure 3A,B illustrates for the high-frequency band the effect of different and decreasing threshold levels (30% and 25%) of the IBC on the detection of irregularities in the IF time series: choosing the wrong level may lead to either underestimation or overestimation of the presence of irregularities and thereby influence reliable computation of the time-frequency parameters. As a first approach, our aim was to remove only those periods from the time series that both researchers unequivocally defined as irregularities.

Systematic inspection of our data revealed that for an accurate correction for irregularities of the mid-frequency fluctuations, the ACIBC with a threshold level of 25 appeared suitable for most time series, wheres as for the high-frequency band an IBC threshold level of 30 was adequate to quantify unequivocal irregular periods.

3.2 Subjects, procedures, and measurements

Data of 39 healthy volunteers (13 females, 26 males; mean age: 36.6 years, SD: 15.3, range: 19 – 68) were obtained from several experiments in which cardio-vascular recordings were made during periods of supine rest and orthostatic challenge [e.g., 9,34].

The recording sessions for the cardiovascular parameters were always performed in the morning. After a stabilization period (of at least 15 min), recordings were obtained during: supine rest (10 min) and orthostatic challenge (active standing or 60 degrees head-up tilt by means of the tilt-table; 10 min). Spontaneous fluctuations in breathing, heart rate, and blood pressure were recorded: the subjects were asked to relax and to breath regularly, not to speak, to move as little as possible, and to stay awake.

ECG, BP (Finapress) and respiration were recorded continuously and analysed according to methods described previously [9,34]. Only time-frequency analyses of the spontaneous variations in heart rate during supine rest and orthostatic challenge will be presented in this paper.

Statistical Analyses

The complete 10-min heart rate variability time series of supine rest was used for the computation of the time-frequency parameters. For the standing period, the first 2 minutes after standing were discarded because, as a first approach, we wanted to describe the time-frequency parameters during a steady state situation (last 8 min period of standing). For the mid- and high-frequency band separately, mean (SD) values of the time-frequency parameters are presented per condition (supine, standing). Differences in mean heart rate and the time-frequency parameters of the mid- and high-frequency band between supine rest and standing were evaluated by means of Student's t-tests for pairwise comparisons. If the parameter was not normally distributed, a non-parametrical test was applied (Wilcoxon test). Statistical analyses were performed using the SPSS for Windows Release 9.0. A p-value of <0.05 was used to indicate a significant effect.

4 Results

Mean heart rate showed a significant increase from supine rest to standing (on average, mean % change: +20%; table 1; figure 5A,B).

Time-frequency parameters of the mid-frequency band

Figure 5A,B and 6A,B show typical examples of spontaneous changes in heart rate, IA, and IF of the mid-frequency band during supine rest and orthostatic challenge of an individual subject. In comparison with supine rest, during standing the IA appears increased (figure 5), whereas the IF appears decreased (figure 6). Furthermore, less data periods are discarded as irregular periods, resulting in longer fragmentation lengths (figure 6). Figure 5 also illustrates an increase in variability of the mid-frequency band (filtered) heart rate from supine rest to standing. On group level, from supine rest to standing, the accepted fraction (+10%), the mean IA (+40%), the mean square IA (+124%), the rejection index (+13%), and the fragmentation length (+23%) increased significantly, whereas the rejected fraction (-32%), the mean IF (-9%), and the acceptation index (-26%) showed a significant decrease (table 1).

Time-frequency parameters of the high-frequency band

Spontaneous changes in heart rate, the IA, and the IF of the high-frequency band during supine rest and standing of an individual subject are presented in figures 7 and 8: from supine rest to standing, the variability of the high-frequency heart rate as well as the IA of the high-frequency component are decreased (figure 7); the IF appears decreased and there are more rejected periods, resulting in shorter fragmentation lengths (figure 8). On group level, from supine rest to standing, the mean IA (-22%), the mean square IA (-135%), the mean IF (-4%), the fragmentation length (-45%), and the interburst interval length (-40%) decreased significantly (table 1). We observed no significant changes from supine rest to standing in the accepted or rejected fractions.

5 Discussion

5.1 Time-frequency parameters during supine rest and orthostatic challenge

Supine rest

On average, 24% of the time periods of the mid- and the high-frequency band were defined as irregularities/discontinuities, indicating that for 76% of the time periods the monocomponent assumption of our method appeared valid. The mean IF of the mid-frequency band during supine rest was 0.11 Hz (mean cycle length: 9.1 sec),

Table 1: Mean (SD) of heart rate and time-frequency parameters of the mid- and high-frequency component during supine rest and standing.

N=39	Supine mean (SD)	Standing mean (SD)	t-test t; p values
Heart Rate (bpm)	67.9 (8.1)	81.8 (10.3)	-8.6; <.001
Mid-frequency band			
Accepted Fraction (%)	76.5 (10.5)	83.9 (12.2)	-4.1; <.001
Rejected Fraction (%)	23.6 (10.5)	16.1 (12.2)	4.1; <.001
Mean IA (bpm)	1.15 (0.5)	1.61 (0.9)	-3.7; =.001
Mean Square IA (ln)	0.38 (0.8)	0.85 (1.2)	-3.4; =.002
Mean IF (Hz)	0.11 (0.007)	0.10 (0.008)	4.2; <.001
Mean Frequency (Hz)	0.11 (0.005)	0.10 (0.006)	5.5; <.001
Acceptation Index*100	2.7 (1.4)	2.0 (1.5)	2.8; =.008
Rejection Index*100	8.0 (1.0)	9.0 (1.6)	-4.2; <.001
Fragmentation Length (sec)	44.6 (23.8)	54.8 (32.2)	-2.0; =.050
Interburst Interval Length (sec)	57.6 (23.9)	62.7 (26.6)	-1.4; NS
High-frequency band			
Accepted Fraction (%)	76.4 (14.6)	73.1 (11.8)	1.6; NS
Rejected Fraction (%)	23.6 (14.6)	26.9 (11.7)	-1.6; NS
Mean IA (bpm)	1.15 (0.6)	0.90 (0.4)	3.2; =.003
Mean Square IA (ln)	0.31 (0.9)	-0.11(0.9)	3.2; =.002
Mean IF (Hz)	0.25 (0.028)	0.24 (0.028)	2.6; =.013
Mean Frequency (Hz)	0.25 (0.025)	0.24 (0.025)	3.2; =.003
Acceptation Index*100	10.3 (7.6)	11.7 (6.7)	-1.1; NS
Rejection Index*100	30.1 (2.6)	29.5 (2.4)	1.2; NS
Fragmentation Length (sec)	23.3 (30.9)	12.9 (11.4)	2.3; =.030
Interburst Interval Length (sec)	28.2 (36.8)	16.8 (12.9)	2.0; =0.50

NS: non-significant

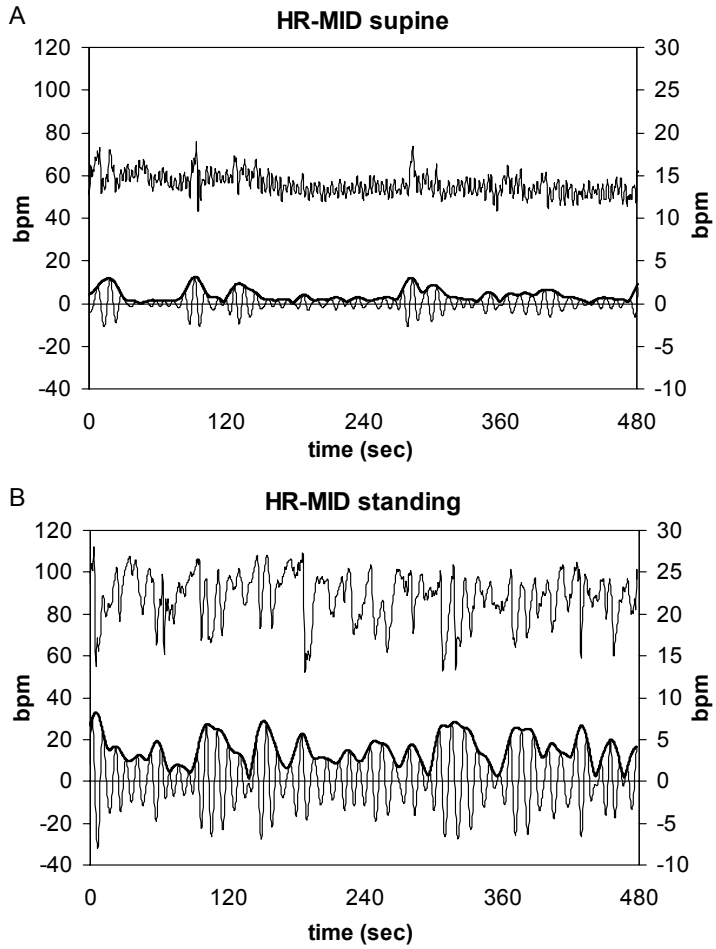

Figure 5. Spontaneous changes in heart rate, mid-frequency band (filtered) heart rate and the IA of the mid-frequency component during supine rest (A) and orthostatic challenge (B). Mean heart rate increases from 55 pm during supine rest to 88 bpm during standing. The SD of the mid-frequency band heart rate increases from 0.9 bpm to 3.0 bpm. Mean IA of the mid-frequency component increases from 1.0 bpm to 3.9 bpm. The scale of the original and unfiltered heart rate in bpm is on the left side and the scale of the filtered heart rate and the IA in bpm on the right side of the graph.

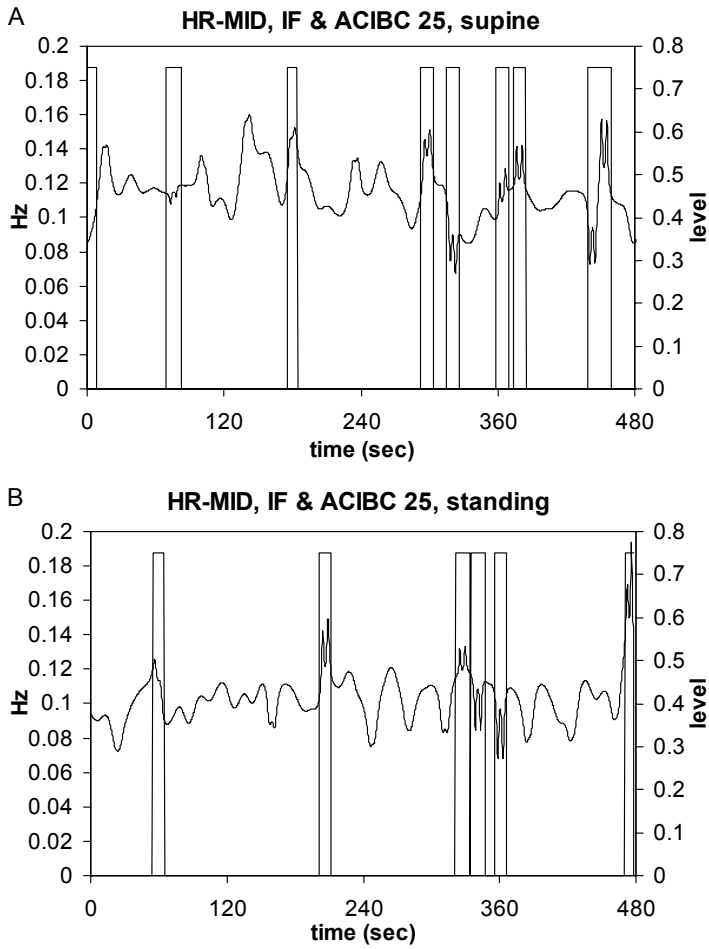

Figure 6. Spontaneous changes in the IF of a mid-frequency band heart rate during supine rest (A) and orthostatic challenge (B). Rejected periods are determined by means of an ACIBC threshold level of 25% and are marked with windows. Mean IF decreases from 0.1158 Hz during supine rest to 0.1003 Hz during standing. The rejected fraction decreases from 18.5% to 12.2%. The scale of the IF in Hz is on the left side and the threshold level of the ACIBC is on the right side of the graph.

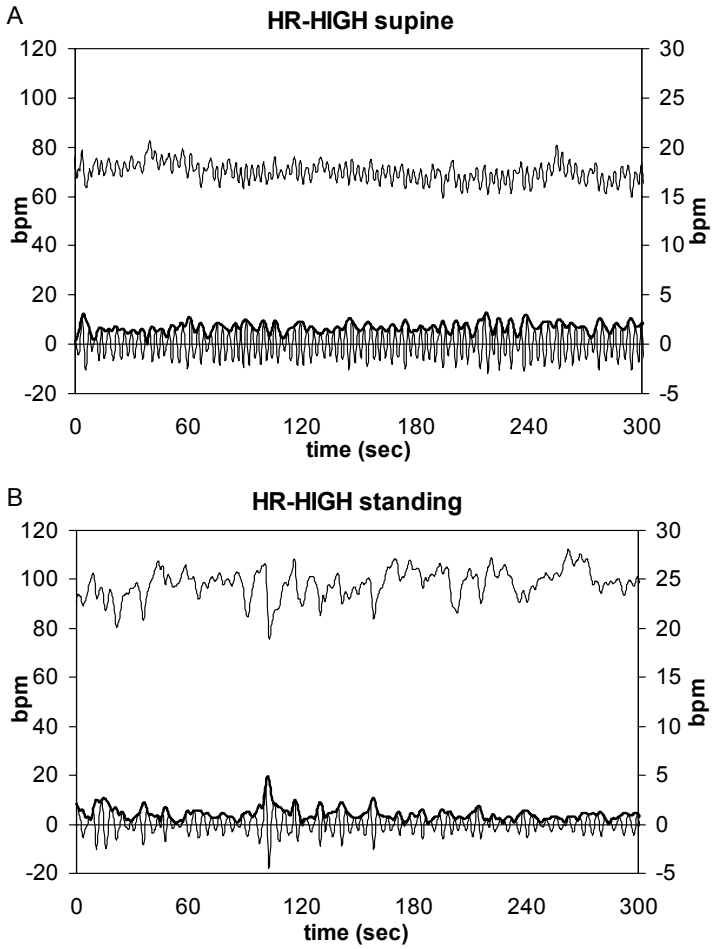

Figure 7. Spontaneous changes in heart rate, high-frequency band (filtered) heart rate and the IA of the high-frequency component during supine rest (A) and orthostatic challenge (B). Mean heart rate increases from 69 bpm during supine rest to 99 bpm during standing. The SD of the high-frequency band heart rate decreases from 1.2 bpm to 0.9 bpm. Mean IA of the high-frequency component decreases from 1.7 bpm during supine rest to 1.1 bpm during standing. The scale of the original and unfiltered heart rate in bpm is on the left side and the scale of the filtered heart rate and the IA in bpm on the right side of the graph.

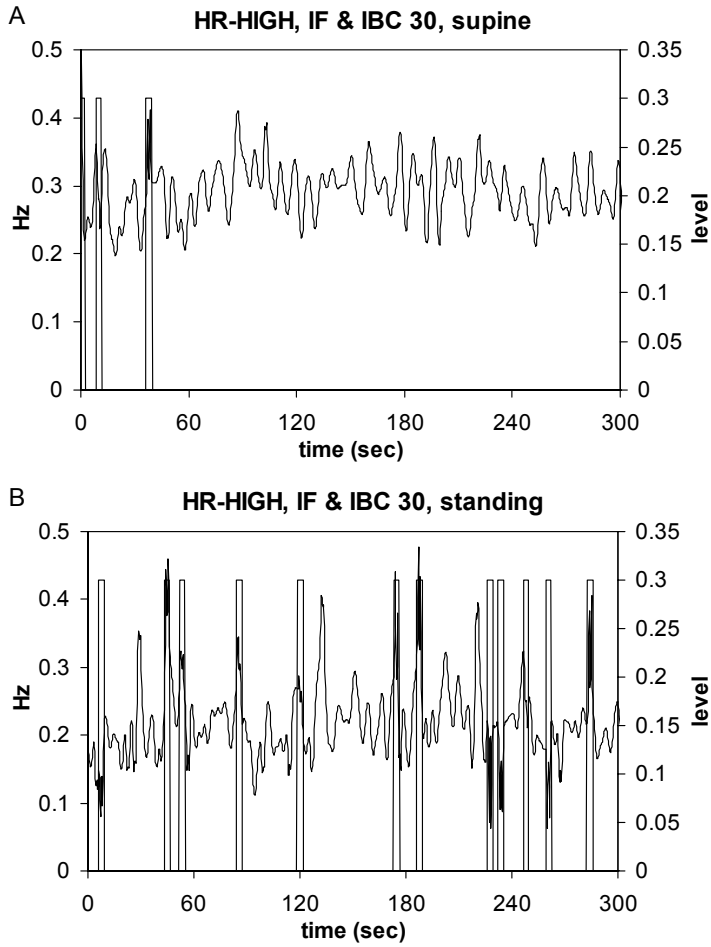

Figure 8. Spontaneous changes in the IF of a high-frequency band heart rate during supine rest (A) and orthostatic challenge (B), derived of the same data set, i.e. the high-frequency heart rate, of figure 7. Rejected periods are determined by means of an IBC threshold level of 30% and are marked with windows. Mean IF decreases from 0.2873 Hz during supine rest to 0.2146 Hz during standing. The rejected fraction increases from 2.1% to 13.6%. The scale of the IF in Hz is on the left side and the threshold level of the ACIBC is on the right side of the graph.

the mean IF of the high-frequency band was 0.25 Hz (mean cycle length: 4 sec). Under the present conditions, we observed a fragmentation length of 45 sec and an interburst interval length of 58 sec for the mid-frequency band and a fragmentation length of 23 sec and an interburst interval length of 28 sec for the high-frequency band. The large standard deviations of these parameters reflect the large inter-individual variability in fragmentation and interburst interval length.

Orthostatic challenge

When changing from supine to standing posture, initial changes in heart rate occur that are different from the steady state variations after prolonged standing (after about 2 min) [35]. Although it is interesting to describe the time-frequency variations of the initial heart rate changes [e.g., 36], in this study our focus was on the time-frequency variations in heart rate during steady state (last 8 min of the 10 min standing period) to explore the relevance of the characteristics of the oscillatory and irregular periods in the heart rate series and compare it with a steady state situation during supine rest.

Mid-frequency band

Based on spectral analyses, mid-frequency band power of heart rate has been shown to increase [e.g., 10,37]. Overall, our results are in line with these studies, although our time-frequency parameters revealed an additional effect of standing on IA and IF: whereas IA increased significantly, IF showed a minor, but significant, decrease. Regarding the characteristics of the oscillatory and irregular periods, the rejected fraction decreased during standing (-32%), an effect that was accompanied by an increase in fragmentation length but no significant change in interburst interval length. On average, about 84% of the mid-frequency signal could be considered as being monocomponent. Apparently, during standing there is an increase in appearance, strength and length of a mid-frequency oscillation as reflected in an increased amplitude, cycle length, and less interference of irregularities.

High-frequency band

Based on spectral analyses, high-frequency power of heart rate has repeatedly been shown to decrease as a result of vagal inhibition [e.g., 10,37,38]. Our time-frequency parameters also revealed a significant decrease of IA, an effect that was accompanied by a small, but significant, decrease of IF (mean cycle length increased from 4 to 4.2 sec, probably reflecting a somewhat slower breathing rate during standing). In contrast to the mid-frequency band, the rejected fraction showed no significant change from supine to standing, although significant decreases in fragmentation length and interburst interval length were observed. It is presently

unclear whether these effects are the result of a more variable or complex breathing pattern from supine to standing posture. Cross-analyses with time-frequency changes in the respiratory signal itself are necessary to further clarify these findings.

5.2 Time-frequency parameters: future developments

As a first approach, the data of this study were quantified by means of selected threshold levels of the IBC and the ACIBC. Although these threshold levels were chosen on the basis of visual screening of a sample of heart rate time series of healthy subjects and patients with autonomic dysfunction by two researchers, we can presently not conclude that the thresholds were optimal for every heart rate time series. Further studies are necessary to optimize the choice of thresholds. However, computations on the basis of the presently used threshold levels showed that it is interesting to quantify time-varying characteristics of signal and irregularities. The significant effect of the changing of posture on the amount of irregularities detected, as well as on the fragmentation length and the interburst interval length indicates that these parameters may have physiological relevance. Furthermore, it also suggests the presence of a periodic process in the occurrence of irregularities that can be influenced by external circumstances. However, since the occurrence of irregularities and interference can be the result of multiple processes (harmonic or sub-harmonic components, quantization or physiological noise, see the Methods-section: 'The behavior of the IF and the IBC') and standard deviations in our group were rather large, these processes need to be further elucidated by studying cardiovascular variability of various patients groups (CHD, hypertension, autonomic failure, neurological and psychiatric disorders) under various conditions (physical strain, psychological stress, cardiovascular and psychoactive drugs).

Complementary to conventional sequential spectral analysis, which has a time resolution of about 2-5 min, our time-frequency method provides instantaneous information of time-varying cardiovascular changes with a time resolution of about 8 sec for the mid-frequency band and about 2.5 sec for the high-frequency band. This high time resolution of the time-varying spectral description, provided by IA and IF, may contribute to a more detailed description of the time-varying dynamics of cardiovascular signals. For instance, periods with phase shifts, i.e., discontinuities in the IF, may be submitted to further analysis, such as cross-correlation between different frequency bands or different cardiovascular time series, to investigate possible dependencies and harmonic relationships between frequency bands. Or, transient changes in cardiovascular variability may be investigated [e.g., 39]. Considering the effect of breathing on heart rate variability, it appears essential in

future studies to include analyses of respiratory parameters and perform cross-correlational studies. The method presented in this paper can be directly applied to other cardiovascular signals (e.g., blood pressure) as well as to respiratory signals; computation of time-dependent changes in transfer functions between two signals is similarly feasible and interesting to perform [7,40].

In summary, we have evaluated a new method to compute time-frequency parameters from cardiovascular time series. Apart from calculating the IA and the IF, characteristics of the oscillatory and irregular periods can be quantified that may be relevant to further unravel the situational- and state-dependent dynamics of homeostatic cardiovascular control processes. As a first approach, the method was applied to describe changes in time-frequency parameters and in the characteristics of the oscillatory and irregular periods from supine to standing posture, under steady state conditions in healthy subjects. The parameters and characteristics discriminated differentially between supine rest and orthostatic challenge. Furthermore, the method can be applied to other cardiovascular time series provided they are monocomponent.

Acknowledgements

The authors like to thank prof. ir. K.H. Wesseling of the department TNO-BMI of the University of Amsterdam for his kind help regarding the preparation of this paper.

References

[1] Akselrod S, Gordon D, Madwed JB, Snidman NC, Shannon DC, and Cohen RJ: Hemodynamic regulation: investigation by spectral analysis. Am J Physiol 249:M867-M875, 1985.

[2] Kitney RI: Beat-by-beat interrelationships between heart rate, blood pressure and respiration. In: Beat-to-beat Investigation of Cardiovascular Function. R.I. Kitney and O. Rompelman, Eds. Oxford: Oxford University Press, pp 146-178,1985.

[3] Sayers BMcA: Analysis of heart rate variability. Ergonomics 16:17-32, 1973.

[4] Sayers BMcA: Signal analysis of heart-rate variability In: The Study of Heart-Rate Variability. R.I. Kitney and O. Rompelman, Eds. Oxford: Clarendon Press, pp 27-58, 1980.

[5] Kobayashi M and Musha T: 1/f Fluctuations of heartbeat period. IEEE Trans Biomed Eng BME-29:456-457, 1982.

[6] Baselli G, Cerutti S, Civardi S, Malliani A, and Pagani M: Cardiovascular variability signals: towards the identification of a closed-loop model of the neural control mechanisms. IEEE Trans Biomed Eng BME-35:1033-1046, 1988.

[7] Saul JP, Berger RD, Albracht P, Stein SP, Chen MH, and Cohen RJ: Transfer function analysis of the circulation: unique insights into cardiovascular regulation. Am J Physiol 261:H1231-H1245, 1991.

[8] Tulen JHM, Man in 't Veld AJ, van Roon AM, Moleman P, van Steenis HG, Blankestijn PJ, and Boomsma F: Spectral analysis of hemodynamics during infusions of epinephrine and norepinephrine in men. J Appl Physiol 76(5):1914-1921, 1994.

[9] Tulen JHM, Bruijn JA, de Man KJ, Pepplinkhuizen L, van den Meiracker AH, and Man in 't Veld AJ: Cardiovascular variability in major depressive disorder and effects of imipramine or mirtazapine (Org 3770). J Clin Psychopharmacol 16(2):135-145, 1996.

[10] Tulen JHM, Boomsma F, and Man in 't Veld AJ: Cardiovascular control and plasma catecholemines during rest and mental stress: effects of posture. Clinical Science 96:567-576, 1999.

[11] Parati G, Castiglioni P, di Renzo M, Omboni S, Pedotti A, and Mancia G: Sequential spectral analysis of 24-hour blood pressure and pulse interval in humans. Hypertension 16:414-421, 1990.

[12] Boashash B: Estimating and interpreting the instantaneous frequency of a signal – part 1: fundamentals. Proc IEEE 80(4):520-538, 1992.

[13] Cohen L: Time-Frequency Analysis. Englewood Cliffs, NJ: Prentice Hall, 1995.

[14] van Steenis HG, Martens WLJ, and Tulen JHM: Quantification of the dynamic behaviour over time of narrow-band components present in heart rate variability by means of the instantaneous amplitude and frequency. submitted a.

[15] van Steenis HG, Martens WLJ, and Tulen JHM: The instantaneous frequency of cardiovascular time series: a comparison of methods. submitted b.

[16] Gabor D: Theory of communication. Proc IEE 93(III):429-457, 1946.

[17] Ville J: Théorie et application de la notion de signal analytique. Cables et Transmissions 2A(1):61-74, 1948.

[18] Wigner E: On the quantum correction for thermodynamic equilibrium. Phys Rev, 40:749-759, 1932.

[19] Boashash B: Time-frequency signal analysis. In: Advances in Spectrum Analysis and Array Processing, Vol. 1. S. Haykin, Ed. Englewood Cliffs, NJ: Prentice Hall, pp 418-517, 1991.

[20] Boashash B and Reilly A: Algorithms for time-frequency signal analysis. In: Time Frequency Signal Analysis – Methods and Applications, chapter 7. B. Boashash, Ed. Longman Cheshire, 1992.

[21] Oppenheim AV, Schafer RW, and Buck JR: Discrete-Time Signal Processing, 2nd edition. Englewood Cliffs, NJ: Prentice Hall, 1999.

[22] Rihaczek A: Signal energy distribution in time and frequency. IEEE Trans. Inform. Theory IT-14:369-374, 1968.

[23] Choi HI and Williams WJ: Improved time-frequency representation of multicomponent signals using exponential kernels. IEEE Trans Acoust Speech, Signal Processing ASSP-37:862-871, 1989.

[24] Cohen L and Lee C: Instantaneous bandwidth. In: Time Frequency Signal Analysis – Methods and Applications, chapter 4. B. Boashash, Ed. Longman Cheshire, 1992.

[25] Bendat JS and Piersol AG: Random Data, Analysis and Measurements Procedures, 2nd edition. New York: John Wiley and Sons, Inc., 1986.

[26] Angelsen BAJ: Instantaneous frequency, mean frequency and variance of mean frequency estimatores for ultrasonic blood velocity doppler signals. IEEE Trans Biomed Eng BME-28:733-741, 1981.

[27] Martens WLJ: The fast time frequency transform (F.T.F.T.): a novel on-line approach to the instantaneous spectrum. 14th International Conference of the IEEE Engineering in Medicine and Biology Society, 1992, Paris.

[28] Martens WLJ: Segmentation of 'rhythmic' and 'noisy' components of sleep EEG, heart rate and respiratory signals based on instantaneous amplitude, frequency, bandwidth and phase. 1st joint BMES/EMBS conference 1999, Atlanta.

[29] Bayly EJ: Spectral analysis of pulse frequency modulation in the nervous system. IEEE Trans Biomed Eng BME-15:257-265, 1968.

[30] Hyndman BW and Mohn RK: A model of the cardiac pacemaker and its use in decoding the information content of cardiac intervals. Automedica 1:239-252, 1975.

[31] Rompelman O: The assessment of fluctuations in heart rate. In: The Study of Heart Rate Variability. R.I. Kitney and O. Rompelman, Eds. Oxford: Clarendon Press, pp 59-77, 1980.

[32] Rompelman O: Spectral analysis of heart-rate variability. In: Psychophysiology of Cardiovascular Control. J.F. Orlebeke, G. Mulder, and L.J.P. van Doornen, Eds. New York: Plenum Press, pp 315-331, 1985.

[33] Flandrin P: Time-Frequency / Time-Scale analysis. San Diego: Academic Press, 1999.

[34] van den Berg F, Tulen JHM, Boomsma F, Noten JBGM, Moleman P, and Pepplinkhuizen L: Effects of alprazolam and lorazepam on catecholaminergic and cardiovascular activity to supine rest, mental load and orthostatic challenge. Psychopharmacology 128:21-30, 1996.

[35] Wieling W: Non-invasive continuous recording of heart rate and blood pressure in the evaluation of neurocardiovascular control. In: Autonomic Failure - A Textbook of Clinical Disorders of the Autonomic Nervous System. R Bannister and CJ Mathias, Eds. Oxford: Oxford University Press, pp 291-311, 1992.

[36] Akselrod S, Os O, Greenberg M, and Keselbrener L: Autonomic response to change of posture among normal and mild-hypertensive adults: investigation by time-dependent spectral analysis. J Auton Nerv Syst 64:33-43, 1997.

[37] Vybiral T, Bryg RJ, Maddens ME, and Boden WE: Effect of passive tilt on sympathetic and parasympathetic components of heart rate variability in normal subjects. Am J Cardiol 63:1117-1120, 1989.

[38] Lipsitz LA, Mietus J, Moody GB, and Goldberger AL: Spectral characteristics of heart rate variability before and during postural tilt. Circulation 81:1803-1810, 1990.

[39] Pola S, Macerata A, Emdin M, and Marchesi C: Estimation of the power spectral density in nonstationary cardiovascular time series: assessing the role of the time-frequency representations (TFR). IEEE Trans Biomed Eng BME-43(1):46-59, 1996.

[40] Parati G, Saul JP, di Rienzo M, and Mancia G: Spectral analysis of blood pressure and heart rate variability in evaluating cardiovascular regulation. A critical appraisal. Hypertension 25:1276-1286, 1995.

CHAPTER 10
SUMMARY AND CONCLUDING REMARKS
SAMENVATTING

1 Heart rate variability

Fourier analysis is often performed to study spontaneous short-term variations in heart rate to obtain estimates of neurocardiac activity. In the Fourier spectrum, two peaks are usually present. One peak near 0.1 and one near 0.3 Hz. The 0.1 Hz peak is probably mediated by the baroreflex and may reflect changes in sympathetic and parasympathetic tone. The 0.3 Hz peak may reflect changes in parasympathetic (vagal) tone. Both peaks have been explained by baroreflex and cardiopulmonary-reflex closed-loop blood pressure control models. The variations in heart rate are called heart rate variability (HRV). The frequency bands around the 0.1 and 0.3 Hz peaks are called the characteristic frequency bands for HRV-analysis. The study of HRV has provided relevant clinical information: reduced HRV appears to predict cardiac events, cardiovascular mortality, and the onset of hypertension. In psychiatric patients, reduced HRV has similarly been studied to explain the increased incidence of cardiovascular mortality and the abnormalities of the autonomic nervous system in affective and anxiety disorders. Furthermore, some of the cardiovascular (side-)effects of psychoactive drugs can be followed in HRV.

HRV is studied in the time-domain and in the frequency-domain. However, time- and frequency-domain results do not fully describe the properties of an HRV-signal. A frequency-domain description does not reveal the frequency components as they change over time and the time-domain description does not show the time components as they change in frequency. This calls for techniques that are able to study amplitude and frequency fluctuations in HRV in the time-frequency domain, and, furthermore, instantaneously. Instantaneous signal properties are properties that can be computed within the time-resolution of the signal. The aim of this research was to develop a time-frequency method that allows the quantification of instantaneous changes in HRV.

In chapter 2 we described eight representations of HRV. A representation of HRV was defined as the beat-to-beat information derived from the ECG and ordered in such a way that it is accessible to the analysis techniques and can be related to physiological processes. A distinction was made between:

- equidistant time series: the interbeat interval series and the heart rate series;
- non-equidistant time series: the interbeat interval function and the instantaneous heart rate function; and
- event series: the cardiac event series, the interbeat interval event series, and the heart rate event series.

Spectral analysis can be applied to each of these HRV-representations.

In the study of time-frequency analysis of HRV, we used the low-pass filtered cardiac event series. This HRV-representation is derived from the cardiac event series. The cardiac event series is a spike-train obtained by replacing the R-waves in the ECG by narrow positive spikes of constant unit impulse generated at the instants that the R-waves are detected. This spike-train is filtered with a zero-phase low-pass filter with cutoff frequency of 0.5 Hz. The filtered continuous-time signal is called the low-pass filtered cardiac event series. After sampling this signal, in our case with a sample frequency of 4 Hz, the resulting equidistant time series can be used for further computations.

2 Spectral analysis

In chapter 3, the instantaneous heart rate spectrum was introduced and compared with the spectrum of counts. The instantaneous heart rate spectrum is the power spectrum of the heart rate event series. The heart rate event series is obtained from the cardiac event series by weighing each spike with the instantaneous heart rate obtained at that instant, multiplied with the duration of the preceding R-R interval. The spectrum of counts is the power spectrum of the cardiac event series. A consequence and drawback of (non-equidistant) event series is the introduction of harmonic distortion in the spectra. This is inherent to this type of sampling. Harmonic distortion implies the presence of sideband components of the mean heart rate into the frequency spectrum below the Nyquist frequency. The spectrum of counts and the instantaneous heart rate spectrum contained the same spectral information, but it was found that the harmonic distortion was smaller in the instantaneous heart rate spectrum than in the spectrum of counts.

Chapter 4 summarized the results of our studies performed with the non-equidistant spectral techniques of chapter 3. Based on our previous research to analyze heart rate and blood pressure variability with non-equidistant spectral techniques, we have observed significant alterations in the powers of the mid- and high-frequency bands. They were associated with:

- challenging the cardiovascular system with various drugs (epinephrine, norepinephrine, clonidine, lorazepam) in healthy subjects;
- the effects of the antidepressants imipramine and mirtazapine in depressed patients;
- the effects of mental and physical stress tests in healthy subjects, depressed patients, and patients with autonomic dysfunctions.

Overall, our experiments confirmed that spectral analysis of heart rate and blood pressure variability can be used for the assessment of the dynamics of neural cardiovascular regulation. However, especially our studies with clinical populations illustrated that it is essential to control for respiratory changes to improve the interpretation of spontaneous short-term cardiovascular variations.

3 Time-frequency analysis: the Wigner-Ville distribution

In chapters 5 and 6, the smoothed Wigner-Ville distribution and the exponential distribution were applied to HRV-, blood pressure variability and respiratory signals. These signals were obtained under various clinical and experimental circumstances. The applications illustrated the potential of the representations to qualitatively describe time-frequency relationships of cardiovascular signals, but failed to provide a quantitative evaluation. The exponential distribution proved to be superior to the smoothed Wigner-Ville distribution because of a better suppression of the cross-terms and a better approximation of the marginal conditions that an ideal time-frequency representation should have.

4 Time-frequency analysis: a new method

In chapter 7 we presented our new method to compute the instantaneous changes in amplitude and frequency within narrow-band HRV-signals. A monocomponent signal is a signal that has only one (time-varying) spectral peak. Our method is applicable to analytical signals that are monocomponent. HRV-signals were filtered with a band-pass filter corresponding to one of the characteristic frequency bands to make the signals narrow-band and monocomponent. Subsequently, the instantaneous amplitude and frequency were computed. The squared instantaneous amplitude is a measure of the time-varying instantaneous power and the instantaneous frequency defines the time-varying frequency location of the spectral peak, both within a narrow frequency band. The spread of the spectral peak is measured by means of the instantaneous bandwidth. In our case, the so-called instantaneous bandwidth coefficient was computed as a measure of the spread. It was illustrated that the instantaneous frequency of HRV-signals may show alternately oscillatory and irregular periods in time. The irregularities in the instantaneous frequency occur at sudden shifts in the instantaneous phase. In turn, the phase shifts may be due to the fact that the signal is locally not completely monocomponent or may be due to random phase fluctuations. The instantaneous bandwidth coefficient was proposed as a time-dependent discriminator between ‘good’ and ‘poor’ fragments in the signal.

By applying a threshold to the instantaneous bandwidth coefficient, oscillatory periods can be selected for further analysis and irregular periods rejected or analyzed separately.

A remark on the instantaneous bandwidth: the variability of a signal in a narrow frequency band is completely described by means of the instantaneous amplitude, frequency, and bandwidth, provided the signal is monocomponent within the frequency band. The algorithm we used for the computation of the instantaneous bandwidth produced a biased instantaneous bandwidth, which we have called the instantaneous bandwidth coefficient. It remains interesting, from signal-analytical as well as physiological viewpoints, to investigate if it is possible to implement and apply a 'true' instantaneous bandwidth. The instantaneous frequency can be interpreted as the average of all frequencies present at an instant, i.e., the conditional average. The instantaneous bandwidth can be interpreted as the associated conditional standard deviation at that instant. It is the spread of frequencies at a particular instant. It is remarkable that the expression for the instantaneous bandwidth of Cohen is only dependent on the instantaneous amplitude. The 'true' instantaneous bandwidth should be dependent on the instantaneous amplitude and the instantaneous frequency, since fluctuations in both contribute to the spread. The possibility should be studied to modify the equation of Cohen with (a) phase dependent term(s) such that it is a 'true' expression for the instantaneous bandwidth while it remains compatible with the theory of Cohen. Including a phase dependent additive term that integrates to zero may be one way to do this.

Chapter 7 also presented a method to derive the shortest possible observation interval for a narrow frequency band, in particular, the characteristic frequency bands. The observation intervals were inversely related to the bandwidth of the frequency bands, as stated by the uncertainty principle of Gabor. If signal properties such as amplitude and frequency can be computed at such an optimal time-resolution, the properties are called instantaneous. The time-resolution of the instantaneous amplitude and frequency of the mid-frequency band of HRV was about 8 s. The time-resolution of the high-frequency band was about 2.5 s.

In chapter 8 our method was compared with three other methods to compute the instantaneous frequency of band-limited, monocomponent, and analytical signals, namely:

- the discrete time-frequency transform;
- the circular mean direction (of the time-slices of the Wigner-Ville distribution);
- and the central finite difference (i.e., the derivative) of the phase of the analytical signal.

In this chapter it was concluded that only at periods in time where there are irregularities or discontinuities due to phase-shifts, there were numerical differences between the four methods, because each method handled these discontinuities differently.

In chapter 9, several statistics were defined to quantitatively describe the time-varying spectral contents and the time-varying distribution of oscillatory and irregular periods. The instantaneous bandwidth coefficient was used to correct the instantaneous frequency and corresponding periods of the instantaneous amplitude for irregularities due to the phase-shifts. For fixed time-intervals, the mean instantaneous amplitude, the mean square instantaneous amplitude, and the mean instantaneous frequency were computed after removing the irregular segments. Additional statistics were calculated reflecting the total duration of the oscillatory and irregular periods and the distribution of these periods in time. The statistics were applied to heart rate data obtained from healthy volunteers during steady state situations of supine rest and orthostatic challenge. The results indicated that for the mid-frequency band about 77% of the total time during supine rest could be considered oscillatory, and about 84% during standing. In the high-frequency band about 77% of the total time during supine rest was oscillatory, and about 73% during standing. From supine rest to orthostatic challenge significant alterations occurred in the mid-frequency band regarding instantaneous amplitude (increase), instantaneous frequency (decrease), as well as in the distribution of oscillatory and irregular periods (increase mean duration of the oscillatory periods). In the high-frequency band, the instantaneous amplitude, frequency and the mean duration of the oscillatory periods decreased significantly. These first results illustrated that our statistics were capable of showing significant alterations to a situation of sympathetic activation and vagal inhibition (orthostatic challenge).

5 Advantages of our time-frequency method

The method presented in this thesis allows the quantification of fast and sustained changes in cardiovascular regulatory processes, as well as the objective assessment of disturbances of these processes. The method can improve our insight into the dynamics of cardiovascular regulation in several areas:

- Traditional spectral techniques do not adequately describe fast changes in the characteristic frequency bands, because several minutes of data are needed for spectral analysis. Our time-frequency method can provide a quantitative analysis of fast changes in amplitude and frequency. Therefore, it can be used to study the

reactivity of the cardiovascular system to mental, physical, and (psycho)-pharmacological stimuli in more detail than before.

- Certain symptoms of psychiatric patients may induce transient disturbances of cardiovascular homeostasis. Anxiety, or behavioral symptoms such as tics, compulsive behaviors, or impulsiveness, may result in short-lasting disturbances of cardiovascular regulatory processes, which may have negative health consequences in the long-term. It will be interesting to evaluate these cardiovascular disturbances by means of our time-frequency method to find out whether and how the effects of these behavioral symptoms are reflected in the instantaneous bandwidth coefficient.

Our time-frequency method needs to be extended to provide a description of the relationships between variations in heart rate, blood pressure, respiration, and/or behavior over time. Theoretically, application to other variability signals seems possible if these signals will prove to be monocomponent.

6 Conclusions

The main conclusions of this thesis can be formulated as follows:

- A time-frequency representation is a powerful tool to observe the instantaneous changes in HRV.
- The instantaneous amplitude and the instantaneous frequency describe the time-varying fluctuations in specified narrow frequency bands in HRV.
- An optimal time-resolution is achieved in terms of Gabor's uncertainty principle.
- The instantaneous bandwidth coefficient discriminates between oscillatory and irregular periods in the instantaneous frequency within a narrow frequency band.
- Based on a level crossing of this instantaneous bandwidth coefficient, several statistics can be defined describing the corrected time-varying spectral contents and the time-varying characteristics of the oscillatory and irregular periods.

1 Hartritme-variabiliteit

Het hart klopt niet met een constante regelmaat, maar de tijd tussen twee opeenvolgende hartslagen varieert. Deze schommelingen in het ritme van de hartslag zijn spontaan of ze kunnen teweeg gebracht worden door psychische of lichamelijke inspanning en geneesmiddelen. De hartslag wordt gemeten met behulp van het electrocardiogram (ECG). Een kenmerkende scherpe piek in het ECG is de R-top. Deze top treedt op als het hart samentrekt om het bloed in de grote lichaamsslagader, de aorta, te pompen. De tijd tussen twee opeenvolgende hartslagen wordt het R-R interval genoemd. Het R-R interval wordt gemeten door in het ECG de tijd tussen de twee opeenvolgende R-toppen te meten. Het hartritme is het aantal hartslagen per minuut. De tijd tussen twee opeenvolgende slagen varieert en deze slag-op-slag variatie wordt hartritme-variabiliteit genoemd (HRV).

Het onderzoek naar HRV heeft belangrijke, klinisch bruikbare informatie opgeleverd: een verminderde HRV voorspelt de kans op hartfalen, sterfte aan hart- en vaatziekten en een blijvend verhoogde bloeddruk. Ook bij psychiatrische patiënten is verminderde HRV onderzocht om de verhoogde kans op sterfte aan hart- en vaatziekten en de afwijkingen in het autonome zenuwstelsel bij stemmingsstoornissen, zoals depressie en angststoornissen te verklaren. Bovendien kunnen de cardiovasculaire effecten van sommige psychoactieve geneesmiddelen gevolgd worden aan de hand van HRV.

We kunnen HRV onderzoeken in het tijdsdomein, in het frequentie-domein en in het tijd-frequentie domein. Om dat te doen hebben we een representatie van HRV nodig.

2 HRV-representaties

In hoofdstuk 2 beschrijven we acht verschillende HRV-representaties. Een HRV-representatie is gedefinieerd als de slag-op-slag informatie (bijvoorbeeld R-R intervallen) verkregen uit het ECG en zodanig gerangschikt dat de informatie verwerkt kan worden door de analysetechnieken en in verband gebracht kan worden met fysiologische processen. We maken een onderscheid tussen:

- Equidistante tijdreeksen: de hartslag-interval tijdreeks en de hartritme tijdreeks. In dit geval worden R-R intervallen of hartritmen op volgorde genummerd en uitgezet als functie van het intervalnummer.
- Niet-equidistante tijdreeksen: de hartslag-interval functie en de instantane hartritme functie. De lengte van het R-R interval of het hartritme wordt bepaald aan het eind van elk R-R interval en uitgezet als functie van de tijd. Deze reeksen zijn niet-equidistant, dit betekent dat de functiewaarden niet regelmatig in de tijd verdeeld zijn.
- Pulsreeksen: de hartslag pulsreeks, de hartritme pulsreeks en de hartslag-interval pulsreeks. In het ECG worden de R-toppen gedetecteerd en op elk detectie-tijdstip wordt er een smalle piek of puls neergezet. De hoogte en breedte van deze puls is zodanig dat de oppervlakte 1 is. Zo onstaat er een rij pulsen die de hartslag pulsreeks wordt genoemd. De hartritme pulsreeks wordt verkregen door elke puls in de hartslag pulsreeks te wegen met het hartritme op dat ogenblik, vermenigvuldigd met de duur van het voorafgaande R-R interval. De hartslag-interval pulsreeks wordt verkregen door elke puls in de hartslag pulsreeks te wegen met het kwadraat van het voorafgaande R-R interval.
- De laagdoorlaat-gefilterde hartslag pulsreeks: dit is een HRV-representatie die verkregen wordt uit de hartslag pulsreeks die we gebruiken in de tijd-frequentie analyse van HRV. De hartslag pulsreeks wordt gefilterd met een laagdoorlaat-filter dat de fase van het signaal niet verandert. Dit betekent dat een gebeurtenis in de tijd, ook wel een tijdcomponent genoemd, niet verschuift in de tijd als gevolg van het filter. Voor het kantelpunt, dat is de scheiding tussen doorlaatgebied en spergebied, van dit filter kiezen we 0.5 Hz. Het gefilterde analoge signaal wordt de laagdoorlaat-gefilterde hartslag pulsreeks genoemd. Na de bemonstering van dit signaal, in ons geval met een frequentie van 4 Hz, kan de resulterende discrete en equidistante tijdreeks gebruikt worden voor verdere analyses.

3 HRV-analyse in het tijdsdomein

Analyses van HRV in het tijdsdomein behelzen o.a. de berekening van het gemiddelde hartritme en het gemiddelde R-R interval in een bepaald tijdsinterval met de bijbehorende standaard deviaties. De standaard deviatie is een maat voor het totale vermogen van de variaties in dat tijdsinterval, respectievelijk de variaties in hartritme en de variaties in R-R intervallen. De veranderingen in de gemiddelden en standaard deviaties van achtereenvolgende tijdsintervallen geven informatie over de veranderingen in HRV over de tijd. Op hun beurt hebben die veranderingen te maken met veranderingen in het cardiovasculaire regelsysteem. De analyses van HRV in het tijdsdomein maken meestal gebruik van equidistante tijdreeksen.

4 HRV-analyse in het frequentie-domein

Met behulp van Fourieranalyse kunnen we HRV in het frequentie-domein onderzoeken. Dit wordt ook wel spectraalanalyse genoemd. Fourieranalyse kan de schommelingen in het hartritme of de R-R intervallen kwantificeren. Met behulp van Fourieranalyse kan een signaal geschreven worden als een som van sinusfuncties, ieder met een specifieke amplitude en frequentie. Er ontstaat zo een een-op-een relatie tussen amplituden en frequenties van de sinusfuncties. Deze relatie stelt het signaal voor als functie van de frequentie. Het signaal is hiermee omgezet van een functie in het tijdsdomein naar een functie in het frequentie-domein. Hierbij gaat geen informatie verloren. Beide representaties van het signaal bevatten dezelfde informatie. Bovengenoemde amplituden zijn complexe getallen. Omdat het kwadraat van de absolute waarde van de amplitude van een sinusfunctie een maat is voor het vermogen van de sinusfunctie, worden de absolute waarden van de amplituden vaak gekwadrateerd. Het resultaat, als functie van de frequentie, wordt het vermogens-spectrum genoemd.

Als een sinusfunctie met een bepaalde frequentie een amplitude heeft die niet nul is, dan zeggen we dat deze frequentie in het signaal voorkomt. Dus met behulp van Fourieranalyse kunnen we berekenen welke frequenties in het signaal voorkomen. Dit worden frequentie-componenten genoemd. Elke frequentie-component zien we in het vermogensspectrum als een waarde bij de bijbehorende frequentie. De waarde is gelijk aan het kwadraat van de absolute waarde van de

amplitude van de bijbehorende sinusfunctie. De frequentie-componenten die voor kunnen komen in de schommelingen in het hartritme signaal van enkele minuten (2-5 min) worden de korte-termijn variaties genoemd.

De spontane korte-termijn variaties worden vaak met behulp van Fourier-analyse bestudeerd om de neurale activiteit (zenuwactiviteit) van de hersenen naar het hart te schatten. Daarvan zijn er zijn twee typen: de sympathische en de parasympathische. Gewoonlijk zijn er twee banden opvallend in het vermogens-spectrum: een band in de buurt van 0.1 Hz en een band in de buurt van 0.3 Hz. Waarschijnlijk weerspiegelt de 0.1 Hz band veranderingen in sympathische activiteit. De 0.3 Hz band weerspiegelt de invloed van de ademhaling op het hartritme en geeft de veranderingen in parasympathische activiteit weer. De banden mogen een spreiding hebben en worden daarom ook frequentie-banden genoemd. De frequentie-banden rond de 0.1 Hz en 0.3 Hz worden de voor de HRV-analyse kenmerkende frequentie-banden genoemd en wel de middenband en de hoge band.

Modellen van gesloten regelsystemen worden gebruikt om het voorkomen van beide banden te verklaren. In zo een model wordt de bloeddruk o.a. door de baroreflex geregeld. Drukopnemers, de zogenaamde baroreceptoren, geven bloeddrukschommelingen via een zenuwbaan, de baroreflex, door aan de hersenen. Door middel van sympatische activiteit wordt het hartritme door de hersenen geregeld om de bloeddrukschommelingen te compenseren. Dit maakt het regelsysteem gesloten.

Het vermogensspectrum wordt gebruikt om de vermogens in beide banden en het totale vermogen van de korte-termijn variaties te berekenen. Dit geeft informatie over de veranderingen in HRV in het frequentie-domein over de tijd. Net als bij de analyses in het tijdsdomein, hebben die veranderingen te maken met veranderingen in het cardiovasculaire regelsysteem. Op elk van bovengenoemde HRV-representaties kan deze Fourieranalyse toegepast worden.

In hoofdstuk 3 introduceren we het instantane hartritme spectrum. Niet het spectrum is instantaan, maar het hartritme. Het hartritme wordt per slag berekend. We vergelijken dit spectrum met het 'tel-spectrum' (spectrum of counts). Het instantane hartritme spectrum is het vermogensspectrum van een hartritme pulsreeks. Het tel-spectrum is het vermogensspectrum van een hartslag pulsreeks.

Pulsreeksen zijn niet-equidistant, dat betekent dat de pulsen niet op regelmatige afstanden in de tijd staan. Het gevolg daarvan is dat er harmonische vervorming in de spectra optreedt. Dit werd in hoofdstuk 3 zijbandvervorming genoemd. Zijbanden zijn waarden in het spectrum die optreden naast de harmonische frequenties van het gemiddelde hartritme. Deze waarden zijn op zich niet interessant voor het onderzoek naar HRV. Harmonische vervorming betekent dat ze kunnen voorkomen in het frequentie-gebied dat wel interessant is voor de studie naar HRV. Dit gebied geeft dus geen juiste weergave van de frequentie-componenten in HRV. Het tel-spectrum en het instantane hartritme spectrum bevatten dezelfde spectrale informatie, dat wil zeggen, dezelfde frequentie-componenten. In hoofdstuk 3 wordt aangetoond dat de harmonische vervorming minder is in het instantane hartritme spectrum dan in het tel-spectrum.

Hoofdstuk 3 beschrijft in het kort ook de methode om van niet-equidistante bloeddruk- en ademhalingsreeksen het spectrum te berekenen. Deze reeksen zijn niet-equidistant omdat de waarden bemonsterd worden op de R-top detectie tijdstippen.

Hoofdstuk 4 vat de resultaten samen van onze studies waarin de spectrale technieken van hoofdstuk 3 toegepast werden op het hartritme, de bloeddruk en de ademhaling. Analyse van hartritme- en bloeddruk-variabiliteit toont significante veranderingen in het vermogen van de middenband en de hoge band aan, gepaard gaand met:

- de belasting van het cardiovasculaire regelsysteem met diverse farmacologische middelen (epinephrine, norepinephrine, clonidine, lorazepam) bij gezonde personen;
- de antidepressiva imipramine en mirtazapine bij depressieve patiënten;
- psychische en fysieke inspanningstesten bij gezonde personen, depressieve patiënten en patiënten met autonome disfuncties.

Over het algemeen bevestigen deze studies dat spectraalanalyse van hartritme- en bloeddruk-variabiliteit gebruikt kan worden om veranderingen in het cardiovasculaire regelsysteem te bestuderen. De studies bij patiëntengroepen tonen aan dat het noodzakelijk is de ademhalingsvariaties er bij te betrekken om de korte-termijn variaties beter te begrijpen.

5 Tijd-frequentie analyse

Hartritme variabiliteit wordt zowel in het tijdsdomein (als functie van de tijd) als in het frequentie-domein (als functie van de frequentie) onderzocht. Beide representaties bevatten dezelfde informatie. Echter, een signaal als functie van frequentie laat niet zien hoe een frequentie-component verandert in de tijd. En een signaal als functie van de tijd laat niet zien hoe een tijdcomponent verandert in frequentie. Anders gezegd, het vermogensspectrum laat zien welke frequentie-componenten er in het signaal aanwezig zijn, maar laat niet zien wanneer ze voorkomen en ook niet hoe de amplitude van een frequentie-component varieert in de tijd. Een signaal, als functie van de tijd, laat zien dat er op een tijdstip activiteit is, maar niet welke frequenties er op dat tijdstip zijn. Deze beperkingen leidden tot de wens te komen tot een analyse in een tijd-frequentie domein. Voor dit doel zijn in de laatste decennia signaal representaties en analyse technieken ontwikkeld waaraan dit proefschrift ook een bijdrage levert.

De instantane eigenschappen van een signaal zijn eigenschappen die binnen de tijdsresolutie van het signaal berekend kunnen worden. De tijdsresolutie van een signaal geeft aan hoe nauwkeurig een gebeurtenis in de tijd gemeten kan worden. Het is het kleinste tijdsverschil tussen twee gebeurtenissen waarbij ze nog als afzonderlijke gebeurtenissen waargenomen kunnen worden.

Een tijd-frequentie methode die veranderingen van de kenmerkende frequentie-componenten (zowel in de tijd als in de frequentie) in HRV instantaan kan kwantificeren, kan een verbeterde interpretatie van HRV-signalen opleveren. Zeker als dat met een hoge tijds- en frequentie-resolutie kan. Dat was het doel van dit onderzoek. We verwachten dat een nauwkeurige tijd-frequentie methode een belangrijke bijdrage kan leveren aan de studie naar de instantane veranderingen van de sympatische en parasympatische activiteit en de invloed van fysieke, psychische en farmacologische prikkels op het cardiovasculaire regelsysteem.

6 De Wigner-Ville distributie

Het vermogensspectrum vertegenwoordigt het vermogen van een signaal uitgesplitst per frequentie-component. Voor elke frequentie-component die aanwezig is in het signaal staat er een waarde in het vermogensspectrum dat het gemiddelde

vermogen van de frequentie-component, over de tijd waarover het vermogens-spectrum berekend is, weergeeft. Zoals al eerder is gezegd, kunnen we niet zien wanneer een frequentie-component aanwezig is. Om dat te kunnen hebben we een methode nodig die de verdeling van het vermogen van een frequentie-component ook in de tijd weergeeft. Zo een weergave van het vermogen van een signaal gelijktijdig in het tijdsdomein en in het frequentie-domein, dat wil zeggen, als functie van de tijd en van de frequentie, heet een tijd-frequentie representatie. Een tijd-frequentie representatie laat de frequentie-componenten zien zoals ze opkomen, in amplitude variëren en weer uitsterven in de tijd.

Een tijd-frequentie representatie kan gemaakt worden van niet-stationaire signalen. Stel dat een signaal verdeeld is in tijdsegmenten en voor elk segment wordt een statistische variabele berekend. Het signaal is stationair als de statistische variabele per segment niet significant verschilt (zie hoofdstuk 1). Een signaal is niet-stationair als het tijdsafhankelijke statistische eigenschappen heeft. In een niet-stationair signaal kunnen de frequentie-componenten sterk variëren. En deze variaties kunnen we dus zichtbaar maken in een tijd-frequentie representatie.

Een voorbeeld van een tijd-frequentie representatie is de Wigner-Ville distributie. De appendix staat uitvoerig stil bij deze representatie. Een nadeel van de Wigner-Ville distributie is het ontstaan van kruistermen. Dit komt omdat de Wigner-Ville distributie een kwadratisch karakter heeft. Kruistermen zijn sinusvormige componenten die onstaan tussen twee autotermen, dat wil zeggen tussen twee frequentie-componenten die enige tijd gelijktijdig aanwezig zijn of tussen twee tijdcomponenten die beide in een frequentie-interval aanwezig zijn. Het geheel van autotermen en kruistermen maakt de interpretatie van de Wigner-Ville distributie erg moeilijk. Varianten van de Wigner-Ville distributie die deze kruistermen onderdrukken zijn de gladde (smoothed) Wigner-Ville distributie en de exponentiële distributie. Deze worden in de hoofdstukken 5 en 6 toegepast op hartritme en bloeddruk variabiliteitssignalen en op ademhalingssignalen. Deze signalen werden verkregen onder diverse klinische en experimentele omstandigheden. De toepassingen tonen de waarde aan van de kwalitieve beschrijving van de tijd-frequentie relaties in cardiovasculaire signalen met behulp van deze representaties. De kwantitatieve beschrijving blijft echter in gebreke want het is moeilijk om goede kwantitatieve

variabelen te definiëren op basis van deze representaties. De exponentiële distributie onderdrukt de kruistermen beter dan de gladde Wigner-Ville distributie.

7 Een nieuwe methode

In hoofdstuk 7 presenteren we onze nieuwe methode om de instantane veranderingen in amplitude en frequentie van HRV-signalen te berekenen. Het HRV-signaal moet aan een aantal eisen voldoen, namelijk, het signaal moet smalbandig, monocomponent en analytisch zijn. Een smalbandig signaal is gedefinieerd in een beperkt frequentie-gebied in het vermogensspectrum, buiten dat gebied heeft het signaal geen frequentie-componenten. Een monocomponent signaal is een signaal dat op ieder tijdstip maar één smalle band in het vermogensspectrum heeft. Die band mag in de tijd wel variëren in amplitude en frequentie. Dus als we op een bepaald tijdstip een instantaan vermogensspectrum maken, dat is een spectrum dat binnen de tijdsresolutie is te berekenen, dan heeft dat spectrum maar één band. Deze band kan een kleine spreiding hebben. Een analytisch signaal is een signaal zonder negatieve frequentie-componenten. Het signaal is dan per definitie complex. Om de instantane amplitude, fase en frequentie van een reëel signaal te berekenen, moet het signaal worden omgezet in een analytisch signaal. Onze methode is toepasbaar op smalbandige, analytische signalen die monocomponent zijn.

Het HRV-signaal wordt gefilterd om het signaal smalbandig en monocomponent te maken. Dit doen we met een banddoorlaat filter dat de fase van het signaal niet verandert en waarvan de doorlaatband overeenkomt met een van de kenmerkende frequentie-banden. Verder heeft dit filter zogenaamde $\cos^2$-flanken. Daardoor heeft het filter in het frequentie-domein steile, bijna ideale flanken. Door te filteren houden we die frequentie-componenten van het signaal over die in het vermogensspectrum in de band van 0.1 Hz of in de band van 0.3 Hz liggen. Het signaal wordt analytisch gemaakt door te filteren met een zogenaamd Hilbertfilter (zie de appendix). Van dit gefilterde signaal worden de instantane amplitude en frequentie berekend met een rekenalgoritme dat beschreven is in hoofdstuk 7. De gekwadrateerde instantane amplitude is een maat voor het tijdsafhankelijke instantane vermogen van het signaal in een smalle frequentie-band. De instantane frequentie bepaalt, binnen een smalle frequentie-band, de tijdsafhankelijke

frequentie-locatie van de spectrale band in het vermogensspectrum. De instantane frequentie kan worden gezien als het gemiddelde van alle frequentie-componenten die op een tijdstip aanwezig zijn. Er wordt toegelicht dat in de instantane frequentie van HRV-signalen afwisselend golfvormige en onregelmatige perioden kunnen voorkomen. De onregelmatigheden werden in de hoofdstukken 7, 8 en 9 toegeschreven aan plotselinge verschuivingen in de instantane fase. De instantane bandbreedte is de spreiding van de spectrale band. De instantane bandbreedte kan gezien worden als de standaard deviatie die bij de instantane frequentie hoort. In ons geval is de instantane bandbreedte coëfficiënt een maat voor de spreiding. We stellen voor om de instantane bandbreedte coëfficiënt te gebruiken om onderscheid te maken tussen golfvormige en onregelmatige signaal fragmenten. Door een drempelniveau aan te leggen in de instantane bandbreedte coëfficiënt, kunnen golfvormige perioden geselecteerd worden om verder geanalyseerd te worden en kunnen onregelmatige perioden genegeerd worden of op een aparte manier geanalyseerd worden.

In hoofdstuk 7 presenteren we ook een methode om in een smalle frequentie-band, in het bijzonder de kenmerkende frequentie-banden, de resolutie van het signaal vast te stellen. De resolutie is omgekeerd evenredig met de bandbreedte van de frequentie-band, zoals de onzekerheidsrelatie van Gabor voorschrijft en hangt alleen af van de eigenschappen van het gebruikte filter. Deze resolutie wordt hier de optimale resolutie genoemd (behorend bij het filter). Als signaaleigenschappen zoals amplitude en frequentie berekend kunnen worden met deze tijdsresolutie, dan noemen we de eigenschappen instantaan. De tijdsresolutie van de instantane amplitude en frequentie in de middenband van HRV was ongeveer 8 s. De tijdsresolutie in de hoge band was ongeveer 2.5 s.

In hoofdstuk 8 vergelijken we onze methode met drie andere methoden die de instantane frequentie van smalbandige, monocomponent en analytische signalen kunnen berekenen. Deze methoden zijn:

- de discrete tijd-frequentie transformatie;
- het 'circulaire' gemiddelde (van de tijdsplakjes in de Wigner-Ville distributie);
- en de discrete afgeleide (central finite difference) van de fase van het analytische signaal.

De conclusie luidt dat er alleen numerieke verschillen tussen de vier methoden zijn op tijdstippen dat er onregelmatigheden optreden.

In hoofdstuk 9 definiëren we diverse variabelen die kwantitatief de tijdsafhankelijke frequentie-veranderingen en de verdeling van de golfvormige en de onregelmatige perioden in de tijd beschrijven. De instantane bandbreedte coëfficiënt wordt gebruikt om de onregelmatige perioden uit de instantane frequentie en de overeenkomstige perioden uit de instantane amplitude te halen. Na de verwijdering van de onregelmatige perioden berekenen we in een vastgesteld tijdsinterval de gemiddelde instantane amplitude, de gemiddelde gekwadrateerde instantane amplitude en de gemiddelde instantane frequentie. Andere variabelen geven de totale duur van de golfvormige en de onregelmatige perioden en de verdeling van deze perioden in de tijd weer. De statistiek wordt toegepast op hartslagdata van gezonde vrijwilligers. De data werden verzameld tijdens rustig liggen (steady state) en tijdens orthostatische belasting, dat is het veroorzaken van een opzettelijke bloeddrukverandering door te gaan staan. De resultaten geven aan dat tijdens liggen de middenband voor 77% van de totale duur beschouwd kon worden als bestaande uit golfvormige perioden. Tijdens staan was dat 84% van de totale duur. De hoge band was tijdens liggen voor 77% golfvormig, tijdens staan was dat 73%. Na overgang van liggen naar staan stijgt de instantane amplitude in de middenband significant, terwijl de instantane frequentie significant daalt. Tevens verandert de verdeling van de golfvormige en de onregelmatige perioden significant omdat de gemiddelde duur van de golfvormige perioden vermindert. In de hoge band dalen zowel de instantane amplitude, de instantane frequentie, als de gemiddelde duur van de golfvormige perioden. Deze eerste resultaten tonen aan dat onze variabelen de omslag van rust naar een toestand van sympathische activatie en parasympatische remming ten gevolge van de orthostatische belasting kunnen weergeven.

8 De voordelen van onze tijd-frequentie methode

De methode, die we in dit proefschrift presenteren, kan snelle en langdurige variaties in het cardiovasculaire regelsysteem kwantificeren en bovendien de verstoring van het systeem objectief vaststellen. Deze methode kan op verschillende manieren ons inzicht in het dynamische gedrag van het cardiovasculair regelsysteem verbeteren:

- De gebruikelijke spectraalanalyse kan de snelle veranderingen in de kenmerkende frequentie-banden niet voldoende beschrijven omdat er telkens enkele minuten nodig zijn voor een spectraalanalyse. Onze tijd-frequentie methode kan de snelle veranderingen in amplitude en frequentie kwantitatief analyseren. De methode kan dus gebruikt worden om vast te stellen hoe het cardiovasculaire regelsysteem reageert op psychische, lichamelijke en (psycho-) farmacologische prikkels, en kan dat gedetailleerder dan voorheen.
- Bepaalde symptomen bij psychiatrische patiënten (angst, tics, dwangmatig en impulsief gedrag) kunnen kortdurende verstoringen in het cardiovasculaire evenwicht veroorzaken. Die verstoringen van het cardiovasculair regelsysteem kunnen op de lange duur een negatieve uitwerking op de gezondheid tot gevolg hebben. Het kan interessant zijn deze verstoringen te onderzoeken met onze tijd-frequentie methode om te zien of en hoe deze psychische symptomen zijn weerspiegeld in de instantane bandbreedte coëfficiënt.

Onze tijd-frequentie methode kan uitgebreid worden om een beschrijving te kunnen geven van de relaties in de tijd tussen veranderingen in hartritme, bloeddruk, ademhaling en gedrag. Het lijkt theoretisch mogelijk om de methode toe te passen op andere variabiliteitssignalen, mits deze monocomponent zijn.

9 Conclusies

De belangrijkste conclusies van dit proefschrift zijn:

- Een tijd-frequentie representatie is een belangrijk hulpmiddel om de instantane veranderingen in HRV te verkennen.
- In een smalle frequentie-band beschrijven de instantane amplitude en de instantane frequentie de amplitude- en frequentie-schommelingen in HRV in de tijd.
- Een optimale tijdsresolutie is bereikt overeenkomstig de onzekerheidsrelatie van Gabor.
- In een smalle frequentie-band kan de instantane bandbreedte coëfficiënt de golfvormige en de onregelmatige perioden in de instantane frequentie vaststellen.
- Door het aanbrengen van niveau's in de instantane bandbreedte coëfficiënt kan de instantane frequentie en amplitude gecorrigeerd worden op onregelmatige perioden. Een aantal variabelen kunnen de gecorrigeerde frequentie-veranderingen

en de verdeling van de golfvormige en de onregelmatige perioden in de tijd kwantitatief beschrijven.

APPENDIX
TIME-FREQUENCY ANALYSIS
GLOSSARY
ABBREVIATIONS

Time-frequency representations have become a common tool in signal analysis. During the past decades time-frequency methods were developed and applied to various bio-medical signals. Each method has its own features and limitations and the literature of time-frequency analysis is extensive. To put our method in context, this section summarizes time-frequency representations that are used in bio-medical signal processing.

Section 2 reviews the short-time Fourier transform. This is one of the oldest time-frequency representations and used in the study of heart rate variability (HRV). Section 3 reviews the wavelet transform. This is a recent time-frequency representation and still in development. Section 4 describes an approach based on the characterization of time-frequency representations by means of a kernel-function, called Cohen's general class of time-frequency representations. Section 5 reviews some special time-frequency representations that are less known.

1 Introductory remarks

A distribution that represents the power of a signal simultaneously in time and frequency is called a (joint) time-frequency representation (e.g., Cohen p:82, 1995). Time-frequency signal analysis does not assume stationarity (e.g., Boashash p:418, 1991). A signal is said to be non-stationary, if it has time-varying statistical properties. Suppose a signal is divided in segments and for each segment a statistic is computed. Possibly, the statistics differ from segment to segment. When the differences are significant, the signal is called non-stationary (see section 2 of chapter 1). The statistical test probably depends on the length of the segments. However, regardless of the length of the segment, if a test demonstrates that a signal is non-stationary, one can still apply time-frequency analysis to this signal. If a signal is non-stationary, there may be significant changes of the frequency components in time (e.g., Boashash p:418, 1991). Transient components can be described with a time-frequency representation.

To interpret a time-frequency representation as a power distribution in the time-frequency plane, a representation should have a number of 'desirable' properties. For now, we mention only four 'desirable' properties P1, P2, P3, and P4 for a time-frequency representation $T(t,f)$ of a signal $x(t)$ with Fourier transform $X(f)$:

P1: a time-frequency representation should be real and non-negative: $T(t,f) \geq 0$;

P2: integration over time yields the power spectral density of the signal:

$\int_{-\infty}^{+\infty} T(t,f)\,dt = |X(f)|^2$;

P3: integration over frequency yields the instantaneous power of the signal:

$$\int_{-\infty}^{+\infty} T(t,f)\,df = |x(t)|^2;$$

P4: The first moments of the time-frequency representation yields the instantaneous frequency $f_i(t)$ of the signal, i.e., the instantaneous frequency is the conditional average of the time-frequency representation at a given time:

$$\frac{\int_{-\infty}^{+\infty} f \cdot T(t,f)\,df}{\int_{-\infty}^{+\infty} T(t,f)\,df} = f_i(t).$$

One can also say that P1, P2, P3, and P4 are conditions that a time-frequency representation should satisfy. For instance, to interpret a time-frequency representation as a power distribution, condition P1 should be satisfied. Or, if condition P3 is not satisfied, the time-frequency representation $T(t,f)$ cannot be interpreted locally as an instantaneous spectrum, i.e., a distribution of the frequencies present in the signal at time t (see section 4 of chapter 2). This applies correspondingly to condition P2. P2 and P3 are called the marginal properties or conditions. These properties and requirements of time-frequency representations are, among others, discussed by Boashash (pp:437-438, 1991), Kootsookos et al. (1992), Hlawatsch et al. (pp:32-34, 1992) and Williams (p:16, 1997) (see chapters 5 and 6).

2 The short-time Fourier transform

One of the oldest and frequently used time-frequency representations is the **short-time Fourier transform**. A complex window $w(t)$, centered around the time origin $t=0$, is shifted in equal steps along the time axis. After each time-step, the Fourier transform of the data segment of the signal $x(t)$ within the time-window is computed:

$$\mathrm{STFT}(t,f) = \int_{-\infty}^{+\infty} x(\tau)\,w^*(\tau - t)\,e^{-2\pi j f \tau}\,d\tau.$$

A possible window function is the Gaussian function as used by Gabor (1946). The squared modulus of the short-time Fourier transform is the time-varying power spectral density of the signal $x(t)$ and is called the **spectrogram**:

$$P_{\mathrm{STFT}}(t,f) = |\mathrm{STFT}(t,f)|^2.$$

At each instant t, $P_{\mathrm{STFT}}(t,f)$ reflects the power of the frequency components. Condition P1 is satisfied. A drawback of the short-time Fourier transform is that the signal and derived parameters are modified by the properties of the time-window. This means that the marginal conditions P2 and P3, and condition P4 are not

satisfied, i.e., the instantaneous frequency cannot be computed as the conditional average of the time-frequency representation at a given time (e.g., Cohen pp:97-101, 1995). An example of a spectrogram of a low-pass filtered cardiac event series is figure A1.

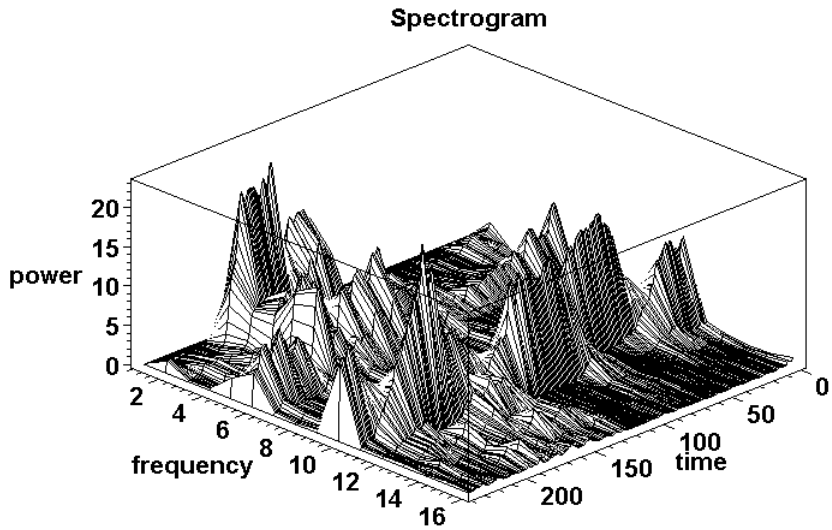

Figure A1. An example of a spectrogram of the first 118 s of the low-pass filtered cardiac event series shown in figure 2A of chapter 1.

Both the time-resolution Δt and the frequency-resolution Δf are dependent on the time-window chosen for the short-time Fourier transform. They are constant throughout the entire time-frequency plane (see figure A2). The frequency-resolution of the time-frequency plane is Δf. This means that two frequency components (two sinusoids) can only be discriminated if they are more than Δf apart. The time-resolution is Δt, which means that two delta pulses can only be discriminated if they are more than Δt apart. Resolution in time and frequency are linked. They cannot be made arbitrarily small simultaneously because of the uncertainty principle of Gabor (1946), which states that: $\Delta t \Delta f \geq 1/4\pi$. Therefore, there is a trade-off between time and frequency localization. A wide time-window yields a poor time-resolution and a good frequency-resolution (figure A2A). A narrow time-window yields a good time-resolution and a poor frequency-resolution (figure A2B). However, the width of the time-window has to be chosen carefully, because a data segment within a wide time-window may be non-stationary. The short-time Fourier transform is discussed, among

others, by Rioul et al. (pp:15-17, 1991), Hlawatsch et al. (pp:23-28, 1992), Cohen (ch.7, 1995), and Qian et al. (pp:46-52, 1996).

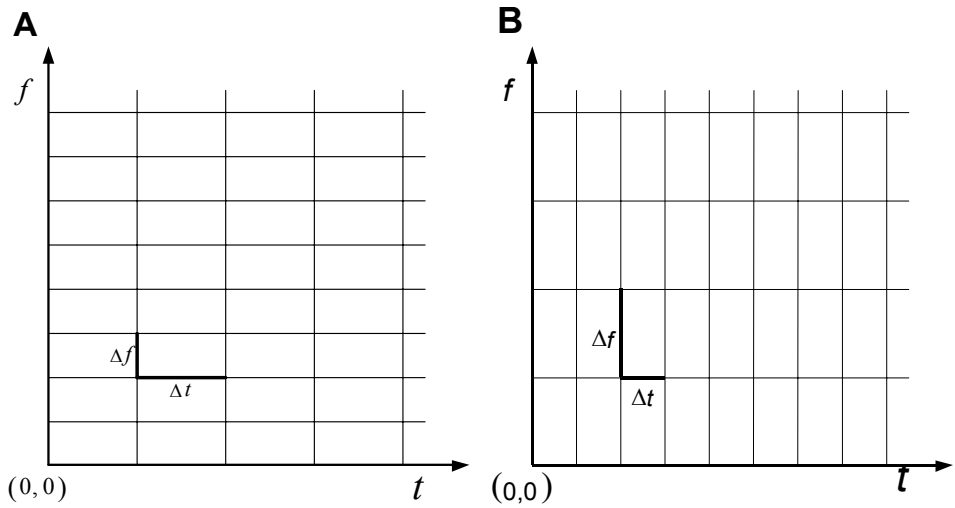

Figure A2. The constant time-frequency resolution of the short-time Fourier transform is illustrated by rectangles in the time-frequency plane (e.g., Rioul et al. p:16, 1991; Qian et al. p:78, 1996). Each rectangle has time-duration Δt and bandwidth Δf. Each rectangle has constant area $\Delta t \Delta f$. A: a wide time-window; B: a narrow time-window.

Keselbrener et al. (1996) implemented an adaptive method, closely related to the short-time Fourier transform, which can be seen as a precursor to the wavelet approach. The method chooses a wide time-window at the lowest frequency component, implying a good frequency-resolution, and narrower time-windows at higher frequency components with increasing time-resolution. They applied this method to HRV-data to quantify with a high time-resolution the effects of vagal stimuli and the transient autonomic changes during a transition from supine to standing in normal subjects and unmedicated mildly hypertensive subjects. Due to the changes in position, sudden changes in heart rate and arterial blood pressure were observed. Their time-frequency method made it possible to hypothesize about the decreasing parasympathetic drive, reflected in the high-frequency components of HRV, and the increasing sympathetic drive, reflected in the low-frequency components of blood pressure variability, during the transition (Akselrod et al., 1997).

3 The wavelet transform

In the computation of the short-time Fourier transform, both the time-resolution Δt and the frequency-resolution Δf of the time-frequency plane are dependent on the chosen time-window. Time- and frequency-resolution are fixed throughout the entire time-frequency plane (see figure A2 of section 2) and they cannot be made arbitrarily small simultaneously because of the uncertainty principle of Gabor. A signal consisting of abrupt changes of short duration superimposed on slow components with long periods, can be analyzed with a short time-window, i.e., with an optimal time-resolution to discriminate the transient events. Alternatively, it can be analyzed with a long time-window, i.e., with an optimal frequency-resolution to discriminate the slow frequency components. With the short-time Fourier transform it cannot be analyzed with both simultaneously.

In contrast to the short-time Fourier transform, the wavelet transform uses a short window at high frequencies and a long window at low frequencies. This time-window is not only localized in time through time-shifting, but also localized in frequency, through time-scaling. This means that at high frequencies, there is a good time-resolution and events of short duration are discriminated in time, and at low frequencies, there is a good frequency-resolution, i.e., long and slow components are discriminated in frequency. As a result, Δt and Δf vary in the time-frequency plane and a multi-resolution time-frequency representation of the signal is obtained (see figure A4 below).

The wavelet transform is a decomposition of a signal onto a set of orthogonal functions. Wavelet analysis is a method that, through this decomposition, analyzes the variations of the power of a signal localized in time as well as in frequency. Let **V** be a function space of which each function x can be written as a linear combination of functions $\{\psi_m, m = ..., -1, 0, 1, ...\}$ in **V**:

$$x(t) = \sum_{m=-\infty}^{\infty} a_m \psi_m(t). \tag{A1}$$

In such a space there exist a set $\{\hat{\psi}_m, m = ..., -1, 0, 1, ...\}$ of functions in **V**, such that each coefficient a_m can be written as:

$$a_m = \int_{-\infty}^{+\infty} x(t) \hat{\psi}_m^*(t)\, dt. \tag{A2}$$

The functions ψ_m are called synthesis functions, and the functions $\hat{\psi}_m$ are called analysis functions. The right hand side of the expression (A1) is the decomposition of the function x onto $\{\psi_m, m = ..., -1, 0, 1, ...\}$. For example, if

$$\psi_m(t) = \hat{\psi}_m(t) = e^{2\pi j \frac{m}{T} t},$$

then expression (A1) is the Fourier series of x and the coefficients a_m in (A2) are the Fourier coefficients of x.

A function $\psi(t)$, called the mother wavelet, is chosen. Three examples of mother wavelets are shown in figure A3. Assume that the mother wavelet is centered in the time- and frequency-domain around time $t = 0$ and center frequency $f = f_0$. The duration σ_t is the standard deviation of $\psi(t)$ with respect to $t = 0$. A wavelet has a band-pass like spectrum. The standard deviation of the spectrum with respect to $f = f_0$ is the bandwidth σ_f.

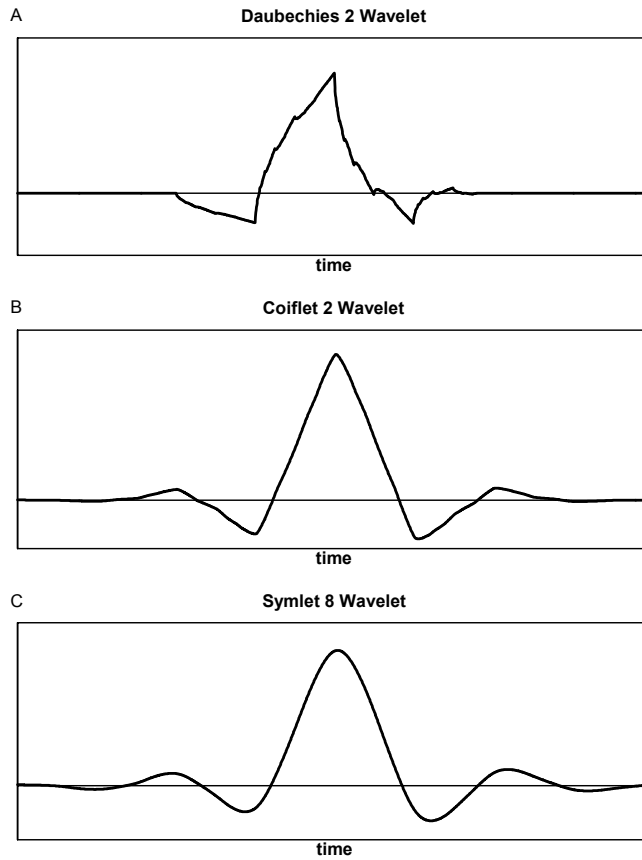

Figure A3. Three examples of mother wavelets. A: a Daubechies wavelet; B: a Coiflet wavelet; C: a Symlet wavelet.

The time-resolution Δt indicates how accurately in time an event can be measured; it is the minimum difference in time between two peaks so that they still can be resolved as distinct peaks in time. Two delta pulses that are less than Δt in

time apart cannot be discriminated in time. The frequency-resolution Δf indicates how accurately the frequency of a sinusoid can be measured; it is the minimum distance in frequency between two sinusoids so that they still can be resolved as distinct peaks in the frequency spectrum. Two frequency components that are less than Δf in frequency apart cannot be discriminated in frequency. Analyzing a signal with a time-window of short duration σ_t yields a good time-resolution but a poor frequency-resolution of the result. Decreasing the duration of an analyzing window by a factor a will improve the time-resolution with a factor a. Analyzing a signal with a time-window of long duration yields a poor time-resolution but a good frequency-resolution of the result. Increasing the duration of an analyzing window by a factor a will improve the frequency-resolution with a factor a.

A set of wavelets, called synthesis wavelets, $\psi_a(t) = \psi(t/a)$ is constructed by time-scaling a mother wavelet with a factor $a > 0$. The effect of the time-scaling is threefold:

- the standard deviation of $\psi(t/a)$ is $a\sigma_t$, therefore the duration of $\psi_a(t)$ becomes $\sigma_t(a) = a\sigma_t$; the time-resolution becomes $\Delta t(a) = a\Delta t$;
- the standard deviation of the spectrum of $\psi(t/a)$ is σ_f / a, therefore the bandwidth of $\psi_a(t)$ becomes $\sigma_f(a) = \sigma_f / a$; the frequency-resolution becomes $\Delta f(a) = \Delta f / a$;
- narrowing the duration increases the mean frequency, broadening the duration decreases the mean frequency: $\psi_a(t)$ is now centered in the frequency-domain around $f(a) = f_0 / a$.

It follows that the relative bandwidth and the relative frequency-resolution are constant:

$\frac{\sigma_f(a)}{f(a)} = \frac{\sigma_f}{f_0}$ and $\frac{\Delta f(a)}{f(a)} = \frac{\Delta f}{f_0}$.

The product of time- and frequency-resolution is constant throughout the time-frequency plane:

$\Delta t(a) \cdot \Delta f(a) = \Delta t \Delta f$

(see figure A4). But, due to the uncertainty principle of Gabor (1946), the resolution in time and frequency cannot be both arbitrarily small.

For instance, if $a = 2$, each scaling means dividing the center frequency by a factor 2, narrowing the bandwidth and the frequency-resolution by a factor 2, and broadening the duration and the time-resolution with a factor 2 (see figure A4).

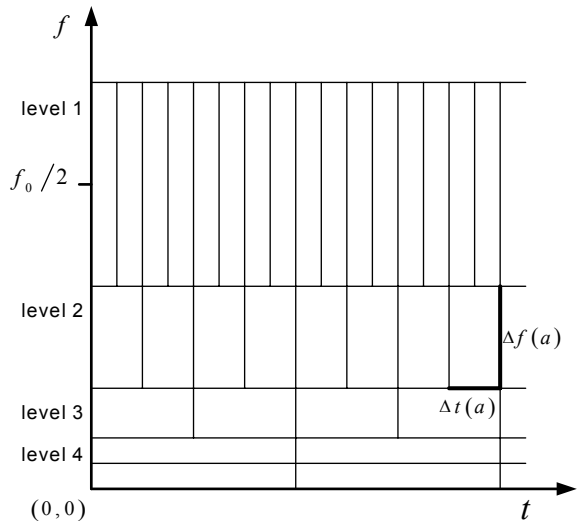

Figure A4. The time-frequency resolution of the wavelet transform is illustrated by rectangles in the time-frequency plane. Each rectangle has time-resolution $\Delta t(a) = a\Delta t$ and frequency-resolution $\Delta f(a) = \Delta f / a$. Each rectangle has constant area $\Delta t \Delta f$. At high frequencies, there is a better time-resolution and a poorer frequency-resolution than at low frequencies. This means that two delta pulses can be discriminated in time at high frequencies. Two sinusoids cannot be discriminated in frequency at high frequencies. At low frequencies, time-resolution is poorer but frequency-resolution is better. This means that two delta pulses cannot be discriminated in time at low frequencies. Two sinusoids can be discriminated in frequency at low frequencies. f_0 is the center of the mother wavelet in the frequency-domain. The levels are the levels of decomposition of the signal into frequency bands.

A **continuous wavelet transform** is defined as the decomposition locally at time t and frequency f of a signal $x(t)$ in **V** onto the analysing wavelets $\hat{\psi}_a(t)$:

$$\mathrm{CWT}(f,t) = \int_{-\infty}^{+\infty} x(\alpha)\hat{\psi}_a^*(\alpha - t)\,d\alpha\,,$$

in which f and a are related by: $a = f_0/f$. The square of the modulus of the continuous wavelet transform is called the **scalogram** of $x(t)$:

$$P_{\mathrm{CWT}}(f,t) = \left|\mathrm{CWT}(f,t)\right|^2.$$

Because the continuous wavelet transform is a decomposition onto an orthogonal basis, it follows that

$$\int_{-\infty}^{+\infty}\int_{-\infty}^{+\infty}\left|\mathrm{CWT}(f,t)\right|^2 df\,dt$$

equals the total energy of the signal $x(t)$. This means that the scalogram $\left|\mathrm{CWT}(f,t)\right|^2$ is a distribution of the energy of the signal in the time-frequency domain expressed in power per frequency unit. The scalogram satisfies condition P1, but does not satisfy the marginal conditions P2 and P3 (see section 1).

Let $a=2$ and denote in this case the synthesis wavelets with $\psi_m(t)=\psi\left(t/2^m\right)$, for $m\in\mathbb{Z}$. The scaled wavelet $\psi_m(t)$ is centered around $f_m=f_0/2^m$, the bandwidth is $\Delta f(m)=\Delta f/2^m$, and the duration is $\Delta t(m)=2^m\Delta t$. Let $x(t)$ be a signal in **V**. Because the synthesis wavelets are localized in time at $t=0$, we cannot decompose $x(t)$ onto the set of synthesis wavelets $\psi_m(t)$. But at each time $t=k2^m$, k is an integer, it is possible to decompose $x(t)$ locally onto a set of time-shifted synthesis wavelets $\psi_m\left(t-k2^m\right)$, which are localized at $t=k2^m$. In other words, there exists a dual wavelet $\hat{\psi}(t)$ and dual analysis wavelets $\hat{\psi}_m(t)=\hat{\psi}\left(t/2^m\right)$ such that, for each signal $x(t)$ in **V**, we can write:

$$x(t)=\sum_{m=-\infty}^{\infty}\sum_{k=-\infty}^{\infty}c_{m,k}\psi_m\left(t-k2^m\right), \tag{A3}$$

with:

$$c_{m,k}=\int_{-\infty}^{+\infty}x(\alpha)\hat{\psi}_m^*\left(\alpha-k2^m\right)d\alpha. \tag{A4}$$

The right hand side of equation (A3) is called the reconstruction of $x(t)$. The numbers $c_{m,k}$ are called wavelet coefficients. The right hand side of equation (A4) is called a **wavelet transform** of $x(t)$:

$$\mathrm{WT}(m,k)=\int_{-\infty}^{+\infty}x(\alpha)\hat{\psi}_m^*\left(\alpha-k2^m\right)d\alpha.$$

Note that this is a convolution of $x(t)$ with the function $\hat{\psi}_m(-t)$. The scalogram:

$$P_{\mathrm{WT}}(m,k)=\left|\mathrm{WT}(m,k)\right|^2=\left|c_{m,k}\right|^2.$$

is the distribution of the energy of the signal in the time-frequency domain.

In the case of a sampled signal, the wavelet transform produces a wavelet coefficient $c_{m,k}$ in each rectangle of figure A4. In this case m ranges from 1 to ∞, because the highest frequency is the sample frequency divided by 2. m is called the level of the decomposition. Figure A4 shows four levels. Each level coincides with a frequency band. Each level contains a signal component. We can use the wavelet coefficients of a level to reconstruct the signal component of that level, i.e., the signal

component of $x(t)$ in that frequency band. This requires the reconstruction of the m^{th}-level component $\tilde{x}_m(t)$ of $x(t)$:

$$\tilde{x}_m(t) = \sum_k c_{m,k} \psi_m\left(t - k2^m\right) \tag{A5}$$

Note that

$$x(t) = \sum_{m=1}^{\infty} \tilde{x}_m(t).$$

Furthermore, an m^{th}-level partial reconstruction $x_m(t)$ of $x(t)$ can be made by:

$$x_m(t) = \sum_{i=m}^{\infty} \tilde{x}_i(t),$$

i.e., all the level components $\tilde{x}_i(t)$ are summed up to the component of level m. One can say that the m^{th}-level partial reconstruction is an approximation of the signal consisting of the low frequency components up to the frequency component of level m.

The literature on wavelet theory is very extensive. We mention only: Rioul et al. (1991), Hlawatsch et al. (1992), Chui (1992), Newland (ch.17, 1993), Akay (ch.8, 1996), Qian et al. (ch.2 and 4, 1996), and Jensen et al. (2001).

An example

Figure A6A presents an IBI-series of 128 s. The series is interpolated and equidistantly resampled with a sample frequency F_s = 16 Hz, i.e., the number of data N = 2048. The time-resolution Δt = 0.0625 s. We want to analyze this time series with the wavelet transform. For this example we have chosen the Coiflet 2 wavelet shown in figure A3B. This wavelet is scaled by the algorithm in such a way that the duration σ_t = 0.0625 s, the bandwidth σ_f = 8 Hz, and such that the wavelet is centered around f_0 = 12 Hz. Then the wavelet transform computes the wavelet coefficients $c_{m,k}$ for a number of levels m.

For the first level, $m = 1$, the center frequency of the scaled wavelet $\psi_1(t)$ is $f_1 = f_0/2$ = 6 Hz, the bandwidth $\sigma_f(1) = \sigma_f/2$ = 4 Hz, and the duration $\sigma_t(1) = 2\sigma_t$ = 0.125 s. This means that level 1 coincides with the frequency band B_1 = [2,4] Hz. The time-resolution in this band is twice the original time-resolution, i.e., $\Delta t(1)$ = 0.125 s, so the wavelet transform only computes $N_1 = N/2$ wavelet coefficients $c_{1,k}$. For the second level, $m = 2$, $f_2 = f_0/4$ = 3 Hz, $\sigma_f(2) = \sigma_f/4$ = 2 Hz, $\sigma_t(2) = 4\sigma_t$ = 0.25 s, $\Delta t(2)$ = 0.25 s, and B_2 = [2,4] Hz. The wavelet transform computes $N_2 = N/4$ wavelets coefficients $c_{2,k}$. Table A1 summarizes this for the first nine levels. In this table, $\Delta t(m)$ is not only the time-resolution of the frequency band B_m, but also the duration of the wavelet ψ_m. Figure A5 shows the band-pass like power spectral

densities of the scaled synthesis wavelets $\psi_5(t)$, $\psi_6(t)$, $\psi_7(t)$, and $\psi_8(t)$, with decreasing center frequencies and decreasing bandwidths.

m	f_m	$\Delta f(m)$	$\Delta t(m)$	B_m	N_m
1	6	4	0.125	[4,8]	1024
2	3	2	0.25	[2,4]	512
3	1.5	1	0.5	[1,2]	256
4	0.75	0.5	1	[0.5,1]	128
5	0.375	0.25	2	[0.25,0.5]	64
6	0.1875	0.125	4	[0.125,0.25]	32
7	0.09375	0.0625	8	[0.0625,0.125]	16
8	0.046875	0.03125	16	[0.03125,0.0625]	8
9	0.0234375	0.015625	32	[0.015625,0.03125]	4
m	$f_0/2^m$	$\Delta f/2^m$	$2^m\Delta t$	$\left[f_m-\frac{\Delta f(m)}{2}, f_m+\frac{\Delta f(m)}{2}\right]$	$N/2^m$

Table A1. Summary of center frequencies, frequency-resolutions, time-resolutions, frequency bands, and number of points for 9 levels of decomposition.

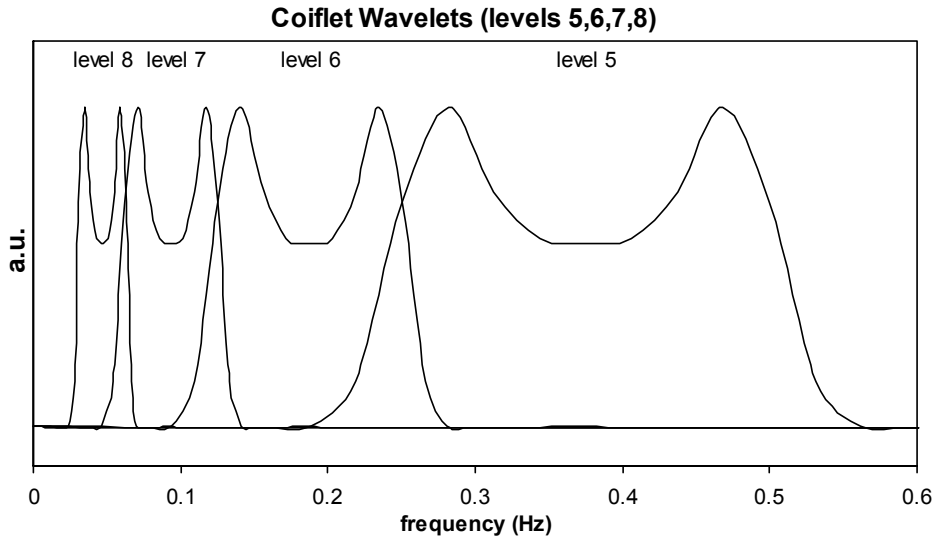

Figure A5. The scaled synthesis Coiflet wavelets of levels 5, 6, 7, and 8 in the frequency domain. The power spectral densities are band-pass like. Table A1 lists the values of the increasing center frequencies and bandwidths.

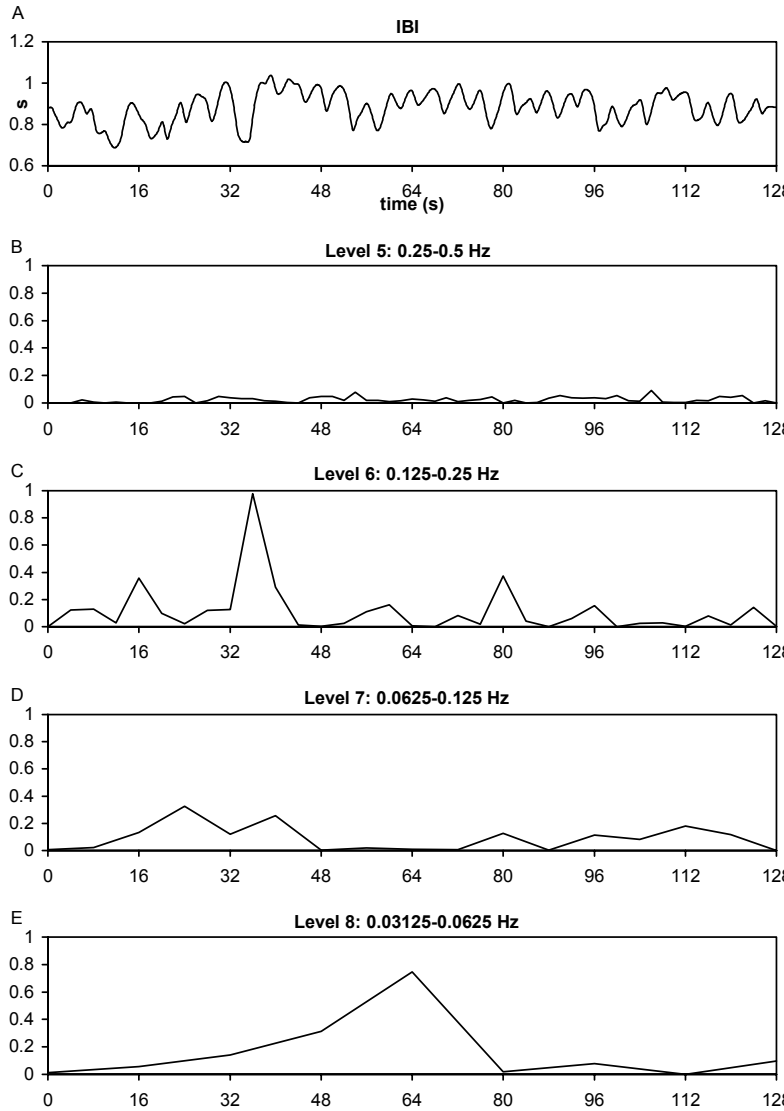

Figure A6. The scalogram $P_{\mathrm{WT}}(m,k)=\left|c_{m,k}\right|^2$ for the levels m =5,6,7, and 8.

The Coiflet wavelet of figure A3 is used. A: the original IBI time series. We used the IBI-data of the Physiological Time-Frequency Analysis Package developed by Houtveen (2001). B,C,D,E: the 5th-, 6th-, 7th-, and 8th-level scalogram; they present the distribution of the energy of the signal in the frequency bands B_5= [0.25,0.5], B_6= [0.125,0.25], B_7= [0.0625,0.125], and B_8= [0.03125,0.0625] Hz, respectively.

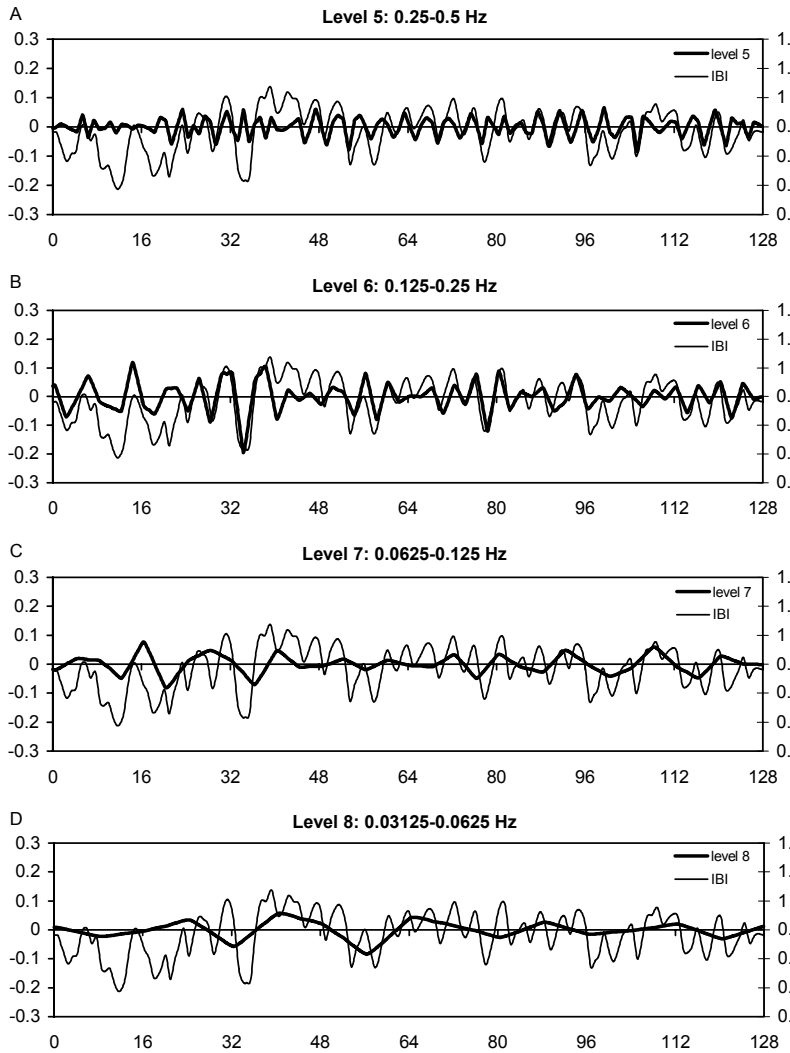

Figure A7. Reconstructed components. The Coiflet wavelet of figure A3 is used. A,B,C,D: the 5^{th}-, 6^{th}-, 7^{th}-, and 8^{th}-level components of the signal in comparison with the original IBI time series. These components are the components of the signal in the frequency bands B_5= [0.25,0.5], B_6= [0.125,0.25], B_7= [0.0625,0.125], and B_8= [0.03125,0.0625] Hz, respectively.

For each level m, the scalogram can be computed, using the wavelet coefficients of that level. The scalogram reflects the spectral density of the signal $x(t)$ in the time-frequency domain at frequency $f_m = f_0/2^m$, i.e., in frequency band B_m. For the levels 5, 6, 7, and 8 the scalograms are plotted in figures A6B, C, D, and E, respectively.

How does the signal component of $x(t)$ in the frequency band B_m look like? For this we have to reconstruct the m^{th}-level component $\tilde{x}_m(t)$ of $x(t)$, using equation (A5). The 5th-, 6th-, 7th-, and 8th-level components are shown in figure A7A, B, C, and D, respectively. For instance, the 7th-level component is the component of $x(t)$ in frequency band [0.0625,0.125] Hz, i.e., the 0.1 Hz rhythm. Finally, the 7th-level partial reconstruction $x_7(t)$ of $x(t)$ is shown in figure A8. One can say that $x_7(t)$ is equal to $x(t)$ without the high frequencies above 0.125 Hz.

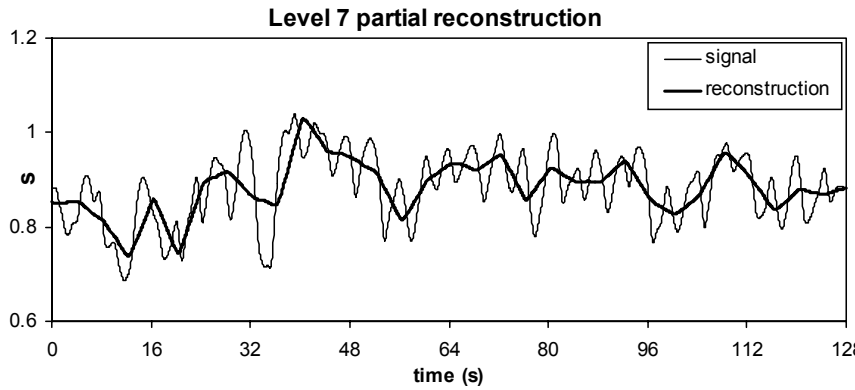

Figure A8. Signal reconstruction. Shown is the 7th-level partial reconstruction of the original IBI time series. This approximation equals the signal without the frequencies above 0.125 Hz.

Comparison with our method

The method described in chapter 7 computes the instantaneous frequency of a monocomponent signal exactly at an optimal time-resolution. A monocomponent signal is a signal that has only one (time-varying) spectral peak. The accuracy with which the frequency of a frequency component can be determined with a wavelet transform depends on the bandwidth σ_f. If the frequency band ranges from 0.07 to 0.15 Hz, i.e., the bandwidth is 0.08 Hz, a component of 0.1 Hz cannot be determined accurately in frequency. Due to the trade-off between duration and bandwidth, a

better frequency-resolution requires a longer time-interval. Therefore, the wavelet transform cannot reach the accuracy of our method.

Figure A5 shows the frequency transfer functions on a linear frequency and amplitude scale of the Coiflet wavelets at levels 8, 7, 6, and 5, i.e., a wavelet filter-bank. Their center frequencies and bandwidths increase each time with a factor 2 (see the table above). Our filter-bank of $\cos^2$-shaped filters was designed conform the physiological definitions of the HRV components, with 'unity-gain' behavior, and an optimal $\sigma_f \sigma_t$ product according to Gabor (see chapter 7). Comparing these two filter-banks, we can make the following comments.

- The wavelet filter-bank does not show 'unity-gain' behavior.
- The filters of the wavelet filter-bank show an overshoot in their pass-bands of 60%, so depending on the frequency of the components, they will be substantially attenuated or affected, whereas our filters have an overshoot better than 0.1%.
- Also in the stop-band of the wavelet filters, there is an attenuation of only 40 dB (1%), so various components will still show minor leakage from adjacent filters; the attenuation in the stop-band of our filters is better than 80 dB.

There is also a remark of a fundamental nature. It is emphasized here that only the squared modulus (or 'power-density') of the wavelet transform is utilized (i.e., the scalogram, figure A6). It can be compared to the square of our instantaneous amplitude (see chapter 7). In our method, we also utilize the phase information contained in the complex analytical signals to yield the instantaneous frequency and bandwidth. The latter is extensively explored regarding its potential to separate oscillatory and irregular ('noisy') periods of the signal over time (chapters 7, 8, and 9).

4 Cohen's general class of time-frequency representations

This section reviews an approach based on the characterization of time-frequency representations by means of a kernel-function. By constructing special kernel-functions one can produce representations with desirable properties. This led to Cohen's general class of time-frequency representations.

4.1 The Wigner-Ville distribution

The Wiener-Khinchine theorem states that the power spectral density $S(f)$ of a stationary stochastic process $x(t)$ is the Fourier transform of the auto-correlation function $R(\tau)$ of the process (e.g., Bendat et al. p:121, 1986):

$$S(f) = F_{\tau \to f} R(\tau) = \int_{-\infty}^{+\infty} R(\tau) e^{-2\pi j f \tau} d\tau \,.$$

To compute the power spectral density of an HRV-signal, this signal has to be stationary. What if an HRV-signal is not stationary? If a signal is not stationary, one has to consider the time-dependent auto-correlation and power spectral density functions. The time-dependent auto-correlation function of an analytical signal $\hat{s}(t)$ (see the appendix of chapter 6) is defined as the product of two points of the signal lying symmetrically around time t at distance $\tau/2$ (e.g., Qian et al. p:104, 1996; Bendat et al. p:456, 1986):

$$R(t,\tau) = \hat{s}\left(t+\frac{\tau}{2}\right)\cdot\hat{s}^{*}\left(t-\frac{\tau}{2}\right)$$

in which τ is called the time-shift or time-lag variable. The time-dependent auto-correlation function is also called local auto-correlation function (Cohen p:137, 1995) or instantaneous auto-correlation function (Steeghs p:30, 1997; Williams p:8, 1997).

The Fourier transform of the local auto-correlation function with respect to the time-shift variable τ is called the **Wigner-Ville distribution** (Wigner, 1932; Ville, 1948):

$$\mathrm{WVD}(t,f) = F_{\tau\to f}R(t,\tau) = \int_{-\infty}^{+\infty} R(t,\tau)e^{-2\pi jf\tau}d\tau\,.$$

For a discussion of the Wigner-Ville distribution see for instance Claasen et al. (1980a; 1980b; 1980c), Boashash (1991; 1992), Cohen (ch.8, 1995), Qian et al. (ch.5, 1996), and Steeghs (pp:29-47, 1997). The Wigner-Ville distribution is interpreted as a power spectral density function, representing the power of the signal $x(t)$ for each point (t,f) of the time-frequency plane. The Wigner-Ville distribution satisfies the marginal conditions P2 and P3 and the total power of the Wigner-Ville distribution in the time-frequency plane equals the total power of the signal. Furthermore, the Wigner-Ville distribution satisfies condition P4: it is possible to use the Wigner-Ville distribution to compute the instantaneous frequency of the signal (see chapters 7 and 8).

4.2 Cross-terms

The Wigner-Ville distribution is not a true density because it may become negative due to cross-terms: the Wigner-Ville distribution does not satisfy condition P1. The cross-terms are due to the bilinear nature of the Wigner-Ville distribution (see equation A14). Suppose $\hat{s}(t)$ consists of two independent pure sinusoids with different frequencies $f_2 > f_1$:

$$\hat{s}(t) = e^{2\pi jf_1t} + e^{2\pi jf_2t}\,.$$

The Wigner-Ville distribution of this analytical function is:

$$\mathrm{WVD}(t,f) = \delta(f-f_1) + \delta(f-f_2) + 2\delta(f-f_h)\cdot\cos(2f_d t) \quad \text{(A6)}$$

in which $f_h = (f_1+f_2)/2$, $f_d = (f_2-f_1)/2$, and $\delta(\cdot)$ is the Dirac delta-function. The first two terms on the right hand side of (A6) are the auto-terms associated with the two sinusoids. The third term is a so-called cross-term. In the time-frequency plane, it is located halfway between the two auto-terms at frequency $f_h = (f_1+f_2)/2$. The cross-term is a sinusoid with frequency $f_d = (f_2-f_1)/2$, i.e., the difference of the frequencies of the two original sine waves. The same applies to two delta-functions in time at different instants $t_2 > t_1$:

$$s(t) = \delta(t-t_1) + \delta(t-t_2).$$

The Wigner-Ville distribution of $s(t)$ is:

$$\mathrm{WVD}(t,f) = \delta(t-t_1) + \delta(t-t_2) + 2\delta(t-t_h)\cdot\cos(2\pi f t_d) \quad \text{(A7)}$$

in which $t_h = (t_1+t_2)/2$ and $t_d = (t_2-t_1)/2$. The first two terms on the right hand side of (A7) are the auto-terms associated with the two events in time. The third term is a so-called cross-term. In the time-frequency plane, it is located halfway between the two auto-terms at time $t_h = (t_1+t_2)/2$. The cross-term is a sinusoid with frequency $t_d = (t_2-t_1)/2$.

This means that between each two frequency components (time components) present in a signal, there appears a cross-term in the time-frequency plane. They can also occur at the location of the auto-terms. One can say that cross-terms are undesirable because they obscure the Wigner-Ville distribution and make it difficult to interpret the distribution. Therefore, one may want to suppress the cross-terms. The ambiguity function plays a role in suppressing the cross-terms of the Wigner-Ville distribution. This is discussed in the next sections. However, if the Wigner-Ville distribution is used to compute signal-parameters one may need the cross-terms; suppressing the cross-terms may lead to incorrect outcomes. An example of a Wigner-Ville distribution with cross-terms is given in figure 4 of chapter 5. Cross-terms are discussed in chapters 5 and 6, and for instance by Cohen (pp:124-127, 1995), Qian et al. (pp:112-118, 1996). Though very small, the spectrogram and the scalogram include also cross-terms (Kadambe et al., 1992; Kootsookos et al., 1992).

4.3 The ambiguity function

The inverse Fourier transform of the local auto-correlation function with respect to the time variable is called the **ambiguity function** (e.g., Boashash p:437, 1991; Cohen p:96, 1995; Qian et al. p:132, 1996; Steeghs p:36, 1997):

$\mathrm{AF}(\nu,\tau) = F^{-1}_{t\to\nu} R(t,\tau) = \int_{-\infty}^{+\infty} R(t,\tau) e^{2\pi j\nu t} dt$.

ν is called the frequency-shift or Doppler-shift variable. The ambiguity function is the Fourier dual of the Wigner-Ville distribution:

$\mathrm{AF}(\nu,\tau) = F^{-1}_{t\to\nu} F^{-1}_{f\to\tau} \mathrm{WVD}(t,f)$

(see figure A9). It is also a time-frequency representation of the signal $\hat{s}(t)$, but now in the (ν,τ)-plane, and it can be seen as a correlation function. For instance, in radar-technology the ambiguity function is used to estimate the distance and velocity of a moving target (Woodward, 1953).

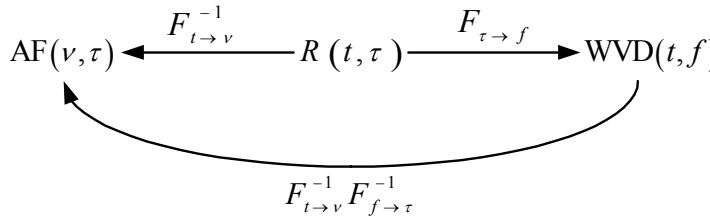

Figure A9. The ambiguity function. The Fourier transform relations between the local auto-correlation function $R(t,\tau)$, the ambiguity function $\mathrm{AF}(\nu,\tau)$, and the Wigner-Ville distribution $\mathrm{WVD}(t,f)$ (e.g., Qian et al. p:133, 1996).

4.4 Cohen's class

In the ambiguity-plane or (ν,τ)-plane, the auto-terms are centered around the origin. The cross-terms, however, are shifted away from the auto-terms. They are located further away from the origin (e.g., Qian et al. p:136, 1996; Steeghs pp:47-50, 1997). If it is possible to window the ambiguity plane with a two-dimensional window that leaves the auto-terms unaltered but suppresses the cross-terms in the ambiguity plane, then the cross-terms in the time-frequency plane will be suppressed too (e.g., Steeghs p:49, 1997). This leads to the concept of the generalized ambiguity function, whereby a two-dimensional function $\varphi(\nu,\tau)$ windows the ambiguity-plane:

$\widetilde{\mathrm{AF}}(\nu,\tau) = \varphi(\nu,\tau)\,\mathrm{AF}(\nu,\tau)$.

The Fourier dual $F_{\tau\to f} F_{\nu\to t} \widetilde{\mathrm{AF}}(\nu,\tau)$ of a generalized ambiguity function is a 'generalized Wigner-Ville distribution'. However, it is in fact a class of time-frequency representations and it is called **Cohen's general class of time-frequency representations**, discussed among others by Boashash (p:436, 1991), Cohen (ch.9, 1995), Qian et al. (p:139, 1996), Steeghs (pp:52-54, 1997), and Williams (p:9, 1997):

$$\rho(t,f) = F_{\tau\to f} F_{\nu\to t}\left[\varphi(\nu,\tau) F^{-1}_{t\to\nu} R(t,\tau)\right] = \int_{-\infty}^{+\infty}\int_{-\infty}^{+\infty}\int_{-\infty}^{+\infty} \varphi(\nu,\tau) R(u,\tau)\, e^{+2\pi j\nu u - 2\pi j t\nu - 2\pi j f\tau}\, du d\nu d\tau$$

(see figure A10).

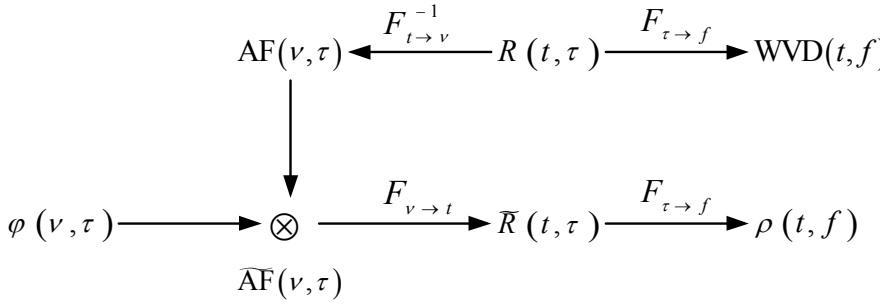

Figure A10. Cohen's general class of time-frequency representations. The Fourier transform relations between the generalized local auto-correlation function $\widetilde{R}(t,\tau)$, the generalized ambiguity function $\widetilde{\mathrm{AF}}(\nu,\tau)$, and Cohen's general class of time-frequency representations (e.g., Cohen pp:136-139, 1995).

The two-dimensional window $\varphi(\nu,\tau)$ of the ambiguity-plane is referred to as the kernel of the time-frequency representation (e.g., Claasen et al., 1980c; Steeghs p:54). The Wigner-Ville distribution belongs to Cohen's general class and has kernel $\varphi(\nu,\tau) = 1$. Other time-frequency representations belonging to Cohen's general class are the spectrogram with kernel

$$\varphi(\nu,\tau) = \int_{-\infty}^{+\infty} w\left(u+\frac{\tau}{2}\right) w^*\left(u-\frac{\tau}{2}\right) e^{-2\pi j\nu u} du$$

in which $w(t)$ is the window function (see section 2), and the **Rihaczek distribution** (Rihaczek, 1968) with kernel

$$\varphi(\nu,\tau) = e^{j\pi\nu\tau/2},$$

(e.g., Boashash, p:434, 1991; Cohen p:138, 1995; Williams p.7, 1997).

The first approach to suppress the cross-terms was the application of a 'smooth'-kernel. The cross-terms were suppressed by smoothing the Wigner-Ville distribution with a two-dimensional filter. This resulting representation is called a **smoothed Wigner-Ville distribution** (see chapter 5) (e.g., Boashash p:472, 1991; Novak, 1993a). Choi et al. (1989) applied an exponential kernel:

$$\varphi(\nu,\tau) = e^{-\nu^2\tau^2/\sigma}.$$

The generalized distribution with this kernel is called the **exponential distribution** (see chapter 6).

To satisfy the 'desirable' conditions of time-frequency representations (section 1) the kernel $\varphi(\nu,\tau)$ is subject to various restrictions and not every kernel can be applied. By constructing special kernel-functions with special constraints one can produce representations with prescribed, desirable properties. The construction of special kernels was also inspired by the question how to get rid of the cross-terms in the Wigner-Ville distribution. This leads to the so-called cross-term reducing 'cone-kernel' applied in the **ZAM-distribution**, and a class of cross-term reducing 'bowtie' shaped kernels. Members of Cohen's class that have cross-term reducing kernels are called **reduced interference distributions**. These are discussed for instance by: Boashash (pp:438,445-451, 1991), Zhao et al. (1991), Hlawatsch et al. (p:41, 1992), Kootsookos et al. (1992), Cohen (pp:141-149, 1995), and Williams (pp:8-20, 1997).

4.5 Applications

Novak et al. (1993a; 1993b; 1999) used time-frequency methods based on a Wigner-Ville distribution to graphically inspect the time-varying frequency contents and the cross time-frequency representation of and between cardiorespiratory signals. Pola et al. (1996) computed the power spectral density of HRV during autonomic tests (tilt test, phenylephrine administration, and Valsalva manoeuvre) by means of several time-frequency methods. They included the spectrogram, a smoothed Wigner-Ville distribution, and the exponential distribution. The spectrogram does not satisfy the marginal conditions. It may have a good time-resolution, though. However, the spectrogram is not very accurate in describing transients, because the time-resolution is dependent on the time-window. The smoothed Wigner-Ville distribution and the exponential distribution have a good time-resolution and both can detect transients with an accuracy of a few samples. Furthermore, a local power spectral density may be estimated, but results are dependent on the suppression of the cross-terms.

5 Other time-frequency representations

A fixed kernel is not capable of suppressing all the cross-terms in the ambiguity plane. Under the condition that the auto-terms and the cross-terms are separated in the ambiguity plane, Baraniuk et al. (1993a) developed an adaptive algorithm that suppresses the cross-terms that lie away from the auto-terms. This means that the algorithm produces an adaptive kernel that is 1 in the region of the auto-terms that lie

around the origin of the ambiguity plane, 0 outside this region, and has smooth edges. The ambiguity function is multiplied with this kernel and the resulting time-frequency representation (i.e., the Fourier dual) is called the **adaptive optimal kernel time-frequency representation** (Baraniuk et al., 1993a; 1993b; 1994; Jones et al., 1995). In fact, the adaptive optimal kernel is signal dependent. Therefore this representation does not belong to Cohen's general class. However, it is expected that this dependency guarantees a good performance for a broad class of signals, because the locations of the auto- and cross-terms depend on the signal (Baraniuk et al., 1993b). The adaptive optimal kernel time-frequency representation generally does not satisfy the conditions of an ideal time-frequency representation, for instance, the marginal conditions. Furthermore, it may not be possible to derive the instantaneous frequency because it contains no phase information. It may still be interesting to apply this representation because of the very good visualization of the time-varying fluctuations in HRV. Pattern recognition analysis may be applied to the adaptive optimal kernel time-frequency representation to identify and describe clusters of activity in the time-frequency plane.

The **Gabor representation** is a decomposition of the signal onto a basis of time-shifted and frequency modulated Gaussian functions (compare this with the short-time Fourier transform and the wavelet transform) (e.g., Hlawatsch et al. pp:28-29, 1992; Qian et al. p:52, 1996).

Another time-frequency representation is the **fast time-frequency transform** and its general formulation, the **discrete time-frequency transform** (Martens, 1992; 1999). This algorithm is the joint computation of the instantaneous amplitude and instantaneous frequency of an analytical signal in certain predefined narrow frequency bands. After filtering the signal, the instantaneous amplitude is the modulus of the resultant analytical signal, and the instantaneous frequency is estimated by means of the argument of the local auto-correlation function of the signal (see chapter 8).

References

Akselrod S, Oz O, Greenberg M, and Keselbrener L. Autonomic response to change of posture among normal and mild-hypertensive adults: investigation by time-dependent spectral analysis. J Autonomic Nervous System 64:33-43, 1997.

Akay M. Detection and estimation methods for biomedical signals. San Diego CA: Academic Press Inc, 1996, ISBN 0120471434.

Baraniuk RG and Jones DL. A signal-dependent time-frequency representation: optimal kernel design. IEEE Trans Signal Proc SP-41(4):1589-1602, 1993a.

Baraniuk RG and Jones DL. Signal-dependent time-frequency analysis using a radially Gaussian kernel. Signal Proc 32:263-284, 1993b.

Baraniuk RG and Jones DL. A signal-dependent time-frequency representation: fast algorithm for optimal kernel design. IEEE Trans Signal Proc SP-42(1):134-145, 1994.

Bendat JS and Piersol AG. Random Data, Analysis and Measurements Procedures, 2nd edition. New York: John Wiley and Sons, Inc., 1986.

Boashash B. Time-frequency signal analysis. In: Advances in Spectrum Analysis and Array Processing, Vol. 1. S. Haykin, Ed. Englewood Cliffs, NJ: Prentice Hall, pp:418-517, 1991.

Boashash B. Estimating and interpreting the instantaneous frequency of a signal – part 1: fundamentals. Proc IEEE 80(4):520-538, 1992.

Choi HI and Williams WJ. Improved time-frequency representation of multicomponent signals using exponential kernels. IEEE Trans Acoust Speech, Signal Processing ASSP-37:862-871, 1989.

Chui CK. An Introduction to Wavelets. New York: Academis Press, 1992.

Claassen TACM and Mecklenbräuker WFG. The Wigner distribution - a tool for time-frequency signal analysis, part I: continuous-time signals. Philips Res J 35:217-250, 1980a.

Claassen TACM and Mecklenbräuker WFG. The Wigner distribution - a tool for time-frequency signal analysis, part II: discrete-time signals. Philips Res J 35:276-300, 1980b.

Claassen TACM and Mecklenbräuker WFG. The Wigner distribution - a tool for time-frequency signal analysis, part III: relations with other time-frequency signal analysis. Philips Res J 35:372-389, 1980c.

Cohen L. Time-Frequency Analysis. Englewood Cliffs, NJ: Prentice Hall Inc, 1995, ISBN 0135945321.

Gabor D. Theory of communication. Proc IEE 93(III):429-457, 1946.

Hlawatsch F and Boudreaux-Bartels GF. Linear and quadratic time-frequency signal representations. IEEE Sig Proc Magazine 9:21-67, 1992.

Houtveen JH. Psychological and physiological responses to stress (Ph.D. Thesis). Amsterdam: University of Amsterdam, 2001.

Jensen A and la Cour-Harbo A. Ripples in Mathematics – The Discrete Wavelet Transform. Berlin-Heidelberg-New York: Springer-Verlag, 2001, ISBN 3540416625.

Jones DL and Baraniuk RG. An adaptive optimal-kernel time-frequency representation. IEEE Trans Signal Proc SP-43(10):2361-2371, 1995.

Kadambe S and Boudreaux-Bartels G. A comparison of the existence of 'cross terms' in the Wigner distribution and the squared magnitude of the wavelet transform and the short time Fourier transform. IEEE Trans Acoust Speech Signal Proc 40(10):2498-2517, 1992.

Keselbrener L and Akselrod S. Selective discrete Fourier transform algorithm for time-frequency analysis: method and application on simulated and cardiovascular signals. IEEE Trans Biomed Eng BME-43(8):789-802, 1996.

Kootsookos PJ, Lovell BC, and Boashash B. A unified approach to the STFT, TFDs and instantaneous frequency. IEEE Trans. Signal Processing 40:1971-1982, 1992.

Martens WLJ. The fast time frequency transform (F.T.F.T.): a novel on-line approach to the instantaneous spectrum. 14th International Conference of the IEEE Engineering in Medicine and Biology Society, 1992, Paris.

Martens WLJ. Segmentation of 'rhythmic' and 'noisy' components of sleep EEG, heart rate and respiratory signals based on instantaneous amplitude, frequency, bandwidth and phase. 1st joint BMES/EMBS conference 1999, Atlanta.

Newland DE. An Introduction to Random Vibrations, Spectral and Wavelet Analysis, 3rd edition. New York: Longman Scientific & Technical, 1993, ISBN 0582215846.

Novak P and Novak V. Time/frequency mapping of the heart rate, blood pressure and respiratory signals. Medical & Biological Engineering & Computing 31(2):103-110, 1993a.

Novak V and Novak P, de Champlain J, Le Blanc AR, Martin R, and Nadeau R. Influence of respiration on heart rate and blood pressure fluctuations. Journal of Applied Physiology 74(2):617-626, 1993b.

Novak V, Reeves AL, Novak P, Low PA, and Sharbrough FW. Time-frequency mapping of R-R interval during complex partial seizures of temporal lobe origin. Journal of the Autonomic Nervous System 77(2-3):195-202, 1999.

Pola S, Macerata A, Emdin M, and Marchesi C. Estimation of the power spectral density in nonstationary cardiovascular time series: assessing the role of the time-frequency representations (TFR). IEEE Trans Biomed Eng BME-43(1):46-59, 1996.

Qian S and Chen D. Joint time-Frequency Analysis – Methods and Applications. Upper Saddle River, NJ: Prentice Hall Inc, 1996, ISBN 0132543842.

Rihaczek A. Signal energy distribution in time and frequency. IEEE Trans. Inform. Theory IT-14:369-374, 1968.

Rioul O and Vetterli M. Wavelets and signal processing. IEEE Sig Proc Magazine 9:14-38, 1991;

Steeghs P. Local power spectra and seismic interpretation (Ph.D. Thesis). Delft: Delft University of Technology, 1997.

Ville J. Théorie et application de la notion de signal analytique. Cables et Transmissions 2A(1):61-74, 1948.

Wigner E. On the quantum correction for thermodynamic equilibrium. Phys Rev 40:749-759, 1932.

Williams WJ. Recent advances in time-frequency representations: some theoretical foundations. In: Time frequency and wavelets in biomedical signal processing. Akay M (ed). John Wiley & Sons, Inc. pp:3-43, 1997, ISBN: 0780311477

Woodward PM. Probability and information theory with application to radar. London: Pergamon Press, 1953.

Zhao Y, Atlas E, and Marks RJ. The use of cone-shaped kernels for generalized time-frequency representations on nonstationary signals. IEEE Trans Acoust Speech Signal Processing ASSP-38:1084-1091, 1990.

Glossary

Aliasing
This is an error that occurs when the ➔sampling frequency is lower than twice the highest frequency contained in the signal.

Ambiguity function
The inverse Fourier transform of the ➔local auto-correlation function with respect to the time variable is called the ambiguity function:

$$\mathrm{AF}(\nu,\tau) = F^{-1}_{t\to\nu} R(t,\tau) = \int_{-\infty}^{+\infty} R(t,\tau) e^{2\pi j\nu t} dt \,,$$

ν is called the frequency-shift or Doppler-shift variable. The ambiguity function plays a role in suppressing the ➔cross-terms of the ➔Wigner-Ville distribution.

Analytic(al) signal
An analytical signal is a signal that has no negative frequency components, equivalently, a signal of which the ➔Fourier transform is equal to 0 for frequencies lower than 0. The analytical signal $\hat{s}(t)$ associated with a real signal $x(t)$ allows us to define the ➔instantaneous amplitude, ➔instantaneous phase, and ➔instantaneous frequency of the real signal $x(t)$.

Autocorrelation function
The autocorrelation function of a complex signal $s(t)$ is defined by:

$$R(\tau) = \int_{-\infty}^{+\infty} s(t) s^*(\tau + t) dt$$

This is a measure of the dependence of a value of a signal at one time on the values of the signal at another time. The autocorrelation function may be used to detect a deterministic component masked in a random background, because the autocorrelation function of deterministic data persist over all time displacements, while the autocorrelation function of stochastic processes tends to zero if the time displacement becomes large (for zero-mean time series).

Auto-term
An auto-term represents the power in the time-frequency plane of a frequency-component or a time-component present in a signal.

Cardiac event series
A cardiac event series is an ➔HRV-representation obtained by representing each R-wave by a narrow positive spike of constant unit area generated at the R-wave occurrence time.

Central Finite Difference
A discrete estimator of the ➔instantaneous frequency is the discrete derivative of the phase $\varphi[n]$ of the discrete analytical time series $\hat{s}[n] = a[n]e^{j\varphi[n]}$. The estimator is the symmetrical discrete derivative:

$$f_i[n] = \frac{1}{2\pi} \cdot \left(\frac{\varphi[n+k] - \varphi[n-k]}{(2k+1)t_s} \right).$$

(t_s is the sample interval.) The discrete differentiation of $\varphi[n]$ must be obtained by subtracting phases at uncorrelated points $\varphi[n+k]$ and $\varphi[n-k]$.

Characteristic frequency components, bands, or rhythms
In the range of ➔short-term variability, three bands can often be distinguished in the ➔power spectrum at frequencies near 0.04, 0.1, and 0.3 Hz. The first band, at 0.04 Hz, is of uncertain origin. The 0.1 Hz band is probably mediated by the baroreflex and reflects the variable sympathetic and parasympathetic tone of the autonomic nervous system. The band near 0.3 Hz may reflect parasympathetic (vagal) tone linked with respiration. In the study of HRV, these bands are called the characteristic frequency components, bands, or rhythms.

Circular mean direction
An estimate of the ➔instantaneous frequency is the circular mean direction of the ➔discrete Wigner-Ville distribution:

$$f_i[n] = \frac{F_s/2}{2\pi} \cdot \arg \sum_{k=0}^{N-1} W[n,k] \cdot e^{2\pi j \cdot k/N}$$

Cross-term
A limitation of the ➔Wigner-Ville distribution is the appearance of cross-terms. They are sinusoidal components that appear between two ➔auto-terms. This means that between two frequency-components that are simultaneously present in a time-interval or between two time-components that are both present in a frequency-interval, there appears a cross-term in the time-frequency plane. The cross-terms are

due to the bilinear nature of the Wigner-Ville distribution. One can say that cross-terms are undesirable because they obscure the Wigner-Ville distribution and make it difficult to interpret the distribution.

Discrete time-frequency transform
The discrete time-frequency transform is the general formulation of the ➔fast time-frequency transform.

Discrete Wigner-Ville distribution
The discrete Wigner-Ville distribution of an discrete analytical time series $\hat{s}[n]$, $n = 0,...,N-1$ is defined by:

$$W[n,k] = \sum_{i=-N_1}^{N_1} \hat{s}[n+i]\hat{s}^*[n-i] \cdot e^{-4\pi j \cdot ik/N}$$

in which $N_1 = N/2$.

ECG
The electrocardiogram.

Envelope
➔Instantaneous amplitude.

Fast time-frequency transform
This algorithm is the joint computation of the instantaneous amplitude and instantaneous frequency of an ➔analytical signal $\hat{s}(t)$ in certain predefined narrow frequency bands. After filtering the signal, the instantaneous amplitude is the modulus of the resultant analytical signal, and the instantaneous frequency is estimated by means of the argument of the local auto-correlation function of the signal $\hat{s}(t)$.

$$f_i(t) \approx \frac{1}{2\pi} \arg R_{\hat{s}\hat{s}}(t,1)$$

Fourier analysis
By means of Fourier analysis, a time-domain function $x(t)$ can be investigated in the frequency-domain. This is also called spectral analysis. A function $x(t)$ can be written as a sum of sinus-functions, each with a specific amplitude and frequency.

There is a ono-to-one relationship between amplitudes and frequencies and this relationship represents the function as a function of frequency. This transforms the function from the time-domain to the frequency-domain and is called the ➔Fourier transform. The square of the absolute value of the amplitude of a sinusoid is a measure of the power of the sinusoid. Therefore, the absolute values of the amplitudes are often squared. The result, as function of the frequency, is called the ➔power spectrum.

Fourier transform
The Fourier transform $X(f)$ of a real or complex function $x(t)$ is defined by:

$X(f) = \int_{-\infty}^{+\infty} x(t) e^{-2\pi jft} dt$.

See also ➔Fourier analysis.

Frequency resolution
The frequency-resolution Δf indicates how accurately the frequency of a sinusoid can be measured; it is the minimum distance in frequency between two sinusoids so that they still can be resolved as distinct peaks in the ➔power spectrum. Two frequency components that are less than Δf in frequency apart cannot be discriminated in frequency.

Heart rate
Heart rate is the number of heartbeats per unit time, conventionally, per minute.

Heart rate event series
The spikes of a ➔cardiac event series represent the R-wave occurrence times. Each spike is weighed with the inverse of the value of the interbeat interval obtained at that R-wave occurrence time, multiplied with the duration of the preceding R-R interval. The result is called the heart rate event series.

Heart rate variability (HRV)
The beat-to-beat fluctuations in ➔heart rate are called heart rate variability.

HRV
➔Heart rate variability.

HRV-representation
A representation of ➔HRV is defined as the beat-to-beat information derived from the ➔ECG and ordered in such a way that it is accessible to the analysis techniques and can be related to physiological processes.

Instantaneous
Instantaneous signal properties are properties that can be computed within the time-resolution of the signal. Computations of a property over a shorter time interval yield adjacently dependent values in time; if computed over a longer time interval, the values will be averaged.

Instantaneous amplitude
Let $\hat{s}(t) = a(t)e^{j\varphi(t)}$ be an ➔analytical signal. The instantaneous amplitude or envelope is the modulus $a(t)$ of $\hat{s}(t)$. The squared instantaneous amplitude is a measure of the time-varying instantaneous power or energy per unit time of the signal within a narrow frequency band.

Instantaneous bandwidth
The ➔instantaneous frequency defines the time-varying frequency location of the spectral peak within a narrow frequency band. Due to a stochastic component, the spectral peak can have a spread. The instantaneous frequency is the average of the spread. The width (in the frequency direction) of the spread of the spectral peak is measured by means of the instantaneous bandwidth, being the associated standard deviation of the average instantaneous frequency.

Instantaneous bandwidth coefficient
The so-called instantaneous bandwidth coefficient is computed by our method as a measure of the ➔instantaneous bandwidth. The instantaneous bandwidth coefficient may serve as a time-varying segmentator of oscillatory versus irregular periods: low values indicate oscillatory properties, high values indicate irregularities.

Instantaneous frequency
Let $\hat{s}(t) = a(t)e^{j\varphi(t)}$ be an ➔analytical signal. The instantaneous frequency $f_i(t)$ is defined as the derivative of the ➔instantaneous phase $\varphi(t)$ of $\hat{s}(t)$:

$$f_i(t) = \frac{1}{2\pi}\frac{d\varphi}{dt}(t).$$

The instantaneous frequency defines the time-varying frequency location of the spectral peak within a narrow frequency band. Due to a stochastic component, the spectral peak can have a spread. The instantaneous frequency is the average of the spread. The width of the spread is called the ➔instantaneous bandwidth.

Instantaneous heart rate
This is the reciprocal of an ➔interbeat interval.

Instantaneous heart rate spectrum
This is a ➔power spectrum of a ➔heart rate event series.

Instantaneous phase
Let $\hat{s}(t) = a(t)e^{j\varphi(t)}$ be an ➔analytical signal. The instantaneous phase is defined as the argument $\varphi(t)$ of $\hat{s}(t)$.

Instantaneous spectrum
The time-varying ➔power spectrum of a signal that can be computed within the ➔time-resolution of the signal.

Interbeat interval
Time duration between two consecutive R-waves in the ECG.

Integral pulse frequency modulation model
System that transforms a continuous input signal into an event series.

Local autocorrelation function
The local ➔auto-correlation function (also called: time-dependent or instantaneous auto-correlation function) of an ➔analytical signal $\hat{s}(t)$ is defined as the product of two points of the signal lying symmetrically around time t at distance $\tau/2$:

$$R(t,\tau) = \hat{s}\left(t+\frac{\tau}{2}\right)\cdot\hat{s}^*\left(t-\frac{\tau}{2}\right),$$

in which τ is called the time-shift or time-lag variable.

Low-pass filtered cardiac event series
The low-pass filtered cardiac event series is an ➔HRV-representation that is derived from a ➔cardiac event series. This spike-train of a cardiac event series is filtered with a ➔zero-phase low-pass filter. Often a cutoff frequency of 0.5 Hz is used. The filtered continuous-time signal is called the low-pass filtered cardiac event series. After sampling this signal the resulting equidistant time series can be used for further computations.

Monocomponent
A monocomponent signal is a signal that has only one (time-varying) spectral band.

Multicomponent
A signal is multicomponent means that the signal's energy is locally distributed in two or more frequency bands.

Non-stationary
A signal is said to be non-stationary, if it has time-varying statistical properties. Suppose a signal is divided in segments and for each segment a statistic is computed. Possibly, the statistics differ from segment to segment. When the differences are significant, the signal is called non-stationary.

Power spectrum
➔Power spectral density.

Power spectral density (function)
The power spectral density or power spectrum describes how the power (or variance) of a time series is distributed with frequency. See also ➔Fourier analysis.

R-R interval
➔Interbeat interval.

Sampling
Extraction of discrete numeric data from an analog continuous signal.

Sampling frequency
Rate of extraction of discrete numeric data from an analog continuous signal.

Short-term variability
The beat-to-beat fluctuations in heart rate present in periods up to several minutes (2-5 min) are called short-term variability.

Spectral analysis
➔Fourier analysis.

Spectrum of counts
A spectrum of counts is the power spectrum of a ➔cardiac event series.

Stationary
See ➔non-stationary.

Time-frequency representation
A distribution that represents the power of a signal simultaneously in time and frequency is called a (joint) time-frequency representation. Time-frequency distributions are used to study ➔non-stationary signals: they give a spectral representation of the signal which is function of time.

Time resolution
The time-resolution Δt indicates how accurately in time an event can be measured; it is the minimum difference in time between two peaks so that they still can be resolved as distinct peaks in time. Two delta pulses that are less than Δt in time apart cannot be discriminated in time.

Time slice
A time-slice T_t at time t of a ➔time-frequency distribution $T(t,f)$ is defined by $T_t = \{T(t,f), \text{all } f\}$. Each time-slice can be viewed as an ➔instantaneous spectrum.

Uncertainty principle of Gabor
Gabor stated that, for a given filter, the product of the width in the time-domain σ_t and the width in the frequency-domain σ_f is greater than or equal to $1/4\pi$. In equation: $\sigma_t \cdot \sigma_f \geq 1/4\pi$. This means that, the wider (or narrower) the bandwidth of a filter is, the shorter (or longer) the corresponding impulse response is in the time-domain. The minimal product is reached for a normal distribution, which is a Gaussian shaped filter. Any other filter shape will deviate from a minimal product.

Wigner-Ville distribution

The Wigner-Ville distribution is a ➔time-frequency representation defined as the ➔Fourier transform of the ➔local auto-correlation function with respect to the time-shift variable τ:

$$\mathrm{WVD}(t,f) = F_{\tau \to f} R(t,\tau) = \int_{-\infty}^{+\infty} R(t,\tau) e^{-2\pi j f \tau} d\tau .$$

Zero-phase filter

A filter that cannot change the phase of a signal.

Reference

Working Group on Blood Pressure and Heart Rate Variability of the European Society of Hypertension. Glossary of terms used in time series analysis of cardiovascular data. Http://www.cbi.polimi.it/glossary/glossary.html

Abbreviations

ACF	autocorrelation function
AM	amplitude modulation
BP	blood pressure
CFD	central finite difference
CMD	circular mean direction
CZT	chirp Z-transform
CWT	color word test
DBP	diastolic blood pressure
DED	discrete exponential distribution
DFT	discrete Fourier transform
DPACF	discrete pseudo autocorrelation function
DTFT	discrete time frequency transform
DWVD	discrete Wigner-Ville transform
ECG	electrocardiogram
ED	exponential distribution
FFT	fast Fourier transform
FM	frequency modulation
FTFT	fast time frequency transform
HR	heart rate
IBI	interbeat interval
IHRS	instantaneous heart rate spectrum
IPFM	integrated pulse frequency modulation
LPFCES	low-pass filtered cardiac event series
PAF	pure autonomic failure
PSD	power spectral density
RSP	respiration
SBP	systolic blood pressure
SOC	spectrum of counts
STFT	short-time Fourier transform
TFD	time-frequency distribution
TFR	time-frequency representation
UTS	uncorrelated time slices
WD	Wigner transform
WVD	Wigner-Ville transform

DANKWOORD
CURRICULUM VITAE
LIST OF PUBLICATIONS

Dankwoord

De werkzaamheden beschreven in dit proefschrift werden uitgevoerd op de afdeling Psychiatrie van het Erasmus MC.

Beste professor Michiel Hengeveld, als hoofd van de afdeling Psychiatrie heb jij me de mogelijkheid gegeven om wetenschappelijk onderzoek te doen. Voor de afdeling ben ik een vreemde eend in de bijt, want wat doet een wiskundige die technisch cardiovasculair onderzoek doet op een afdeling Psychiatrie? Toch had je vertrouwen in me. Hartelijk dank daarvoor en voor het faciliterend werk dat je voor me hebt verricht. In verband met een moeilijke situatie op onze afdeling heb je dit werk overgenomen van professor Lolke Pepplinkhuizen. Beste Lolke, ik wil je bedanken voor je initiërend werk en ik betreur het dat de zaken zo gelopen zijn.

Beste professor Karel Wesseling, je hebt veel werk in dit proefschrift zitten en heel veel heb ik van je geleerd. Hartelijk dank voor het vertrouwen dat je in mij stelde en voor alles wat je voor me hebt gedaan.

Beste professor Arie Man in 't Veld, het is jammer dat je om persoonlijke omstandigheden mij niet langer kon begeleiden. Ik wil je bij deze bedanken voor jouw aandeel in het werk.

Beste doctor Joke Tulen, mijn dagelijkse begeleidster. Om jou te bedanken schieten woorden eigenlijk te kort. Ik heb zoveel van je geleerd. Je hebt me de ruimte gelaten een eigen richting te zoeken in het wetenschappelijk onderzoek. Ik wil je bedanken voor je leiding, je geduld, je vertrouwen en je vriendschap. Ik ben je erkentelijk voor het vele werk dat je voor me verzet hebt. We werken al heel lang samen en ik hoop dat onze samenwerking nog vele jaren zal duren. Van nu af aan zal ik weer meer tijd hebben voor het lab.

Beste Wim Martens, mijn tweede dagelijkse begeleider. Ik wil je bedanken voor de vele inspirerende en vruchtbare gesprekken. Veel signaal-analyse heb je mij geleerd en altijd had je het geduld om het me nog een keer uit te leggen. Ik hoop nog veel met je te kunnen samenwerken.

Ik wil de leden van de kleine en grote promotiecommissie bedanken voor hun (lees)werk en de bereidheid plaats te nemen in de commissies. Beste professor Solange Akselrod, hartelijk dank voor je bereidheid over te komen uit Tel Aviv om in mijn promotiecommissie plaats te nemen.

Beste dominee Peter van Helden en lieve Jolanda Geerlings, jullie hebben mij er doorheen geholpen toen de dagen voor mij wel erg donker waren. Jullie beurden mij op door, ieder op eigen wijze, veel met mij te praten. Dank jullie wel.

Beste Anita Volkers en beste Dirk Stronks, mijn mede promovendi, dank jullie wel voor jullie collegiale samenwerking, steun en gezelligheid.

Voor alles wat jullie voor me hebben gedaan, wil ik bedanken: de afdeling Psychiatrie; het secretariaat, met name Tini Zaanen en Marga Bosbaan; mijn lieve paranimfen Jannie Teekman en Jolanda Geerlings; de afdeling Klinische Neurofysiologie, Karel Mechelse, Ton Mus en Lourens van Briemen; de HTS-stagiaires; de koffiekamerkletsgroep; hervormde en gereformeerde gemeenteleden, voor jullie belangstelling; mijn lieve ouders; mijn zusters Martha, Riet en Willy en broer Jan, jammer dat onze vader, moeder en Rien dit niet meer mee kunnen maken; en iedereen die ik niet vergeten ben maar hier niet met name kan noemen.

Tot slot, dank en eer ik de Eeuwige.

Curriculum Vitae

Huibert Goosen (Hugo) van Steenis werd op 19 april 1952 geboren te Herwijnen. Hij doorliep het MULO-B en het HAVO en ging in 1970 wiskunde studeren aan de Rijksuniversiteit Utrecht. Daar deed hij eerst de leraren-opleiding MO-B wiskunde. Na een wiskundige specialisatie in de algemene topologie (gegeneraliseerde metrische ruimten) werd het doctoraal examen behaald in juni 1979. Van 1979 tot 1981 vervulde hij zijn vervangende dienstplicht bij de afdeling Neurologie van de Erasmus Universiteit Rotterdam. Daarna volgde in oktober 1982 een aanstelling als computer-programmeur op de afdeling Klinische Neurofysiologie van het Academisch Ziekenhuis Rotterdam-Dijkzigt. In april 1995 kreeg hij een aanstelling als wetenschappelijk onderzoeker bij het Instituut Psychiatrie van de Erasmus Universiteit Rotterdam. Daar is hij medewerker van het Psychofysiologisch Laboratorium. Onder leiding van het hoofd van het laboratorium, dr. Joke Tulen, kwam hij tot de samenstelling van dit proefschrift.

List of publications:

[1] Tulen JHM, Moleman P, van Steenis HG, Boomsma F. Characterization of stress reactions to the Stroop Color Word Test. Pharmacology Biochemistry & Behavior, 32(1):9-15, 1989.

[2] Tulen JHM, Moleman P, Boomsma F, van Steenis HG, van den Heuij VJHM. Dose-dependent effects of intravenous lorazepam on cardiovascular activity, plasma catecholamines and psychological function during rest and mental stress. Psychopharmacology, 105:77-83, 1991.

[3] Tulen JHM, Man in 't Veld AJ, van Steenis HG, Mechelse K. Sleep patterns and blood pressure variability in patients with pure autonomic failure. Clinical Autonomic Research, 1:309-315, 1991.

[4] van Steenis HG, Tulen JHM. A comparison of two methods to calculate the heart rate spectrum based on non-equidistant sampling. In: Proceedings of the 13th Annual International Conference of the IEEE Engineering in Medicine and Biology Society, J.H. Nagel, W.M. Smith (eds.). IEEE, vol. 13(2): 670-671, 1991.

[5] Tulen JHM, Moleman P, van de Wetering BJM, Kruijk M, von Saher RA, Boomsma F, van Steenis HG, Man in 't Veld AJ. Responses to cumulative doses of clonidine in healthy volunteers: cardiovascular, noradrenergic and subjective parameters. European Neuropsychopharmacology, 1(3):466, 1991.

[6] Tulen JHM, van de Wetering BJM, Kruijk M, von Saher RA, Moleman P, van Steenis HG, Boomsma F, Man in 't Veld AJ. Cardiovascular, noradrenergic and sedative responses to four doses of clonidine in a placebo-controlled design. Biological Psychiatry, 32:485-500, 1992.

[7] Tulen JHM, Man in 't Veld AJ, van Roon AM, Moleman P, van Steenis HG, Blankestijn PJ, Boomsma F. Spectral analysis of haemodynamics during 'stress-levels' of adrenaline and noradrenaline. Psychophysiology, 29(suppl):S71, 1992 (Abstract).

[8] Tulen JHM, Mulder G, Pepplinkhuizen L, Man in 't Veld AJ, van Steenis HG, Moleman P. Effects of lorazepam on cardiovascular variability during rest and mental stress. Psychophysiology, 29(suppl):S71, 1992 (Abstract).

[9] Tulen JHM, Moleman P, Blankestijn PJ, Man in 't Veld AJ, van Steenis HG, Boomsma F. Psychological, cardiovascular and endocrine changes to 6 hours of continuous infusion of epinephrine or norepinephrine in healthy volunteers. Psychosomatic Medicine, 55:61-69, 1993.

[10] Tulen JHM, Smeets FML, Man in 't Veld AJ, van Steenis HG, van de Wetering BJM, Moleman P. Cardiovascular variability after clonidine challenge: assessment of dose-dependent temporal effects by means of spectral analysis. Journal of Cardiovascular Pharmacology, 22:112-119, 1993.

[11] Tulen JHM, van de Wetering BJM, Luteijn LB, Boomsma F, Smeets F, van Steenis HG. Stability of baselines in a repeated measurement design: Details of cardiovascular variability, plasma catecholamines, and subjective mood. Journal of Psychophysiology, 7(1):85, 1993 (Abstract).

[12] Tulen JHM, van de Wetering BJM, Kruijk M, von Saher R, Moleman P, Boomsma F, van Steenis HG, Man in 't Veld AJ. Dose-related effects of clonidine i.v. on subjective mood, cardiovascular activity, and noradrenergic function in healthy volunteers. Journal of Psychophysiology, 7(1):86, 1993 (Abstract).

[13] van Steenis HG, Tulen JHM. Wigner-Ville time-frequency signal analysis of spontaneous fluctuations in cardiovascular time series. In: Extended Abstracts. Vijfde Workshop Computers in de Psychologie, F.J. Maarse, K.M.G. Kattenpoel Oude Heerink (eds.), 6-7 mei, 1993. Nijmeegs Instituut voor Cognitie en Informatie, Katholieke Universiteit Nijmegen, pp:88-90. ISBN 90-373-0189-4.

[14] Tulen JHM, Mulder G, Pepplinkhuizen L, Man in 't Veld AJ, van Steenis HG, Moleman P. Effects of lorazepam on cardiac vagal tone during rest and mental stress: assessment by means of spectral analysis. Psychopharmacology, 114:81-89, 1994.

[15] Tulen JHM, Man in 't Veld AJ, van Roon AM, Moleman P, van Steenis HG, Blankestijn PJ, Boomsma F. Spectral analysis of hemodynamics during infusions of epinephrine or norepinephrine in men. Journal of Applied Physiology, 76:1914-1921, 1994.

[16] van Steenis HG, Tulen JHM, Mulder LJM. Heart rate variability spectra based on non-equidistant sampling: the spectrum of counts and the instantaneous heart rate spectrum. Medical Engineering and Physics 16:355-362, 1994.

[17] Tulen JHM, van Steenis HG, Martens WLJ, Man in 't Veld AJ. Functional requirements for an ambulatory hemodynamic monitor. In: Dynamic analysis using body fixed sensors, P.H. Veltink, R.C. van Lummel (eds.). The Hague, McRoberts BV, pp:113-114, 1994. ISBN 90-9007328-0.

[18] van Steenis HG, Tulen JHM. Examining nonequidistantly-sampled cardiovascular time series by means of the Wigner-Ville distribution. In: F.J. Maarse, A.E. Akkerman, A.N. Brand, L.J.M. Mulder, M.J. van der Stelt (eds.),

Computers in Psychology: Applications, methods, and instrumentation. Lisse: Swets & Zeitlinger. Chapter 13, pp:151-166, 1994. ISSN 0925-9244.

[19] Tulen JHM, van Steenis HG, Pepplinkhuizen L, Man in 't Veld AJ. Quantification of autonomic cardiac regulation in psychopharmacological research. In: Measurement of heart rate and blood pressure variability in man. Methods, mechanisms and clinical applications of continuous finger blood pressure measurement. A.J. Man in 't Veld, G.A. van Montfrans, G.J. Langewouters, K.I. Lie, G. Mancia (eds.). Van Zuiden Communications B.V., Alphen aan den Rijn, The Netherlands, 1995, chapter 8, pp:61-72. ISBN 90-75141-14-9.

[20] van den Meiracker AH, Tulen JHM, Man in 't Veld AJ, van Steenis HG, Balk AHMM, Schalekamp MADH. Autonomic nervous system activity and short-term blood pressure variability. In: Measurement of heart rate and blood pressure variability in man. Methods, mechanisms and clinical applications of continuous finger blood pressure measurement. A.J. Man in 't Veld, G.A. van Montfrans, G.J. Langewouters, K.I. Lie, G. Mancia (eds.). Van Zuiden Communications B.V., Alphen aan den Rijn, The Netherlands, 1995, chapter 9, pp:73-80. ISBN 90-75141-14-9.

[21] van Steenis HG, Tulen JHM. Time-frequency analysis of cardiovascular signals using the exponential distribution. Psychophysiology 32(supplement 1):S73, 1995 (abstract).

[22] van Steenis HG, Tulen JHM. The exponential distribution applied to nonequidistantly sampled cardiovascular time series. Computers and Biomedical Research 29:174-193, 1996.

[23] Tulen JHM, van den Berg F, Bussmann JBJ, van Herel ECG, van Steenis HG. Ambulatory monitoring of kinematic and physiological parameters in psychophysiological research. In: Zesde Workshop Computers in de Psychologie. Beurs voor Computertoepassingen in de Gedragswetenschappen, B.P.L.M. den Brinker, P.J. Beek, A.P. Hollander, R.T. Nieuwboer (eds.). IFKB, Amsterdam 2-3 mei 1996, pp:132-134. ISBN 90-9009529-2.

[24] Tulen JHM, Bussmann JBJ, van Steenis HG, Pepplinkhuizen L, Man in 't Veld AJ. A novel tool to quantify physical activities: ambulatory accelerometry in psychopharmacology. Journal of Clinical Psychopharmacology 17:202-207, 1997.

[25] van Steenis HG, Tulen JHM. The effect of physical activities on cardiovascular variability in ambulatory situations. In: Proceedings - 19th International Conference - IEEE/EMBS, Oct. 30 - Nov. 2, 1997, Chicago, Il., USA, pp: 105-108. ISBN: 0-7803-4262-3.

[26] Tulen JHM, Bussmann JBJ, van Steenis HG, van den Berg F, van Herel ECG. Accelerometry in cardiovascular psychophysiology: new perspectives for ambulatory research. In: Cognitive ergonomics, clinical assessment and computer-assisted learning, B.P.L.M. den Brinker, P.J. Beek, A.N. Brand, F.J. Maarse, L.J.M. Mulder (eds). Lisse: Swets & Zeitlinger, pp:176-186, 1999, ISBN 90-265-1553-7.

[27] van Steenis HG, Martens WLJ, Tulen JHM. A new method to estimate the instantaneous frequency and bandwidth of cardiovascular time series. In: Proceedings of The First Joint BMES/EMBS Conference 'Serving humanity, Advancing technology', Oct. 13-16, 1999, Atlanta, USA, pp: 1011. ISBN: 0-7803-5683-7.

[28] van Steenis HG, Martens WLJ, Tulen JHM. Quantification of the dynamic behavior over time of narrow-band components present in heart rate variability by means of the instantaneous amplitude and frequency. Submitted.

[29] van Steenis HG, Martens WLJ, Tulen JHM. The instantaneous frequency of cardiovascular time series: a comparison of methods. Computer Methods and Programs in Biomedicine, accepted.

[30] van Steenis HG, Martens WLJ, Tulen JHM. Time-frequency parameters of heart rate variability – using instantaneous amplitude and frequency to unravel the dynamics of cardiovascular control processes. IEEE Engineering in Medicine and Biology Magazine, in press.